Investigation of glutamate receptors in human pancreatic β-cells and their role in insulin secretion.

Claire Heather Caygill

A thesis submitted in partial fulfilment of the requirements of the University of the West of England, Bristol for the degree of Doctor of Philosophy

This research programme was carried out in collaboration with the University of Bristol

Faculty of Health and Applied Sciences, University of the West of England, Bristol, 2020

May 2020

Acknowledgements

I would firstly like to thank my supervisor Aniko Varadi for providing me with valued help and guidance throughout my PhD. I would also like to thank my second supervisor Elek Molnar for allowing me to use his laboratory at Bristol University at the beginning of my studies and for providing helpful suggestions during the course of my PhD.

A massive thank you also goes to my girlfriend, Beth, for putting up with me after a bad day in the lab and for being my rock through the most difficult of times. I can't imagine getting this far without your support.

I would last, but not least, like to both thank and dedicate this body of work to my Mam and Dad. You both believed in me, even when I didn't believe in myself. Your unwavering encouragement and support enabled me to keep going and have the belief that I could make it to the end. My only regret is that I was unable to finish in time for Dad to see it, but I hope I have made you both proud.

Abstract

Background and Aims: β-cells share many similarities and features with neuronal cells, including the expression of proteins specialised for synaptic transmission. Glutamate receptors (GluRs) are key players in cellular communication throughout the central nervous system (CNS) and are activated by the major excitatory neurotransmitter glutamate. GluRs are also thought to be present in pancreatic β-cells, where they modulate insulin secretion, however there are many conflicting reports over the presence and function of GluRs particularly in human β-cells. Furthermore, autoantibodies to various GluRs have been associated with diseases of the CNS such as autoimmune encephalitis and epilepsy. It is unclear whether these receptors are also targets on β-cells in patients with Type 1 Diabetes (T1D). The aims of this project were *(i)* to identify GluRs, specifically Kainate receptor (KAR) subunits, expressed in the human β-cell line, EndoC- βh1; *(ii)* to elucidate their role in insulin secretion and *(iii)* to identify if GluR subunits on the β-cell surface are targeted by the immune system in T1D.

Materials and Methods: GluR expression was investigated in EndoC-βh1 human β-cells, both at the mRNA and protein levels using RT-PCR and immunoblotting, respectively. To measure the cell surface targeting of KARs in response to glucose stimulation, biotinylation experiments were carried out using EndoC- βh1 cells. Autoantibodies to KAR subunits were detected in sera from T1D patients (n=40) and aged-matched controls (n=40) using immunocytochemistry. The effect of KAR activation on insulin secretion was measured in the presence of kainate and various GluR agonists/antagonists using the Mercodia human insulin ELISA kit. To investigate if the KAR subunit GluK2 is specifically involved in glucose-stimulated insulin secretion (GSIS) a GluK2 knockdown using GluK2 shRNA lentivirus was attempted.

Results and Conclusions: KAR subunits Gluk2 and Gluk5 and the supporting auxiliary subunits Neto1 and Neto2 are expressed in EndoC-βh1 cells. The presence of GluK2 protein in EndoC-βH1 cells was confirmed using immunoblots, suggesting that functional kainate receptors can be formed. However, neither GluK2, GluK5, GluN1 nor GluN1 plus GluN2B are antigenic targets in T1D patients. The subcellular localisation of KAR was observed to be dynamically regulated as glucose stimulation significantly increased the cell surface targeting of GluK2. Lentiviral knock-down of GluK2 was unsuccessful in both INS-1 and EndoC-βH1 cells and it was therefore not possible to assess of GluK2 was specifically involved in GSIS. However, high glucose and kainate significantly increased insulin secretion compared to high glucose alone. Furthermore, high glucose and kainate induced insulin secretion from EndoC-βH1 cells was significantly reduced by the kainate receptor antagonist, NBQX, suggesting a functional role for KARs in insulin secretion and that KAR activation augments insulin secretion in human β-cells.

Posters, presentations and publications

- Caygill, CH., Craig, TJ., Dayan, C., Gillespie, K., Hayward, K., Molnar, E., Varadi, A. Investigation of glutamate receptors in human pancreatic β-cells and their potential role in insulin secretion. **Poster Presentation**. Islet Study Group Symposium. Potsdam, Germany (5th – 7th October 2018)

- Caygill, CH., Dwomoh, L., Molnar, E., Gillespie, K., Craig, TJ., Varadi, A. Investigation of glutamate receptors in human pancreatic β-cells and their potential role as autoantigens in Type 1 Diabetes. **Oral Presentation**. CRIB Annual Postgraduate Research Conference. UWE (22nd June 2018).

- Caygill, CH., Dwomoh, L., Molnar, E., Gillespie, K., Craig, TJ., Varadi, A. Investigation of glutamate receptors in human pancreatic β-cells and their potential role as autoantigens in Type 1 Diabetes. **Poster Presentation**. CRIB Annual Postgraduate Research Conference. UWE (19th June 2017).

- Caygill, CH., Dwomoh, L., Molnar, E., Gillespie, K., Craig, TJ., Varadi, A. Investigation of glutamate receptors in human pancreatic β-cells and their potential role as autoantigens in Type 1 Diabetes. **Poster Presentation**. CRIB Annual Meeting. UWE (11th January 2017).

- Caygill, CH., Hayward, K., Molnar, E., Gillespie, K., Varadi, A. The role of pancreatic islet cell glutamate receptors in endocrine hormone secretion and in the development of Type 1 Diabetes. **Poster Presentation**. Doctoral Training Alliance Summer Meeting. UWE (20th July 2016).

Abbreviations

AMPA (α-amino-3-hydroxy-5-methyl-4-isoxazolepropionic acid)

APS (ammonium persulphate)

ATD (amino terminal domain)

ATP (adenosine triphosphate)

CNS (central nervous system)

CSF (cerebral spinal fluid)

CTD (carboxy terminal domain)

DCI (3,4-Dichloroisocoumarin)

DEPC (Diethylpyrocarbonate)

DHPG ((*S*)-3,5-dihydroxyphenylglycine)

DMEM (Dulbecco's modified Eagle's medium)

DMSO (dimethyl sulphoxide)

EDTA (ethylenediaminetetraacetic acid)

ELISA (Enzyme-Linked Immunosorbent Assay)

EPSC (excitatory post-synaptic potential)

FBS (foetal bovine serum)

FCS (foetal calf serum)

FTD (frontotemporal dementia)

GAD (glutamate decarboxylase)

GCK (glucokinase)

GDM (gestational diabetes mellitus)

GFP (green fluorescent protein)

GluR (Glutamate receptor)

GLUT (glucose transporter)

GPCR (G-protein-coupled receptor)

GSIS (Glucose-stimulated insulin secretion)

GWAS (genome-wide association studies)

Gyki-52466 (Gyki-hydrochloride)

HLA (human leukocyte antigen)

IA-2 (islet-autoantigen-2)

IAA (insulin)

IBMX (3-isobutyl-1-methylxanthine)

ICA (islet cell autoantigen)

iGluR (ionotropic glutamate receptor)

IL2 (Interleukin 2)

IPSC (inhibitory post-synaptic current)

KAR (Kainate receptors)

LBD (ligand-binding domain)

mGluR (metabotropic glutamate receptor)

MODY (maturity-onset diabetes of the young)

MSG (monosodium glutamate)

NBQX (2,3-dihydroxy-6-nitro-7-sulfamoyl-benzon[f]quinoxaline-2,3-dione)

NDM (neonatal diabetes mellitus)

NMDAR (*N*-methyl-D-aspartate receptors)

NOD (non-obese diabetic)

PBS (phosphate buffered saline)

PEI (polyethylenimine)

PKA (protein kinase A)

PKC (protein kinase C)

PLC (phospholipase C)

RP (reserve pool)

RRP (readily releasable pool)

SDS (sodium dodecyl sulfate)

SG (secretory granules)

siRNA (short interfering RNA)

SLE (systemic lupus erythematosus)

T1D (type 1 diabetes)

T2D (type 2 diabetes)

TCA (tricarboxylic acid)

TMD (transmembrane domain)

VDCC (voltage-dependent Ca^{2+} channel)

VFD (venus flytrap domain)

ZnT8 (zinc transporter 8)

Table of contents

Table of figures

Table of tables

1. Introduction

1.1. The Islet of Langerhans

The endocrine pancreas accounts for 1 – 2 % of pancreas mass, which is comprised of the Islet of Langerhans, named after Paul Langerhans (1847 – 1888) who first distinguished the cluster of cells that make up the Islet of Langerhans. Pancreatic islets are made up of five different cell types; glucagon secreting α-cells make up 30% of the islet, insulin secreting β-cells account for 60% and the remaining 10 % are made up of δ-cells which produce somatostatin, PP (gamma) cells which secrete pancreatic polypeptide and epsilon cells which produce ghrelin (Da Silva Xavier, 2018).

The structure and composition of cells within islets has been shown to differ between species (Cabrera et al., 2006; Rorsman and Ashcroft, 2018). Human islets are considered to have a more random distribution of the different islet cell types (Cabrera et al., 2006; Da Silva Xavier, 2018) (Figure 1.1a). Whereas, in rodent islets there is a highly ordered structure, with β-cells being the predominant cell type making up the core of the islet and smaller numbers of α, δ, PP and epsilon cells surrounding the periphery, creating a 'mantle' structure (Pfeifer et al., 2015; Steiner et al., 2010) (Figure 1.1c). However, Bonner-Weir et al., 2015, have demonstrated that the majority human islets do resemble the rodent mantle-core arrangement, but there is a much bigger variability between islets from human pancreas than there is between islets from rodents. Despite islet architecture showing variation between different species, the cell composition remains the same and always includes α-, β- and δ-cells (Figure 1.1).

The pancreas is well vascularised and despite the Islets of Langerhans only accounting for 1 – 2 % of the pancreas, it receives roughly 10 % of the total pancreatic blood supply and the number of fenestrae is approximately ten times higher in islets than in the exocrine capillaries (Henderson and Moss, 1985; Jansson et al., 2016). Vascularisation of the islets of Langerhans is essential to allow β-cells and α-cells to respond quickly to changes in blood glucose levels and maintain glucose homeostasis (Diez et al., 2017). Studies also report differences between human and rodent vascularisation and innervation, both of which being less dense in humans (Brissova et al., 2015; Hart and Powers, 2019; Pfeifer et al., 2015; Rodriguez-Diaz et al., 2011).
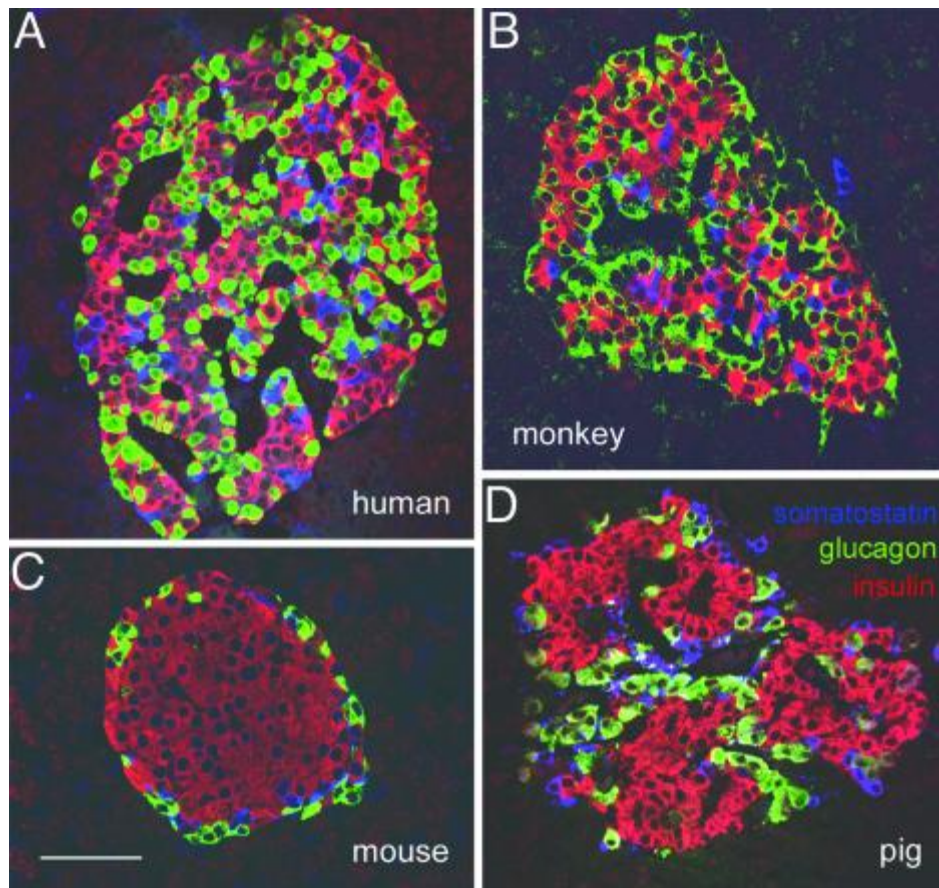
Figure 1.1. The architecture of the islets of Langerhans varies between different mammalian species. Architectural differences in the islets of Langerhans can be seen from immunostained pancreatic sections taken from A) human, B) monkey, C) mouse and D) pig. Immunoreactive antibodies towards insulin (produced by β-cells, shown in red), glucagon (produced by α-cells, shown in green) and somatostatin (produced by δ-cells, shown in blue) were used identify the different cell types in the islet of Langerhans. The scale bare represents 50 µM. Image is taken from Cabrera et al., 2006.

1.2. Glucose Homeostasis

The primary role of the endocrine pancreas is to regulate glucose levels in the blood and to keep it maintained within 4 – 6 mM (Röder et al., 2016). Variation outside of the normal glucose range can have catastrophic effects on the body. If blood glucose levels fall below 3.9 mM then an individual is described as being hypoglycaemic and left in this condition it can result in seizures or coma (Pawaskar et al., 2018). It is now known that even a short period of energy depletion in the brain can result in irreversible damage, highlighting the importance of maintaining blood glucose levels (Nirmalan and Nirmalan, 2017). Conversely, if glucose levels become too high, resulting in hyperglycaemia, the body can begin to breakdown fat as an energy source, leading to the production of ketone bodies and metabolic acidosis, resulting in changes in blood pH, eventually leading to coma (Fayfman et al., 2017). Both hyper- and hypoglycaemia if left untreated are fatal.

The body is able to maintain glucose homeostasis primarily through the actions of hormones secreted by the islets of Langerhans. The two most significant hormones in this process are glucagon and insulin.

1.2.1. The role of insulin in glucose homeostasis

Insulin is produced by β-cells in the islets of Langerhans and has the opposite effect of glucagon. When blood glucose levels are raised insulin is released by β-cells and results in glucose uptake by skeletal muscles, liver and adipose tissue and the conversion of glucose to glycogen (Nirmalan and Nirmalan, 2017) (Figure 1.2.).

1.2.2. The role of glucagon in glucose homoestasis

Glucagon is produced by the α-cells of the islets of Langerhans and its effects are primarily exerted on the liver. Glucagon is released by α-cells when blood glucose levels are low and results in glycogenolysis (glycogen breakdown into glucose) and gluconeogenesis (formation of new glucose) in the liver (Briant et al., 2016; Wendt and Eliasson, 2020). As a result, glucagon causes an increase in blood glucose levels (Figure 1.2).
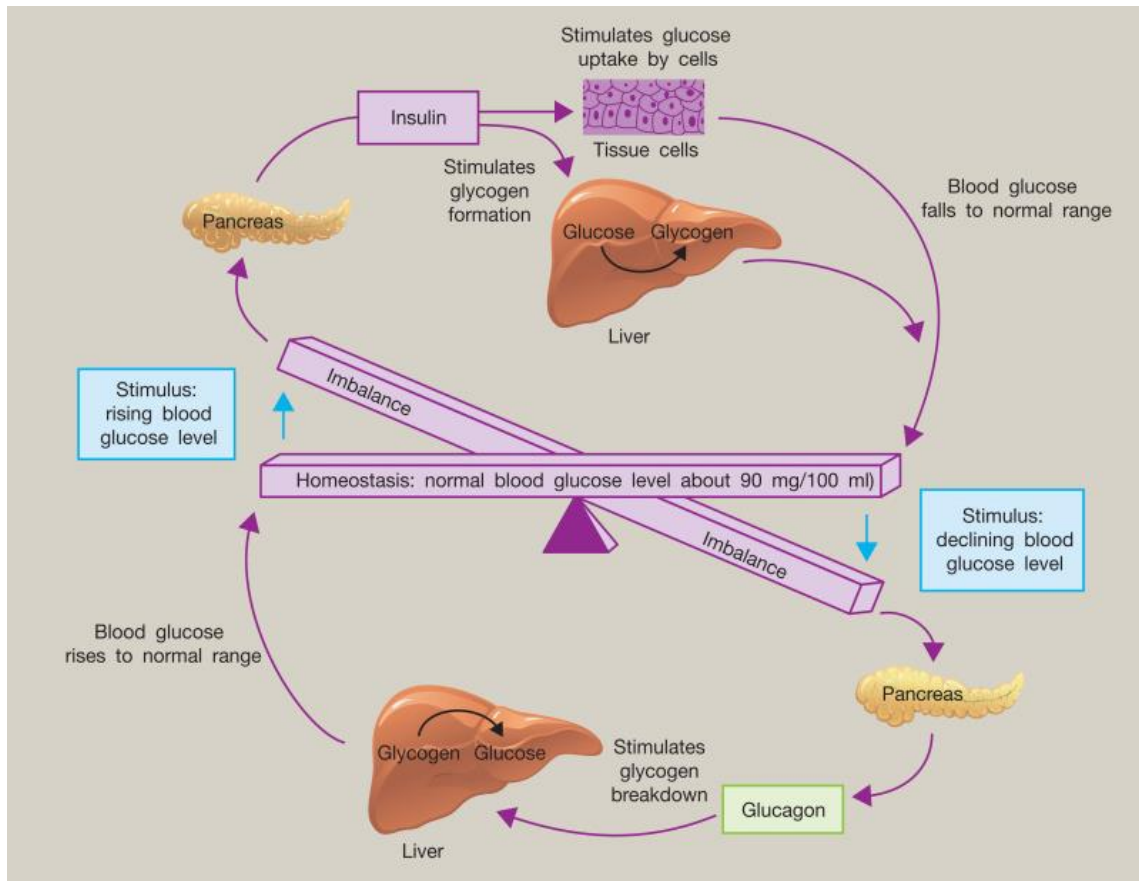
Figure 1.2. The hormonal control of glucose homeostasis. Blood glucose control is achieved through the balance of insulin and glucose secretion in response to high or low glucose. When blood glucose levels rise the β-cells of the pancreas are stimulated to produce insulin, resulting in glucose conversion to glycogen by the liver and glucose uptake by muscle tissue. Thus, allowing blood glucose levels to return to normal range. If blood glucose levels decline then the α-cells of the pancreas are stimulated to produce glucagon, which causes glycogen to be converted to glucose by the liver, resulting in blood glucose levels to rise and return to the normal range. Image taken from Nirmalan and Nirmalan, 2017.

1.3. Insulin secretion from pancreatic β-cells and mode of action

Upon ingestion of food, blood glucose levels begin to rise, creating a concentration gradient between the blood and the inside of β-cells. Glucose can then be transported via facilitated diffusion into the β-cell. This diffusion occurs via glucose transporters (Gluts) located on the plasma membrane of the β-cell. In humans, the predominant Glut used for glucose transport across the β-cell membrane is Glut1, whereas Glut2 is primarily used in rodents (Rorsman and Ashcroft, 2018). Once inside the cell, glucose is phosphorylated by glucokinase and undergoes glycolysis to yield pyruvate, which is utilised by the mitochondria in the tricarboxylic acid cycle (TCA cycle) to produce adenosine triphosphate (ATP) (Figure 1.3). Increased ATP within the cell then results in the closure of ATP-sensitive K^+ channels, depolarisation of the membrane and activation of voltage-dependent Ca^{2+} channels (VDCCs). Activation of VDCCs causes an influx of Ca^{2+} and triggers the exocytosis of insulin via secretory granules (Nirmalan and Nirmalan, 2017) (Figure 1.3).
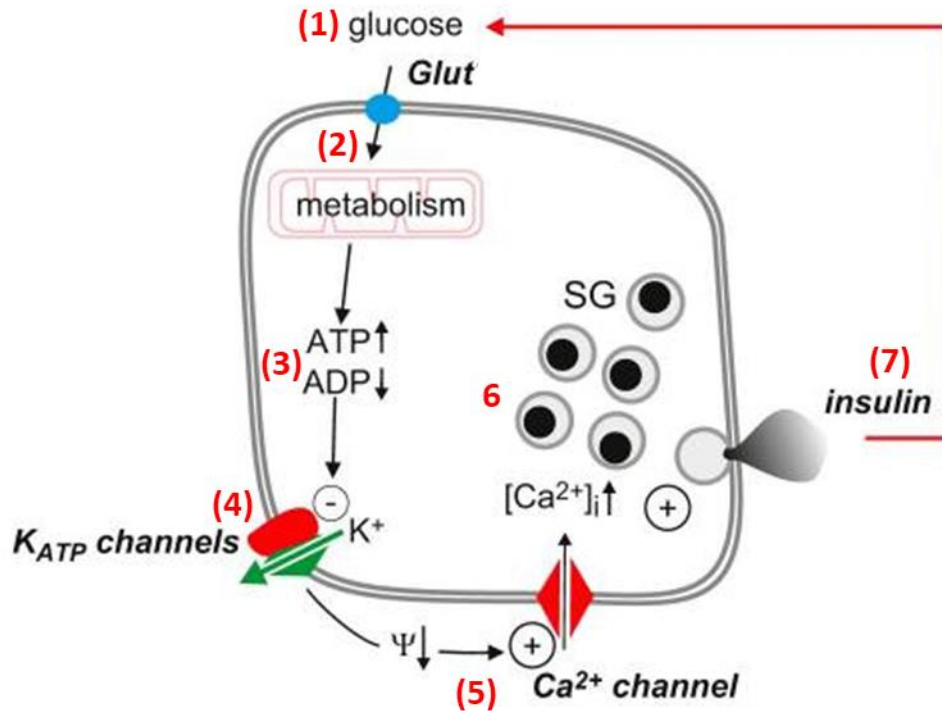
Figure 1.3. Mechanism of glucose-stimulated insulin secretion from a pancreatic β-cell. Glucose is transported into the β-cell via the glucose transporter (Glut) (1). Once inside the cell, glucose undergoes glycolysis to produce pyruvate which can be utilised by the mitochondria in the tricarboxylic acid (TCA) cycle (2). The TCA cycle causes increased levels of adenosine triphosphate (ATP) (3). Increased ATP then causes ATP-sensitive K^+ channels to close (4), resulting in a decreased membrane potential (Ψ) and activation of voltage-dependent Ca^{2+} channels (VDCCs) (5). Open VDCCs allow the influx of Ca^{2+} and triggers the formation of insulin containing secretory granules (SG) (6). Finally, insulin is released from the β-cell via exocytosis of SGs (7). Figure adapted from Rorsman and Ashcroft, 2018.

Glucose-stimulated insulin secretion (GSIS) from β-cells is a biphasic mechanism (Pedersen et al., 2019). The first phase lasts less than 10 minutes and results from the release of insulin from the readily releasable pool (RRP), which includes granules that are biochemically ready for release from the membrane as soon as depolarisation occurs. Roughly only 1 – 2 % of all β-cell insulin granules make up the RRP and are depleted following depolarisation (Rorsman and Ashcroft, 2018). The second phase occurs much more slowly, over approximately 60 minutes, where the reserve pool (RP) of insulin are trafficked to the plasma membrane for release (Rorsman and Braun, 2013) (Figure 1.4).

Once insulin has been released from β-cells it binds to insulin receptors on skeletal muscle, liver and adipose tissues. Binding of insulin to the insulin receptor results in a downstream signalling cascade which leads to translocation of Glut4 to the cell membrane. As a result, glucose can enter the cells via facilitated diffusion and be utilised by the cells for ATP production (Nirmalan and Nirmalan, 2017; Richter and Hargreaves, 2013).
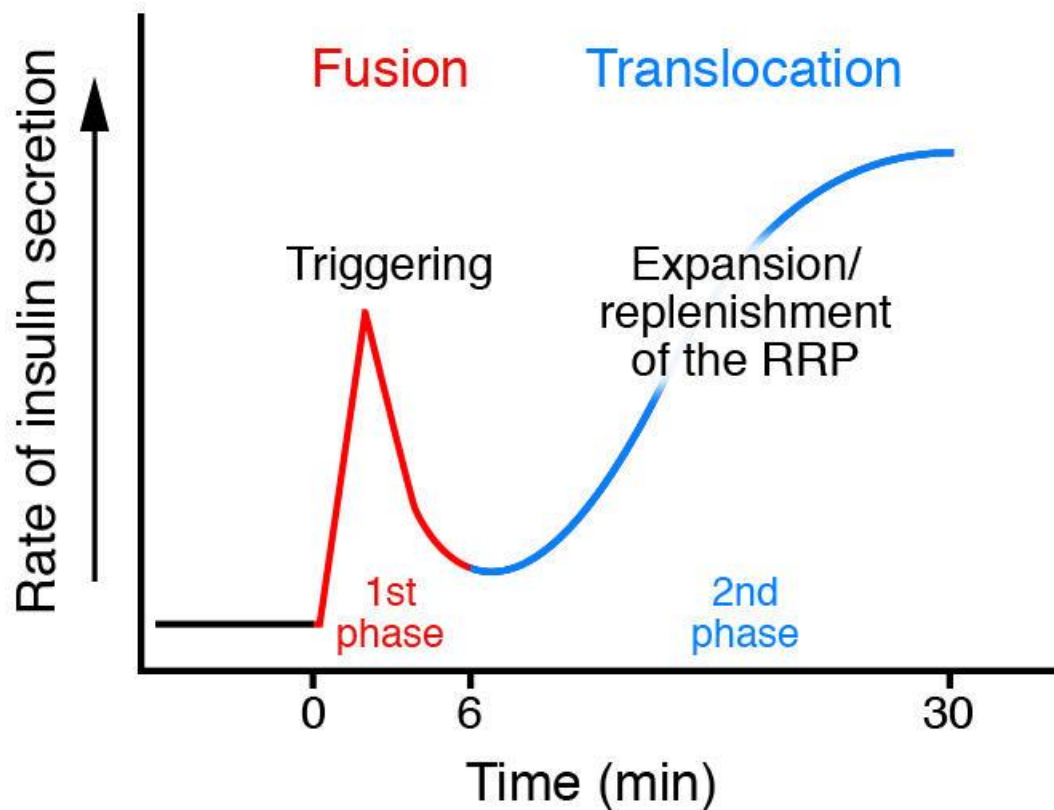
Figure 1.4. Biphasic insulin secretion from pancreatic β-cells. Insulin is released from β-cells in a biphasic manner where during the first phase (red line), insulin is released from the readily releasable pool (RRP), which is comprised of insulin granules which are fused to the membrane and are ready for immediate release. The first phase lasts less than 10 minutes and depletes the RRP. The second phase of insulin release occurs when the reserve pool (RP) of insulin is trafficked to the plasma membrane fusion site for release or replenishes the RRP. The second phase occurs over approximately 60 minutes. Image taken from Aizawa and Komatsu, 2005.

1.4. Diabetes Mellitus

1.4.1. <u>Definition and Prevalence of Diabetes Mellitus</u>

Diabetes mellitus is a group of chronic metabolic conditions that occur due to defects in either insulin secretion, insulin action or both. The lack of insulin action or secretion results in the body being unable to process glucose, leading to hyperglycaemia (Saberzadeh-Ardestani et al., 2018, IDF Diabetes Atlas, 2017). Diabetes can result in numerous complications such as, cardiovascular disease (Raghavan et al., 2019), kidney disease (Alicic et al., 2017), retinopathy (Selvaraj et al., 2017) bone fragility (Ferrari et al., 2018) and if left untreated can result in death. As well as physical complications, individuals with diabetes have been shown to have an increased risk of depression compared to the general population (Chireh et al., 2019), highlighting the difficulties faced by those living with the disease.

According to the IDF Diabetes Atlas, 2017 there are currently 425 million people affected by diabetes and this figure could rise to as many as 629 million by 2045. Globally, cases of diabetes are set to rise substantially across all continents (Figure 1.5). Diabetes treatment and care has become a major global burden with reported healthcare costs to have reached USD 727 billion. In the UK, 1 in 15 people have diabetes and the number of people with diabetes has risen from 1.4 million in 1996 to 3.8 million in 2018 (NHS Digital, 2018) and costs the NHS £192 million per week (Hex et al., 2012).
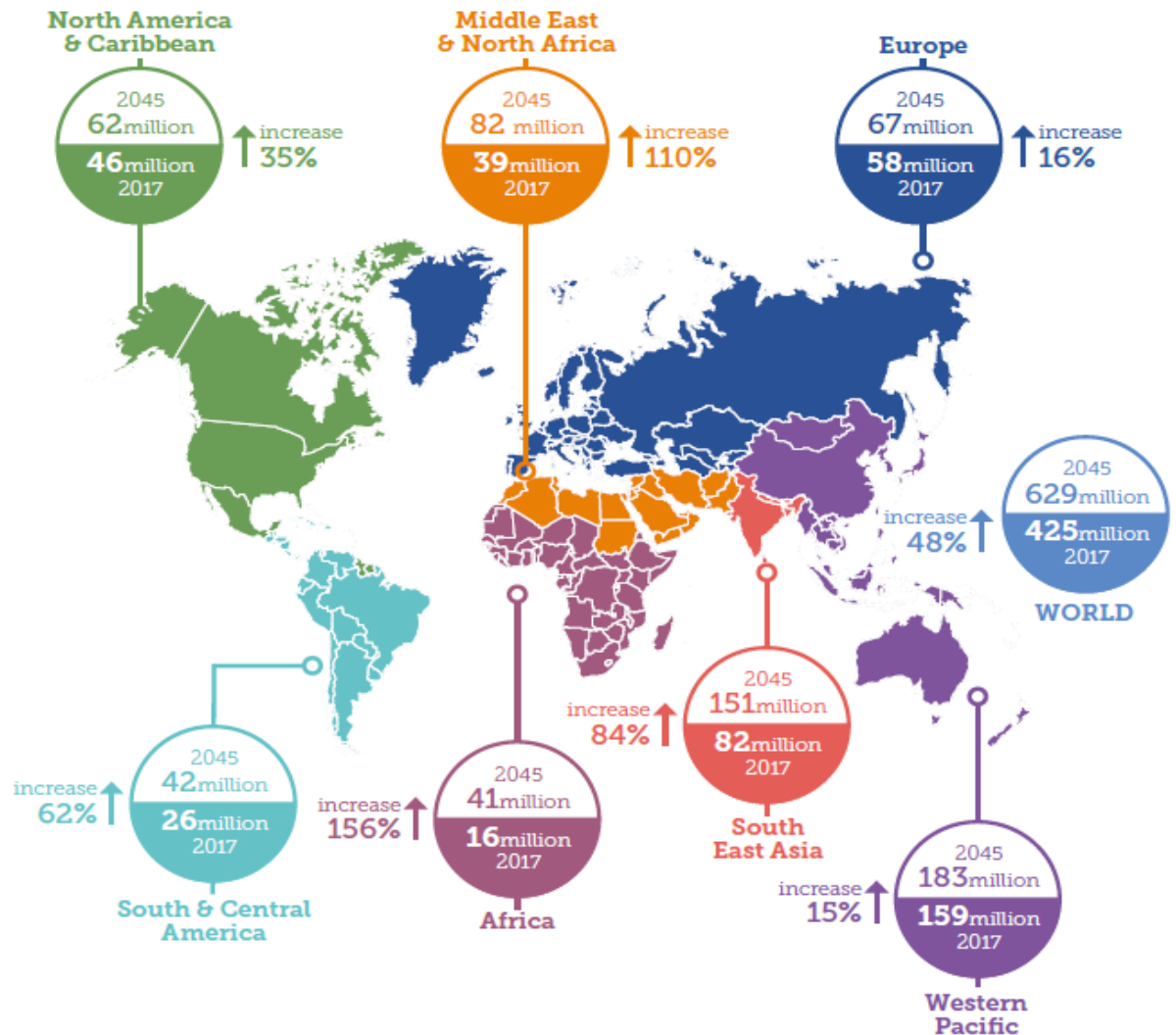
Figure 1.5. Number of people with diabetes worldwide and per region in 2017 and 2045 (20-79 years). The number of cases of diabetes is growing worldwide, with low and middle income countries showing the biggest increase. Figure available from International Diabetes Federation (https://diabetesatlas.org/ , last accessed 25/04/2019).

1.4.2. <u>Classification of Diabetes Mellitus</u>

Diabetes mellitus describes a group of metabolic diseases which can be classified into four general categories; 1) type 1 diabetes (T1D), 2) type 2 diabetes (T2D), 3) gestational diabetes mellitus (GDM) and 4) diabetes due to other causes, such as; neonatal diabetes (NDM), maturity-onset diabetes of the young (MODY) and diseases of the pancreas (American Diabetes Association, 2018).

The majority of people with diabetes have T2D and account for 90% of all diabetes cases (NHS Digital, National Diabetes Audit, 2017/2018). Individuals with T2D are still able to produce insulin, but the insulin they produce is insufficient to maintain glucose homeostasis. T1D accounts for 8% of diabetes cases in the UK and results from the destruction of insulin producing β-cells in the pancreas (Saberzadeh-Ardestani et al., 2018). The remaining 2% of diabetes cases arise from GDM or diabetes due to other causes. GDM is diabetes which occurs in pregnant woman at the second or third trimester, causing hyperglycaemia of varying severity (Chiefari et al., 2017). GDM prevalence is rising and has been found to reflect the prevalence of T2D within a population (Zhu and Zhang, 2016), adding to the current diabetes pandemic. In the majority of GDM cases, diabetes disappears after birth. However, it has been shown that women with a history of GDM are seven times more likely to develop T2D later on in life, with women who develop GDM in their first and second pregnancies being three times as likely of early T2D onset within three years of the second delivery (Bellamy et al., 2009; Bernstein et al., 2019).

MODY and NDM are both monogenic forms of diabetes. MODY has a higher occurrence compared to NDM and results from a genetic defect in insulin

producing β-cells and limits the cells ability to produce insulin (Firdous et al., 2018). There are currently 14 different genes known in which mutations could lead to the development of MODY and diagnosis of the condition is reliant on genetic screening (Firdous et al., 2018). NDM is diabetes which presents in the first 6 months of life and has more than 20 known genetic causes, with prognosis dependent on which gene is affected (Lemelman et al., 2018).

As a whole diabetes presents with vast heterogeneity, making correct diagnosis and classification of diabetes challenging. However, treatment management varies depending on which type of diabetes a patient has, so ensuring correct classification is essential for patient outcomes.

1.4.3. Type 1 Diabetes

T1D is a life-long and if left untreated, a life-threatening disease which is caused by the mass destruction of insulin producing β-cells in the islet of Langerhans (Saberzadeh-Ardestani et al., 2018). Patients with T1D are unable to convert glucose into glycogen and as a result enter a hyperglycaemic state and in severe cases ketoacidosis (Siller et al., 2016). T1D was formally known as juvenile diabetes as it was thought to only present itself in the young. However, research now indicates that incidences of adult-onset T1D are becoming more common (Lee et al., 2019; Thomas et al., 2018; Weng et al., 2018). This highlights the increasing difficulty in diagnosing T1D as many cases maybe misdiagnosed as T2D due to the age of onset. There is an estimated 40 million people living with T1D worldwide and recent research has shown that this figure is set to rise, as a 3.4% increase per annum in incidence rate has been noted across European countries (Patterson et al., 2019; Tuomilehto, 2013) (Figure 1.6).
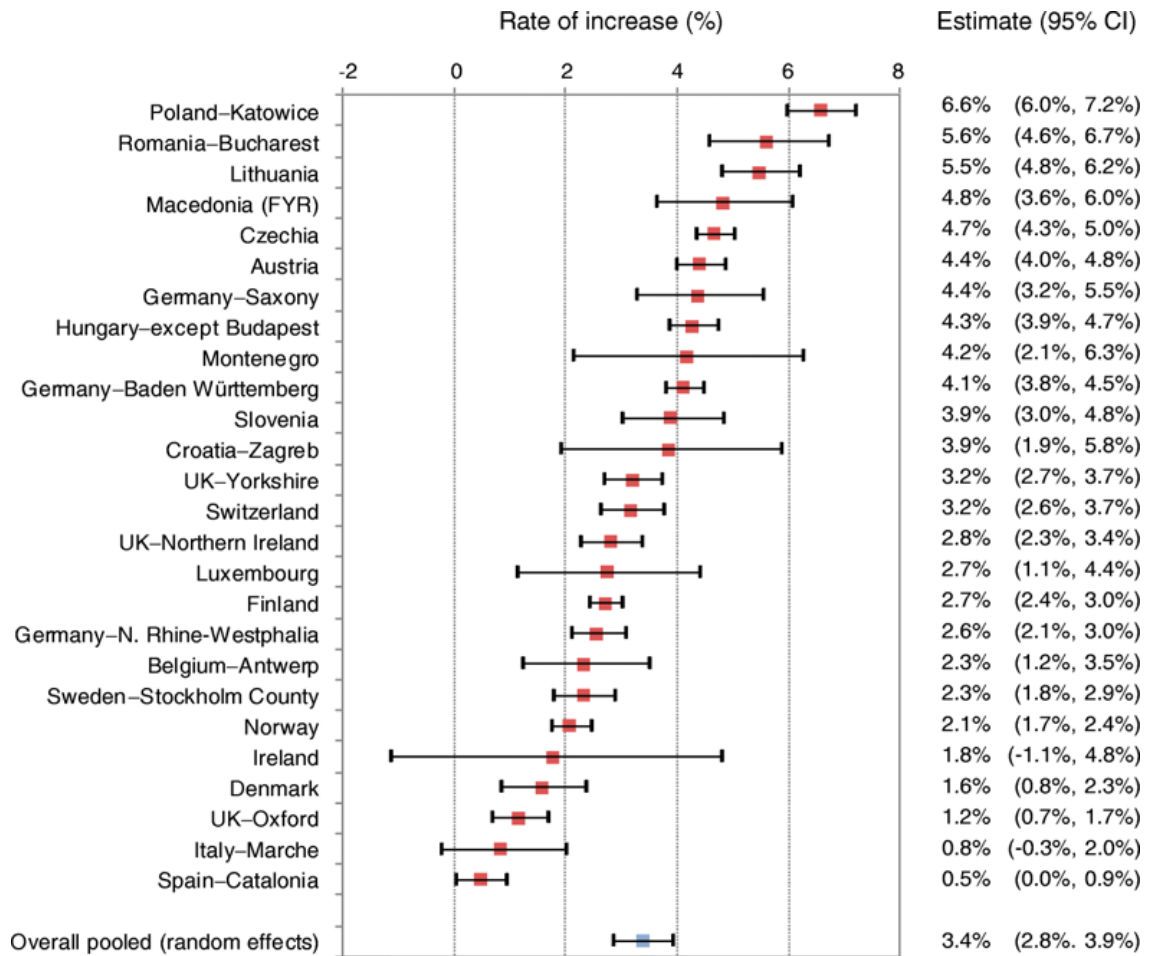
Figure 1.6. Estimated rates of annual increase of Type 1 Diabetes across 26 European centres. Data from 26 European centres shows an increase in T1D across all countries, with a ranging increase from 0.5 % in Spain to 6.6 % in Poland. The overall pooled increase across all 26 centres is 3.4 %. Figure taken from Patterson et al., 2019.

The cause of T1D is currently unknown, however, it is thought that it results from an interplay of genetic and environmental factors resulting in an uncontrolled immune response and autoimmunity (Saberzadeh-Ardestani et al., 2018) (Figure 1.7). There is evidence that the environment plays a role in T1D as the incidence and prevalence of T1D varies globally, ranging from more than 60 cases per 100,000 reported each year in Finland to only 0.1 per 100,000 cases per year in China (Atkinson et al., 2014). Studies have also indicated a seasonal link between incidences of T1D, further supporting the role of an environmental trigger for T1D (Rogers et al., 2017). There have been many studies suggesting numerous environmental risk factors which could be associated with T1D, such as gut microbiota reduction and the "hygiene hypothesis" (Toniolo et al., 2019). In support of this, children born by caesarean section have been shown to have an increased risk of developing T1D later in life (Magne et al., 2017; Peters et al., 2018), with a recent paper identifying shared molecular changes between children born by caesarean section and children who developed T1D (Laimighofer et al., 2019). Numerous dietary factors have also been associated with T1D, such as; cow's milk (Chia et al., 2018), breast feeding (Frederiksen et al., 2013; Lund-Blix et al., 2017) and gluten intake (Antvorskov et al., 2018; Gorelick et al., 2017). Further to this, excess BMI has been reported to accelerate autoimmunity and may lead to earlier onset of T1D in children (Ferrara-Cook et al., 2020). A study has even suggested that reduced natural selection may be involved in the increased rates of T1D (You and Henneberg, 2016). Epigentics is also suggested to be involved, with T1D patients having increased DNA methylation variability compared to their healthy twin siblings and healthy

unrelated individuals (Paul et al., 2016). Despite all the environmental evidence, no one exposure has been proven as the cause of T1D.

Through the use of genome-wide association studies (GWAS) over 60 susceptibility loci have been identified which are thought to explain roughly 80% of the heritability of T1D (Pociot, 2017). The most significant genetic association is with changes in the human leukocyte antigen (HLA), accounting for more than 50% of the genetic risk in T1D (Nakayama et al., 2015). HLA class II molecules present exogenous antigens to T lymphocytes, initiating the immune response. Alterations in genes encoding HLA molecules may predispose individuals to triggering autoimmunity, destroying β-cells and ultimately developing T1D (Regnell and Lernmark, 2017). Other non-HLA genes affecting T1D susceptibility are often genes associated with the immune system and even β-cell function. Some of the most notable of these are; *INS, PTPN22* and *IL2RA. PTPN22* codes for protein tyrosine phosphatase and is expressed in high levels in neutrophils and natural killer cells (Tizaoui et al., 2019). Interleukin 2 (IL2) has an essential role in maintaining the function of CD4$^+$ regulatory T cells, which help to regulate autoimmunity. *IL2RA* encodes the α subunit of the IL2 receptor and alterations in this gene are thought to lead to reduced IL2 signalling in regulatory T cells of T1D patients (Andreone et al., 2018). Finally, *INS* has the strongest association to T1D of all the non-HLA susceptibility genes and codes for preproinsulin. It is of note that this is the only susceptibility gene that also codes for a known T1D autoantigen (Regnell and Lernmark, 2017). Through the identification of genetic susceptibility loci researchers are beginning to be able to stratify the risk of individuals to go on to develop β-cell autoimmunity and eventually T1D (Bonifacio et al., 2018). However, genetic risk alone is not enough to account for or predict

all cases of T1D. An overview of the genetic and environmental aetiologies which may be involved in T1Ds is shown in Figure 1.7.
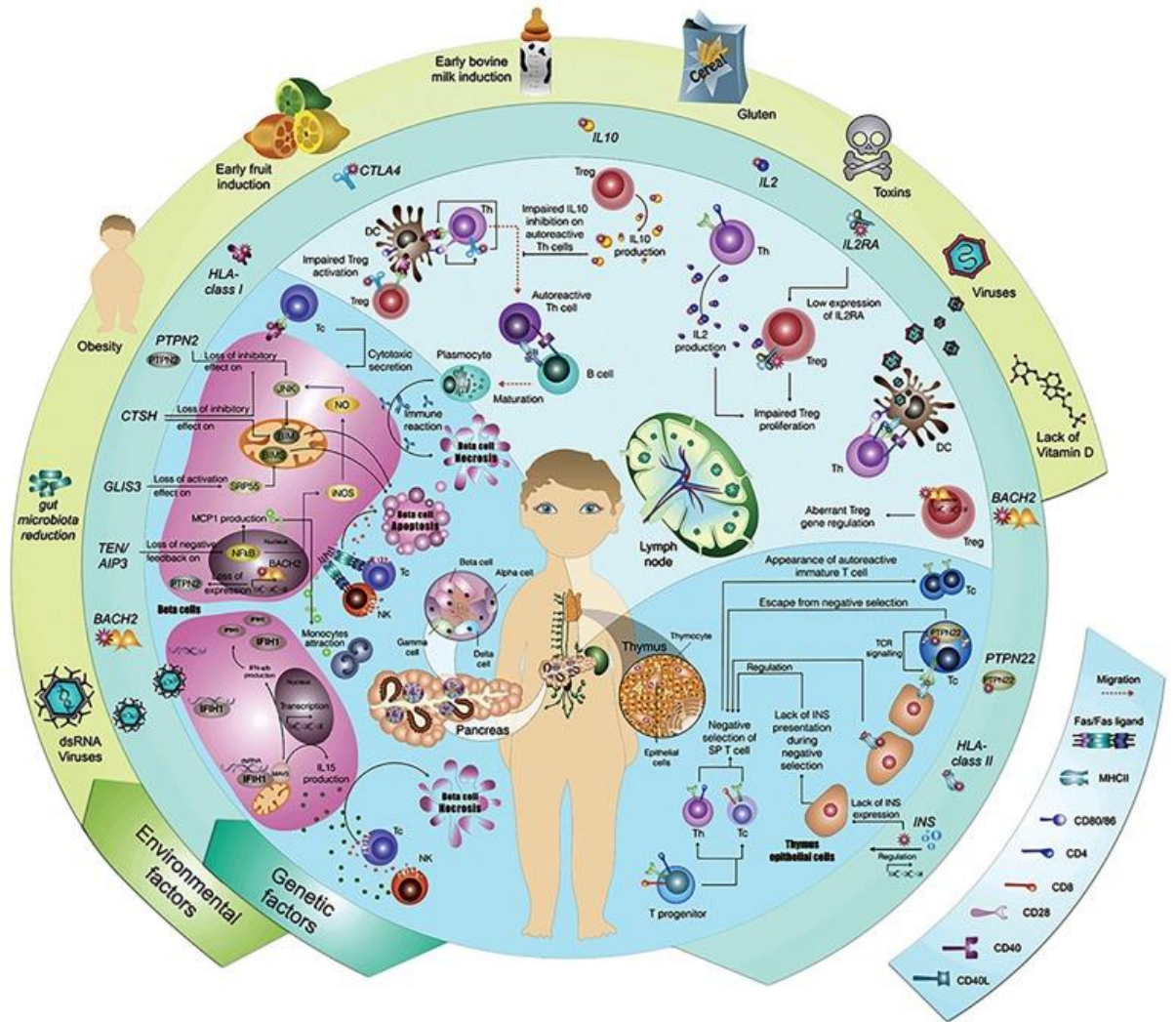
Figure 1.7. Representation of the genetic and environmental factors associated with T1D. The outer green ring represents environmental factors associated with T1D, whilst the middle blue ring displays genetic susceptibility alleles associated with T1D. The central circle indicates the mechanism of action for each of the environmental and genetic factors on causing T1D. Figure taken from Saberzadeh-Ardestani et al., 2018.

1.4.4. <u>Autoantibodies and Type 1 Diabetes Mellitus</u>

As discussed, it is now considered that islet autoimmunity is the first stage of disease in T1D (Insel et al., 2015; Rewers and Ludvigsson, 2016). There are currently four significant known autoantibodies associated with T1D which target β-cell proteins. The target proteins are: glutamate decarboxylase (GAD), insulin (IAA), islet-autoantigen-2 (IA-2) and zinc transporter 8 (ZnT8) (Jacobsen et al., 2018). It has been known for many years that detection of any of these autoantibodies in an individual's serum is predictive of T1D onset, especially if the individual is positive for more than one autoantibody (Bingley et al., 1994). Further to this, a study recruited new-borns with increased risk of developing T1D and measured their autoantibody levels regularly over many years. It was found that by age 15, 12.7% of children with a single autoantibody had developed diabetes, compared to 61.6% who had two autoantibodies and 79.1% for those who had three autoantibodies (Ziegler et al., 2013); highlighting the predictive value of autoantibodies in T1D.

Although they can act as a predictor, it is unlikely that any of these autoantibodies are the cause of T1D. All of the currently known autoantibody targets are intracellular β-cell proteins, as shown in Figure 1.8. Therefore, they will probably only be targeted by the immune system after the β-cell has already been destroyed and are unlikely to be the 'primary antigens' in triggering β-cell destruction at the early stages of T1D. Autoantibodies for these intracellular β-cell proteins are more likely to be as a result of "epitope spreading", which is when there is an increase in the number of islet autoantigens as the disease progresses into a more chronic state (McLaughlin et al., 2015). The antibodies produced as a result of epitope spreading are distinct from and non-crossreactive with the

disease-causing epitope. Epitope spreading is thought to occur by an initial activation of T cells, which leads to B cell activation and heightened antigen presentation. This heightened antigen presentation leads to antigen expansion beyond the initial disease causing antigen (Cornaby et al., 2015; Didona and Di Zenzo, 2018). However, it is likely that there are more autoantibodies to be discovered as there are some individuals whose sera are positive for islet cell autoantigen (ICA) but do not show immunoreactivity with any of the currently identified autoantibodies (Wenzlau and Hutton, 2013). Recently numerous other autoantibodies have been discovered which may also be associated with T1D, however, none so far appear act as the primary trigger of disease (Shi et al., 2019; So et al., 2018). It is possible that a currently unknown surface antigen is the first target for the immune system, leading to β-cell death and presentation of the already known intracellular autoantigens. Identifying the primary antigen target in T1D is vital as it would allow for the development of new therapies which could help to treat and prevent the disease.
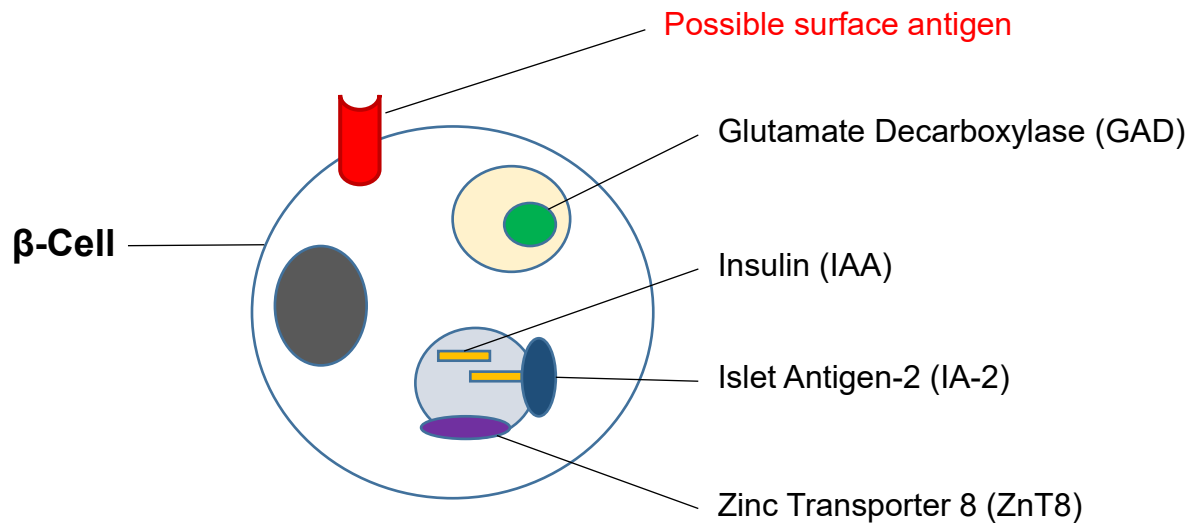
Figure 1.8. Pancreatic β cell and the location of known autoantibody targets in Type 1 Diabetes. All known autoantibodies associated with T1D have intracellular β-cell targets, as a result none of them are thought to be the "primary trigger" for the disease. The figure also shows the extracellular location of a potential antibody target which may be the initial target for the immune system in T1D. The figure is adapted from: http://www.bristol.ac.uk/clinical-sciences/research/diabetes/research/autoantibodies/, last accessed 25/04/2019.

1.5. Models of Type 1 Diabetes and pancreatic β-cells

The study of T1D is notoriously difficult for many reasons. First of all, the majority of patients remain undiagnosed until most functional β-cells have been destroyed; allowing for the onset of clinical symptoms to occur (Rojas et al., 2018) (Figure 1.9). As a result of this, any form of prevention that could be used, such as immunosuppressant therapy, may no longer be as effective as the majority of β-cells which have been targeted by the immune system have already been wiped out. To aid this the Juvenile Diabetes Research Foundation (JDRF), the Endocrine Society and the American Diabetes Association have proposed that T1D actually starts with islet autoimmunity, rather than when clinical symptoms and hyperglycaemia occur (Insel et al., 2015). Furthermore, there is an argument that T1D clinical trials are targeting patients at the wrong time and they should be receiving treatment as soon as autoimmune markers in T1D are present or even before (Bonifacio et al., 2017; Coppieters and von Herrath, 2018). However, this is controversial and raises ethical and safety questions in providing treatment to otherwise clinically healthy individuals. New research is now aiming to utilise β-cell regeneration to one day cure T1D and replace the β-cells destroyed by the immune system (Kuljanin et al., 2019; Mahdipour et al., 2019; Yi et al., 2020; Zhong and Jiang, 2019). While studies on non-obese diabetic (NOD) mice demonstrated if autoimmunity and islet inflammation are stopped it is possible for new β-cells to be formed (Akirav et al., 2008). This suggests that if the primary target of the autoimmune system in T1D can be identified and haulted, patients with T1D may have the potential to recover from the disease and regain β cell function.

The use of human islets for research purposes poses numerous problems as they can only be obtained from cadavers and require a specialist to properly excise the islets. Human islets have also been found to have very high variability from both one person to another and even between islets from the same individual (Bonner-Weir et al., 2015). For this reason, many researchers chose to use animal models as the islets are easier to acquire and in rodents show much less heterogeneity between samples. However, as described previously there are differences between human and other species islets, so they are still not the perfect model. There are many β-cell lines which can be used to study β-cell function, however, none exactly replicate a human β-cell so multiple models are sometimes required (Green et al., 2018). Many T1D breakthroughs and discoveries have been made using these research models, however, there is still a need for a consistent human model β-cell.
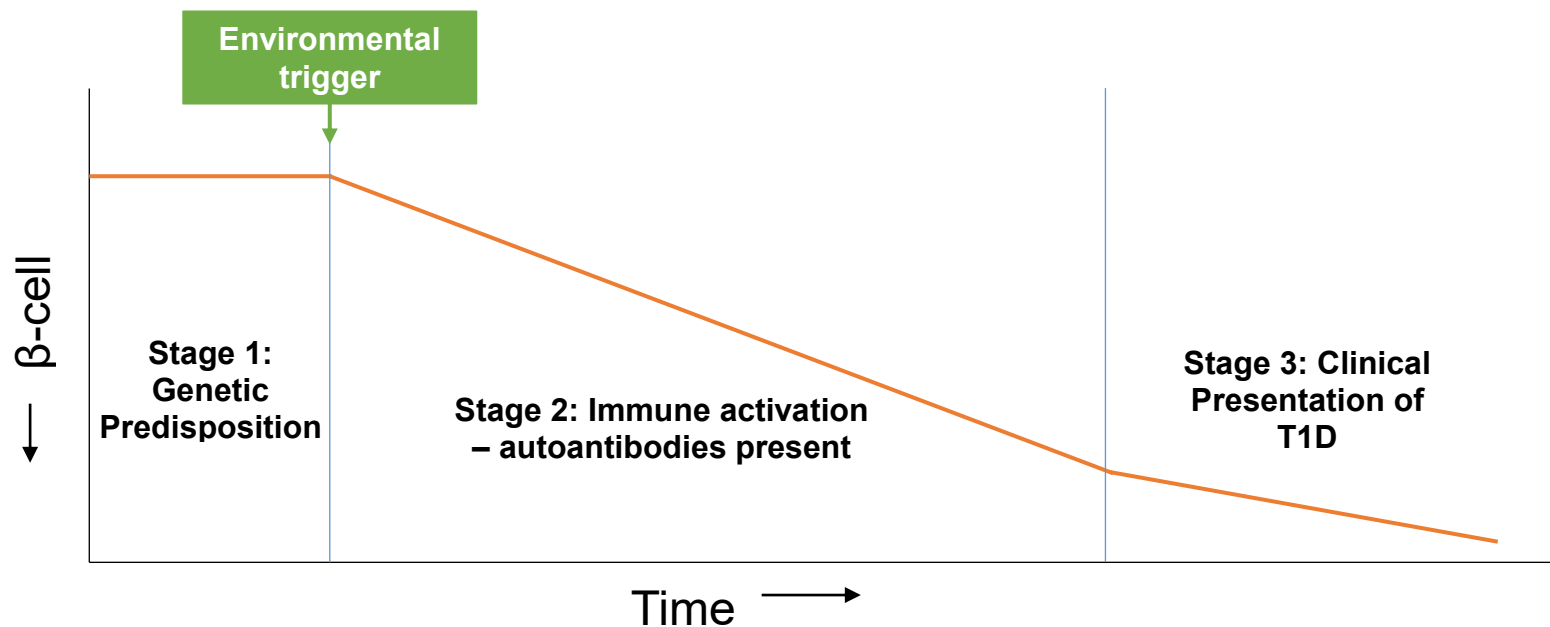
Figure 1.9. Timeline of Type 1 Diabetes disease initiation and progression. Prior to clinical diagnosis of T1D a genetic predisposition increases the chances of an individual developing T1D (stage 1). It is thought that some form of environmental trigger (virus, dietary trigger, microbiome etc.) then causes activation of the immune system and signals β-cell death and formation of autoantibodies (stage 2). The β-cell mass of T1D patients decreases over time until there are no longer enough cells to maintain glucose homeostasis through insulin secretion and clinical symptoms begin to be presented (stage 3). Figure has been adapted from https://www.diapedia.org/type-1-diabetes-mellitus/2104328117/natural-history-of-pre-type-1-diabetes , last accessed 30/04/19.

1.6. EndoC-βH1 cell line – human beta-cell line

As discussed in section 1.5, the study of pancreatic cells and their physiology has been difficult due to a lack of human pancreatic samples and no functional human cell lines. However, a human pancreatic β cell line produced from human foetal pancreatic buds which have been transduced with a lentiviral vector expressing SV40LT (an oncoprotein derived from polyomavirus SV40), under the control of the insulin promoter; named EndoC-βH1 has now been produced (Ravassard et al., 2011). The EndoC-βH1 cell line was shown to express the β-cell transcription factors PDX1, MAFA, NKX6-1, PAX6 and NEUROD1 (Ravassard et al., 2011). These cells also express mRNA for other important β cell markers, for example; glucokinase (GCK) which acts as a glucose sensor and SLC2A2, a glucose transporter (Ravassard et al., 2011). More recent studies have also shown that EndoC-βH1 cells show commonality of gene expression when compared to human islets and primary β-cells (Lawlor et al., 2019). Importantly, it has been shown that EndoC-βH1 cells respond to glucose-stimulated insulin secretion (GSIS), with publications reporting a roughly two or three-fold increase in insulin secretion in the presence of high glucose, compared to low glucose conditions (Andersson et al., 2015; Fred et al., 2015; Hastoy et al., 2018; Tsonkova et al., 2018).

Characterisation of EndoC-βH1 cells revealed their physiological response to glucose is controlled in the same way as is seen in human β-cells, which was described previously in section 1.3. Gurgul-Convey et al., 2016 found that, much like human β-cells, EndoC-βH1 cells use Glut1 and Glut2 glucose transporters to internalise glucose from outside of the cell. EndoC-βH1 cells then uses glucokinase to phosphorylate glucose, leading to glycolysis and pyruvate

production. Pyruvate can then be used by the mitochondria in TCA cycle to produce ATP from ADP. The subsequent increase in intracellular ATP then triggers the exocytosis of insulin via secretory granules by closure of ATP-sensitive K+ channels and opening of VDCC's (Figure 1.3) (Gurgul-Convey et al., 2016). These cells are therefore ideally suited for use as a human β-cell model to investigate glucose-sensitive hormone secretion.

Numerous studies have already begun to use the EndoC-βH1 cell line as a model of human β-cells to uncover new susceptibility genes (Ndiaye et al., 2017), understand β-cell dedifferentiation (Diedisheim et al., 2018), as well as identification of novel drug targets (Tsonkova et al., 2018). As a result, these cells have the potential to be used to elucidate some of the conflicting data on β-cell function and physiology in humans.

1.7. Glutamate receptors

L-glutamate is the major excitatory neurotransmitter in the mammalian central nervous system (CNS). In the CNS, glutamate is produced in the brain as the blood-brain-barrier prevents the majority of blood-borne glutamate from entering the CNS (Mahan, 2019). Glutamate acts as a neurotransmitter through its actions on Glutamate receptors (GluRs), which initiates numerous neuronal functions such as; fast synaptic transmission, learning and memory, motor processing and autonomic sensing (Mahan, 2019). There are two classes of GluRs; ionotropic (iGluR) and metabotropic (mGluR). iGluRs are glutamate-gated ion channels and mGluRs are G-protein coupled receptors (Ribeiro et al., 2017; Zhu and Gouaux, 2017). GluRs are located on the cell surface of neuronal cells and as a result of their conformation can only be activated by glutamate found in the extracellular fluid (Zhou and Danbolt, 2014). Glutamate homeostasis is required in the CNS, as concentrations which are too low or too high can be very damaging for neuronal cells. Glutamate is therefore actively taken up by glutamate transporters located predominantly on glial cells and released at nerve terminals to allow balance within the CNS (O'Donovan et al., 2017). The essential role of glutamate transporters to take in glutamate is highlighted as there is no known enzyme which is able to degrade glutamate in the extracellular space (Mahan, 2019). It is therefore necessary for neuronal cells to be able to detect when to release and when to take up glutamate and maintain homeostasis. Too much glutamate and neuronal cells begin to die and despite it being an important neurotransmitter, it is now known that it is also a neurotoxin. Neuronal cell death due to excessive GluR activation has been termed 'excitotoxicity' and is thought to lead to seizures and be the primary cause of neuronal cell death in neurological disorders such

as; Alzheimer's disease, traumatic brain injury and motor neurone disease (Magi et al., 2019; Vishnoi et al., 2016). On the other hand, too little glutamate has been associated with psychosis and schizophrenia (Hernaus and Amelsvoort, 2018), further emphasising the importance of glutamate and its regulation.

1.7.1. Ionotropic Glutamate Receptors (iGluRs)

Activation of iGluRs within the CNS results in basal excitatory synaptic transmission and synaptic plasticity (Zhu and Gouaux, 2017). iGluRs can be further subdivided based on their sequence homology, electrophysiological properties and pharmacological selectivity into three main subtypes; AMPA (α-amino-3-hydroxy-5-methyl-4-isoxazolepropionic acid), kainate and NMDA (N-methyl-D-aspartate) receptors (Hogan-Cann and Anderson, 2016). Within the CNS iGluRs are located at the synaptic cleft, where upon binding of glutamate to the ligand-binding domain (LDM), allow the influx of Ca^{2+} and Na^+ , resulting in excitatory synaptic transmission (Mayer, 2017; Zhu and Gouaux, 2017). iGluRs share some sequence homology and architecture, despite having large differences in their gating kinetics and pharmacology (Twomey and Sobolevsky, 2018). All are composed of four protein subunits, 3 of which are transmembrane spanning, and form a central ion channel pore (Mayer, 2017). iGluRs can be divided into four layered domains; the amino terminal domain (ATD), which is required for receptor trafficking and assembly, the ligand binding domain (LBD), the transmembrane domain (TMD) which forms pores to allow the influx of Ca^{2+} and Na^+ through the postsynaptic membrane and the intracellular C-terminal domain (CTD) (Twomey and Sobolevsky, 2018). The basic structure of iGluRs when at rest, activated and desensitised is shown in Figure 1.10.
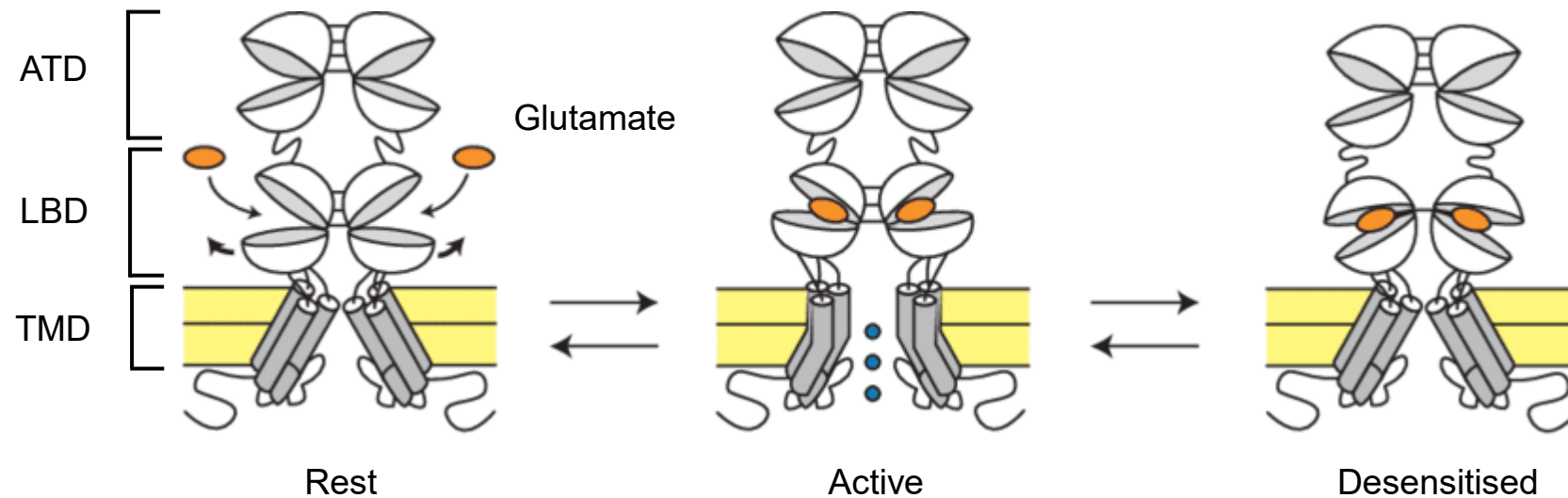
Figure 1.10. Structural overview of iGluRs at rest, activated and desensitised. iGluRs can are formed of a transmembrane domain (TMD), ligand-binding domain (LBD) and amino terminal domain (ATD). Upon iGluR activation via binding of glutamate to the LBD, iGluRs undergo a conformational change, creating a pore in the TMD and allowing the passage of ions through the post-synaptic membrane. Following activation, iGluRs become desensitised and the pore in the TMD is closed to prevent over-stimulation of neuronal synapses. Figure is modified from Smart and Paoletti, 2012.

1.8. Kainate Receptors (KARs)

1.8.1. <u>KAR subunit classification and receptor organisation</u>

Kainate receptors (KARs) are composed of five different subunits; GluK1, GluK2, GluK3, GluK4 and GluK5, encoded by the genes GRIK1 – 5, and assemble as either homo- or heterotetrameric receptors (Evans et al., 2019). Similar to the other iGluRs, KAR subunits come together form a functional receptor made up of a transmembrane domain (TMD), ligand-binding domain (LBD), amino terminal domain (ATD) and an intracellular C-terminal domain (CTD) (Twomey and Sobolevsky, 2018) (Figure 1.10). KAR subunits have been split into two groups; low affinity subunits and high affinity subunits based on their affinity to kainate. Low affinity subunits comprise GluK1 – 3 and have an affinity to kainate in the range of 50 – 100 nM. Whereas the high affinity subunits have an affinity to kainate in the 5 – 15 nM range and are made up GluK4 or GluK5 (Hadzic et al., 2017). Studies have shown that low affinity subunits are able to form both homomeric and heteromeric receptors, whereas high affinity subunits can only form functional receptors when in combination with GluK1 – 3 subunits.

1.8.2. <u>KAR localisation in the CNS</u>

In comparison to the other iGluRs, KAR localisation in the CNS is less well studied. This is likely to be due to a number of factors including; inadequate pharmacological tools, poor antibody quality, fewer mRNA copies per cell and low amounts of receptor proteins (Hadzic et al., 2017). However, it has been established that the most predominant subunit combination in the brain is GluK2 and GluK5 receptors (Mahan, 2019); which is supported by evidence that GluK2 and GluK5 subunits form the most stable receptors compared to any other KAR subunit combinations (Zhao et al., 2017). In adult mouse hippocampus and

cerebellum it has been shown that GluK2 and GluK3 were the major KAR subunits expressed, along with GluK5. Whereas, GluK4 and GluK1 expression levels were either very low or below the detection threshold (Watanabe-Iida et al., 2016). However, species differences between mouse and human GluK4 expression have been observed, with GluK4 being more abundant in the human cortex compared to mouse (Zeng et al., 2012). KAR subunits are thought to have differing roles within the CNS, for example, GluK2 is thought to play a role in synaptic incorporation, whereas synapse specificity in the hippocampus is reliant on GluK4 and GluK5 subunits (Evans et al., 2019). On top of this, studies have suggested that KARs play a role in neuronal development as they are expressed in the embryonic brain (Hadzic et al., 2017) and KAR overexpression promotes dendritic growth in pyramidal cells and interneurons (Jack et al., 2018), highlighting the importance of KARs in the CNS.

1.8.3. <u>KAR Auxiliary Proteins</u>

Research has shown that proteins interact with KARs to influence their function, trafficking and surface expression (Evans et al., 2017, 2019) and are termed auxiliary subunits. Some of the proteins which have been shown to interact with KARs are; PSD-95, N-Cadherin and C1q-like proteins (Falcón-Moya1 et al., 2018; Fièvre et al., 2016; Kilinc, 2018; Suzuki and Kamiya, 2016). However, by far the most extensively researched KAR auxiliary proteins are Neto1 and Neto2, which associate with KARs through binding to the GluK1 – 3 subunits (Evans et al., 2019). Recent studies have demonstrated that Neto1 may be involved in dendritic growth and differentiation when expressed with GluK1 (Jack et al., 2018). Neto1 has also been shown to be necessary for the formation of KAR-containing synapses in interneurons, as Neto1 deficient interneurons have

significantly impaired dendritic and axonal targeting (Orav et al., 2019). It has been demonstrated that expression of GluK2 in HEK293 cells is enhanced by the co-expression of Neto1 or Neto2 auxiliary subunits, suggesting a further role for these proteins in KAR trafficking (Palacios-Filardo et al., 2016). Importantly, it has been revealed that the Neto proteins slow the deactivation and desensitisation of KARs which explains the differing gating kinetics of KARs in vivo compared to studies in vitro which over express KAR subunits without Neto auxiliary proteins (Evans et al., 2019; Sheng et al., 2017). This strengthens the importance of Neto subunits in KAR function.

1.8.4. <u>Role of KARs in the CNS</u>

KARs are a unique subgroup of iGluRs as they not only have functional roles at the pre- and post-synaptic terminus, but they are also able to exert metabotropic mechanisms of action (Negrete-Díaz et al., 2018). Despite being present post-synaptically, they do not exert much excitatory post-synaptic potential (EPSC) in comparison to AMPA receptors. In CA1 pyramidal cells KARs exert virtually no EPSCs at all (Sheng et al., 2017), however, studies have shown that they have some control over AMPA receptors to induce LTP through metabotropic mechanisms when they are activated at post-synaptic terminals (Petrovic et al., 2017). Pre-synaptically, KARs appear to exert bidirectional control over glutamate release and are therefore able to regulate both excitatory and inhibitory control over neurotransmitter release (Hadzic et al., 2017). In the cerebellum, pre-synaptic KARs have been shown to facilitate glutamate release and enhance synaptic transmission via activation of PKA signalling (Falcón-Moya et al., 2018). KARs are also able to downregulate GABA release from interneurons to reduce inhibitory post-synaptic currents (IPSCs) (Evans et al., 2017; Hadzic et al., 2017).

On the other hand, a recent study has shown that activation of KARs in the hippocampus results in fast synaptic inhibition, with activation of KARs being proposed as a method to reduce glutamatergic activity during hyperexcitability (Garand et al., 2019). The role of KARs within the CNS still remains to be fully elucidated, however, research has shown that KARs are complex iGluRs with roles in both inhibition and excitation (Blakemore et al., 2018) at neuronal synapses and further studies are still needed to uncover KAR function.

1.9. NMDA and AMPA Receptors

1.9.1. NMDA Receptors

NMDA receptors consist of seven subunits; GluN1, GluN2A – D and GluN3A – B. NDMA receptors form from heterotetrameric assembly of the different subunits (Hansen et al., 2018). GluN1 is an obligatory subunit and is present in all functional NMDA receptors as it contains an essential glycine binding site (Spitzer et al., 2016). NMDA receptors differ to AMPA and kainate receptors because they act as coincidence detectors and need both glutamate and glycine binding to allow the opening of the ion pore (Hansen et al., 2018). NMDA receptors are also under the control of a voltage-dependent Mg^{2+} block, which when the receptor is at rest prevents ion channel opening (Hansen et al., 2018; Spitzer et al., 2016). Studies have also shown that NMDA receptors mediate slow synaptic transmission compared to AMPA and kainate receptors. When activated NMDA receptors have a much slower desensitisation rate, producing longer synaptic currents which aid long term synaptic potentiation and depression (Granger et al., 2011; Iacobucci and Popescu, 2018; Zhu and Gouaux, 2017).

1.9.2. <u>AMPA Receptors</u>

AMPA receptors consist of four subunits; GluA1 – 4 and are able to form both homo- and heterotetrameric receptors, but preferentially form heterotetrameric receptors in the brain (Kamalova and Nakagawa, 2020; Zhao et al., 2017). AMPA receptors regulate fast excitatory transmission in the CNS and unlike NMDA receptors, exhibit extremely fast channel kinetics in the sub-millisecond timescale (Greger et al., 2017). AMPA receptors are the main regulators of synaptic plasticity in the CNS, which is controlled by their trafficking in and out of synapses, subunit composition and phosphorylation state (Greger et al., 2017). Trafficking of AMPA receptors away from the synapse, thus reducing synaptic strength, results in long-term depression which is essential for specific types of learning and memory (Migues et al., 2016; Opendak et al., 2018).

1.10. Glutamate receptors in Pancreatic Islets

Neuronal cells and the cells of the islet of Langerhans have been shown to have many common features and traits including expression of neuropeptides (Rodnoi et al., 2017), RNA splicing regulators (Juan-Mateu et al., 2017) and shared gene expression (Atouf et al., 1997; Perillo et al., 2018). It has also been observed that insulin storage and secretion by β-cells is achieved by the same mechanisms as neuronal cells to secrete neurotransmitters (Arntfield and van der Kooy, 2011; Eberhard, 2013). It is therefore not surprising to note that islet cells have been shown to express neuronal cell surface receptors and are able to release neurotransmitters (Korol et al., 2018; Otter and Lammert, 2016). One such receptor which has been identified in islet cells are GluRs. The expression of the different GluRs in islet cells is summarised in Tables 1.1 – 1.3.

Although the presence of GluRs in pancreatic islets has been established, there are numerous conflicting reports regarding the involvement of these receptors in endocrine regulation and which GluR subtypes are expressed by which islet cells. Additionally, the molecular composition and characteristics of GluRs have not yet been established in pancreatic islet cells. However, it is expected that their composition will be similar to that seen in the CNS (Figure 1.10).

Previous studies on rat pancreatic islets found evidence of AMPA and kainate receptor mRNAs but failed to find the presence of any NMDA receptors (Inagaki et al., 1995). In contrast, other studies have demonstrated the presence of NMDA receptors in pancreatic islets and that pancreas-specific deletion of *GluN1* resulted in an increase in glucose stimulated insulin secretion both *in vitro* and *in vivo* (Marquard et al., 2015). Further studies have also identified a role for NMDA receptors in regulating β-cell excitability and reducing insulin secretion (Patterson et al., 2016; Wu et al., 2017). This provides evidence that NMDA receptors are present in islet cells and do play a role in insulin secretion within these cells. However, it may be that NMDA receptors act to suppress insulin release rather than increase it. In support of this, a clinical trial with T2D patients used the NMDA receptor antagonist dextromethorphan to treat participants and showed that individuals who had received the drug had lower blood glucose and increased insulin secretion compared with patients who received a placebo (Marquard et al., 2015). Dextromethorphan acts as a non-competitive receptor antagonist which binds to an allosteric site on the NMDA receptor to prevent it's activation by the ligand (Pechnick and Poland, 2004).

Similarly, contradictory evidence has been found for the presence of AMPA receptors in pancreatic islets. Some studies have reported that functional AMPA

receptors can only be found exclusively in α-cells and not in β-cells in human, mouse and monkey islets (Cabrera et al., 2008; Cho et al., 2010). It has also been reported that AMPA receptor expression on α-cells is significantly increased in fasting mouse islets and that they contribute to increased glucagon secretion when exposed to long-term high glucose concentrations (Zhang et al., 2016). However, other data has shown functional AMPA receptors in mouse islets that are able to increase intracellular calcium and ultimately increase insulin secretion (Tönnes et al., 1999). In addition, AMPA and kainate receptor agonists, but not NMDA, increased insulin release from rat islets and perfused pancreas (Bertrand et al., 1992; Inagaki et al., 1995). Whilst a more recent study has identified AMPAR receptors in rat β-cells, which in a streptozotocin-induced diabetic model show altered expression compared to healthy controls and prevented the release of insulin from the cells (Jayanarayanan et al., 2015).

In contrast to NMDA and AMPA receptors, very few studies have identified a role for kainate receptors and islet cell function and as shown in Table 1.2 there are mixed reports of successfully identifying kainate receptors in islet cells. Some studies have shown that human α-cells respond to 100 μM kainate, however, the response in rat α-cells was less evident (Köhler et al., 2012). Similar to this, Molnár et al., 1995, found no significant increase in insulin secretion in rat islets treated with 0.5 mM kainate, suggesting that there may be a species difference between human and murine responses to kainate receptor agonists. Further studies on human β-cells are required to fully elucidate kainate receptors role in insulin secretion and regulation.

Table 1.1. AMPA receptor subunit mRNA and protein found in pancreatic islets and cell lines. References from which the data were obtained are listed below. [1] (Bramswig et al., 2013) [2] (Cabrera et al., 2008) [3] (Nica et al., 2013) [4] (Huang et al., 2017) [5] (Wu et al., 2012) [6] (Inagaki et al., 1995) [7] (Kutlu et al., 2009) [8] (Dorrell et al., 2011) [9] (Eizirik et al., 2012) [10] (Benner et al., 2014) [11] (Gonoi et al., 1994) [12] (Weaver et al., 1996) [13] (Molnár et al., 1995) [14] (Zhang et al., 2016) [15] (Jayanarayanan et al., 2015). Empty boxes represent no data.

AMPA			Human Islet/β-cell	Mouse Islet/β-cell	Rat Islet/β-cell	RINm5F (Rat)	MIN6 (Mouse)	INS-1 (Rat)	HIT T15 (Hamster)
GluA1	RNA	Positive	1-3	4, 5	4, 6		4	7	
		Negative	7-9	4, 10		4, 6	11		
	Protein	Positive			12				
		Negative	2			13	13		13
GluA2	RNA	Positive	1-3, 8, 9	4, 5, 10	4, 6, 7	4, 6	4, 11	7	
		Negative	7						
	Protein	Positive	2	5, 14	12, 15				
		Negative							
GluA3	RNA	Positive	1-3, 7-9	4, 5, 10	4, 6, 7		4, 11	7	
		Negative				4, 6			
	Protein	Positive	2	14	12				
		Negative							
GluA4	RNA	Positive	1-3, 8, 9	4, 5	4, 7	4	4	7	
		Negative	7	10	6	6	11		
	Protein	Positive			15				
		Negative	2		12				

Table 1.2. Kainate receptor subunit mRNA and protein found in pancreatic islets and cell lines. References from which the data were obtained are listed below. [1] (Bramswig et al., 2013) [2] (Cabrera et al., 2008) [3] (Nica et al., 2013) [4] (Huang et al., 2017) [5] (Wu et al., 2012) [6] (Inagaki et al., 1995) [7] (Kutlu et al., 2009) [8] (Dorrell et al., 2011) [9] (Eizirik et al., 2012) [10] (Benner et al., 2014) [11] (Gonoi et al., 1994) [12] (Weaver et al., 1996) [13] (Molnár et al., 1995). Empty boxes represent no data.

Kainate			Human Islet/β-cell	Mouse Islet/β-cell	Rat Islet/β-cell	RINm5F (Rat)	MIN6 (Mouse)	INS-1 (Rat)	HIT T15 (Hamster)
GluK1	RNA	Positive	1-3, 9	4	4,7	4,6		7	
		Negative	7,8	10	6		4, 11		
	Protein	Positive							
		Negative							
GluK2	RNA	Positive	1-3, 8, 9	4, 10	4,6,7	4	4	7	
		Negative	7			6	11		
	Protein	Positive							
		Negative			12				
GluK3	RNA	Positive	1-3, 7, 9	4	4, 6, 7	4	4	7	
		Negative	8	10		6			
	Protein	Positive							
		Negative			12				
GluK4	RNA	Positive	1, 3, 9	4, 10	4, 6, 7	4	4	7	
		Negative	7, 8			6	11		
	Protein	Positive							
		Negative							
GluK5	RNA	Positive	1-3, 8, 9	10	6, 7	6	11	7	
		Negative	7						
	Protein	Positive			13	13	13		13
		Negative			12				

Table 1.3. NMDA receptor subunit mRNA and protein found in pancreatic islets and cell lines. References from which the data were obtained are listed below. [1] (Bramswig et al., 2013) [2] (Nica et al., 2013) [3] (Huang et al., 2017) [4] (Inagaki et al., 1995) [5] (Kutlu et al., 2009) [6] (Dorrell et al., 2011) [7] (Eizirik et al., 2012) [8] (Benner et al., 2014) [9] (Gonoi et al., 1994) [10] (Weaver et al., 1996) [11] (Molnár et al., 1995) [12] (Wu et al., 2017) [13] (Atouf et al., 1997) [14] (Patterson et al., 2016). Empty boxes represent no data.

NMDA			Human Islet/β-cell	Mouse Islet/β-cell	Rat Islet/β-cell	RINm5F (Rat)	MIN6 (Mouse)	INS-1 (Rat)	HIT T15 (Hamster)	BRIN-D11 (Rat)
GluN1	RNA	Positive	1, 2, 6, 7, 16	3, 8	3, 4, 5	3, 4	3, 9	5, 13		
		Negative	5							
	Protein	Positive			11	11	11	12	11	14
		Negative				10				
GluN2A	RNA	Positive	1, 2	3	3, 4, 5	3	3	5		
		Negative	5-7	8		4	9			
	Protein	Positive								
		Negative								
GluN2B	RNA	Positive	1, 5, 7	3	3, 5	3	3	5		
		Negative	2, 6	8	4	4	9			
	Protein	Positive								
		Negative								
GluN2C	RNA	Positive	1,2, 6, 7	3, 8	3, 4, 5	3	3, 9	5		
		Negative	5				4			
	Protein	Positive								
		Negative								
GluN2D	RNA	Positive	1, 2, 6, 7	3, 8	3, 4, 5	3, 4	3, 9	5		
		Negative	5							
	Protein	Positive								
		Negative								
GluN3A	RNA	Positive	1, 2, 6, 7	3, 8	3, 5	3	3	5		
		Negative	5							
	Protein	Positive								
		Negative								
GluN3B	RNA	Positive	1, 6, 7	3, 8	3, 5	3	3	5		
		Negative	5							
	Protein	Positive								
		Negative								

1.11. Glutamate receptor autoimmunity and excitotoxicity in disease

Previous studies have already shown autoantibodies to GluRs are associated with numerous autoimmune diseases of the CNS such as; limbic encephalitis (Lai et al., 2009), paraneoplastic cerebella ataxia (Sillevis Smitt et al., 2000), anti-NMDA receptor encephalitis (Gresa-Arribas et al., 2014), Rasmussen encephalitis (Fukuyama et al., 2015) and in up to 30% of epilepsy patients (Levite, 2014). In such diseases the immune system predominantly targets NMDA and AMPA receptors, with some cases showing targeting of mGluR subunits (Dalmau et al., 2017).

1.11.1. <u>NMDA Receptors as autoantigen targets in autoimmune diseases of the</u>
<u>CNS</u>

The main syndrome associated with NMDA receptor autoantibodies is anti-NMDA receptor encephalitis in which the GluN1 subunit is targeted (Dalmau et al., 2017). Detection of these autoantibodies relies on assays which maintain the original receptor confirmation, such as cell-based assays (Dalmau et al., 2017). Anti-NMDA receptor encephalitis patients usually present with memory deficits, psychiatric dysfunctions, epilepsy, autonomic dysfunction and in the early stages prodromal headache (Balu et al., 2019; Ma et al., 2019). Autoantibodies targeted against NMDA receptors in autoimmune encephalitis have been shown to alter the distribution and number of NMDA receptors found on the cell surface of synapses (Ladépêche et al., 2018), which is thought to result in NMDA-related excitotoxity and interference with glutamatergic transmission (Manto et al., 2010). Patient outcome and recovery is often dependant on fast treatment with immunotherapy (Balu et al., 2019) and provided treatment is received 80% of patients recover or substantially improve

(Dalmau et al., 2017). Interestingly, it has been shown that viral infection of Herpes Simplex Virus can lead to anti-NMDA receptor encephalitis if it enters the CNS, thus representing a link between viral infection and autoimmunity (Duarte et al., 2019).

Autoantibodies which target GluN2A and GluN2B subunits have also been associated with systemic lupus erythematosus (SLE), which is potentially fatal and causes brain atrophy and neuropsychiatric manifestations (Arinuma, 2018). Studies have been able to demonstrate that introduction of autoantibodies from SLE patient cerebral spinal fluid (CSF) into mice caused olfactory dysfunction, changes in learning and memory and behaviour (Kapadia et al., 2017; Levite, 2014). Kapadia et al., 2017 was also able to show that administration of SLE patient CSF on neurons resulted in a rapid influx of extracellular Ca^{2+} which is thought to also lead to neuron excitotoxicity and cell death.

1.11.2. AMPA Receptors as autoantigen targets in autoimmune diseases of the CNS

Autoantibodies against AMPA receptors have been associated with CNS diseases such as limbic encephalitis, epilepsy and even dementia (Borroni et al., 2017; Dalmau et al., 2017; Geis et al., 2019; Levite, 2014). It has been reported that up 30% of patients with epilepsy have anti-AMPAR-GluR3 antibodies in their serum (Levite, 2014). One study reported that individuals with epilepsy who were anti-AMPAR-GluR3 positive were much more likely to have learning, attention and psychiatric problems compared to individuals who also suffered from epilepsy but were antibody negative (Goldberg-Stern et al., 2014). It thought that the presence of autoantibodies leads to the disruption of the normal cycling of AMPA receptors to

and from the cell surface, resulting in fewer AMPA receptors on the neuronal surface and increased intrinsic excitability (Fang et al., 2017; Peng et al., 2015).

More recently, anti-AMPA receptor autoantibodies have been linked with frontotemporal dementia (FTD) (Benussi et al., 2019). One study has reported that 23% of FTD patient sera was positive for anti-GluR3 antibodies and of those there was an inverse correlation between anti-GluR3 titre and age of onset; the higher the antibody titre, the younger the age of onset (Borroni et al., 2017).

As of now, there have been no reported cases of autoimmune CNS diseases involving kainate receptor autoantibodies.

1.12. Possible role of GluRs in T1D

Research has shown over-activation of GluRs kills neurons by excitotoxicity (Goldberg-Stern et al., 2014; Levite, 2014). As mentioned previously it has been shown that dextromethorphan, a NMDA receptor antagonist, not only results in higher glucose-stimulated insulin release, but also decreases cell death in T2D islets (Marquard et al., 2015). A study has also concluded that over-activation of NMDA receptors in β-cells when exposed to chronic high glucose reduced cell viability, but *GluN1* knockdown eliminated these effects, reduced inflammatory cytokines and improved β-cell function (Huang et al., 2017). It is hypothesised that GluRs are overstimulated by the presence of autoantibodies, causing excitotoxicity in the pancreatic β-cells, leading to their death.

There is also growing evidence that glutamate receptors could play a role in T1D. Di Cairano et al., 2011 used human islets and β- and α-cell lines to show that chronic

exposure to glutamate resulted in cytotoxicity and cell death in β cells, while α cells remained unaffected. On top of this, a study used Wistar rats to explore the effects of dietary consumption of monosodium glutamate (MSG) on glucose metabolism and pancreatic islet morphology (Boonnate et al., 2015). They showed that rats which consumed MSG had a significanlty lower β-cell mass, but their glucose tolerance and serum insulin stayed the same as that seen in the control group (Boonnate et al., 2015) and could be representative of the early stages of T1D. Whilst a longitudinal study, with children who later progressed to T1D, found that 9-18 months prior to seroconversion serum levels of glutamic acid were 32-fold higher than those seen in healthy controls (Oresic et al., 2008) and further stuides have indicated that plasma glutamate levels are significantly higher in diabetics than in healthy controls (Huang et al., 2017). Preliminary studies have identified autoantibodies to recombinant GluR proteins in sera obtained from T1D patients, suggesting that GluRs are a promising potential target for the immune system in T1D. Taken together, this suggests that glutamate and over activation of it's receptor by autoantibodies could play a novel role in T1D pathogenesis (Figure 1.11).
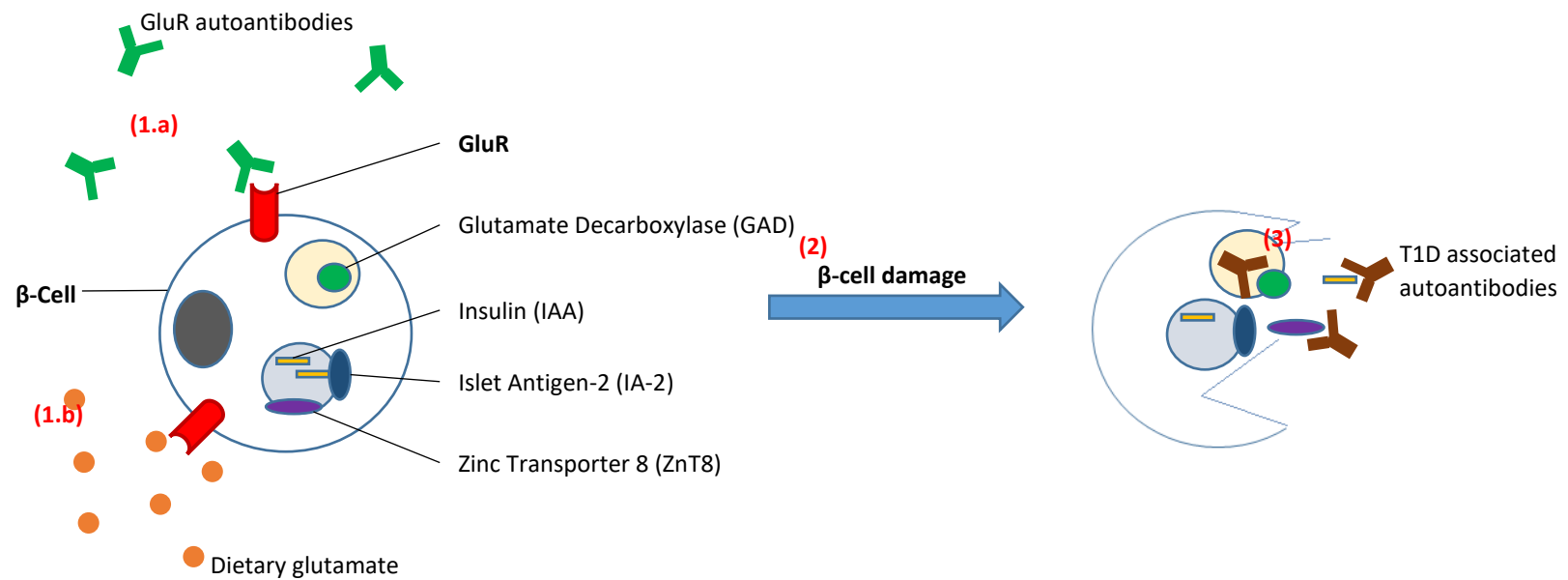
Figure 1.11. Proposed mechanism of β-cell damage through overactivation of GluRs in T1D. GluRs on the β-cell surface are targeted by the immune system via GluR autoantibodies (1.a.) or are overactivated by excess dietary glutamate (1.b.), which leads to excitotoxicity and β-cell damage (2). Following β-cell damage the immune system is exposed to intracellular β-cell proteins and produces autoantibodies which are associated with T1D (GAD, IAA, IA-2 and ZnT8 autoantibodies) as a result of epitope spreading (3).

1.13. Aims and objectives of the project

This project aims to investigate GluRs and their role in hormone secretion in human pancreatic β-cells, as well as their potential involvement in T1D pathogenesis. Specifically, there are three main objectives for this project:

1. To identify GluRs, specifically KAR subunits, expressed in the human β-cell line, EndoC-βH1. This will be investigated by using RT-PCR to identify KAR subunit mRNA and western blotting to elucidate if KAR subunits are expressed as protein by EndoC-βH1 cells.

2. To elucidate what role KARs play in insulin secretion by developing a lentivirus which can knockdown GluK2 subunit protein production in EndoC-βH1 cells and characterising glucose-stimulated insulin secretion in β-cells following GluK2 knockdown or by blocking GluR function by GluR antagonists.

3. To identify if GluR subunits on the β-cell surface are targeted by the immune system in T1D. The project aims to develop an autoantibody assay to detect GluR autoantibodies which can be used to identify the presence or absence of GluR autoantibodies in T1D patient serum samples and healthy control serum.

2. Glutamate receptors in human β-cells and their role in insulin secretion

2.1 Background

Although there have been several studies which aimed to establish the presence of glutamate receptor (GluR) subunit mRNA and protein, there have been numerous conflicting reports of successful and unsuccessful identification of iGluRs in β-cells (outlined in Tables 1.1 – 1.3). In particular, Kainate receptors have been largely understudied in both the CNS and in pancreatic β-cells. However, as described in section 1.7.4 KARs role in the CNS is beginning to be elucidated and they are now thought to play a significant roles in both neurotransmitter excitation and inhibition (Blakemore et al., 2018). It is therefore important to establish if KARs are present in human β-cells and if so, do they also play a significant role in hormone secretion and homeostasis within β-cells.

As discussed in section 1.4 there is not yet a consistent model for the study of human β-cells and their function. However, EndoC-βH1 is a human β-cell line which has been shown to have functional glucose stimulated insulin secretion (GSIS), as well as expressing many β-cell markers (Hastoy et al., 2018; Jahan et al., 2018; Kracht et al., 2018; Lawlor et al., 2019; Tyka et al., 2019). The EndoC-βH1 cell line is emerging as an important tool for investigating β-cell characterisation and function. Thus, this current study aims to use the human β-cell line, EndoC-βH1, to investigate the presence of various iGluRs, in particular KARs, and establish their role in insulin secretion.

2.2 Materials and Methods

2.2.1 <u>Materials</u>

Table 2.1. List of materials. Complete list of materials and suppliers which were used for the current study.

Material	Supplier
(*S*)-3,5-dihydroxyphenylglycine (DHPG, 0805)	Tocris, Bristol, UK.
1,10-Phenanthroline (131377)	Sigma-Aldrich, Poole, UK
2,3-dihydroxy-6-nitro-7-sulfamoyl-benzon[f]quinoxaline-2,3-dione (NBQX, 0373)	Tocris, Bristol, UK.
2S,3S,4S)-Carboxy-4-(1-methylethenyl)-3-pyrrolidineacetic acid (kainate, 0222)	Tocris, Bristol, UK.
3,4-Dichloroisocoumarin (DCI, D7910)	Sigma-Aldrich, Poole, UK
3-isobutyl-1-methylxanthine (IBMX, 2845)	Tocris, Bristol, UK.
Acetic acid (A6283)	Sigma-Aldrich, Poole, UK
Agarose (BIO-41025)	Bioline, London, UK.
Ammonium persulphate (A3678)	Sigma-Aldrich, Poole, UK
Antibiotic-antimycotic (A5955)	Sigma-Aldrich, Poole, UK
Anti-CaV2.1 (PA5-77295)	Thermo Fisher Scientific Inc, Rockford, USA
Anti-GluK2 (ab124702)	Abcam®, Cambridge, UK.
Anti-GluR6/7 antibody (04-921)	Merck Millipore, Watford, UK
Anti-Grik5 antibody (ab67408)	Abcam®, Cambridge, UK.
Anti-Human Alexa Flour 488 (10226402)	Fisher Scientific, Loughborough, UK
Anti-KA2/GRIK5 antibody (06-315)	Merck Millipore, Watford, UK
Anti-Na, K-ATPase (#3010)	Cell Signaling Technology®, Danvers, MA, USA.
Anti-NR2A (AB1555P)	Merck Millipore, Watford, UK
Anti-NR2A antibody (07-632)	Merck Millipore, Watford, UK
Anti-NR2B antibody (06-600) antibody	Merck Millipore, Watford, UK
Anti-PAN-AMPAR antibody	University of Bristol, Bristol, UK
Anti-Rabbit Alexa Flour 568 (10032302)	Fisher Scientific, Loughborough, UK
Anti-β-tubulin antibody (T8328)	Sigma-Aldrich, Poole, UK
Atto Horiz Blot semi-dry blotter (2322413)	Atto, Tokyo, Japan

beta-2-mercaptoethanol (M3148)	Sigma-Aldrich, Poole, UK
BIOTAQ™ DNA polymerase (BIO-21040)	BioRad®, Hertfordshire, UK.
Bovine serum albumin fraction V (10775835001)	Sigma-Aldrich, Poole, UK
Calcium Chloride Dihydrate (CaCl$_2$-2H$_2$O) (C3306)	Sigma-Aldrich, Poole, UK
Chloroform (C7559)	Sigma-Aldrich, Poole, UK
cOmplete™ Mini EDTA-free Protease Inhibitor Cocktail (04693159001)	Sigma-Aldrich, Poole, UK
CutSmart® buffer	New England BioLabs®, Hitchin, UK
DAKO fluorescence mounting medium (S3023)	Agilent Technologies LDA, Stockport, UK
DEPC-treated water (95284)	Sigma-Aldrich, Poole, UK
DH5α competent cells (18265017)	Thermo Fisher Scientific Inc, Rockford, USA
Dimethyl sulphoxide (DMSO)	Sigma-Aldrich, Poole, UK
DMEM High glucose (41965039)	Thermo Fisher Scientific Inc, Rockford, USA
DMEM no glucose (11966-025)	Thermo Fisher Scientific Inc, Rockford, USA
DNA Engine Dyad® thermal cycler system (PTC-0220)	BioRad®, Hertfordshire, UK.
Dulbecco's phosphate buffered saline (D8537)	Sigma-Aldrich, Poole, UK
E64 (E3132)	Sigma-Aldrich, Poole, UK
EndoC-βH1 cell line	EndoCells, Paris, France.
Ethanol (02860)	Sigma-Aldrich, Poole, UK
Ethylene glycol-bis(2-aminoethylether)-N,N,N',N'-tetraacetic acid (EGTA) (E3889)	Sigma-Aldrich, Poole, UK
Ethylenediaminetetraacetic acid (EDTA) (EDS)	Sigma-Aldrich, Poole, UK
extra-thick blot filter paper (1703966)	BioRad®, Hertfordshire, UK.
Fetal bovine serum (F6178)	Sigma-Aldrich, Poole, UK
Fibronectin from bovine plasma (F1141)	Sigma-Aldrich, Poole, UK
FluoroChem® Q System	Alpha Innotech, Devon, UK.
GeneJET Gel Extraction and DNA Cleanup Micro Kit (K0831)	Thermo Fisher Scientific Inc, Rockford, USA
GeneJET Plasmid Miniprep Kit (K0502)	Thermo Fisher Scientific Inc, Rockford, USA
Glycerol (G5516)	Sigma-Aldrich, Poole, UK
Glycine (G8898)	Sigma-Aldrich, Poole, UK

Goat anti-human secondary antibody (A0170)	Sigma-Aldrich, Poole, UK
Goat anti-rabbit secondary antibody (A0545)	Sigma-Aldrich, Poole, UK
Gyki-hydrochloride (Gyki-52466, 1454)	Tocris, Bristol, UK.
HEK293T (Human Embryonic Kidney cell line) cells	American Type Culture Collection, Manassas, VA, USA.
Hepes sodium salt (H3784)	Sigma-Aldrich, Poole, UK
Human Insulin ELISA Kit (10-1113-10)	Mercodia, Uppsala, Sweden.
Human transferrin (T8158)	Sigma-Aldrich, Poole, UK
Immobilon Western Chemiluminescent HRP Substrate (WBKLS0500)	Merck Millipore, Watford, UK
Immobilon®-P PVDF (IPVH00010)	Merck Millipore, Watford, UK
INS-1 cell line	University of Bristol, Bristol, UK
IRDye© 800CW Anti-Mouse IgG (926-32210)	Li-Cor Biosciences, Cambridge, UK
Isopropanol (I9516)	Sigma-Aldrich, Poole, UK
L-glutamine (25030081)	Thermo Fisher Scientific Inc, Rockford, USA
Ligase I	New England BioLabs®, Hitchin, UK
Marvel original dried skimmed milk <1 % fat	Chivers Ireland Ltd, Dublin, IR.
Methanol (322415)	Sigma-Aldrich, Poole, UK
Mini-PROTEAN® short plates (1653308)	BioRad®, Hertfordshire, UK.
Mini-PROTEAN® Spacer Plates with 1.5 mm Integrated Spacers (1653312)	BioRad®, Hertfordshire, UK.
Mini-PROTEAN® Tetra Vertical Electrophoresis Cell (1658006)	BioRad®, Hertfordshire, UK.
Mini-sub® cell GT system (1704406)	BioRad®, Hertfordshire, UK.
MISSION® lentiviral packing mix (SHP001)	Sigma-Aldrich, Poole, UK
MK-801 (0924)	Tocris, Bristol, UK.
Mr Frosty (5100 0001)	Thermo Fisher Scientific Inc, Rockford, USA
NanoDrop™ 1000 spectrophotometer	Thermo Fisher Scientific Inc, Rockford, USA
Nicotinamide (481907)	VWR, Radnor, USA
NMDAR1 (D65B7) antibody (5704)	Cell Signaling Technology®, Danvers, MA, USA.
Odessy® Fc Imaging System	Li-Cor Biosciences, Cambridge, UK
Opti-MEM® (31985070)	Thermo Fisher Scientific Inc, Rockford, USA
Phenylmethlysulfonyl fluoride (PMSF) (PMSF-RO)	Sigma-Aldrich, Poole, UK

Pierce™ BCA Protein Assay Kit (23225)	Thermo Fisher Scientific Inc, Rockford, USA
Polyethylenimine (PEI), poly-l-lysine (P8920)	Sigma-Aldrich, Poole, UK
Potter-Elvehjem Tissue Grinder (14231-384)	VWR, Radnor, USA
precision plus protein™ dual colour (1610374)	BioRad®, Hertfordshire, UK.
Restriction enzymes (*BamHI*, *HindIII*, *PacI, xhoI*)	New England BioLabs®, Hitchin, UK
RQ1 RNase-Free DNase (M6101)	Promega, Southampton, UK
Sodium Bicarbonate (NaHCO$_3$) (S5761)	Sigma-Aldrich, Poole, UK
Sodium deoxycholate (D6750)	Sigma-Aldrich, Poole, UK
Sodium dodecyl sulfate (L3771)	Sigma-Aldrich, Poole, UK
Sodium orthovanadate (S6508)	Sigma-Aldrich, Poole, UK
Sodium selenite (S1382)	Sigma-Aldrich, Poole, UK
Streptavidin agarose beads (S1638)	Sigma-Aldrich, Poole, UK
Sulfo-NHS-Biotin (21217)	Thermo Fisher Scientific Inc, Rockford, USA
tetro cDNA synthesis kit (BIO-65043)	BioRad®, Hertfordshire, UK.
Tri-reagent® (93289)	Sigma-Aldrich, Poole, UK
Triton X-100 (93443)	Sigma-Aldrich, Poole, UK
Trizma® Base (T1503)	Sigma-Aldrich, Poole, UK
Trypsin-EDTA solution (59417C)	Sigma-Aldrich, Poole, UK
TWEEN®20 (P1379)	Sigma-Aldrich, Poole, UK
Wide mini-sub® cell GT system (1704405EDU)	BioRad®, Hertfordshire, UK.

2.2.2 Cell Culture

EndoC-βH1

EndoC-βH1 cells (EndoCells, Paris, France) produced from human foetal pancreatic buds, is a human pancreatic β cell line which has been transduced with a lentiviral vector expressing SV40LT (an oncoprotein derived from polyomavirus SV40), under the control of the insulin promoter (Ravassard et al., 2011). Before the EndoC-βH1 cells were seeded flasks were coated with coating medium (DMEM 25 mM glucose, 2 μg/ml fibronectin (Sigma-Aldrich, Poole, UK) and 1 % ECM gel from Engelbreth-Holm-Swarm murine sarcoma (Sigma-Aldrich, Poole, UK)) and incubated at 37°C between 1 and 24 hours. EndoC-βH1 cells were maintained in coated flasks with culture medium consisting of DMEM 5.6 mM glucose supplemented with 2 w/v % BSA fraction V (Roche Diagnostics, Mannheim, Germany), 10 mM nicotinamide (VWR, Radnor, USA), 50 μM 2-mercaptoethanol (Sigma-Aldrich, Poole, UK), 5.5 μg/ml transferrin (Sigma-Aldrich, Poole, UK) and 6.7 ng/ml sodium selenite (Sigma-Aldrich, Poole, UK). Cells were seeded at an initial density of $7.5 \times 10^4 \, /cm^2$ at 37°C in humidified air and 5 % CO_2.

At 90 % confluency the cells were washed with phosphate buffered saline (PBS) and then detached with 0.2 5% Trypsin-EDTA at 37°C in humidified air and 5 % CO_2. Once the cells were detached an equal volume of neutralising medium (80 % phosphate buffered saline [PBS] and 20 % foetal calf serum FCS) was added to the cell suspension, transferred to a sterile universal tube and centrifuged at 1000 x g for 3 minutes. The supernatant was then discarded, and the cells were sub-cultured into either T75 or T25 flasks. Cells were used between passages 45 and 76.

HEK293T (American Type Culture Collection, Manassas, VA, USA) human embryonic kidney cells, have been transformed with sheared fragments of adenovirus type 5 DNA (Graham et al., 1977). The cells were maintained in growth medium consisting of Dulbecco's modified Eagle's medium (DMEM), supplemented with 10 % foetal bovine serum (FBS), 1 % antibiotic-antimycotic and 1 % L-glutamate. Cells were seeded at an initial density of 2.8 x 10^4/cm^2 at 37°C in humidified air and 5 % CO_2. HEK293T cells were passaged as described under EndoC-βH1 cells, except HEK293T growth medium is used in place of neutralising medium. Cells were used between passages 9 and 30. For the purpose of this study HEK293T cells were used for the production of GluR subunit protein via transient transfection of GluR subunit plasmids (Method section 2.2.7) as they have been shown to have good transfection efficiency and protein yield (Longo et al., 2013). The GluR subunit protein was then used as GluR subunit positive control protein samples (Method section 2.2.9) and for detection of GluR autoantibodies (Method section 3.2.4).

2.2.2 Thawing and establishing stored cells

Cells were removed from liquid nitrogen and placed immediately into a 37°C water bath for 1 to 2 minutes. Thawed cells were then pipetted aseptically into a sterile universal tube containing 9 ml of cell line specific culture medium (see section 2.1.1) and centrifuged for 5 minutes at 700 x g at room temperature. The supernatant was then removed, and cells were re-suspended with 5 ml culture medium for EndoC-βH1 or 10 ml culture medium for HEK293T and put into 75cm^2 flasks.

2.2.3 Storing cell lines in liquid nitrogen

Confluent cells were washed with PBS, trypsinised and re-suspended in neutralising medium for EndoC-βH1 cells or culture medium for HEK293T cells. The cell suspension was then centrifuged for 5 minutes at 700 x g and the supernatant discarded before re-suspending in freezing medium, containing 10 % dimethyl sulphoxide (DMSO) and 90 % fetal calf serum (FCS) for EndoC-βH1 and DMEM (25 mM glucose) 10 % FBS, 10 % DMSO and 2 mM glutamine for HEK293T. The cell suspensions were aliquoted into 1 ml cryovials and placed in a Mr Frosty (Thermo Fisher Scientific Inc, Rockford, USA) in a -80°C freezer overnight. The next day the cryovials were moved into liquid nitrogen for long term storage.

2.2.4 Preparation of total cell lysates

Confluent T25 flask or 60 cm^2 dishes were washed three times with ice cold PBS and then incubated on ice for 10 minutes with 500 µl cold lysis buffer containing 0.5 % sodium deoxycholate, 1 % Triton X-100, 0.1 % SDS, 25 mM Tris (pH 7.5), 150 mM NaCl, 0.1 mM EDTA, 1x complete mini EDTA free protease inhibitor (Sigma-Aldrich, Poole, UK), 200 mM sodium orthovanadate and 100 mM phenylmethysulfonyl fluoride. The cells were then scrapped and transferred to Eppendorf tubes, and incubated at 4°C on a rotator for 30 minutes. Cell lysates were centrifuged at 13,000 x g at 4°C for 15 minutes. The supernatant was removed and then aliquoted and stored at -80° until further use.

2.2.5 Preparation of total cell lysates using Sodium Bicarbonate (NaHCO$_3$) for immunochemical detection of NMDA and AMPA receptors

Confluent T25 flasks were washed three times with PBS before adding 1 ml ice cold 10 mM NaHCO$_3$ with 1 x complete mini EDTA free protease inhibitor (Sigma-Aldrich, Poole, UK). The cells were then scraped from the flask and transferred to an Eppendorf tube on ice. The cells were then passed through a 21G x 1.5" (0.8 x 38 mm) needle approximately 30 times, aliquoted and stored at -80°C until future use.

2.2.6 Determination of protein concentration

The protein concentration of the samples was then quantified according to the manufacturer's instructions using the Pierce™ BCA Protein Assay Kit (Thermo Fisher Scientific Inc, Rockford, USA).

2.2.7 HEK293T cell transfection for immunoblotting

HEK293T cells were seeded as described above onto 60 cm^2 dishes with seeding density of 1.6 x 10^3 /cm^2 and incubated at 37 °C in humidified air and 5 % CO$_2$ for 24 hours.

Cells were then transiently transfected with plasmids encoding KAR subunit DNA (GluK2 or GluK5) as described previously (Gallyas et al., 2003; Pickard et al., 2000). 4 µg DNA and 14 µg polyethylenimine (PEI) transfection agent (Sigma-Aldrich, Poole, UK) was mixed in 500 µl Opti-MEM and incubated at room temperature for 20 minutes. Following the incubation, the DNA-PEI-Opti-MEM solution was added onto the HEK293T cells. The cells were then incubated at 37 °C in humidified air and 5 % CO$_2$ for 48-72 hours before cells were lysed for use in immunoblotting.

2.2.8 Separation of proteins on SDS-PAGE

The protein samples (10 μg – 50 μg) were mixed with sample loading buffer (10 % β-mercaptoethanol, 10 % glycerol, 2 % sodium dodecyl sulfate (SDS) and 62.5 mM Tris(hydroxymethyl)aminomethane (Tris-)-HCl, pH6.8 om deionised water) at a 1:1 ratio. Samples were then centrifuged at 13,000 x g for 30 seconds and boiled for 5 minutes at 95 °C and centrifuged briefly. Samples were kept at room temperature before loading onto a pre-prepared 10 well acrylamide gel consisting of a 10 % running gel (10 % acrylamide/Bis-acrylamide, 0.375 M Tris-HCl pH8.8, 1 % SDS, 1 % ammonium persulphate (APS), 0.04 % TEMED in sterile water) and a 5 % stacking gel (5 % acrylamide/Bis-acrylamide, 0.125M Tris-HCl pH6.8, 1 % SDS, 1 % ammonium persulfate APS and 0.01 % TEMED in sterile water) made using 1.5 mm BioRad® gel plates. A precision plus protein™ dual colour (BioRad®, Hertfordshire, UK) standard weight marker was used. The BioRad® plates containing the gel were then assembled into the BioRad® gel tank according to the manufacturer's instructions (BioRad® Hertfordshire, UK). The tank was then filled with SDS-PAGE running buffer (25 mM Tris, 192 mM glycine and 0.1 % SDS). The gel was then run for 20 minutes at 90 V, then at 130 V for 30 minutes to 1 hour.

2.2.9 Immunochemical detection of proteins

Proteins were transferred on to an Immobilon®-P PVDF membrane, which had been activated with absolute methanol for 10 minutes, using an Atto Horizblot (Atto, Tokyo, Japan) dry blotter with transfer buffer (10 % 10 x SDS-PAGE running buffer 20 % absolute methanol and 70 % ddH$_2$O) for 110 minutes at 9 V.

2.2.10 Blocking and immunochemical probing of the membrane

After the transfer, the membrane was blocked in 5 % dried, fat free milk in TBS (50 mM Tris and 150 mM NaCl with deionised water, pH7.4) supplemented with 0.1 % TWEEN®20 (TBST) for one hour. The membrane was then incubated at 4°C overnight on a shaker with the appropriate primary antibody (Table 2.2) or serum sample from patients with Type 1 diabetes or healthy controls (all serum samples diluted 1:200) diluted in TBST containing 5 % dried, fat free milk.

The membrane was then washed 6 times for 5 minutes with TBST and incubated at room temperature with a goat anti-rabbit secondary antibody (Sigma-Aldrich, Poole, UK) or if using human serum a goat anti-human secondary antibody (Sigma-Aldrich, Poole, UK) for 1 hour. The membrane was washed 6 times for 5 minute each with TBST. The bound antibody membrane was then developed with Immobilon Western Chemiluminescent HRP Substrate as per the manufacturer's instructions (Merck Millipore, Watford, UK) and imaged using Odessy® Fc (Li-Cor Biosciences, Cambridge, UK) Imaging System.

Table 2.2. Table of primary and secondary antibodies used for immunoblot. B = bovine, H = human, R = rat, Rb = rabbit, F = fish, M = mouse, Hm = hamster, Mk = monkey, Z = zebra

Antibody	Species Specificity	Source	Concentration	Supplier
Anti-GluR6/7 (aka GluK2/3) (04-921)	H, R	Rabbit	0.125 µg/ml	Merck Millipore
Anti-GluK2 (ab124702)	M, R, H	Rabbit	0.085 µg/ml	Abcam
Anti-GRIK5 (06-315)	R, Rb	Rabbit	1 µg/ml	Merck Millipore
Anti-GRIK5 (ab67408)	M, R, H	Rabbit	1 µg/ml	Abcam®
Anti-NMDAR1 (#5704) (aka GluN1)	H, M, R	Rabbit	0.295µg/ml	Cell Signalling Technology®
Anti-NMDAR2A (07-632) (aka GluN2A)	M, R	Rabbit	1µg/ml	Merck Millipore
Anti-NMDAR2A (AB1555P) (aka GluN2A)	H, M, R, F	Rabbit	0.2 µg/ml	Merck Millipore
Anti-NMDAR2B (AB1557P) (aka GluN2B)	H, R	Rabbit	0.2 µg/ml	Merck Millipore
Anti-Pan-AMPAR	R, H	Rabbit	0.075 µg/ml	University of Bristol
Anti-CaV2.1 (PA5-77295)	H, M, R	Rabbit	0.8 µg/ml	Thermo Fisher Scientific
Anti-Na, K-ATPase (#3010)	H, M, R, Hm, Mk, Z	Rabbit	0.031 µg/ml	Cell Signalling Technology®
Anti-β-tubulin (T8328)	B, H, M, R	Mouse	0.67 µg/ml	Sigma-Aldrich®
Anti-Human IgG	H	Goat	0.22 µg/ml	Sigma-Aldrich®
Anti-Rabbit IgG (AQ132P)	R	Goat	0.08 µg/ml	Sigma-Aldrich®
IRDye© 800CW Anti-Mouse IgG (926-32210)	M	Goat	0.05 µg/ml	Li-Cor Biosciences UK Limited

2.2.11 RNA extraction from EndoC-βH1 monolayer cells and rat brain tissue

Confluent EndoC-βH1 cells were washed with PBS at 37°C, trypsinised and re-suspended in neutralising medium. The cell suspension was then centrifuged for 5 minutes at 700 x g in a sterile Eppendorf tube and the supernatant discarded. Tri-reagent® (Sigma-Aldrich, Poole, UK) was then added to the cells and homogenised with a Potter-Elvehjem Tissue Grinder (VWR, Radnor, USA). The EndoC-βH1-Tri-reagent® solution was then left at room temperature for 10 minutes before adding 200 µl chloroform and shaken vigorously for 15 seconds. The tubes were then left at room temperature for a further 10 minutes before being centrifuged at 18,000 x g for 15 minutes. Following centrifugation, the clear aqueous layer containing the RNA was transferred to a sterile Eppendorf and 500 µl 100 % isopropanol was added, mixed and left to stand for 10 minutes. The samples were then spun again at 13 500 x g for 10 minutes to reveal the RNA pellet, which was mixed with 300 µl 75 % ethanol and centrifuged at 5 000 x g for 5 min. Finally, the ethanol was removed, and the pellet re-suspended in Diethylpyrocarbonate (DEPC)-treated water. Samples were quantified using a NanoDrop™ 1000 spectrophotometer (Thermo Scientific, Runcorn, UK). Each sample was read as wavelengths 260 nm and 280 nm to calculate the RNA quantity and purity.

The same procedure was then carried out using 200 mg rat brain tissue beginning with homogenisation of the tissue with 3ml Tri-reagent®.

2.2.12 Genomic DNA removal from RNA samples using DNase treatment

RNA samples were treated with RQ1 RNase-Free DNase following the manufacturer's instructions (Promega, Southampton, UK). The samples were then

quantified again using the NanoDrop™ 1000 spectrophotometer (Thermo Scientific, Runcorn, UK). Each sample was read at wavelengths 260 nm and 280 nm to calculate the RNA quantity and purity, only samples with a 260/280 reading between 1.8 and 2 were used. All RNA samples were kept at -80°C.

2.2.13 cDNA synthesis from EndoC-βH1 and rat brain RNA

cDNA was produced from 3000 ng EndoC-βH1 and rat brain RNA using the tetro cDNA synthesis kit, following the manufacturer's instructions (Bioline, London, UK). cDNA was then stored at -20°C.

2.2.14 PCR amplification of iGluR subunit mRNA from EndoC-βH1 and rat brain cDNA

EndoC-βH1 and rat brain cDNA was used for PCR to amplify kainate receptor subunit mRNA. All primers were designed using National Centre for Biotechnology Information (NCBI) Primer Blast (website: http://www.ncbi.nlm.nih.gov/tools/primer-blast/) and were optimised using a temperature gradient PCR (range of temperatures from 50°C to 65°C) with varying $MgCl_2$ concentrations (1 mM to 4 mM). Primers used are shown in Table 2.3. All reactions were carried out with 2.5 µl 10x NH_4 reaction buffer (Bioline, London, UK) 2 mM dNTP, 0.5 µl BIOTAQ™ DNA polymerase (Bioline, London, UK), 0.8 pmol/µl forward and reverse primers, cDNA (2 µl – 10 µl) and $MgCl_2$ (1 mM to 3 mM) and ddH_2O to a final volume of 25 µl. A range of cDNA volumes was used to allow detection of low abundance mRNA. PCR was carried out using a DNA Engine Dyad® thermal cycler system (BioRad®, Hertfordshire, UK).

Table 2.3. Table showing all primer sequences and their targets, along with the product size, temperature and MgCl$_2$ concentration used for RT-PCR.

Subunit Name	Gene and accession number	Specificity	Forward Primer (5'-3')	Reverse Primer (5'-3')	Size (bp)	Annealing Temperature (°C)	MgCl$_2$ (mM)
Gluk1	*Grik1* (NM_010348)	*Mus musculus, Homo sapiens* and *Rattus norvegicus*	TCAGACTCGCTGGAA ACACC (Position: 949-968)	TGCTTCAGTTGTCATC ACGC (Position: 1519-1500)	571	60	2.0
Gluk2	*Grik2* (NM_021956.4)	*Homo sapiens* and *Rattus norvegicus*	CATGCAGCAAGGTTC TGAGC (Position: 2150-2169)	GTTTGCCTTCCTCTTG CAGC (Position: 2664-2645)	515	58.4	1.5
Gluk3	*Grik3* (NM_181373)	*Rattus norvegicus* and *Homo sapiens*	CCGAGGTCCTAATGT CACCG (Position: 1397-1416)	AGGGCTGAATCTGGC AATGA (Position: 1895-1876)	499	56	2.0
Gluk4	*Grik4* (NM_012572)	*Rattus norvegicus* and *Homo sapiens*	CCACCATCCTGGAAA ACCCA (Position: 1338-1357)	CCAGGTTGGCTGTGT ACGAT (Position: 1997-1978)	660	56	2.0
Gluk5	*Grik5* (NM_001301030. 1)	*Rattus norvegicus* and *Homo sapiens*	AGAACCAACTACACC CTGCG (Position: 1153-1172)	GTCTGCCTTCCGGTT GATGA (Position: 1527-1508)	375	57.4	3.0
Neto1	*Neto1* (NM_001201465)	*Rattus norvegicus* and *Homo sapiens*	CACCAGTGGGACTGT CATTG (Positions 1304-1323)	TCTGCCACATCTGCA AAGTC (Position:1525-1505)	216	50.2	2.0
Neto2	*Neto2* (NM_001201477)	*Rattus norvegicus* and *Homo sapiens*	TTTGCTTCGCCAAATT ATCC (Position:582-601)	TTAATGGAGGGCTTTT CACG (Position: 801-782)	220	50.2	2.0
Beta-actin	*ACTB* (NM_001101.3)	*Rattus norvegicus* and *Homo sapiens*	CATGGATGATGATATC GC (Position: 83-101)	CCACACGCAGCTCAT TGT (Position: 373-355)	290	60	2.0
Beta-actin	*ACTB* (NM_007393.5)	*Mus musculus, Homo sapiens* and *Rattus norvegicus*	GCCTTCCTTCTTGGG TATGGAA (Position: 897-919)	CAGCTCAGTAACAGT CCGCC (Position: 1256-1236)	359	60	2.0

2.2.15 <u>Agarose Gel Electrophoresis of amplified iGluR subunit mRNA</u>

PCR samples were mixed and loaded with DNA loading buffer (Bioline, London, UK) onto a premade 2 % agarose gel submerged in TAE (40 mM Tris, 20 mM acetic acid and 1 mM ethylenediaminetetraacetic acid [EDTA]). The samples were then run in either a mini-sub® cell GT or wide mini-sub® cell GT system (BioRad®, Hertfordshire, UK) at 100V for 30 minutes to an hour. The gel was then imaged using a FluoroChem® Q (Alpha Innotech, Devon, UK) imaging system.

2.2.16 <u>Small hairpin RNA (shRNA) lenti-viral knock-down of GluK2</u>

shRNAs primers were designed using the GRIK2 mRNA sequence (NM_021956.2). shRNAs primers consisted of a 21-nucleotide sense and antisense sequence separated with a 9 nucleotide loop structure (TTCAAGAGA), a 5' AAAAA overhang and *Bg1II* or *Xho1* restriction sites (Figure 2.1). Primers corresponding to the shRNA sequence were then synthesised (Table 2.4).

Figure 2.1. GluK2 targeting shRNA annealed primers. Primers constructed with short interfering RNA (siRNA) sense and antisense

sequencing matching to *GRIK2* and a containing a hairpin loop sequence, as well as the restriction sites *Bg1II* and *XhoI*.

Table 2.4. Table showing all shRNA primer sequences and their target species.

Gene and accession number	Target species	Sequence number	Forward Primer 5' – 3'	Reverse Primer 5' – 3'
GRIK2 (NM_021956.2)	*Homo sapiens*	1	GATCCCCCCCAATACT ACCCTTACCTATTTCA AGAGAATAGGTAAGGG TAGTATTGGGTTTTTC	TCGAGAAAAACCCAAT ACTACCCTTACCTATT CTCTTGAAATAGGTAA GGGTAGTATTGGGGGG
		2	GATCCCCCCTCTGATT ATGCTTTCCTAATTCA AGAGATTAGGAAAGCA TAATCAGAGGTTTTTC	TCGAGAAAAACCTCTG ATTATGCTTTCCTAA TCTCTTGAATTAGGAA AGCATAATCAGAGGGGG
		3	GATCCCCCCAATCGTT CTTTGATTGTTACTCG AGTAACAATCAAAGAA CGATTGGTTTTTC	TCGAGAAAAACCAATC GTTCTTTGATTGTTAC TCGAGTAACAATCAAA GAACGATTGGGGG

2.2.17 <u>Cloning shRNA oligonucleotides into pSUPER-neo-GFP</u>

shRNA primers were mixed to a concentration of 100 µM in TE buffer. 2 µl of the forward primer and 2 µl of the reverse primer were mixed and heated at 95 °C for 4 minutes, before leaving at room temperature for 2 hours to cool and anneal the primers. After 1 h 250 µl H_2O was added and vortexed briefly. 1 µl primer mix was then ligated with 1 µl cut pSUPER-neo-GFP vector and 2 µl ligase (New England BioLabs®, Hitchin, UK) for 10 minutes at room temperature. The ligated primers and pSUPER-neo-GFP were then added to DH5α competent cells on ice for 30 minutes and transformed by heat shock at 42 °C for 45 seconds. The cells were then left on ice for a further 2 minutes and plated onto 100 µg/ml ampicillin agar plates and incubated at 37 °C overnight. The following day colonies were picked and grown in 3 ml LB Broth with 100 µg/ml ampicillin overnight at 37°C. Plasmid DNA was then extracted using the Thermo Scientific GeneJET Plasmid Miniprep Kit (Thermo Scientific, Runcorn, UK). All plasmids were screened by performing a restriction digest with *Hind*III and *BamH*I. 1 µl *HindIII*, 1 µl *BamHI*, 3 µl 10 x CutSmart® buffer (New England BioLabs®, Hitchin, UK), 20 µl H_2O and 5 µl plasmid were mixed and incubated at 37°C for 2 hours, before loading and separating on a 0.8% agarose gel for 1 hour at 100 V. Plasmids which were successfully ligated with annealed shRNA primers resulted in the removal of the *HindIII* restriction site and were therefore only cut by *BamHI* and appeared as one band. Unsuccessful ligations have the *HindIII* restriction site intact so were cut by both *BamHI* and *HindIII* and appeared as two bands. Positive plasmids were sent for sequencing to confirm the successful integration of the *GRIK2* shRNA sequence into pSUPER-neo-GFP (Source Bioscience, Nottingham, UK; Appendix I).

2.2.18 Cloning shRNA and the H1 promoter from pSUPER-neo-GFP into pXLG3-PX-GFP-IRES-WPRE vector

Using the pSUPER-neo-GFP vector containing the shRNA sequence as a template, a PCR was performed using a forward primer which contains the *PacI* restriction site and corresponds to the beginning H1 promoter in pSUPER-neo-GFP (5'-CACTTAATTAAGAACGCTGACGTCATCAACCC-3') and a reverse primer which corresponds to M13 Rev (5'-GTCATAGCTGTTTCCTG-3') (Figure 2.2a). The PCR was carried out using an annealing temperature of 55 $^{\circ}$C, 10 % 10x NH$_4$ reaction buffer (Bioline, London, UK) 2 mM dNTP, 2 % BIOTAQ™ DNA polymerase (Bioline, London, UK), 0.8 pmol/μl forward and reverse primers, 8 % cDNA and 2 mM MgCl$_2$. PCR was carried out using a DNA Engine Dyad® thermal cycler system (BioRad®, Hertfordshire, UK).

A PCR clean-up was then done using GeneJET Gel Extraction and DNA Cleanup Micro Kit (Thermo Scientific, Runcorn, UK), followed by a restriction digest with 50 μl PCR product, 2 μl *pacI* , 2 μl *xhoI* and 10 μl 10 x CutSmart® buffer (New England BioLabs®, Hitchin, UK) and 36 μl H$_2$O at 37 $^{\circ}$C for 2 hours. A second PCR cleanup was carried out using the entire restriction digested PCR product with GeneJET Gel Extraction and DNA Cleanup Micro Kit (Thermo Scientific, Runcorn, UK). The eluted insert (Figure 2.2b) was then diluted 1:5 with ddH$_2$O and ligated in a 1:1:2 ratio with cut pXLG3-PX-GFP-IRES-WPRE vector and ligase I (Bioline, London, UK) for 10 minutes at room temperature. The ligated vector was then added to XL1-blue competent cells on ice for 30 minutes and transformed by heat shock at 42 $^{\circ}$C for 45 seconds. The cells were then left on ice for a further 2 minutes and plated onto 100 μg/ml ampicillin agar plates and incubated at 37 $^{\circ}$C overnight. The following day colonies were picked and grown

in 3 ml LB Broth with 100 μg/ml ampicillin overnight at 37 °C. Plasmid DNA was then extracted using the Thermo Scientific GeneJET Plasmid Miniprep Kit (Thermo Scientific, Runcorn, UK). All plasmids were sequenced to confirm the presence of shRNA in the vector (Source Bioscience, Nottingham, UK; Appendix I).

A.

$PacI$
Restriction
site   H1 Promoter

FP: 5'-CACTTAATTAAGAACGCTGACGTCATCAACCC-3'
RP: 5'-GTCATAGCTGTTTCCTG-3'

M13 Reverse

B.

Figure 2.2. PCR primers to isolate GRIK2 shRNA sequence and H1 promoter from pSUPER-neo-GFP plasmid. A) pSUPER-neo-GFP plasmids containing GRIK2 shRNA sequence was used as template DNA to amplify the GRIK2 shRNA sequence as well as the H1 promoter required for shRNA expression. Forward and reverse primers (FP and RP) were used which amplify from the multiple cloning site M13 Reverse and from the beginning of the H1 promoter in pSUPER-neo-GFP. B.) Linear structure of the PCR product generated, H1 promoter controls GRIK2 shRNA expression and $PacI$ and $XhoI$ restriction sites are required to insert the sequence into the pXLG3-PX-GFP-IRES-WPRE plasmid used for virus production.

2.2.19 Production of *GRIK2* shRNA Lentivirus

HEK293T cells were split and seeded with 1 x 10^6 cells in T25 flasks as described in section 1.2.1. The following day cells were washed twice with 3 ml PBS at 37 ºC. 2 µg pXLG3-PX-GFP-IRES-WPRE vector containing shRNA, 2 µg MISSION® lentiviral packing mix (Sigma-Aldrich, Poole, UK) and 12 µg PEI transfection reagent were mixed in 2 ml DMEM (25 mM glucose), supplemented with 10 % foetal bovine serum (FBS), 1 % antibiotic-antimycotic and 1 % L-glutamate and incubated at room temperature for 30 minutes. Cells were washed with 3 ml of warm DMEM and then incubated with the transfection reagent and plasmid mix for 4h. The media was then removed and replaced with 4 ml fresh media. 48 hours post-transfection, the virus-containing media was removed from the flask, sterilised by passing it through a 0.45 µm filter, aliquoted into cryovials and stored at -80 ºC for future use.

2.2.20 Viral infection of EndoC-βH1 or INS-1 cells to knock-down GluK2

EndoC-βH1 cells were grown in 6 well plates for 24 hours and treated with 100 µl *GRIK2* shRNA lentivirus or 100 µl non-specific shRNA control lentivirus, which was used as a viral control. Cells with virus were incubated at 37 ºC in humidified air and 5 % CO_2 for 72 hours. Successful viral infection was confirmed by the observation of GFP fluorescence from the cells. Cells were then washed 3 times with PBS and twice with EndoC-βH1 complete media, both at 37 ºC, and incubated for a further 24 hours. The total cell lysate was then collected every 24 hours over 4 days. Total cell lysates were then separated by SDS-PAGE and immunoblotted with a GluK2/3 antibody (method section 2.2.8 – 2.2.10) to determine if the virus had successfully knocked down *GRIK2*.

Plasmids encoding rat targeting *GRIK2* shRNA for virus production were gifted by University of Bristol and were used with rat INS-1 cells in the same method as used with EndoC-βH1 cells, described above.

2.2.21 <u>Glucose-stimulated insulin secretion (GSIS) assay</u>

EndoC-βH1 cells were seeded as described in section 2.1.1 onto 96 well plates at a seeding density of 70 x 10^3 cells per well. The cells were incubated at 37°C in humidified air and 5 % CO_2 for 48 hours. After two days the medium was changed to glucose starving medium (glucose free DMEM, 2.8 mM glucose, 2 % albumin from bovine serum fraction V, 50 µM 2-mercaptoethanol, 10 mM nicotinamide, 5.5 µg/ml transferrin, 6.7 ng/ml sodium selenite) and incubated overnight for 12 - 18 hours. The glucose starving medium was removed and Krebs-Ringer solution (115 mM NaCl, 24 mM $NaHCO_3$, 5 mM KCl, 1 mM $MgCl_2$, 1 mM $CaCl_2$-$2H_2O$, 0.2 % BSA, 10 mM Hepes, made up to volume with sterile H_2O) supplemented with 2.8 mM glucose was added and cells were incubated for an hour and then replaced with Krebs-Ringer buffer supplemented with 0.5 mM glucose or 20 mM glucose containing the appropriate treatments for 1 hour (Figure 2.3). All experiments were conducted in triplicate. For the treatments the following drugs were used: 2S,3S,4S)-Carboxy-4-(1-methylethenyl)-3-pyrrolidineacetic acid (kainate); 2,3-dihydroxy-6-nitro-7-sulfamoyl-benzon[f]quinoxaline-2,3-dione (NBQX) (kainate and AMPA receptor antagonist (Yu and Miller, 1995)); Gyki-hydrochloride (Gyki-52466) (AMPA receptor antagonist (Rzeski et al., 2001)); (*S*)-3,5-dihydroxyphenylglycine (DHPG) (Group 1 mGluR agonist (Wiśniewski and Car, 2002)) and 3-isobutyl-1-methylxanthine (IBMX) (phosphodiesterase inhibitor which raises intracellular cAMP (Parsons et al., 1988)).

The supernatant was then removed and centrifuged at 700 x g for 5 minutes at 4°C, the resulting supernatant was recovered and stored at -20°C for up to four weeks before measuring the amount of secreted insulin.

50 µl cell lysis solution (1 ml 1 M Tris (pH 8.0), 500 µl Triton X-100, 5 ml Glycerol, 1.37 ml 5 M NaCl, 500 µl 0.2 M EGTA, 41.63 ml H_2O with 1x protease inhibitor cocktail tablet (Roche complete mini EDTA-free per 10ml) was added to each well and centrifuged at 700 x g for 5 minutes at 4°C. Samples were then also stored at -20 °C for up to four weeks before measuring retained insulin.
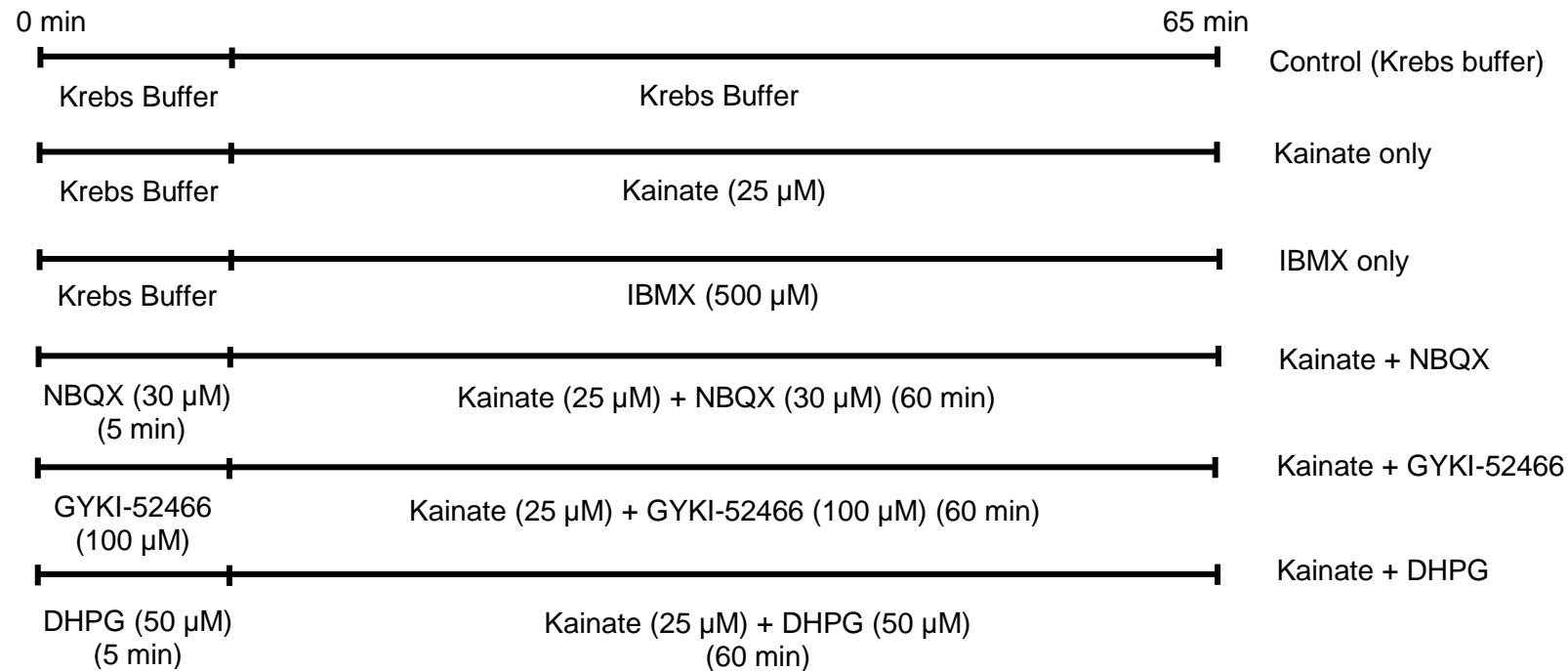
Figure 2.3. Summary of the treatments and drug combinations used for the GSIS assay. EndoC-βH1 cells were grown in glucose-starving medium containing 2.8 mM glucose for 12 – 18 hours. Cells were incubated in KREB-Ringer solution supplemented with 0.5 mM glucose for 1 hour and then pre-incubated with 20 mM glucose or 0.5 mM glucose (these were the controls). The treated cells were incubated with 20 mM glucose or 0.5 mM glucose and NBQX; GYKI or DHPG for five minutes. Cells were then incubated with 20 mM glucose, 0.5 mM glucose, 20 mM glucose or 0.5 mM glucose and glutamate receptor agonists and antagonists for a further 1 hour.

2.2.22 Quantification of secreted and retained insulin

Insulin was determined by using a human insulin Enzyme-Linked Immunosorbent Assay (ELISA) Kit (Mercodia, Uppsala, Sweden). ELISA was carried out following the manufacturers' instructions (Mercodia, Uppsala, Sweden). Samples containing secreted insulin and retained insulin were diluted in 1:10 and 1:1000 with H_2O, respectively, with the exception of IBMX and KCl treated cells which were diluted 1:40 for secreted insulin. Insulin values for both secreted and retained insulin were then calculated using a standard curve derived from known standards (Mercodia, Uppsala, Sweden).

2.2.23 Statistical analysis

Statistical analysis of GSIS data was carried out using one-way *ANOVA* with Bonferroni correction using IBM® SPSS® Statistics 23 software (IBM®, Portsmouth, UK). Differences between means were considered statistically significant if the *p* value was less than 0.05. Results were analysed from 5 – 10 independent experiments conducted in triplicate.

2.2.24 Cell-surface Biotinylation of EndoC-βH1 protein

EndoC-βH1 cells were grown in T25 flasks to confluency. The cells were washed two times with PBS at room temperature, followed by two washes with 10 mM Na-Borate (pH 8.2), 0.15 M NaCl. Excess liquid was removed from the flask and 2 ml 10 mM Na-Borate (pH 8.2), 0.15 M NaCl was added, along with 50 µg/ml sulfo-NHS-Biotin (Thermo Fisher Scientific Inc, Rockford, USA). The cells were then left at room temperature for 5 minutes and then all liquid was removed and a further 2 ml 10 mM Na-Borate (pH8.2), 0.15 M NaCl was added with 50 µg/ml sulfo-NHS-Biotin (Thermo Fisher Scientific Inc, Rockford, USA). The cells were

left for a further 10 minutes at room temperature, after which, 30 µl 1 M NH_4Cl was added to the flask for 5 minutes. The cells were then washed three times with TBS and lysed with 1 ml TBS containing 1 % Triton X-100, 93 µM 3,4-Dichloroisocoumarin (DCI), 50 µM E64 and 122 µM 1,10-Phenanthroline and moved to an Eppendorf tube and kept on ice for 15 minutes. The sample was centrifuged for 10 minutes at 700 x g at 4 °C, supernatant removed and transferred to a fresh Eppendorf tube. 100 µl of sample was put into a separate Eppendorf tube and 500 µl cold acetone was added and left at -20 °C until flocculated. The sample was then centrifuged at 700 x g at 4 °C for 15 minutes, the acetone was removed and the pellet resuspended in 50 µl sample loading buffer (10 % β-mercaptoethanol, 10 % glycerol, 2 % sodium dodecyl sulfate (SDS) and 62.5 mM Tris(hydroxymethyl)aminomethane (Tris-)-HCl, pH6.8 om deionised water), heated for 5 minutes at 95 °C, then frozen at -80 °C until electrophoresis. This sample is the total cell content. The remaining supernatant was then mixed with 50 µl of a 1:1 suspension of streptavidin agarose in TBS, 1 % Triton X-100 for 1 hour at 4 °C with mixing by rotation. The beads were then washed three times with TBS, 1 % Triton X-100 and once with 50 mM Tris-HCl (pH7.5). The membrane proteins were eluted by heating at 95 °C with 50 µl sample loading buffer for 2 minutes. The stripped beads were pelleted by centrifugation at 700 x g for 2 minutes. The supernatant was then snap frozen in liquid nitrogen and stored at -80 °C until electrophoresis.

2.3 Results

2.3.1 Kainate receptor subunit mRNA is expressed in EndoC-βH1

To assess if EndoC-βH1 cells express glutamate receptors (GluRs), specifically kainate receptors (KARs), and could be used as a model to investigate the role of GluRs in insulin secretion, RT-PCR was carried out using EndoC-βH1 cDNA (as described in section 2.2.14 of Methods). Primers for kainate receptor subunits (GluK1-5) and the auxiliary subunits (Neto1 and Neto2) were designed using the National Centre for Biotechnology Information (NCBI) Primer Blast software and are shown in Table 2.3 (Methods section 2.2.14) with expected PCR product size, annealing temperatures and $MgCl_2$ concentrations used.

GluK2 and GluK5 mRNA was amplified and produced visible bands of 516 bp and 375 bp, respectively (Fig. 2.4). The KAR auxiliary subunits Neto1 and Neto2 are also expressed in both EndoC-βH1 cells and rat brain, PCR amplification producing products with the expected size (Fig. 2.5). Sequencing of the GluK2, GluK5, Neto1 and Neto2 PCR products confirmed their identity (Source Bioscience, PLC, Nottingham, UK).

In contrast, KAR subunit mRNA for GluK1, GluK3 and GluK4 was not detected by RT-PCR from EndoC-βH1 cell but all five KAR subunits were detected in rat brain. The house keeping gene β-actin was amplified in all samples tested which ensured the integrity of the cDNA used and that the steps of the PCR reaction worked. Control samples containing cDNA in the absence of reverse transcriptase were used to detect the presence of genomic DNA contamination. A sample without cDNA template was used as a negative control to check for any PCR contamination. Neither negative controls resulted in any PCR products.
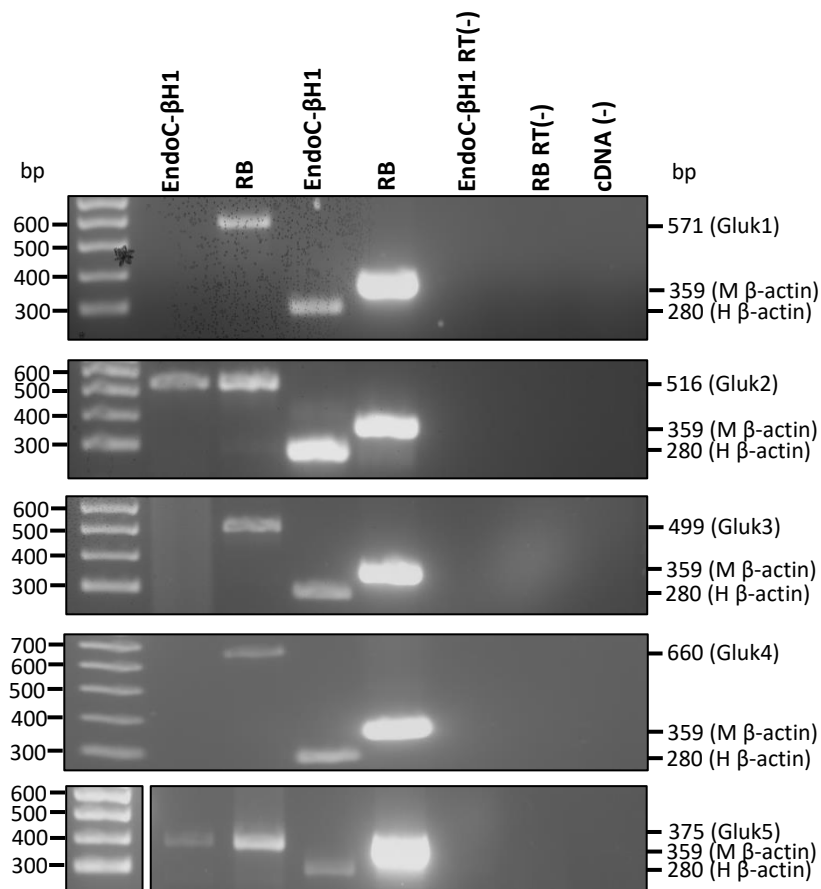
Figure 2.4. RT-PCR analysis of kainate receptor subunit (GluK1-5) mRNA expression in EndoC-βH1 cells and rat brain (RB). Kainate receptor (KAR) subunit specific primers were used (Table 2.3) to amplify each subunit. cDNA was synthesised using 3 µg total RNA (Method section 2.2.13). β-actin was amplified as a positive control and produced 280 bp and 359 bp bands in human and rodent samples, respectively. Samples excluding reverse trancriptase in the RT reaction (EndoC-βH1 RT(-) and RB RT(-)) were used to detect the presence of genomic DNA contamination. A sample without cDNA template was used as a control for PCR (cDNA (-)) contamination. The size of the DNA marker (BioRad®, Hertfordshire, UK) is indicated on the left in base pairs (bp) and the expected PCR product size for each reaction is indicated on the right. Figure is representative of three independent experiments.
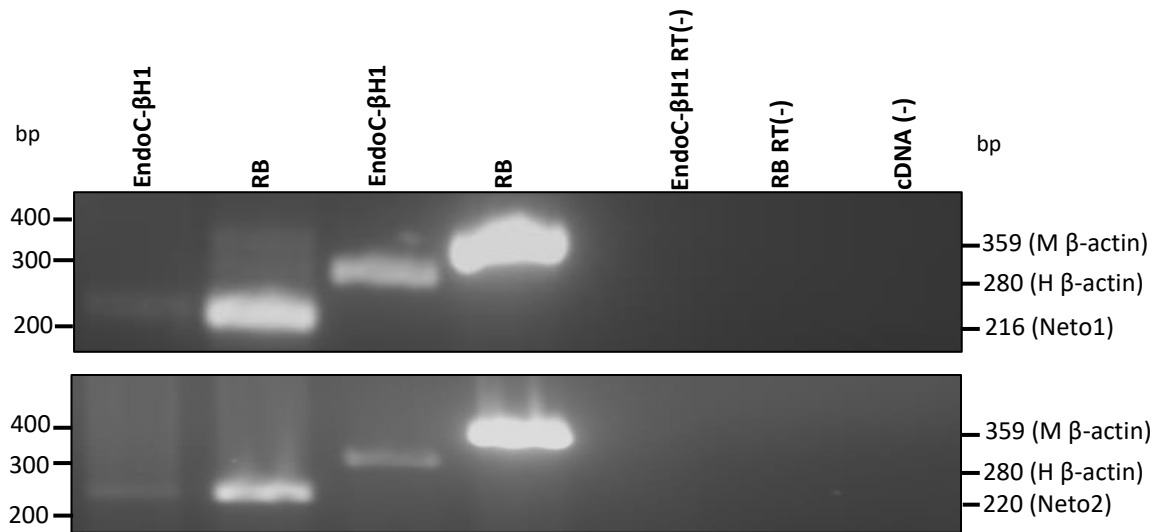
Figure 2.5. RT-PCR analysis of kainate receptor auxiliary subunits Neto1 and Neto2 mRNA expression in EndoC-βH1 cells and rat brain (RB). Neto1 and Neto2 subunit specific primers were used (Table 2.3) to amplify each subunit. cDNA was synthetised using 3 µg total RNA (Method section 2.2.13). β-actin was amplified as a positive control and produced 280 bp and 359 bp bands in human and rodent samples, respectively. Samples excluding reverse trancriptase in the RT reaction (EndoC-βH1 RT(-) and RB RT(-)) were used to detect the presence of genomic DNA contamination. A sample without cDNA template was used as a control for PCR (cDNA (-)) contamination. The size of the DNA marker (BioRad®, Hertfordshire, UK) is indicated on the left in base pairs (bp) and the expected PCR product size for each reaction is indicated on the right. Figure is representative of three independent experiments.

2.3.2 EndoC-βH1 cells produce kainate receptor subunit proteins

Immunoblots were carried out using EndoC-βH1 protein lysate to access if any of the mRNA detected in the cells is translated into protein and therefore, potentially form a functional KAR. GluK2/3 and GluK5 specific commercial antibodies were used as described in section 2.2.10 of the Methods. HEK293T cells which had been transfected with GluK2 or GluK5 plasmids (section 2.2.7 of Methods) and rat brain protein homogenate were used as positive controls. Protein homogenate from untransfected HEK293T cells was used as a negative control.

EndoC-βH1 cells produce GluK2/3 protein, as a clear band was detected at the expected molecular weight (115 kDa, Fig. 2.6). All positive controls also showed a band at 115 kDa, which was absent in the negative control. For GluK5, two different antibodies were used to try and detect this subunit in EndoC-βH1 cells. No GluK5 protein was detectable in EndoC-βH1 cells (Fig. 2.7), but this antibody was not specific for the human GluK5 (Appendix II), which may explain the absence of a specific band. A second anti-GluK5 antibody, which was specific for human GluK5 was then used (Figure 2.8) and a strong band at the correct size was clearly seen. However, the negative control also showed a much weaker band with a similar molecular weight. Furthermore, many non-specific protein bands were also detected. Based on the results, it is not clear whether GluK5 protein is produced in this cell line.
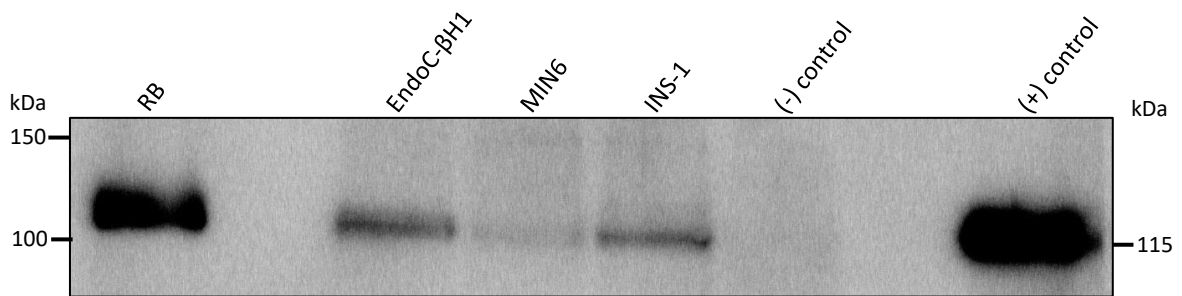
Figure 2.6. Immunoblot analysis of GluK2 proteins in EndoC-βH1, MIN6 and INS-1 pancreatic β-cells. Homogenates from human EndoC-βH1, mouse MIN6 and rat INS-1 cells were prepared. Proteins (50 µg per lane) were separated by SDS-PAGE and transferred to immobilon membranes (Method section 2.2.10). Homogenates from rat brain (RB; 25 µg) and HEK293T cells overexpressing GluK2 (25 µg; (+) control) were used as positive controls. HEK293T cell homogenate (50 µg; (-) control) was used as a negative control. Immunoblots were probed with a rabbit polyclonal anti-GluK2/3 antibody (0.125 µg/ml; Millipore UK Limited) overnight at 4°C. Immunoblots were then probed with a secondary anti-rabbit IgG antibody (0.08 µg/ml; Sigma-Aldrich®) for 1 hour. Immunoblots were imaged by chemiluminescence using the Odessy® Fc (Li-Cor Biosciences) Imaging System. The molecular weight markers (Bio-Rad®) are shown on the left in kilodaltons (kDa). The expected size of GluK2 is indicated on the right. Figure is representative of three independent experiments.
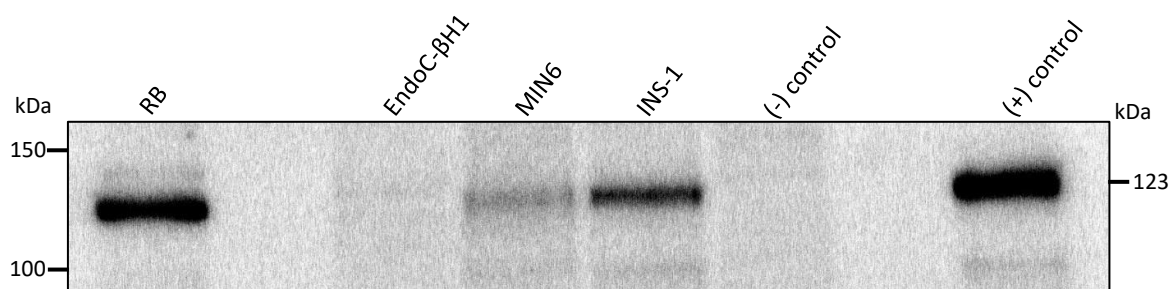
Figure 2.7. Immunoblot analysis of GluK5 proteins in EndoC-βH1, MIN6 and INS-1 pancreatic β-cells. Homogenates from human EndoC-βH1, mouse MIN6 and rat INS-1 cells were prepared. Proteins (50 µg per lane) were separated by SDS-PAGE and transferred to immobilon membranes (Method section 2.2.10). Homogenates from rat brain (RB; 25 µg) and HEK293T cells overexpressing GluK5 (25 µg; (+) control) were used as positive controls. HEK293T cell homogenate (50 µg; (-) control) was used as a negative control. Immunoblots were probed with a rabbit polyclonal anti-GRIK5 antibody (1 µg/ml; Millipore UK Limited) overnight at 4°C. Immunoblots were then probed with a secondary anti-rabbit IgG antibody (0.08 µg/ml; Sigma-Aldrich®) for 1 hour. Immunoblots were imaged by chemiluminescence using the Odessy® Fc (Li-Cor Biosciences) Imaging System. The molecular weight markers (Bio-Rad®) are shown on the left in kilodaltons (kDa). The expected size of GluK5 is indicated on the right. Figure is representative of four independent experiments.
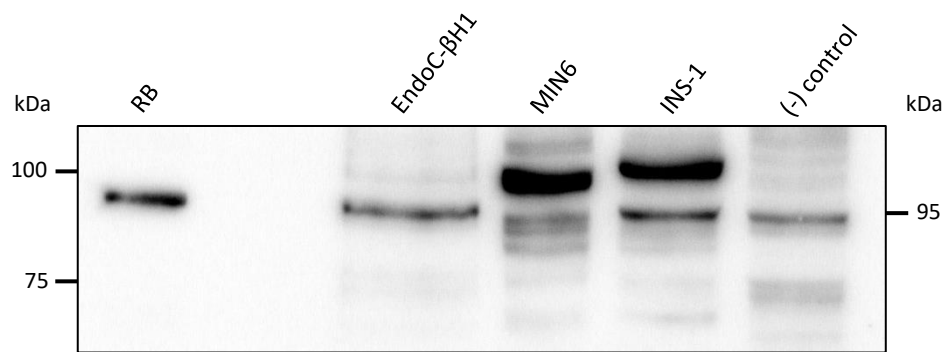
Figure 2.8. Immunoblot analysis of GluK5 proteins in EndoC-βH1, MIN6 and INS-1 pancreatic β-cells. Homogenates from the human EndoC-βH1, mouse MIN6 and rat INS-1 cells were prepared. Proteins (50 µg per lane) were separated by SDS-PAGE and transferred to immobilon membranes (Method section 2.2.10). Rat brain homogenate (RB; 25 µg) was used as a positive control. HEK293T cell homogenate (50 µg; (-) control) was used as a negative control. Immunoblots were probed with a rabbit polyclonal anti-GRIK5 antibody (1 µg/ml; Abcam®) overnight at 4°C. Immunoblots were then probed with a secondary anti-rabbit IgG antibody (0.08 µg/ml; Sigma-Aldrich®) for 1 hour. Immunoblots were imaged by chemiluminescence using the Odessy® Fc (Li-Cor Biosciences) Imaging System. The molecular weight markers (Bio-Rad®) are shown on the left in kilodaltons (kDa). The expected size of GRIK5 is indicated on the right. Figure is representative of six independent experiments.

2.3.3 Detection of NMDA and AMPA receptor subunit proteins in EndoC-βH1 and INS-1 cells

To investigate if EndoC-βH1 and INS-1 cells express any other ionotropic glutamate receptor subunits, protein homogenate from a crude protein extraction, using sodium bicarbonate, was obtained (Methods section 2.2.5). This method of obtaining protein from EndoC-βH1 and INS-1 cells ensured no protein was lost through centrifugation. Specific antibodies for GluN1, GluN2A, GluN2B and AMPAR subunits were used as described in section 2.2.10 of the Methods. Rat brain homogenate was used as a positive control for all immunoblots.

EndoC-βH1 cells only produced protein for the NMDA receptor subunit GluN2B (Fig. 2.9, D) and not for either of the other two NMDA receptor subunits (Fig 2.9, B and C). INS-1 cells did not show any expression for any of the NMDA receptor subunits tested. AMPA receptors were not detected in either EndoC-βH1 or INS-1 cells (Figure 1.6 A.). The rat brain positive control was detected in all blots whilst the HEK293T negative control showed no specific bands.
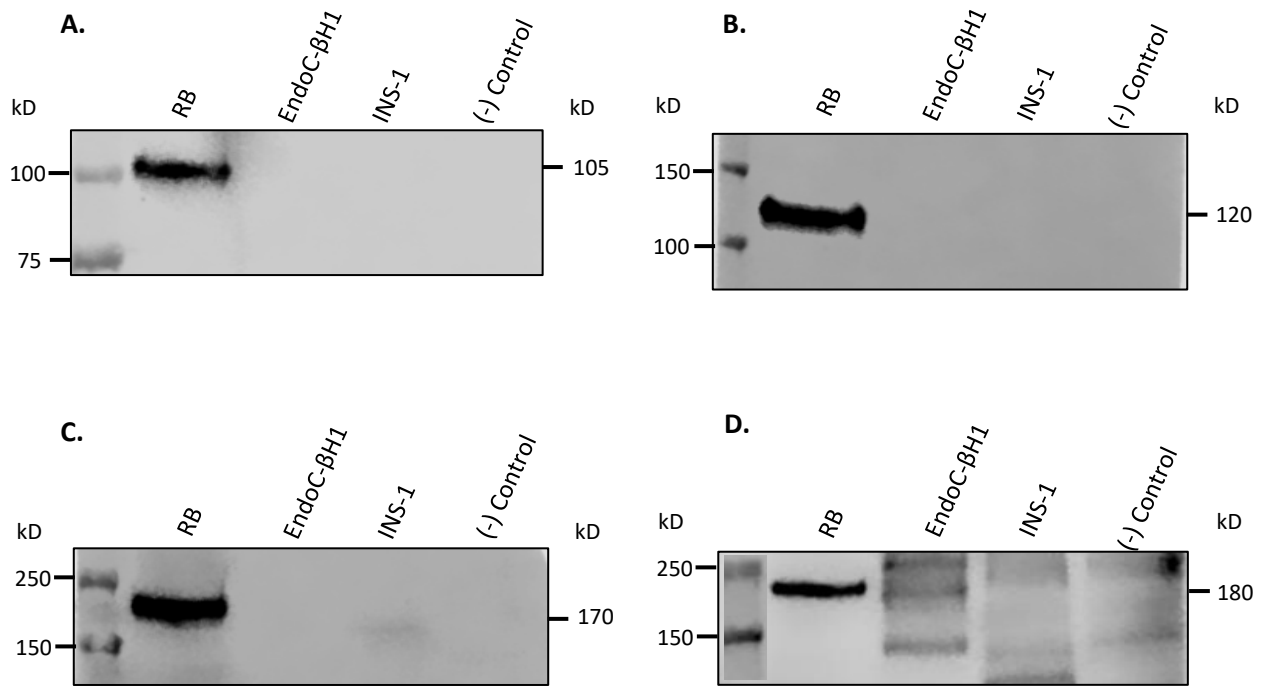
Figure 2.9. Immunoblot analysis of AMPA and NMDA receptor subunit proteins in EndoC-βH1 and INS-1 pancreatic β-cells. Crude protein homogenates from the human EndoC-βH1 and rat INS-1 cells were prepared. Proteins (50 µg per lane) were separated by SDS-PAGE and transferred to immobilon membranes (Method section 2.2.10). Rat brain homogenate (RB; 25 µg) was used as a positive control for all immunoblots. HEK293T cell homogenate ((-) Control; 50 µg) was used as a negative control. Immunoblots were probed with; A) a rabbit anti-PAN-AMPAR antibody (0.075 µg/ml; University of Bristol); B) rabbit anti-NMDAR1 antibody (0.295µg/ml; Cell Signalling Technology®); C) a rabbit anti-NMDAR2A antibody (0.2 µg/ml; Millipore UK Limited) or D) a rabbit anti-NMDAR2B antibody (0.2 µg/ml; Millipore UK Limited) overnight at 4°C. Immunoblots were then probed with a secondary anti-rabbit IgG antibody (0.08 µg/ml; Sigma-Aldrich®) for 1 hour. Immunoblots were imaged by chemiluminescence using the Odessy® Fc (Li-Cor Biosciences) Imaging System. The molecular weight markers (Bio-Rad®) are shown on the left in kilodaltons (kDa). The expected size of AMPAR (A.); NMDAR1 (B.); NMDAR2B (C.) and

NMDAR2B (D.) is indicated on the right. Figure is representative of three independent experiments.

2.3.4 <u>GluK2 protein production was unchanged following shRNA lentivirus treatment</u>

In order to investigate if the KARs, specifically GluK2, are involved in GSIS a GluK2 knockdown using GluK2 shRNA lentivirus was attempted.

GluK2 shRNA virus was successfully made with sequence 2 (Table 2.4 Methods section). GluK2 shRNA virus infected 81 % (± 3.1%, calculated from three separate images) of EndoC-βH1 cells when treated with 50 µl of supernatant containing virus (Method section 2.2.20), as indicated by EndoC-βH1 cells producing green fluorescent protein (GFP) (Figure 2.10). However, immunblotting of protein homogenate from days 4 – 7 post-viral infection revealed no reduction in GluK2 protein detected compared to cells which were not exposed to 50 µl or 100 µl virus containing supernatant (Figure 2.11a). Similarly, and as expected, EndoC-βH1 cells which were infected with non-specific shRNA control virus showed no difference in GluK2 protein production compared to cells not exposed to virus (Figure 2.11b).

EndoC-βH1 cell is a slow growing cell line, it was therefore possible that GluK2 was recycled by the cells at a rate too slow to allow efficient knockdown of GluK2 by the virus. To encourage GluK2 protein recycling EndoC-βH1 cells were treated with 25 µM, 50 µM or 100 µM kainate at the time of viral infection and then again 72 hours after infection. Treatment of EndoC-βH1 cells with kainate and GluK2 shRNA virus did not result in knockdown of GluK2 (Figure 2.12).

Two rat specific GluK2 shRNA virus were then used to infect INS-1 cells. Both viruses infected INS-1 cells, indicated by the cells producing GFP (51% ± 9.1% for virus 1 and 61.7% ± 17% for virus, calculated from three separate images)

(Figure 2.13). However, immunoblotting of protein homogenate from days 4 – 8 post-viral infection again showed no reduction in GluK2 protein production compared to cells which were not exposed to GluK shRNA virus or cells treated with a non-specific shRNA virus control (Figure 2.14).

GluK2 production was not reduced in either human EndoC-βH1 cells or rat INS-1 cells.
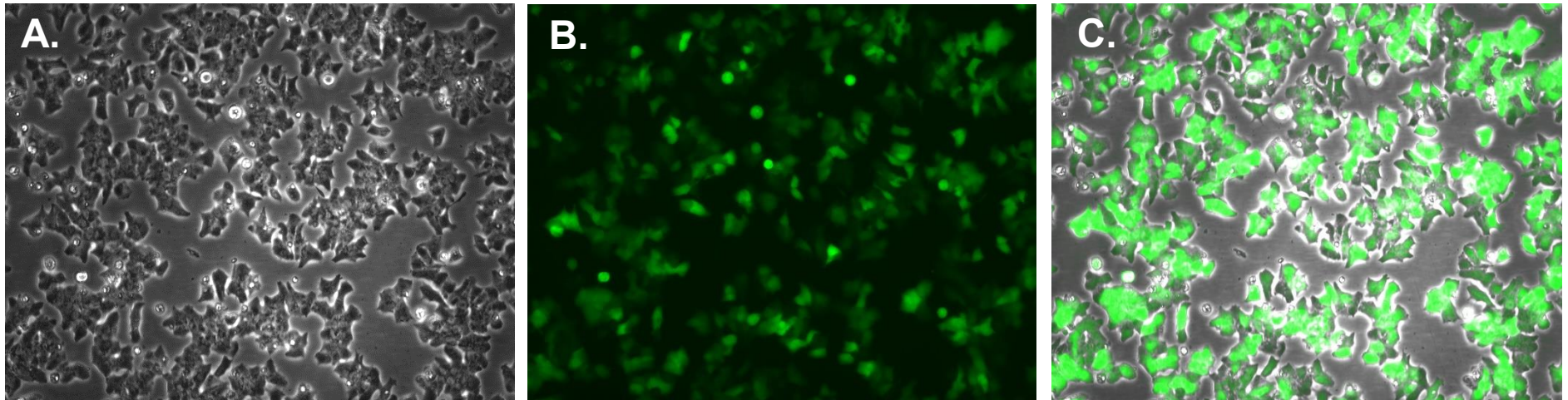
Figure 2.10. GRIK2 shRNA lentivirus effectively infected EndoC-βH1 cells. EndoC-βH1 cells were infected with 50 µl GRIK2 shRNA lentivirus per well in a 6-well plate and incubated for 72 hours. A) Bright-field (BF) of EndoC-βH1 cells. B) EndoC-βH1 successfully infected with GRIK2 shRNA lentivirus expressing GFP. C) Merge image of BF and GFP showing successful infection of EndoC-βH1 cells following 72 hour incubation with GRIK2 shRNA lentivirus. Images taken with Nikon Eclipse Inverted Fluorescence Microscope 20x objective.
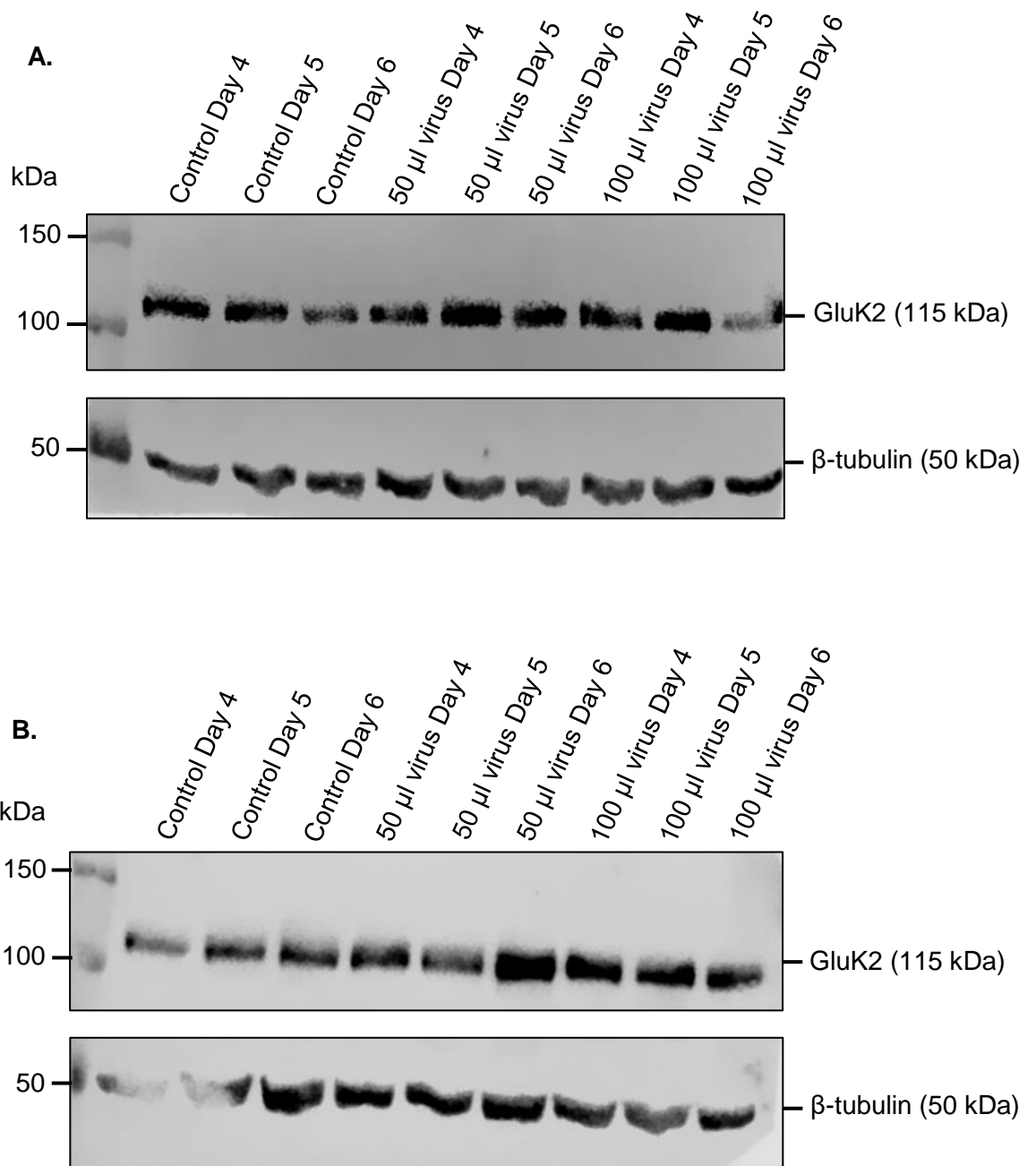
Figure 2.11. Exposure to GluK2 shRNA or non-specific shRNA lentivirus did not reduce GRIK2 production in EndoC-βH1 cells. A lentivirus which contained either A) GluK2 shRNA or B) non-specific shRNA did not reduce GluK2 protein production. EndoC-βH1 cells were grown in 6 well plates and treated with 50 μl or 100 μl of GluK2 or non-specific shRNA lentivirus for 72 hours. Cells were then washed 3 x with PBS and incubated with fresh media. On days 4, 5 and 6

post lentiviral infection protein lysate was collected as described in the Methods section. The protein lysate was then separated by SDS-PAGE and proteins transferred to immobilon membranes (Methods section). Immunoblots were probed with a rabbit polyclonal anti-GluK2/3 antibody (0.125 µg/ml; Millipore UK Limited) overnight at 4 °C. Immunoblots were then probed with a secondary anti-rabbit IgG antibody (0.08 µg/ml; Sigma-Aldrich®) for 1 hour. Immunoblots were imaged by chemiluminescence using the Odessy® Fc (Li-Cor Biosciences) Imaging System. Immunoblots were also probed with mouse anti-β-tubulin (0.67 µg/ml; Sigma-Aldrich®), followed by a secondary IRDye© 800CW Anti-Mouse IgG antibody to assess total protein loading. The molecular weight markers (Bio-Rad) are shown on the left in kilodaltons (kDa). The expected size of GluK2 and β-tubulin is indicated on the right. Images are representative of two independent experiments.
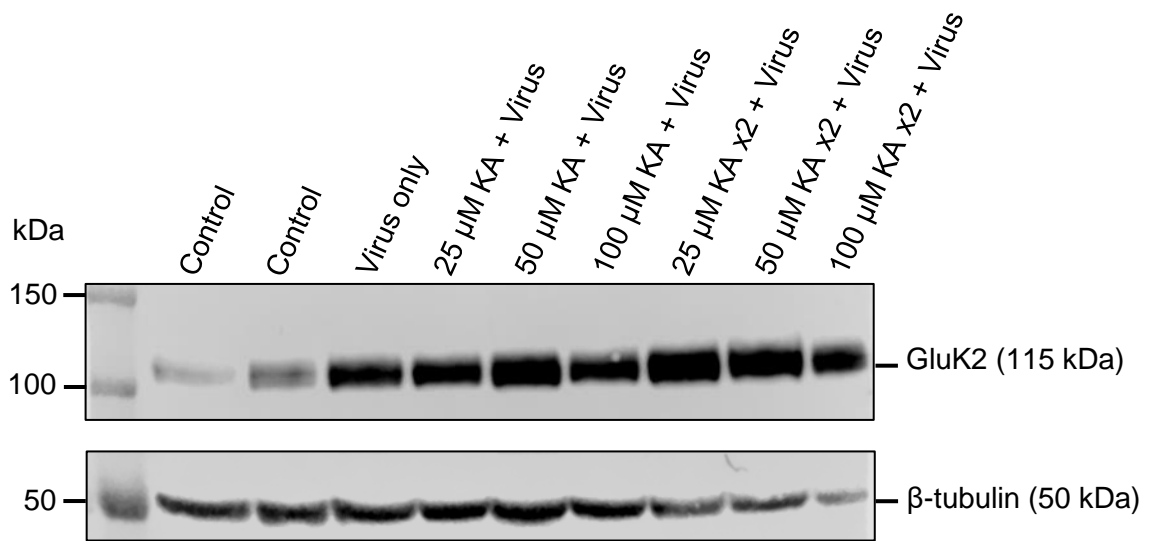
Figure 2.12. Exposure to GRIK2 shRNA lentivirus and Kainate did not reduce GRIK2 production in EndoC-βH1 cells. EndoC-βH1 cells were grown in 6 well plates and treated with 100 µl of GRIK2 shRNA lentivirus and 25 µM, 50 µM or 100 µM Kainate (KA + Virus) for 72 hours. Cells were then washed 3 x with PBS and incubated with fresh media or media containing 25 µM, 50 µM or 100 µM Kainate (KA x2 + Virus). 7 days post lentiviral infection protein lysate was collected as described in the Methods section. EndoC-βH1 cells not exposed to any lentivirus and were used as controls for normal GluK2 protein production and protein lysate was collected at the same time as infected cell protein lysate. The protein lysate was then separated by SDS-PAGE and proteins transferred to immobilon membranes (Methods section). Immunoblots were probed with a rabbit polyclonal anti-GluK2/3 antibody (0.125 µg/ml; Millipore UK Limited) overnight at 4°C. Immunoblots were then probed with a secondary anti-rabbit IgG antibody (0.08 µg/ml; Sigma-Aldrich®) for 1 hour. Immunoblots were imaged by chemiluminescence using the Odessy® Fc (Li-Cor Biosciences) Imaging System. Immunoblots were also probed with mouse anti-β-tubulin (0.67 µg/ml; Sigma-

Aldrich®), followed by a secondary IRDye© 800CW Anti-Mouse IgG antibody to assess total protein loading. The molecular weight markers (Bio-Rad) are shown on the left in kilodaltons (kDa). The expected size of GluK2 and β-tubulin is indicated on the right. Image is representative of one experiment.

Virus 1.
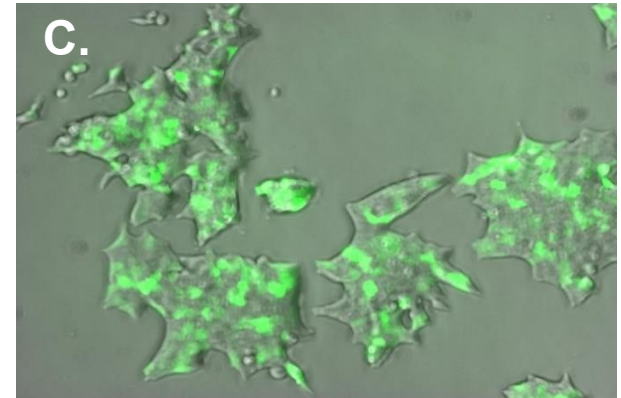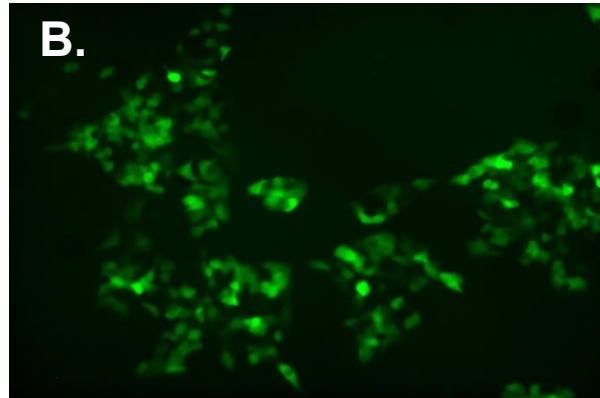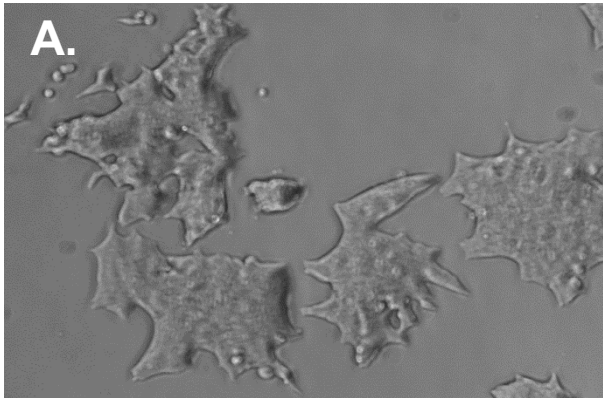
Virus 2.
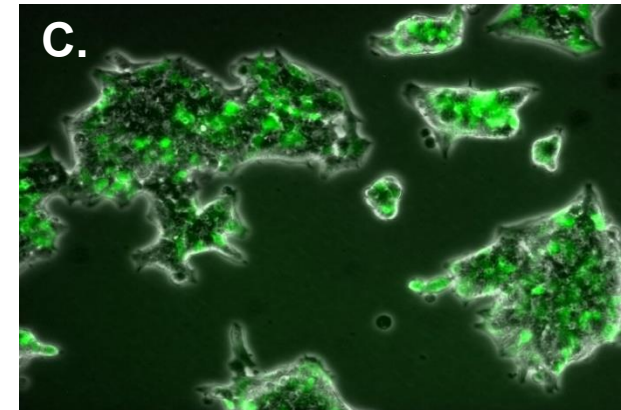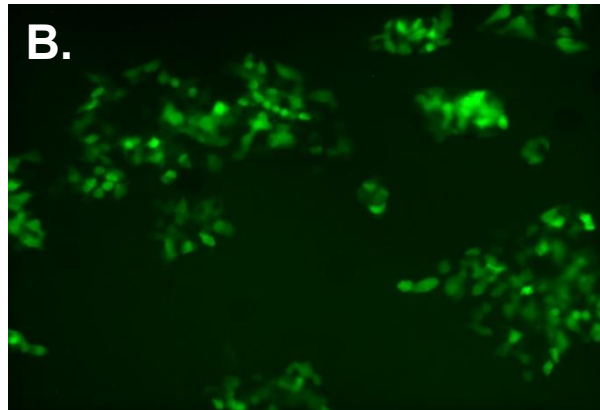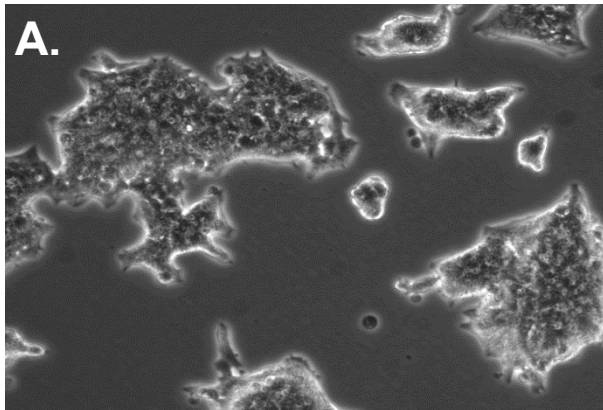
Figure 2.13. Rat GluK2 shRNA lentivirus (1) and (2) effectively infected INS-1 cells. INS-1 cells were infected with 100 μl rat GRIK2 shRNA lentivirus (1) or (2) per well in a 6-well plate and incubated for 72 hours. A) Bright-field (BF) of INS-1 cells. B) INS-1 successfully infected with GRIK2 shRNA lentivirus expressing GFP. C) Merge image of BF and GFP showing infection of INS-1 cells following 72 hour incubation with rat GRIK2 shRNA lentivirus. Images taken with Nikon Eclipse Inverted Fluorescence Microscope 20x objective.

A.
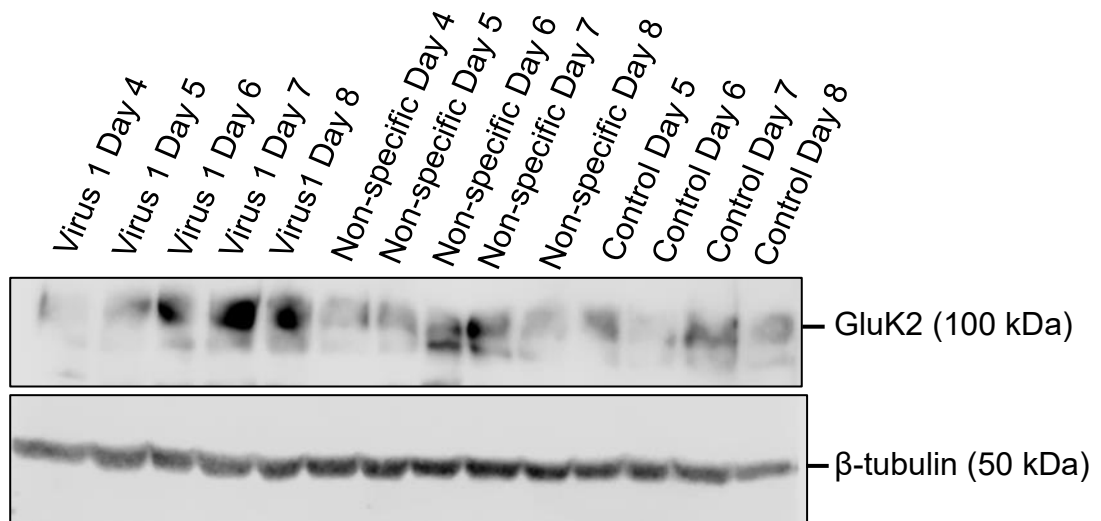
B.
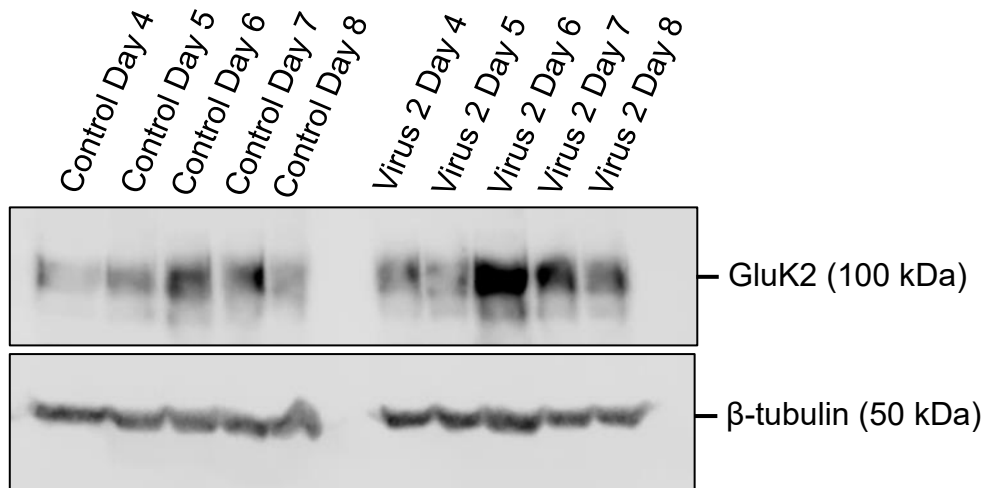
Figure 2.14. Exposure to GluK2 shRNA virus 1, 2 or non-specific shRNA lentivirus did not reduce GRIK2 production in INS-1 cells. A lentivirus which contained either A) GluK2 shRNA virus 1 or non-specific shRNA virus or B) GluK2 shRNA virus 2 did not reduce GluK2 protein production. INS-1 cells were grown in 6 well plates and treated with 100 µl of GluK2 shRNA virus 1, 2 or non-specific shRNA lentivirus for 72 hours. Cells were then washed 3 x with PBS and incubated with fresh media. On days 4, 5, 6, 7 and 8 post lentiviral infection protein lysate was collected as described in the Methods section. The protein

lysate was then separated by SDS-PAGE and proteins transferred to immobilon membranes (Methods section). Immunoblots were probed with a rabbit monoclonal anti-GluK2 antibody (0.085 µg/ml; Abcam) overnight at 4°C. Immunoblots were then probed with a secondary anti-rabbit IgG antibody (0.08 µg/ml; Sigma-Aldrich®) for 1 hour. Immunoblots were imaged by chemiluminescence using the Odessy® Fc (Li-Cor Biosciences) Imaging System. Immunoblots were also probed with mouse anti-β-tubulin (0.67 µg/ml; Sigma-Aldrich®), followed by a secondary IRDye© 800CW Anti-Mouse IgG antibody to assess total protein loading. The expected size of GluK2 and β-tubulin is indicated on the right in kilodaltons (kDa). Images are representative of two individual experiments.

2.3.5 Glutamate receptor activation increases glucose stimulated insulin secretion (GSIS) in EndoC-βH1 cells

Following the unsuccessful knock down of KAR subunits using shRNA lentivirus, it was then decided to use various GluR agonists and antagonists to elucidate GluRs role in insulin secretion from human β-cells. The human β-cell's primary function is to secrete insulin in response to maintain blood-glucose homeostasis (Da Silva Xavier, 2018). To establish if EndoC-βH1 cells respond to glucose, a glucose-stimulated insulin secretion (GSIS) assay was performed (Methods section 2.2.21). Retained and secreted insulin were measured using Human Insulin ELISA (Mercodia, Uppsala, Sweden). A calibration curve using known standards was also obtained from the ELISA (Figure 2.15). The optical density of the test samples was inserted into the equation ($y = mx + c$) from the calibration curve. Calibration curves were only used to quantify data if they had an R^2 value great than 0.95. Following treatments (described in Methods section 2.2.21), the retained and secreted insulin from EndoC-βH1 cells was measured and the percentage of insulin secreted from the total insulin (retained insulin plus secreted insulin) was calculated.

EndoC-βH1 cells showed a significant two-fold increase in insulin secretion when treated with 20 mM glucose, compared with cells treated with 0.5 mM glucose ($p = 0.000385$; Figure 2.16). EndoC-βH1 cells also responded to increased intracellular cyclic AMP (cAMP), as demonstrated with the phosphodiesterase inhibitor IBMX (Komatsu et al., 2002). Cells treated with 20 mM glucose and 0.5 mM IBMX showed a more than five-fold increase in insulin secretion compared to cells treated with 20 mM glucose alone ($p = 0.000014$; Figure 2.17).

Results from PCR and immune blotting have shown that KARs are found in EndoC-βH1 cells (Sections 2.3.1 and 2.3.2). To establish if these KARs affect β-cell insulin secretion various GluR agonists and antagonists were used during GSIS (as described in Method section 2.2.21).

Kainate and 20 mM glucose induced a 1.3 fold increase in insulin secretion compared to cells treated with 20 mM glucose alone ($p = 0.034$; Figure 2.18). Cells which were pre-incubated with the KAR and AMPAR antagonist, NBQX, before treatment with high glucose and kainate blocked kainate induced insulin secretion, indicating that KAR activation increases GSIS.

When GSIS was conducted in low glucose (0.5 mM) there was no significant increase in insulin secretion between low glucose alone and low glucose plus kainate. There was also no significant difference in insulin secretion between low glucose alone and cells pre-treated with NBQX before treatment with low glucose and kainate (Figure 2.19).

To ensure the effect of NBQX was due to KARs and not AMPAR antagonism, EndoC-βH1 cells were also pre-incubated with GYKI-52466, an AMPAR-specific antagonist (Rzeski et al., 2001). Pre-treatment with GYKI-52466 did not block the effects of kainate on insulin secretion and there was no significant difference between cells treated with high glucose and kainate compared to those pre-treated with GYKI-52466 (Figure 2.18).

KARs can exert both ionotropic and metabotropic functions involving G-proteins and second messengers (Marshall et al., 2018; Petrovic et al., 2017). To investigate if KAR effect on insulin secretion could be potentiated by metabotropic receptor activation, the mGluR1 receptor agonist, DHPG (Wiśniewski and Car,

2002), was used during GSIS. EndoC-βH1 cells which were incubated with DHPG before treatment with 20 mM glucose and kainate showed no significant difference in insulin secretion compared to cells which were only treated with 20 mM glucose and kainate (Fig.2.18).
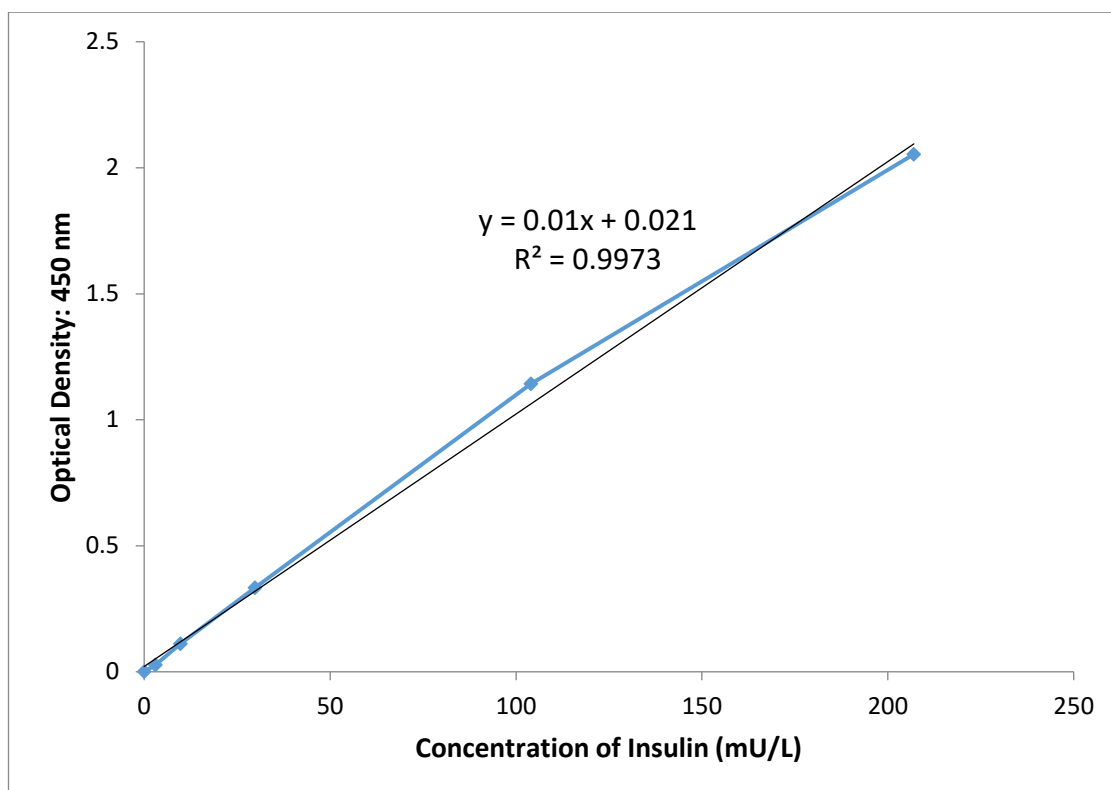
Figure 2.15. Example calibration curve of human insulin ELISA standards with optical density (450 nm) plotted against concentration of insulin (mU/L). An equation for the R^2 value was calculated using the curve, which was then used to calculate the concentration of insulin produced from the EndoC-βH1 cells after treatments. Figure is representative example of the calibration curves used to calculate insulin secretion.
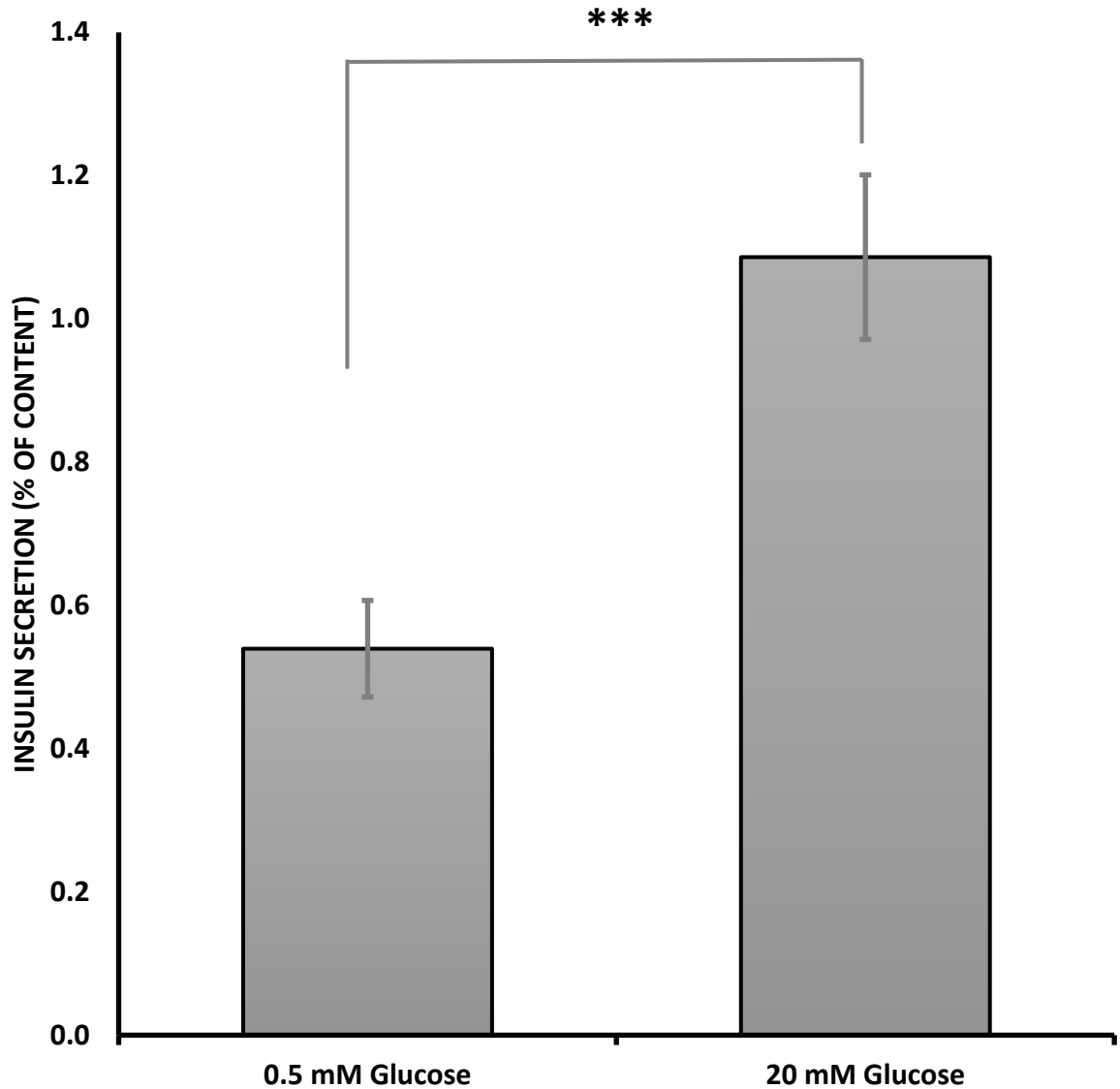
Figure 2.16. Effect of non-stimulatory and stimulatory glucose on insulin secretion in EndoC-βH1 cells. EndoC-βH1 cells were grown in glucose-starving medium containing 2.8 mM glucose for 12 – 18 hours. Cells were incubated in KREB-Ringer solution supplemented with 0.5 mM glucose for 1 hour and were then incubated with 0.5 mM glucose or 20 mM glucose for a further 1 hour. Total and released insulin were quantified by Human Insulin ELISA (Mercodia) as described in the Methods section. Results are shown as the percentage insulin secretion in relation to the total insulin content ± SEM from 10 separate experiments conducted in triplicate. Means were compared by students t-test. ***$p < 0.001$
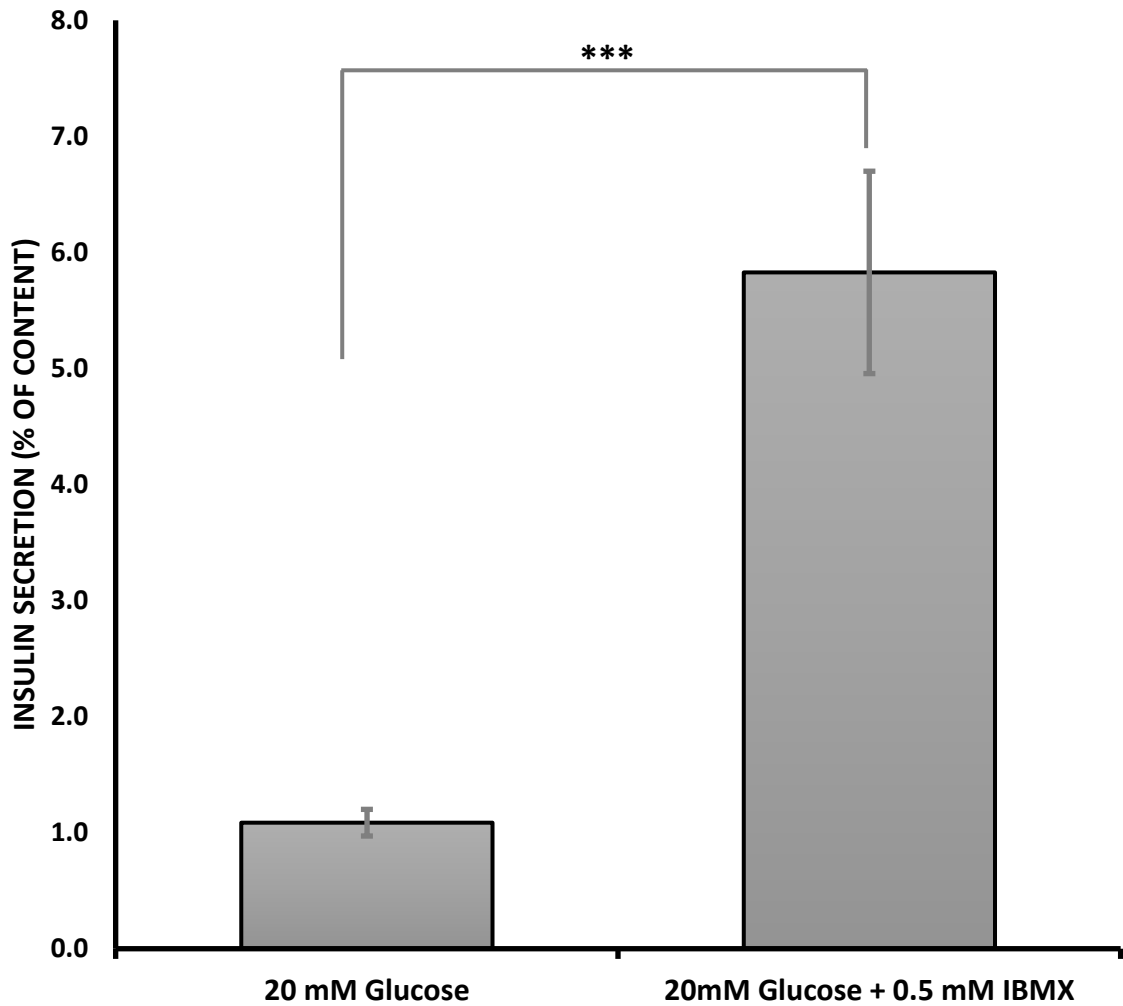
Figure 2.17. Effect of stimulatory glucose and IBMX on insulin secretion in EndoC-βH1 cells. EndoC-βH1 cells were grown in glucose-starving medium containing 2.8 mM glucose for 12 – 18 hours. Cells were incubated in KREB-Ringer solution supplemented with 0.5 mM glucose for 1 hour and were then incubated with 20 mM glucose or 20 mM glucose and IBMX for a further 1 hour. Total and released insulin were quantified by Human Insulin ELISA (Mercodia) as described in the Methods section. Results are shown as the percentage insulin secretion in relation to the total insulin content ± SEM from 11 separate experiments conducted in triplicate. Means were compared by students t-test. ***$p < 0.001$.

Kainate (25 µM)	-	+	+	+	+
NBQX (30 µM)	-	-	+	-	-
GYKI (100 µM)	-	-	-	+	-
DHPG (50 µM)	-	-	-	-	+
Glucose (20 mM)	+	+	+	+	+
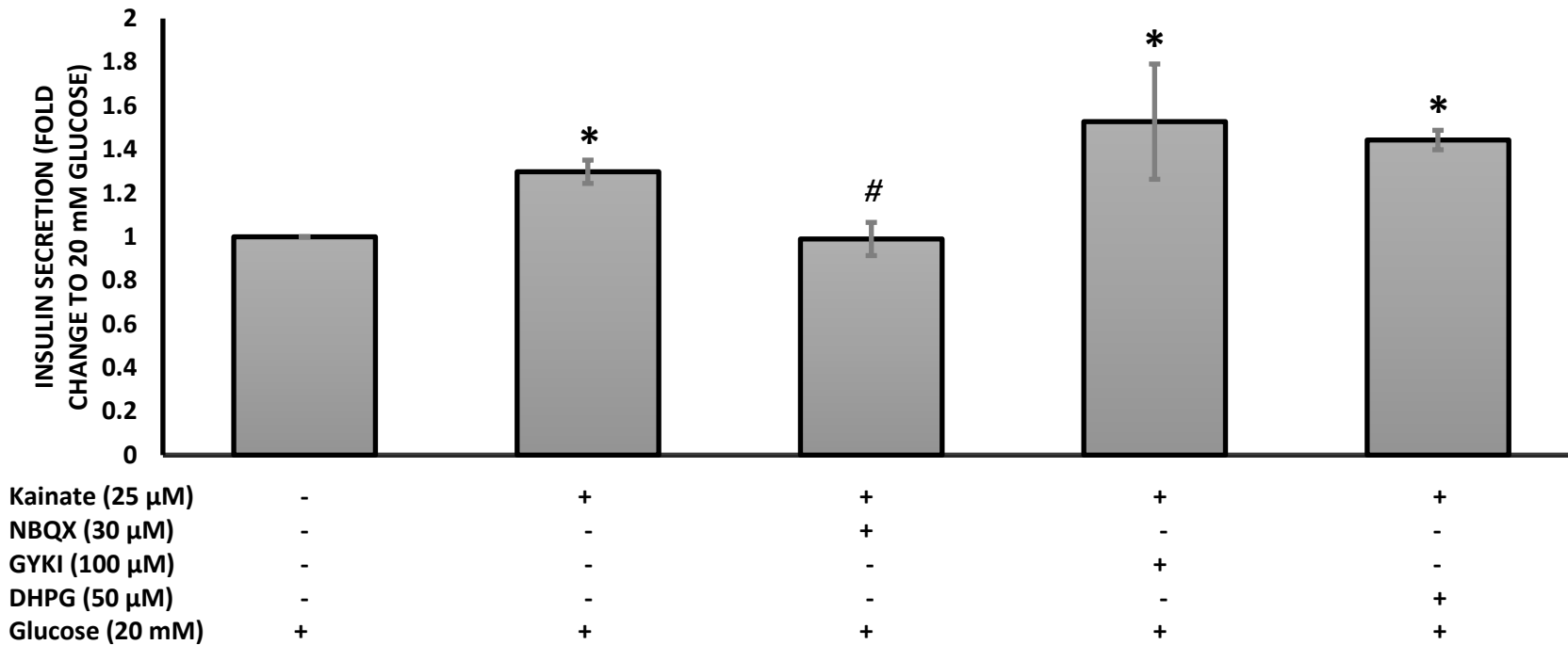
Figure 2.18. Effect of glutamate receptor agonists and antagonists on glucose-stimulated insulin secretion in EndoC-βH1 cells.

EndoC-βH1 cells were grown in glucose-starving medium containing 2.8 mM glucose for 12 – 18 hours. Cells were incubated in KREB-Ringer solution supplemented with 0.5 mM glucose for 1 hour and then pre- incubated with 20 mM glucose or 20 mM glucose and NBQX; GYKI or DHPG for five minutes. Cells were then incubated with 20 mM glucose, 20 mM glucose and glutamate receptor agonists and antagonists for a further 1 hour. Total and released insulin were quantified by Human Insulin ELISA (Mercodia) as described in the Methods section. Results are shown as the mean fold change compared to 20 mM glucose ± SEM from 5 - 11 separate experiments conducted in triplicate. Means were compared by One-Way ANOVA followed by Bonferroni correction. * $p < 0.05$ compared to 20 mM glucose, # $p < 0.05$ compared to 20 mM glucose plus kainate.
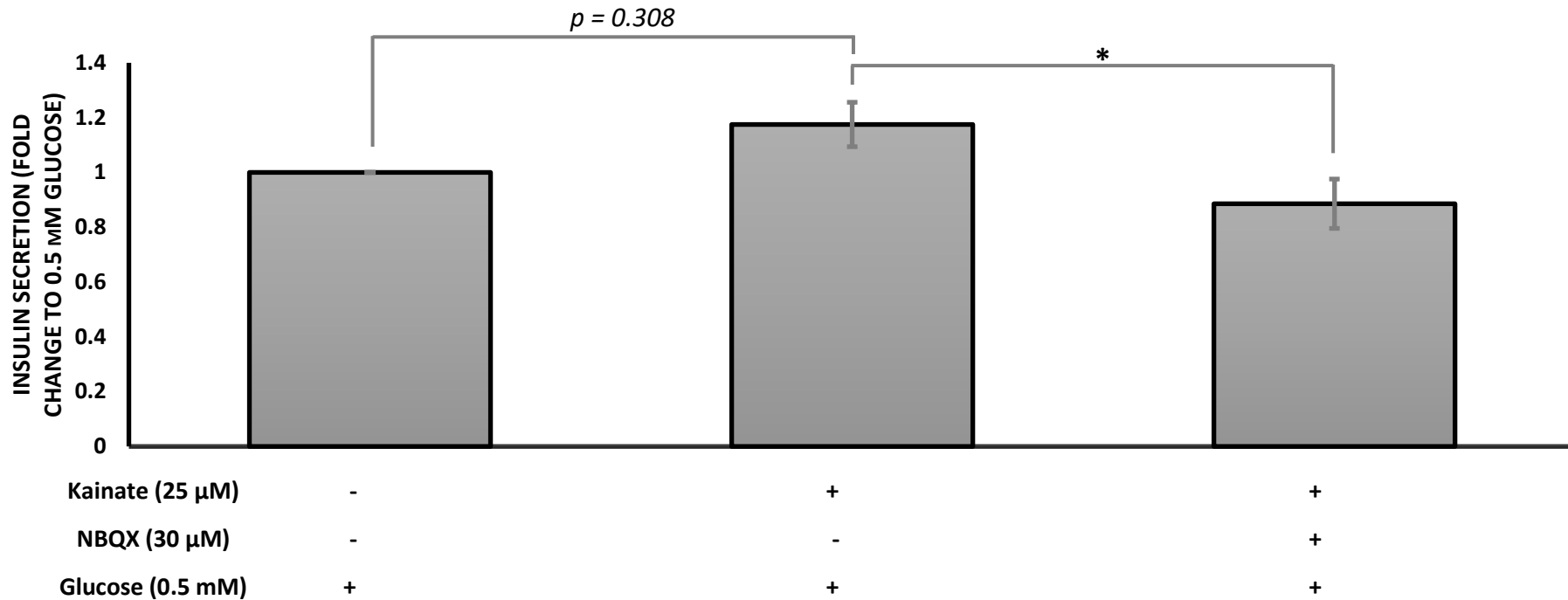
Figure 2.19. Effect of Kainate receptor agonists and antagonists on insulin secretion in EndoC-βH1 cells in non-stimulatory glucose. EndoC-βH1 cells were grown in glucose-starving medium containing 2.8 mM glucose for 12 – 18 hours. Cells were incubated in KREB-Ringer solution supplemented with 0.5 mM glucose for 1 hour and then pre- incubated with 0.5 mM glucose or 0.5 mM glucose and NBQX. Cells were then incubated with 0.5 mM glucose, 0.5 mM glucose and Kainate receptor agonists and antagonists for a further 1 hour. Total and released insulin were quantified by Human Insulin ELISA (Mercodia) as described in the Methods section. Results are shown as the mean fold change compared to 0.5 mM glucose ± SEM from 5 separate experiments conducted in triplicate. Means were compared by One-way ANOVA followed by Bonferroni correction. *$p<0.05$

2.3.6 Exposure to high glucose induces surface translocation of GluK2 in EndoC-βH1 cells.

To investigate if KAR membrane localisation was affected by different glucose concentrations EndoC-βH1 cells were treated with 0.5 mM glucose or 20 mM glucose for 1 hour, after which membrane protein fractions were obtained (Methods section 2.2.24). GluK2 protein was then visualised via immunoblotting (Methods section 2.2.8 – 2.210). Within neuronal cells protein kinase A (PKA) pathway activation influences KAR activity (Andrade-Talavera et al., 2013; Falcón-Moya et al., 2018), however, KAR trafficking is thought to be independent of this pathway (Sun et al., 2014). To investigate if this was also true in human β-cells, EndoC-βH1 cells were also treated with IBMX, which rises intracellular cAMP and activates PKA. (Komatsu et al., 2002).

Immunoblot detection of cell surface and total GluK2 protein revealed that surface expression of GluK2 is variable between blots (Figure 2.20). However, normalisation of the blots shows that cell surface expression of GluK2 is significantly increased when EndoC-βH1 cells are treated with 20 mM glucose, compared to cells which are treated with 0.5 mM glucose (Figure 2.21a). The total GluK2 in 0.5 mM glucose was not significantly different to that in 20 mM glucose (Figure 2.21b).

There was no significant difference seen between either surface expressed or total GluK2 protein when cells were treated with 20 mM glucose or 20 mM glucose and IBMX (Figure 2.22).

Immobilon® PVDF membranes containing cell surface and total proteins were re-probed with an anti-CaV2.1 (Life Technologies Limited, Paisley, UK) and anti-

Na,K-ATPase (Cell Signalling Technology®, Leiden, UK) antibodies, however, surface expressed protein was unable to be detected with either antibody (Figure 2.23).
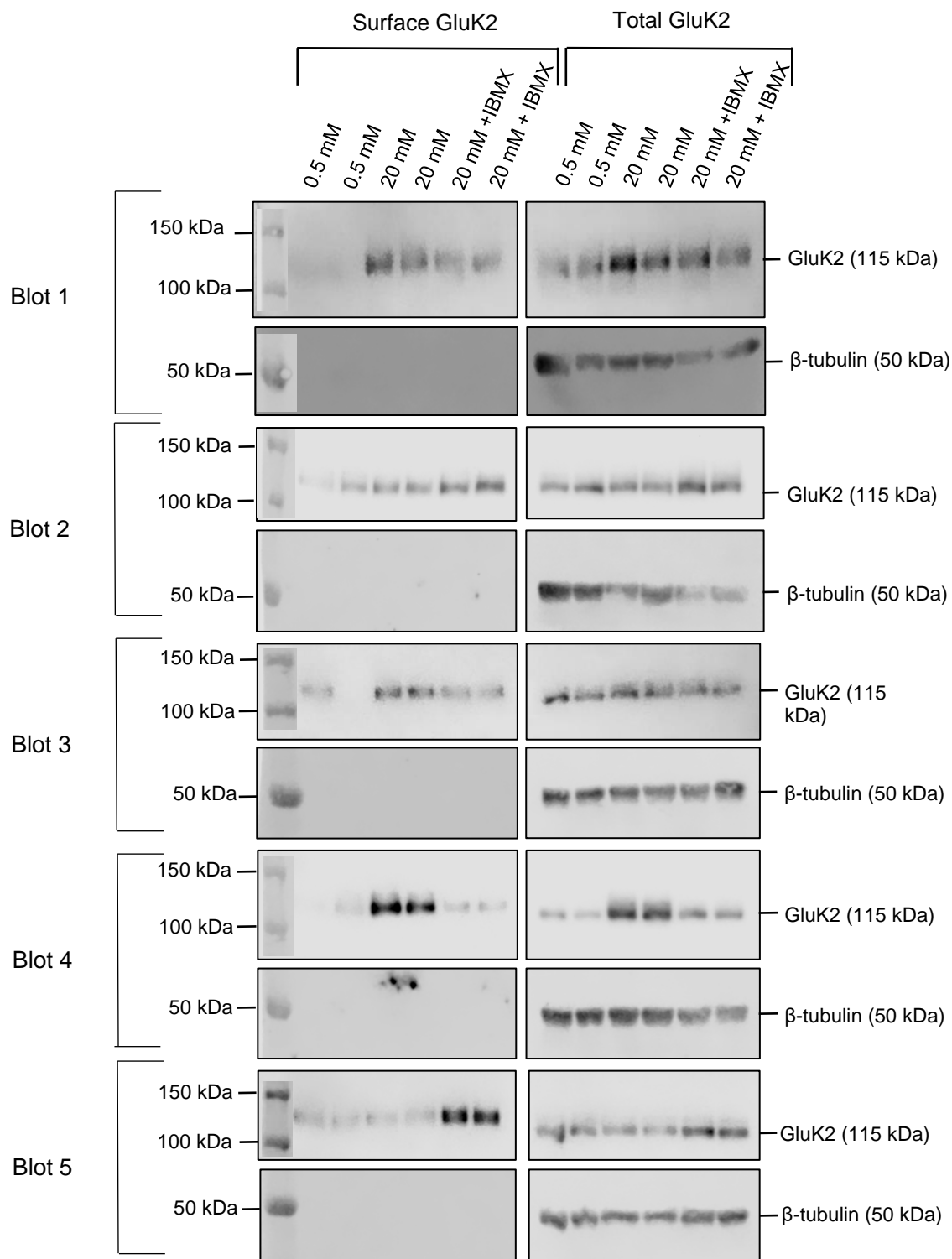
Figure 2.20. Surface expression of GluK2 in EndoC-βH1 pancreatic β-cells.

EndoC-βH1 cells were grown in glucose-starving medium containing 2.8 mM glucose for 12 – 18 hours. Cells were incubated in KREB-Ringer solution supplemented with 0.5 mM glucose for 1 hour. Cells were then incubated with KREB-Ringer solution supplemented with 0.5 mM glucose, 20 mM glucose or 20

mM glucose and IBMX (500 µM) for a further 1 hour. The surface proteins were separated from the total cell protein by cell surface biotinylation assay (as described in Methods section). Surface and total protein samples were then separated by SDS-PAGE and proteins transferred to immobilon membranes (Methods section). Immunoblots were probed with a rabbit polyclonal anti-GluR6/7 antibody (0.125 µg/ml; Millipore UK Limited) overnight at 4°C. Immunoblots were then probed with a secondary anti-rabbit IgG antibody (0.08 µg/ml; Sigma-Aldrich®) for 1 hour. Immunoblots were imaged by chemiluminescence using the Odessy® Fc (Li-Cor Biosciences) Imaging System. Immunoblots were also probed with mouse anti-β-tubulin (0.67 µg/ml; Sigma-Aldrich®), followed by a secondary IRDye© 800CW Anti-Mouse IgG antibody to assess total protein loading. The molecular weight markers (Bio-Rad) are shown on the left in kilodaltons (kDa). The expected size of GluK2 is indicated on the right. Lysates were loaded in duplicate. The experiment was conducted 5 times and the results of each immunoblot are shown.
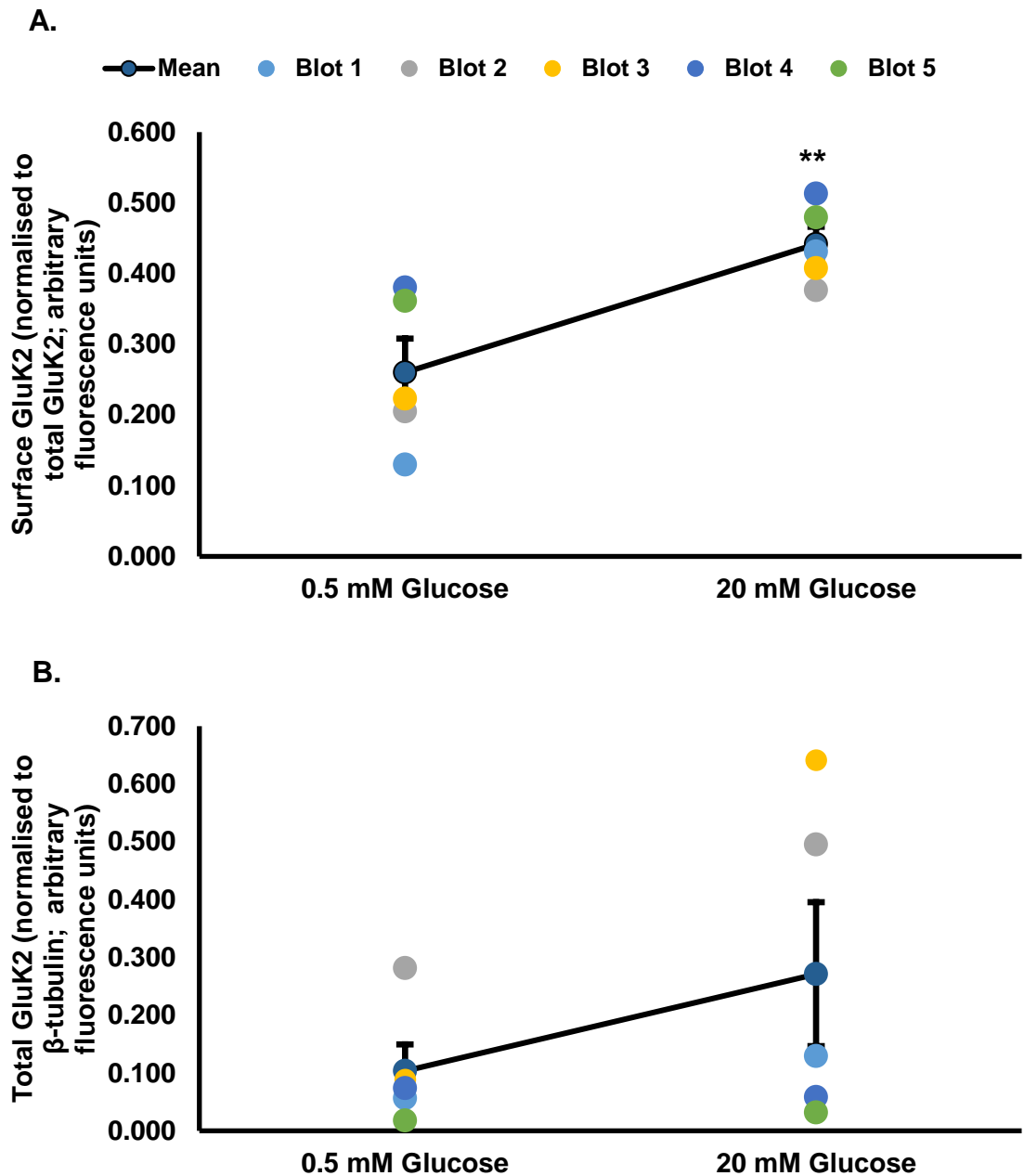
Figure 2.21. Effect of non-stimulatory glucose (0.5 mM) and stimulatory glucose (20 mM) GluK2 protein production. A) Chart showing the surface expression of GluK2 normalised against total GluK2 signal for each immunoblot. B) Chart showing the total expression of GluK2 normalised against β-tubulin signal for each immunoblot. Immunoblots were analysed using Image Studio™ Lite software. The black line represents the mean ± SEM from the 5 individual experiments conducted. Means were compared by students t-test. ** $p < 0.01$
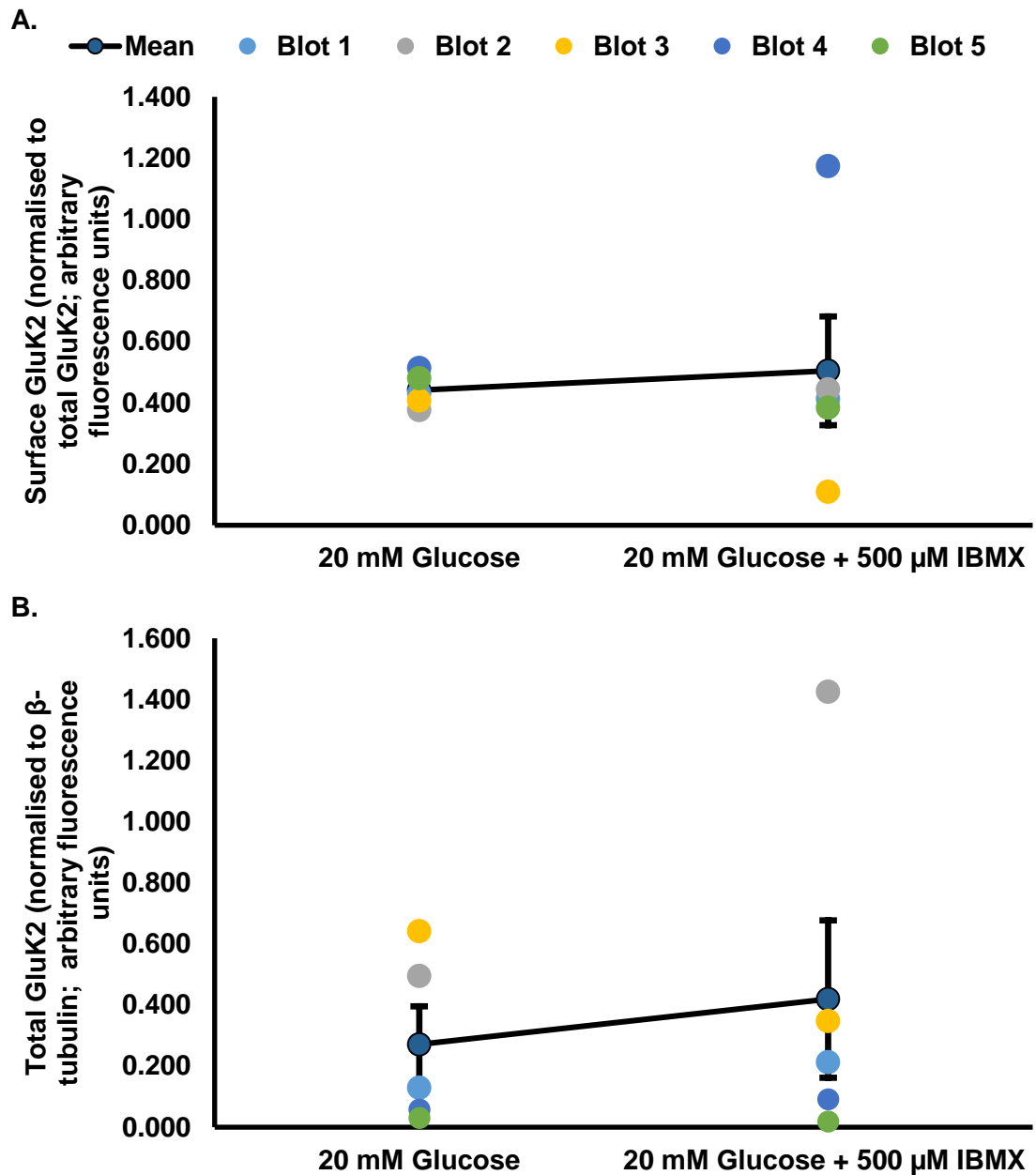
Figure 2.22. Effect of stimulatory glucose (20 mM) and stimulatory glucose (20 mM) with IBMX (500 µM) on GluK2 expression. A) Chart showing the surface expression of GluK2 normalised against total GluK2 signal for each immunoblot. B) Chart showing the total expression of GluK2 normalised against β-tubulin signal for each immunoblot. Immunoblots were analysed using Image Studio™ Lite software. The black line represents the mean ± SEM from the 5 individual experiments conducted. Means were compared by students t-test.
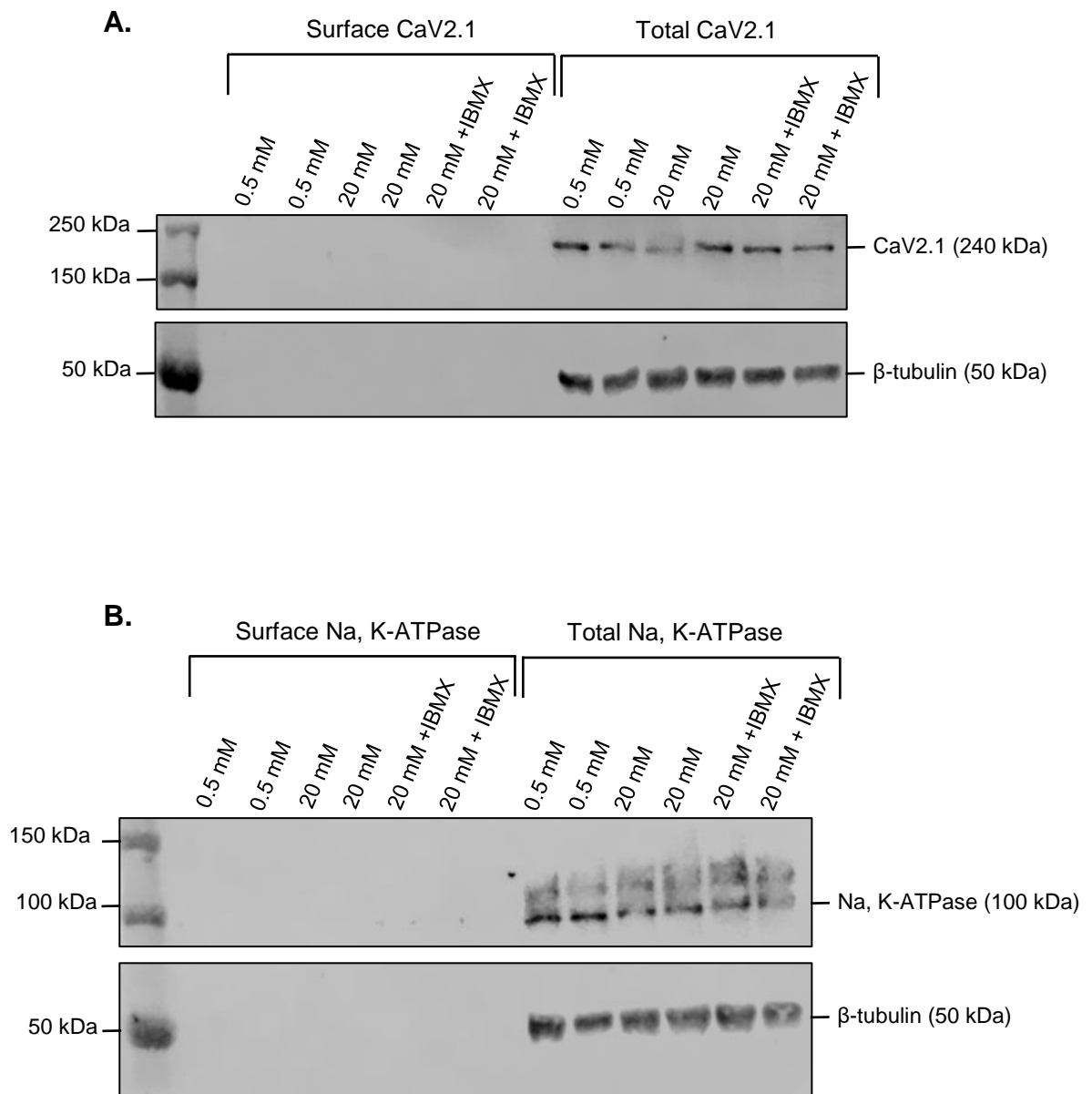
Figure 2.23. CaV2.1 and Na, K-ATPase surface protein was undetectable EndoC-βH1 pancreatic β-cells. EndoC-βH1 cells were grown in glucose-starving medium containing 2.8 mM glucose for 12 – 18 hours. Cells were incubated in KREB-Ringer solution supplemented with 0.5 mM glucose for 1 hour. Cells were then incubated with KREB-Ringer solution supplemented with 0.5 mM glucose, 20 mM glucose or 20 mM glucose and IBMX (500 µM) for a further 1 hour. The surface proteins were separated from the total cell protein by cell surface biotinylation assay (as described in Methods section). Surface and total

protein samples were then separated by SDS-PAGE and proteins transferred to immobilon membranes (Methods section). Immunoblots were probed with either A) rabbit polyclonal anti-CaV2.1 (0.8 µg/ml; Life Technologies Limited, Paisley, UK) or B) rabbit polyclonal anti-Na,K-ATPase (0.031 µg/ml; Cell Signalling Technology®, Leiden, UK) overnight at 4°C. Immunoblots were then probed with a secondary anti-rabbit IgG antibody (0.08 µg/ml; Sigma-Aldrich®) for 1 hour. Immunoblots were imaged by chemiluminescence using the Odessy® Fc (Li-Cor Biosciences) Imaging System. Immunoblots were also probed with mouse anti-β-tubulin (0.67 µg/ml; Sigma-Aldrich®), followed by a secondary IRDye© 800CW Anti-Mouse IgG antibody to assess total protein loading. The molecular weight markers (Bio-Rad) are shown on the left in kilodaltons (kDa). The expected size of CaV2.1 and Na, K-ATPase is indicated on the right. Lysates were loaded in duplicate. Figure is representative of four independent experiments.

2.4   Discussion

Comparatively to AMPAR and NMDARs, very little is known about KARs in both the CNS and in pancreatic β-cells. Within β-cells there has been conflicting reports on the presence and function of KARs between human islets and murine cell lines (Table 1.2 and section 1.10). However, the development of the human β-cell line, EndoC-βH1, has provided the opportunity to investigate KAR molecular composition and their role in insulin secretion.

2.4.1   KAR subunits are present in the human β-cell line EndoC-βH1

RT-PCR analysis in this study successfully identified GluK2 and GluK5 mRNA from EndoC-βH1 cells (Figure 2.4). The identification of GluK2 and GluK5 mRNA is very significant as it suggests that functional receptors could be formed in EndoC-βH1 cells. It is also important to note that because of the presence of GluK2, it is possible for the formation of either homomeric, low-affinity KARs or heteromeric, high-affinity KARs when in combination with GluK5 (Hadzic et al., 2017). Previous studies have reported the presence of GluK2 and GluK5 subunit specific mRNA from β-cells isolated from human islets (Bramswig et al., 2013; Dorrell et al., 2011; Eizirik et al., 2012; Nica et al., 2013), however these studies also identified other KAR subunits (GluK1, GluK3 and GluK4) which were not found in EndoC-βH1 cells. These results may therefore infer a difference in the molecular composition of KARs in β-cells isolated from human islets and that seen in the human β-cell line EndoC-βH1. However, this may be explained in part due to the heterogenic nature of β-cells isolated from human islets which have been shown to display a diverse genetic profile from one β-cell to another (Bader et al., 2016; Dorrell et al., 2016). The islet cell isolation Methods used in previous studies can also result in cell types other than β-cells being mixed together and

could include other islet cell types and not just a pure β-cell sample, as is seen when using the EndoC-βH1 β-cell line (Dorrell et al., 2008; Prasad and Groop, 2016). The current study therefore identifies for the first time the KAR subunit molecular composition of pure human β-cells.

Up until now the only study to identify KAR subunit proteins in β-cells is Molnar *et al.,* 1995, who successfully identified GluK5 protein from rat islets and the rat/mouse cell lines RINm5F, MIN6 and HIT T15. However, Molnar *et al.*, 1995 did not test human β-cells and GluK5 is cannot to form a functional receptor alone. It was therefore essential to investigate if both GluK2 and GluK5 proteins are produced in human EndoC-βH1 cells to establish if functional KARs can be formed. The current study showed that EndoC-βH1 cells do produce GluK2 protein (Figure 2.6) but was could not to confirm if GluK5 protein is produced. Two different anti-GluK5 antibodies were used. The first anti-GluK5 antibody was not specific for human GluK5 and could not be detected using EndoC-βH1 protein homogenate (Figure 2.7). Indeed, when the epitope sequence for the antibody was compared to the complimentary sequence for human GluK5, it revealed two amino acid changes (Appendix II). Both amino acid changes were threonine to alanine; threonine is a hydrophilic amino acid and so will likely lie on the outside of the structure, whereas alanine is hydrophobic so will be buried inside the structure (Barnes and Gray, 2003). It is likely that these amino acid changes would have affected the epitopes tertiary structure and prevented binding of the antibody to the human GluK5. A second antibody which was specific for human GluK5 was then used to overcome this, however, the specificity of the antibody was poor and positive bands were seen even in the negative control (Figure 2.8). Therefore, the presence of GluK5 protein in EndoC-βH1 cells could not be

confirmed. The identification of GluK2 protein is important because as stated previously, GluK2 can form functional KARs without any other KAR subunits, meaning that even if GluK5 protein is not produced by the cells, functional homomeric GluK2 containing KARs can still be produced. However, the identification of GluK5 mRNA suggests that the EndoC-βH1 cell line is likely to produce GluK5 proteins, which in turn allow the formation of both homo- and heteromeric KARs with low and high affinity to kainite. Within β-cells this would suggest that much lower levels of extracellular glutamate are required to activate KARs than if only homomeric GluK2 containing KARs were present due to GluK5's higher affinity for glutamate (Hadzic et al., 2017). This is the first study to identify KAR subunit mRNA and protein in the EndoC-βH1 cell line. Table 1.2 has been updated to highlight the KAR subunits which have been identified in EndoC-βH1 cells from the current study and are shown in Table 2.5.

Table 2.5. Kainate receptor subunit mRNA and protein found in pancreatic islets and cell lines. References from which the data were obtained are listed below. [1] (Bramswig et al., 2013) [2] (Cabrera et al., 2008) [3] (Nica et al., 2013) [4] (Huang et al., 2017) [5] (Wu et al., 2012) [6] (Inagaki et al., 1995) [7] (Kutlu et al., 2009) [8] (Dorrell et al., 2011) [9] (Eizirik et al., 2012) [10] (Benner et al., 2014) [11] (Gonoi et al., 1994) [12] (Weaver et al., 1996) [13] (Molnár et al., 1995). Data obtained from the current study is shown in red and empty boxes represent no data.

Kainate			EndoC-βH1	Human Islet/β-cell	Mouse Islet/β-cell	Rat Islet/β-cell	RINm5F (Rat)	MIN6 (Mouse)	INS-1 (Rat)	HIT T15 (Hamster)
GluK1	RNA	Positive		1-3, 9	4	4,7	4,6		7	
		Negative	*	7,8	10	6		4, 11		
	Protein	Positive								
		Negative								
GluK2	RNA	Positive	*	1-3, 8, 9	4, 10	4,6,7	4	4	7	
		Negative		7			6	11		
	Protein	Positive	*							
		Negative				12				
GluK3	RNA	Positive		1-3, 7, 9	4	4, 6, 7	4	4	7	
		Negative	*	8	10		6			
	Protein	Positive								
		Negative				12				
GluK4	RNA	Positive		1, 3, 9	4, 10	4, 6, 7	4	4	7	
		Negative	*	7, 8			6	11		
	Protein	Positive								
		Negative								
GluK5	RNA	Positive	*	1-3, 8, 9	10	6, 7	6	11	7	
		Negative		7						
	Protein	Positive				13	13	13		13
		Negative				12				

115

2.4.2 KAR auxiliary subunits Neto1 and Neto2 are expressed in EndoC-βH1 cells

Neto1 and Neto2 auxiliary proteins have been shown to play a significant role in KAR expression and function within the CNS (section 1.8.3). Specifically Neto subunits have been shown to enhance the expression of GluK2 in HEK293 cells (Palacios-Filardo et al., 2016). The current study identified transcripts for both Neto1 and Neto2 subunits (Figure 2.5) from EndoC-βH1 cells and aligns well with previous studies which have reported expression of Neto1 and Neto2 mRNA in human β-cells (Bramswig et al., 2013; Eizirik et al., 2012; Kutlu et al., 2009; Nica et al., 2013). This suggests that as seen in the CNS, Neto subunits may be used in β-cells to modulate KAR expression and function, as is seen in neuronal cells (Evans et al., 2017, 2019).

2.4.3 GluN2B protein is produced by EndoC-βH1 cells, but no other NMDAR or AMPAR subunit proteins could be identified

In the current study only protein for the NMDAR subunit GluN2B was found to be produced by EndoC-βH1 cells, no other iGluR subunits were detected (Figure 2.9). INS-1 cell protein homogenate was tested simultaneously with EndoC-βH1 cells and was not found to produce any NMDAR or AMPAR subunit proteins. However, another study using INS-1 cells has reported that NMDAR subunit proteins are produced (Wu et al., 2017). There have also been other studies which report AMPAR and NMDAR subunit proteins in various other β-cell lines (Gonoi et al., 1994; Patterson et al., 2016; Weaver et al., 1996). However, it should be noted that due to time limitations, the immunoblots for NMDAR and AMPAR receptor subunits were not checked with a house-keeping antibody to ensure the integrity of the protein samples. It is therefore possible that there was

an issue with the samples used for immunoblotting of NMDAR and AMPAR subunits. In addition to this, the positive control used was rat brain and was processed separately to the EndoC-βH1 and INS-1 homogenate and therefore cannot be used to infer the integrity of the other samples. It is also interesting that Wu et al., 2017 observed that only 43 % of INS-1 cells express detectable levels of GluN1 protein and most of these cells express GluN1 at low levels. Due to this, it is possible that a larger amount of protein is necessary to be loaded in order to detect NDMAR subunits for immunoblotting. If time was not limiting, I would repeat these immunoblots with a larger protein sample (60 μg or more) whilst simultaneously probing for a house-keeping protein, such as β-tubulin, to act as a further positive control to check the integrity of the samples being used. Since NMDARs and AMPARs are membrane spanning proteins it may also be that some receptors were not properly extracted from the membrane and linearised by the SDS in the lysis buffer. Rath et al., 2009, demonstrated that incomplete denaturation of membrane proteins by SDS can alter the proteins ability to travel through SDS-Page gels. If NMDARs protein is not expressed by all β-cells, as is seen by Wu *et al.*, 2017, then incomplete denaturation will further reduce the amount of protein which can bind to the antibody. One possible solution to this could be to use a native gel so that linearization of the protein is not necessary to detect the presence of the subunits, avoiding a reduction in viable protein for antibody binding.

2.4.4 GluK2 shRNA lentivirus did not to reduce production of GluK2 in EndoC-βH1 or INS-1 cells

GluK2 shRNA lentiviral knock down of GluK2 was attempted in both EndoC-βH1 and INS-1 cell lines. Despite successfully producing viruses which infected both

cell lines (Figure 2.10 and Figure 2.13) there was no reduction in GluK2 production in either cell line (Figure 2.11 and Figure 2.14). The EndoC-βH1 cell line is very slow growing and has a doubling time of 174 hours (Andersson et al., 2015). It was therefore possible that the GluK2 shRNA virus could not reduce protein production of GluK2 because GluK2 was trafficked back into the cell at a much slower rate than in other cell lines. Proteins which have a slow turnover will not be affected by shRNA targeted knockdown as quickly and effectively as higher turnover proteins (Wu et al., 2004). To encourage GluK2 protein recycling and clear GluK2 receptors which had formed on the cell-surface before lentivirus infection, EndoC-βH1 cells were treated with 25 µM, 50 µM or 100 µM kainate at the time of viral infection and then again 72 hours after infection. However, this did not result in any changes in GluK2 protein production (Figure 2.12). It is also possible that the GluK2 shRNA virus designed for targeting of EndoC-βH1 cells had a problem with the H1 promoter region, which is responsible for driving RNA polymerase III to transcribe the shRNA sequence inside the cell. If the H1 promoter region was ineffective then the virus cannot induce the production of GluK2 targeted shRNA and a reduction in GluK2 protein would not be possible. One study recommended that multiple promoters are used to produce more reliable and effective gene silencing (Lambeth et al., 2010) and would be utilised in future experiments to try to improve GluK2 knock down. It should also be noted that out of the three shRNA sequences attempted only one virus was successfully made to target GluK2 in EndoC-βH1 cells. The literature recommends that a minimum of two different viruses be used to try and improve the chances of a successful knock down (Moore et al., 2010), but due to time constraints it was not possible design and try a fourth sequence.

Designing shRNA for protein knockdown is difficult as there is no guarantee of gene silencing for a given shRNA sequence until it has been experimentally tested and proven, as such it can be a very time consuming process, which despite using multiple shRNA sequences can still result in failure to knockdown the protein target. It was therefore hoped that using GluK2 shRNA viruses which were a gift from the University of Bristol and had previously been shown to effectively reduce GluK2 protein production in rodent neuronal cells (Appendix III) would be similarly effective in INS-1 cells. However, as previously noted the two viruses used in INS-1 cells showed no reduction in GluK2 protein production. This may have been due to the different cell types which were used as one study has reported that the target gene abundance is a determining factor on the efficiency of the knockdown (Hong et al., 2014). It is possible that GluK2 protein is more abundant in neurons compared to INS-1 cells and may explain why successful shRNA knockdown of GluK2 in neuronal cells may not be translated in the INS-1 cell line.

2.4.5 EndoC-βH1 cells show increased insulin secretion in response to stimulatory glucose

After numerous unsuccessful attempts to knock down GluK2 using shRNA lentivirus, it was decided instead to use various GluR agonists and antagonists, to determine GluRs role in insulin secretion. Before using EndoC-βH1 cells to assess KAR function in relation to insulin secretion it was important to establish that EndoC-βH1 cells were responding to glucose. EndoC-βH1 cells showed a significant two-fold increase in insulin secretion when treated with 20 mM glucose, compared with cells treated with 0.5 mM glucose (Fig.2.16). This is comparable to other published data which observe between 2- and 3-fold

increase in insulin secretion after high glucose treatment (Giorgio et al., 2019; Hastoy et al., 2018; Tsonkova et al., 2018). However, other studies have reported a smaller response to glucose with only a roughly 1.5 fold increase in insulin secretion when treated with stimulatory glucose concentrations (Krizhanovskii et al., 2017; Oleson et al., 2015). During the study it was observed that the EndoC-βH1 cells did not consistently respond to glucose and as such any experiments conducted where there was a less than 1.3-fold increase in insulin secretion at a stimulatory glucose level compared to non-stimulatory glucose level were not included. As a result, any future studies conducted with this cell line should have a successful GSIS prior to any experiments being carried out. This is to ensure that the EndoC-βH1 cells have a phenotype which is appropriate for studies using human β-cells and can secrete insulin in response to stimulatory glucose concentrations. Some recent studies have suggested that changes in media and growing EndoC-βH1 cells as pseudoislets improves their GSIS (Krizhanovskii et al., 2017; Teraoku and Lenzen, 2017) and should therefore also be taken into consideration when planning future experiments with this cell line. EndoC-βH1 cells did, however, consistently respond to treatment with stimulatory glucose and IBMX, showing a five-fold increase in insulin secretion compared to 0.5 mM glucose (Figure 2.17).

2.4.6 <u>KAR activation increases GSIS in EndoC-βH1 cells</u>

The present study has demonstrated for the first time that GSIS from EndoC-βH1 cells is enhanced by 25 µM kainate in combination with 20 mM glucose and resulted in a significant increase in insulin secretion compared to cells treated with 20 mM glucose alone (p = 0.034; Figure 2.18). There was, however, no significant differences in insulin secretion when cells were treated with 25 µM

kainate and 0.5 mM glucose (Figure 2.19), compared to cells treated with 0.5 mM glucose only. These results are comparable to studies which demonstrated that extracellular glutamate can enhance GSIS when murine pancreatic islets are treated with stimulatory glucose, but has no effect on basal insulin secretion (Bertrand et al., 1992; Wu et al., 2012). A further study observed that isolated rat islets showed increased insulin secretion when treated with kainite at varying concentrations (0.01, 0.1 and 1 mM) and 8.3 mM glucose (Inagaki et al., 1995). Conversely to the current study, Gonoi *et al.*, 1994, observed that kainate stimulated insulin secretion in MIN6 cells at non-stimulatory glucose levels. However, Gonoi *et al.*, 1994, used 0.5 mM kainate and at this concentration is known to activate AMPARs (Lee et al., 2004) as well as KARs, so it may be that the increased insulin secretion observed was due to AMPAR activation and not KARs. Another conflicting study reported that kainate (0.5 mM) resulted in no significant increase in GSIS in rat islets in the presence of either 3.3 mM, 8.3 mM or 16.7 mM glucose (Molnár et al., 1995), demonstrating the variability of results seen in rat islets and murine cell lines. The current study has importantly elucidated the response of human β-cells to kainate.

Pre-incubation of EndoC-βH1 with the AMPAR and KAR specific antagonist, NBQX, blocked kainate induced insulin secretion in the presence of stimulatory glucose concentrations (Figure 2.18), confirming that activation of GluRs potentiates insulin secretion. To ensure that increased insulin secretion was as a result of KAR activation and not AMPARs, EndoC-βH1 cells were also pre-incubated with the AMPAR specific antagonist GYKI-52466 before treatment with kainate and stimulatory glucose concentrations. Blocking of AMPARs with GYKI-52466 did not prevent kainate induced insulin secretion (Figure 2.18), thus

confirming that increased insulin secretion was as a result of KAR activation and not AMPARs.

In the CNS, KARs can exert both ionotropic and metabotropic functions involving G-proteins and second messengers (Marshall et al., 2018; Petrovic et al., 2017). The current study therefore investigated if insulin secretion in EndoC-βH1 cells could be potentiated further by pre-treating cells with the mGluR1 receptor agonist, DHPG. However, no significant change was observed between cells pre-treated with DHPG prior to treatment with kainate and 20 mM glucose compared to cells treated with kainate and 20 mM glucose alone. This result is similar to that seen in a study which treated MIN6 cells with DHPG and 25 mM glucose and found no difference in insulin secretion compared to control (Brice et al., 2002). However, the Brice *et al.*, 2002 also reported that DHPG did cause a significant increase in insulin secretion when the cells were in the presence of non-stimulatory glucose. It has been shown that mGluR activation can potentiate iGluR activity (Wallis et al., 2015), however, in neuronal cells both mGluRs and iGluRs exert their effects on many of the same downstream targets such as Ca^{2+} influx and PKA (Reiner and Levitz, 2018). It may therefore, be that pre-treatment of EndoC-βH1 cells with DHPG to activate mGluR1 does not enhance insulin secretion compared to treatment with stimulatory glucose concentrations and kainate alone because mGluR1 and KARs are acting upon the same downstream targets which are already exerting a physiologically saturated response by the effects of DHPG and cannot be exacerbated further by activation of KARs. Future experiments using a range of glucose levels and DHPG treatment without kainate could be done to confirm if mGluR activation can increase insulin secretion.

As discussed in section 1.3, insulin secretion is triggered by the depolarisation of the β-cell through the influx of Ca^{2+} through VDCC's (Nirmalan and Nirmalan, 2017). Within neurons, activation of KARs similarly allows the influx of Ca^{2+} ions to induce excitatory synaptic transmission (Falcón-Moya et al., 2018; Mayer, 2017; Zhu and Gouaux, 2017). KARs may therefore potentiate GSIS by being activated by an increase in extracellular glutamate in the blood following a glutamate-rich meal and consequently allow further influx of Ca^{2+} ions (Figure 2.24). Several studies have also found that activation of iGluRs regulates glucose import through enabling the trafficking of Gluts to the cell surface of neuronal cells (Ferreira et al., 2011; Saab et al., 2016) and therefore may aid insulin secretion via a similar manner in pancreatic β-cells. Finally, KARs are known to exert mGluR effects in neuronal cells by activating PKA, leading to increased glutamate release (Falcón-Moya et al., 2018). If KARs within β-cells can activate PKA it would also explain how activation of KARs leads to increased insulin secretion as PKA activation is directly linked to insulin secretion (Tomas et al., 2019) (Figure 2.24).
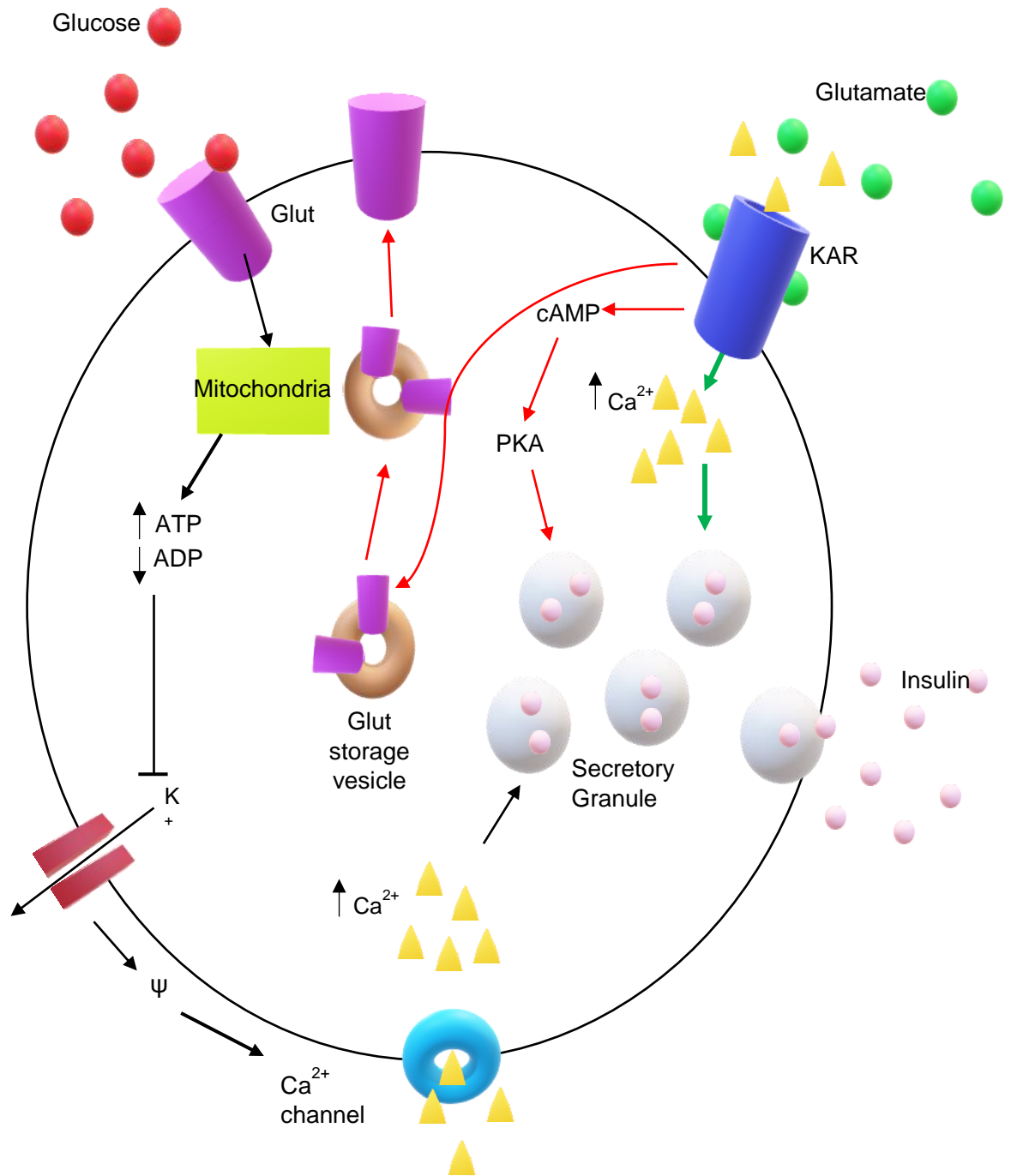
Figure 2.24. Mechanism of potentiated glucose-stimulated insulin secretion from a pancreatic β-cell by KAR activation. Glucose is transported into the β-cell via the glucose transporter (Glut). Once inside the cell, glucose undergoes glycolysis to produce pyruvate which can be utilised by the mitochondria in the tricarboxylic acid (TCA) cycle. The TCA cycle causes increased levels of adenosine triphosphate (ATP) and decreased adenosine diphosphate (ADP).

Increased ATP then causes ATP-sensitive K^+ channels to close, resulting in a decreased membrane potential (Ψ) and activation of voltage-dependent Ca^{2+} channels (VDCCs), allowing the influx of Ca^{2+}. Simultaneously extracellular glutamate from the blood activates KARs, resulting in a further influx of Ca^{2+} and a further decrease in membrane potential. Membrane depolarisation triggers the formation of insulin containing secretory granules (SG) from the RRP and the RP. KARs exert metabotropic effects by increasing cAMP which in turn activates PKA. PKA then further perpetuates the formation of insulin containing SGs. Simultaneously KAR activation promotes the trafficking of Gluts to the cell surface. Finally, insulin is released from the β-cell via SGs. KARs proposed ionotropic effects on insulin secretion are shown by green arrows and metabotropic effects are shown by red arrows.

2.4.7 High glucose induces cell surface translocation of GluK2 in EndoC-βH1 cells

Cell surface biotinylation experiments in the current study have established that the surface expression of GluK2 is significantly increased in EndoC-βH1 cells in response to glucose stimulation (Figure 2.20 and 2.21a). However, the total GluK2 level showed no significant difference between stimulatory and non-stimulatory glucose conditions (Figure 2.21b). Figure 2.20 demonstrates that in non-stimulatory glucose conditions KAR surface expression is very low and as a result of this, it would be expected that activation of KARs by agonists would have very little physiological effects as there are few KARs being expressed on the surface for the agonist to interact with. These results therefore further support the current studies finding that EndoC-βH1 cells in non-stimulatory glucose treated with kainate are unable to induce increased insulin secretion (Figure 2.19) and it is unsurprising that kainate and non-stimulatory glucose was unable to induce insulin secretion as there are so few surface KARs being expressed. It may be that EndoC-βH1 cells only express KARs in stimulatory glucose conditions in order to prevent unwanted activation of the β-cells and subsequent release of insulin, helping to maintain glucose homeostasis by only allowing insulin secretion when blood glucose levels are high. A further study using kidney cells also observed that high glucose caused an increase in iGluR expression (Roshanravan et al., 2016). However, a study using a diabetic rat model resulting in hyperglycaemia resulted in a significant reduction in GluK2/3 protein levels in the retina after 12 weeks of diabetes (Santiago et al., 2009), suggesting that chronic exposure to stimulatory glucose may results in reduced iGluR expression. Further studies exposing EndoC-βH1 cells to stimulatory glucose over varied time

points to show both chronic and short incubation would help to elucidate how over long periods stimulatory glucose can affect GluK2 expression.

Treating EndoC-βH1 cells with high glucose and IBMX did not result in any significant changes in either surface or total expression of GluK2 (Figure 2.20 and 2.22). This result was surprising as it was expected that IBMX would further increase GluK2 surface expression as it activates PKA to induce insulin secretion, a pathway which is hypothesised to be associated with KAR metabotropic activity within β-cells (Figure 2.24). However, despite having downstream effects on the PKA pathway, within neuronal cells KAR trafficking to the cell surface is independent of the PKA pathway (Martin and Henley, 2004; Sun et al., 2014). If KARs in β-cells behave in a similar manner to neuronal KARs then induction of the PKA pathway will not induce KARs to be exocytosed to the β-cell surface and it is therefore not surprising that there was no difference in GluK2 surface expression between β-cells treated with 20 mM glucose and cells treated with 20 mM and IBMX. Other studies have also noted that KAR expression and activation are dependent upon the strength of the stimulus used and have shown that low to moderate stimulation increased KAR synaptic transmission but strong stimulation decreased synaptic transmission (González-González and Henley, 2013; Schmitz et al., 2003). β-cells treated with IBMX induces a response which is much larger than is physiologically normal for the cells, as such it may have the effect of preventing KAR surface expression, rather than increasing it, as is seen with neuronal cells when given a strong stimulus. This may further explain why IBMX failed to cause an increase in GluK2 surface expression.

To ensure that high glucose didn't cause upregulation of all β-cell surface proteins, the membranes used were attempted to be re-probed with either anti-

Cav2.1 or anti-Na,K-ATPase antibodies. Both Cav2.1 and Na, K-ATPase surface expression has previously been shown to be unaffected by changes in glucose concentrations (Huang et al., 2017). However, neither antibodies detected the proteins in the membrane fraction and therefore it could not be established if high glucose resulted specifically in upregulation of GluK2 or if it affected all surface proteins (Figure 2.23). Cav2.1 and Na, K-ATPase may not have been detected in the membrane fraction because the process of stripping membranes of the original primary and secondary antibody can result in loss of antigen for antibody to bind to (Bass et al., 2017). Due to the slow growing nature of the EndoC-βH1 cell line used the number of cells and therefore amount of membrane homogenate available to use was limited, as such the current study could not use a larger quantity of membrane protein to try and prevent total loss of Cav2.1 and Na, K-ATPase antigen in the membrane homogenate after stripping.

3 Detecting autoantibodies to iGluRs in serum from newly diagnosed patients with Type 1 Diabetes (T1D)

3.1 Background

As discussed in section 1.4.4, all currently known autoantibodies associated with T1D target intracellular proteins and are more likely to be a result of epitope spreading than a primary cause of the disease (McLaughlin et al., 2015). It is likely that there are more autoantibodies to be discovered which are associated with T1D, as some individuals have been shown to be islet cell autoantigen positive, but do not demonstrated immunoreactivity with any of the currently known T1D associated autoantibodies (Wenzlau and Hutton, 2013). It is possible that a currently unknown surface antigen is the first target for the immune system, leading to β-cell death and presentation of the already known intracellular autoantigens. Identification of novel cell surface immune targets could help to identify a trigger for the disease. One such immune target is GluRs, as they are transmembrane proteins with extracellular domains which could be the initial antigen targeted by the immune system in T1D. Furthermore, numerous autoantibodies targeting GluRs have already been associated with diseases of the CNS (section 1.11), providing evidence that targeting of these receptors can lead to and initiate disease (Dalmau et al., 2017; Geis et al., 2019). The current study therefore aimed to identify autoantibodies which target GluR subunits from T1D patient serum.

There are multiple methodologies for autoantibody detection, such as the previously recognised 'gold standard' in T1D research, radio-binding assays (RBA), which are both highly sensitive and specific (Lampasona et al., 2019). However, RBAs come with legislative and logistically issues due to the

unavoidable use of radiation for the assay. More traditional methods such as immunoblotting can be useful for screening of autoantibodies as the SDS-Page gel separates all proteins based on size and positive bands produced from serum autoantibodies can be directly analysed to see if they bind to proteins of a similar molecular weight as the proposed antigen target (Zampieri et al., 2000). Immunoblotting is frequently used for autoantibody detection (Banjara et al., 2017; Mørkholt et al., 2018) and is a cheap and simple method. Enzyme-linked immunosorbent assay (ELISA) is also commonly used as it allows high efficiency and high through-put of samples, however, developing new ELISAs can be arduous and time-consuming. ELISAs are also susceptible to reporting false positives (Sakamoto et al., 2018). Finally, cell-based immunofluorescent assays can be used to allow for the screening of confirmation-dependent autoantibodies and helps to prevent potential epitope sites from being altered or blocked by previous sample preparation (Gastaldi et al., 2017; Ricken et al., 2018). However, this method does not give any information on the size of the protein being targeted so any positive results need to be tested and confirmed using another technique, such as immunoblotting. The current study utilised both immunoblotting and cell-based assays to detect autoantibodies which target GluRs.

3.2 Materials and Methods

3.2.1 Materials

All materials can be found in section 2.2.1.

3.2.2 Methods

Culture of HEK293T cells is discussed in section 2.2.1, preparation of total cell lysates in section 2.2.4, separation of proteins on SDS-PAGE and immunoblotting are outlined in sections 2.2.8 – 2.2.10.

3.2.3 HEK293T transient transfection for immunocytochemistry

Before plating the HEK293T cells 13 mm round glass coverslips were placed into 24 well plates and coated with 100 µl poly-l-lysine (Sigma-Aldrich, Poole, UK) in PBS for 30 minutes. The coverslips were washed three times with PBS and HEK293T cells were seeded as described in section 2.2.1 onto the coverslips at a density of 1.25 x 10^5 cells per well and incubated at 37°C in humidified air and 5 % CO_2 for 24 hours.

Cells were then transiently transfected with GluK2, GluK5 (same as described in section 2.2.7), GluN1 or GluN1 plus GluN2B plasmids, as described previously (Köhr et al., 1994). For single transfections 500 ng DNA and 1.75 µg polyethylenimine (PEI) (Sigma-Aldrich, Poole, UK) was mixed in 100 µl Opti-MEM™ and incubated at room temperature for 20 minutes. For the co-transfection of GluN1 plus GluN2B, 100 ng GluN1 plasmid DNA and 400 ng GluN2B plasmid DNA was mixed with 1.75 µg PEI in 100 µl Opti-MEM. Following the incubation, the DNA-PEI-Opti-MEM solution was pipetted onto the HEK293 cells. Cells transfected with NMDAR subunits were also incubated with the NMDAR non-competitive antagonist, MK-801 (10 µM) (Bio-Techne, Abingdon,

UK) which was added to the media prior to transfection. Cells were incubated at 37°C in humidified air and 5 % CO_2 for 48 hours before cells were fixed for immunocytochemistry.

3.2.4 <u>Immunocytochemistry of HEK293T cells</u>

Forty-eight hours after transfection the cells were washed three times with 500 µl sterile PBS and then fixed with 250 µl ice cold 100 % methanol for 5 – 10 minutes. Next, the cells were washed again with PBS for 5 minutes, followed by incubation with 100 mM Glycine in PBS (pH8.5) for 5 minutes and finally with 10 % FBS in PBS for 5 minutes. After which the cells were washed twice with PBS. The HEK293T cells were then permeabilised with 0.2 % Triton X-100 in PBS for 20 minutes at room temperature. Cells were washed three times with PBS and blocked in 3 % BSA in PBS for 15 minutes. Primary antibodies were added to 3 % BSA, at dilutions shown in Table 3.1 and incubated with the cells for 1 hour at room temperature. Cells were then washed three times with PBS before incubating for 30 minutes in darkness with the fluorescent secondary antibody diluted in 3 % BSA (dilutions used in Table 3.1). Finally, cells were washed three times with PBS, ensuring the cells remained in the dark. The coverslips were then mounted onto slides using DAKO fluorescence mounting medium (Agilent Technologies LDA, Stockport, UK) containing 300 nM DAPI.

Table 3.1. Table of Antibodies used for immunohistochemistry detection of GluR subunit autoantibodies from patient serum.

Antibody	Species Specificity	Source	Concentration/ Dilution	Supplier	Secondary Antibody
Anti-GluR6/7 (aka GluK2/3) (04-921)	H, R	Rabbit	0.025 µg/ml	Millipore UK Limited	0.4 µg/ml Anti-Rabbit Alexa Fluor 568 (10032302, Fisher Scientific, Loughborough, UK)
Anti-GRIK5 (06-315)	R, Rb	Rabbit	0.1 µg/ml	Millipore UK Limited	0.4 µg/ml Anti-Rabbit Alexa Fluor 568 (10032302, Fisher Scientific, Loughborough, UK)
Anti-NMDAR1 (#5704) (aka GluN1)	H, M, R	Rabbit	0.295 µg/ml	Cell Signalling Technology ®	0.4 µg/ml Anti-Rabbit Alexa Fluor 568 (10032302, Fisher Scientific, Loughborough, UK)
Anti-NMDAR2 B (AB1557P) (aka GluN2B)	H, R	Rabbit	0.2 µg/ml	Millipore UK Limited	0.4 µg/ml Anti-Rabbit Alexa Fluor 568 (10032302, Fisher Scientific, Loughborough, UK)
Human Serum	-	-	1:100	Gifted by Cardiff University	0.04 µg/ml Anti-Human Alexa Fluor 488 (10226402, Fisher Scientific, Loughborough, UK)

3.2.5 Details of T1D patients and healthy controls

Forty newly diagnosed T1D patient serum and forty age-matched healthy control serum were obtained by University Hospital of Wales (Wales, UK). All T1D patient serum were positive for at least one T1D associated autoantibody. Details of the T1D patients and age-matched healthy controls is shown in Table 3.2.

Table 3.2. Patient serum sample ID, gender and age of serum samples used for GluR autoantibody detection. 40 newly diagnosed T1D patient serum were obtained by University Hospital of Wales (Wales, UK), along with 40 gender and age-matched healthy control serum samples to be used for GluR autoantibody detection.

T1D Patient Serum			Healthy Control Serum		
Sample ID	Gender	Age	Sample ID	Gender	Age
ND603	F	39	1	F	39
ND604	M	38	2	M	38
ND605	M	44	3	M	44
ND607	F	40	4	F	40
ND609	F	47	5	F	47
ND614	F	29	6	F	29
ND615	F	37	7	F	37
ND637	F	45	8	F	45
ND638	F	43	9	F	43
ND650	M	46	10	M	46
ND662	F	48	11	F	48
ND674	M	47	12	M	47
ND675	F	38	13	F	38
ND490	M	46	14	M	46
ND488	F	29	15	F	29
ND450	M	50	16	M	50
ND419	F	50	17	F	50
ND517	M	40	18	M	40
ND522	F	42	19	F	42
ND530	M	29	20	M	29
ND534	M	35	21	M	35
ND548	F	30	22	F	30
ND568	M	48	23	M	48
ND398	M	47	24	M	47
ND358	F	42	25	F	42
ND397	M	48	26	M	48
ND557	M	43	27	M	43
ND456	M	39	28	M	39
ND455	M	45	29	M	45
ND365	F	52	30	F	52
ND667	M	44	31	M	44
ND512	F	46	32	F	46
ND596	F	42	33	F	42
ND494	F	47	34	F	47
ND507	M	51	35	M	51
ND480	M	50	36	M	50
ND533	M	42	37	M	42
ND609	F	47	38	F	47
ND366	F	47	39	F	47
ND541	M	50	40	M	50

3.2.6 Fluorescence imaging

GluK2 and GluK5 slides were imaged on Nikon Eclipse TE300 inverted microscope and GluN1 and GluN1/GluN2B slides were imaged on Nikon E80i Fluorescence Photomicroscope. Five representative images were taken of each slide and autoantibody staining was scored from 0 to 4, as described previously (Leite et al., 2008). Table 3.3 outlines the scoring system used.

Table 3.3. Outline of autoantibody scoring system used with patient serum samples, adapted from Leite et al., 2008.

Score	Description
0	No labelling of GluR subunit expressing cells by serum samples.
0.5	Very weak labelling of very few GluR subunit expressing cells with no co-localisation with the commercial GluR subunit antibody staining.
1	Weak labelling of some of the GluR subunit expressing cells with co-localisation with the commercial GluR subunit antibody staining.
2	Moderate labelling of some (~20 – 50 %) of GluR subunit expressing cells, with precise co-localisation with the commercial GluR subunit antibody staining.
3	Moderate/strong labelling of ~50 – 80 % of GluR subunit expressing cells, with perfect co-localisation with the commercial GluR subunit antibody staining.
4	Strong labelling of virtually all GluR subunit expressing cells, with perfect co-localisation with the commercial GluR subunit antibody staining.

3.3 Results

3.3.1 Detection of autoantibodies using immunoblots

Ionotropic glutamate receptors (iGluRs) could be extracellular targets for the immune system in T1D, leading to destruction of insulin producing β-cells. To investigate this HEK293T cells over expressing iGluR subunits cell lysate was run on SDS-PAGE gel (Methods section 3.2.2). Sera from newly diagnosed T1D patients and healthy controls (Table 3.2) were then used to detect GluK2 or GluK5 autoantibodies with the HEK293T cell system, described above (Methods section 3.2.2). To ensure that HEK293T cells were overexpressing GluK2/GluK5 and GluK2 or GluK5 protein was produced, immunoblot analysis was carried out using commercial GluK5 and GluK2/3 specific primary antibodies (Merck Millipore, Watford, UK; Figure 3.1). This sample was used as a positive control to ensure that the cell lysate contained GluK2 or GluK5 protein which could be detected by antibodies. In total, 27 serum samples were tested, 14 from T1D patients and 13 from healthy controls (Figure 3.2 and 3.3). All serum samples tested showed many non-specific bands, which did not allow identification of positive reactions. Serum samples which appeared to show immuno-reactivity at the expected size also showed the same bands in the non-transfected HEK293T cell lysate used as a negative control. In conclusion, it was not possible to establish if T1D serum contained GluK2 or GluK5 autoantibodies using this approach.
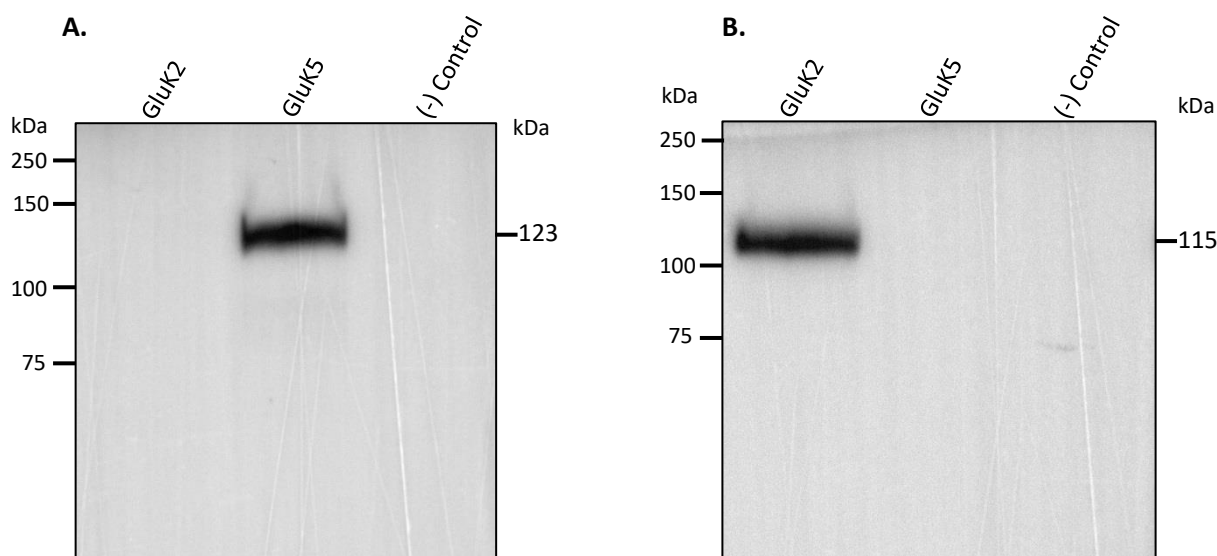
Figure 3.1. GluK2 and GluK5 proteins produced by HEK293T cells following transient transfection. Total cell homogenates from HEK293T cells overexpressing GluK5 (A) or GluK2 (B) were prepared. Proteins (40 µg per lane) were separated by SDS-PAGE and transferred to immobilon membranes (Method section 3.2.2). Untransfected HEK293T cell homogenate was used as a negative control (- Control). Immunoblots were probed with a commercial rabbit polyclonal anti-GluR6/7 antibody (0.125 µg/ml; Millipore UK Limited) to detect GluK2 protein or a commercial rabbit polyclonal anti-GRIK5 antibody (1 µg/ml; Millipore UK Limited) to detect GluK5 protien overnight at 4°C. Immunoblots were then probed with a secondary anti-rabbit IgG antibody (0.08 µg/ml; Sigma-Aldrich®) for 1 hour. Immunoblots were imaged by chemiluminescence using the Odessy® Fc (Li-Cor Biosciences, Cambridge, UK) Imaging System. The molecular weight markers (Bio-Rad®) are shown on the left in kilodaltons (kDa). The expected size of the overexpressed GluK2 and GluK5 is indicated on the right. Figure is representative of three independent experiments.
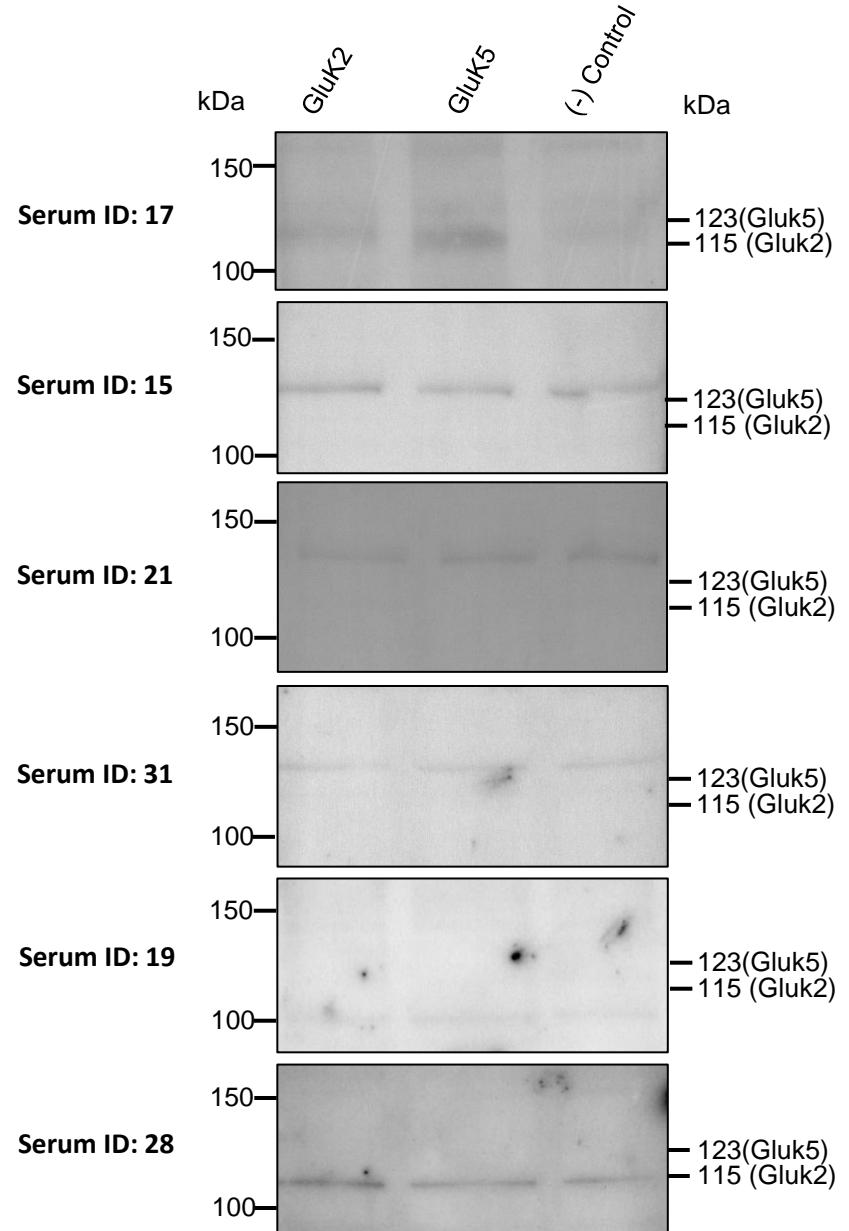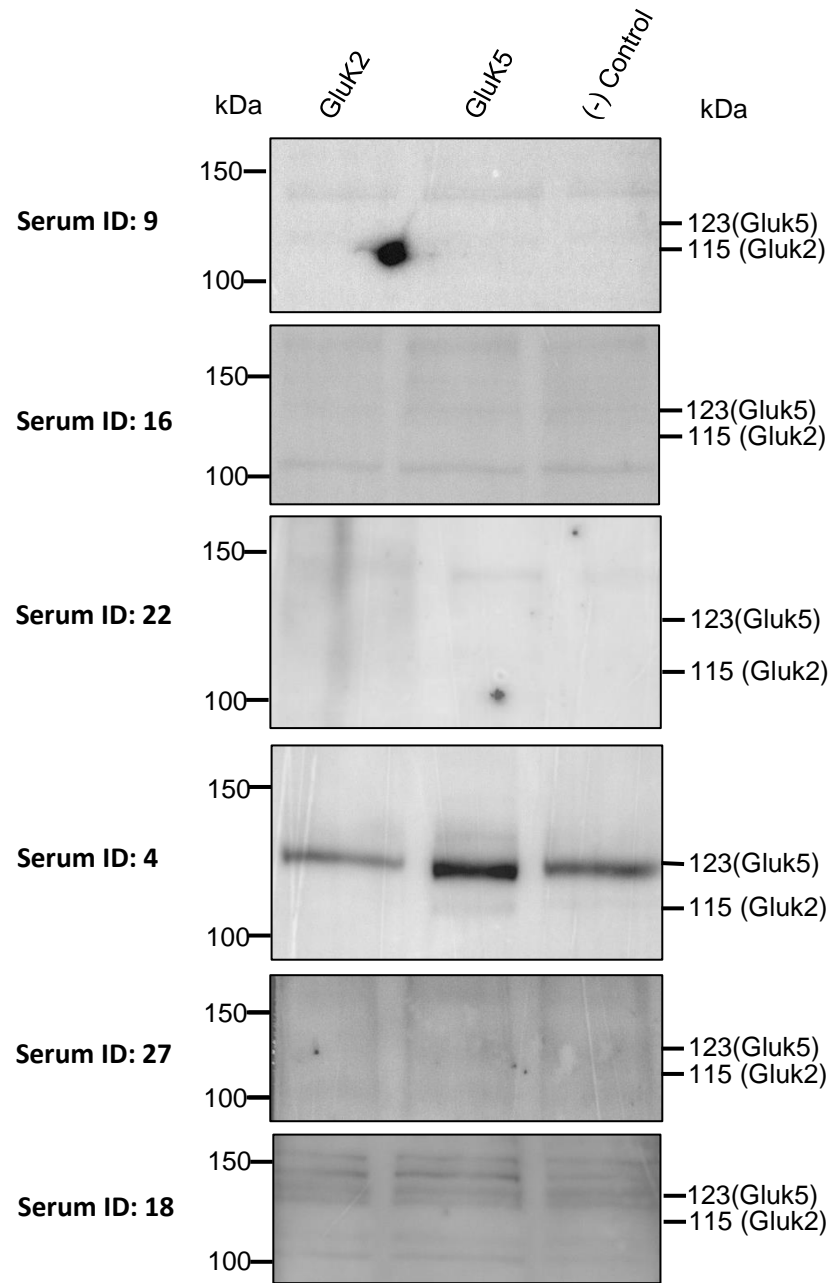
Figure 3.2. Detection of GluK2 and Gluk5 using healthy control serum by immunoblots. Homogenates from HEK293T cells producing GluK2 or GluK5 proteins were prepared. Proteins (40 µg per lane) were separated by SDS-PAGE and transferred to immobilon membranes (Method section 3.2.2). Cell homogenates from untrasfected HEK293T cells were used as a negative control ((-) control). Immunoblots were probed with healthy control serum (1:200 dilution) overnight at 4°C. Immunoblots were then probed with a commercial secondary anti-human IgG antibody (0.55 µg/ml; Sigma-Aldrich®) for 1 hour. Immunoblots were imaged by the enhanced chemiluminescence detection system and Syngene gel imaging and analysis system (Syngene, Cambridge, UK). The serum sample ID is indicated on the let (Table 3.2 for sample details), along with the molecular weight markers (Bio-Rad®) in kilodaltons (kDa). The expected size of GluK2 and GluK5 is indicated on the right. Figure is representative of one independent experiment.
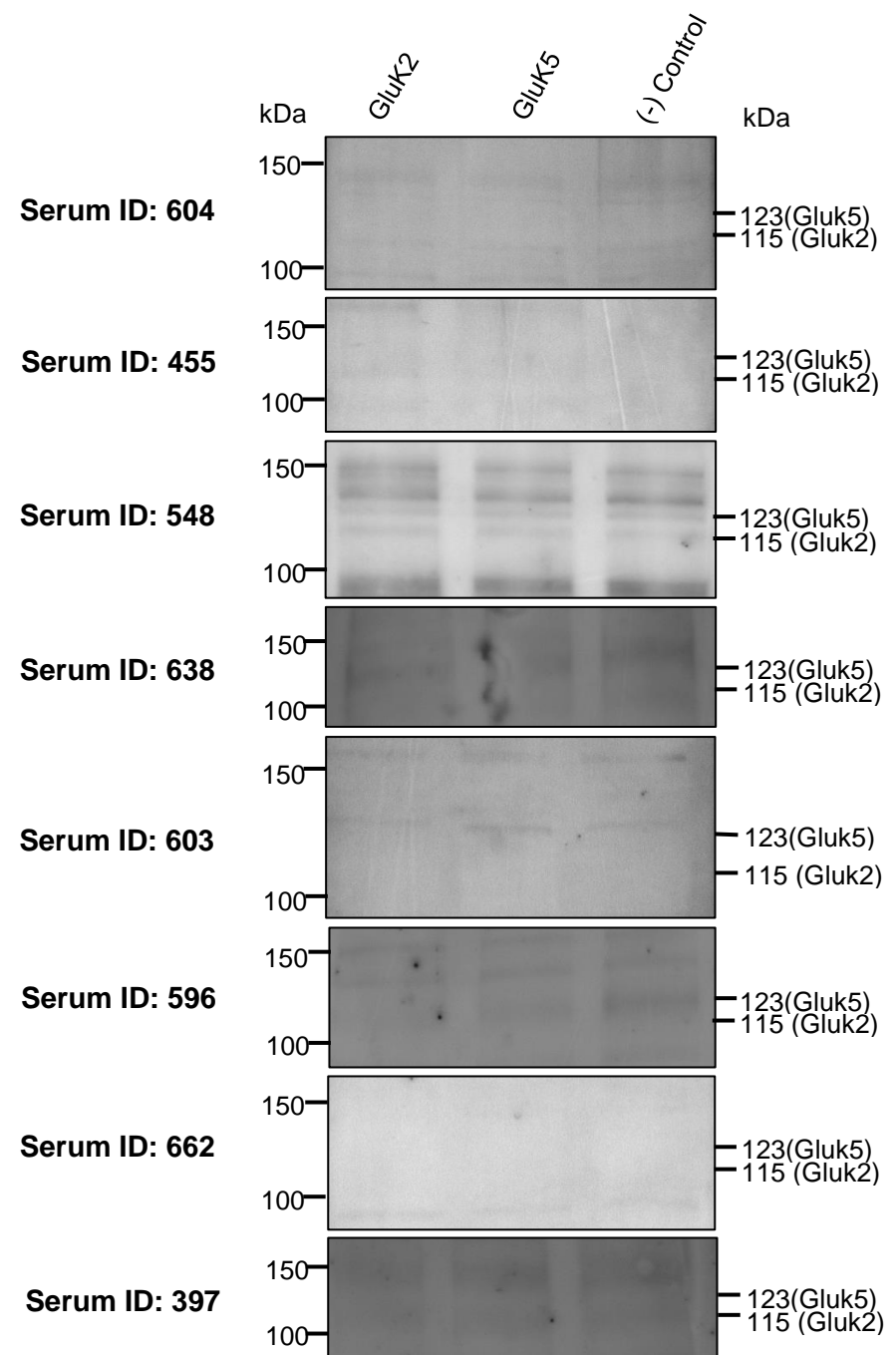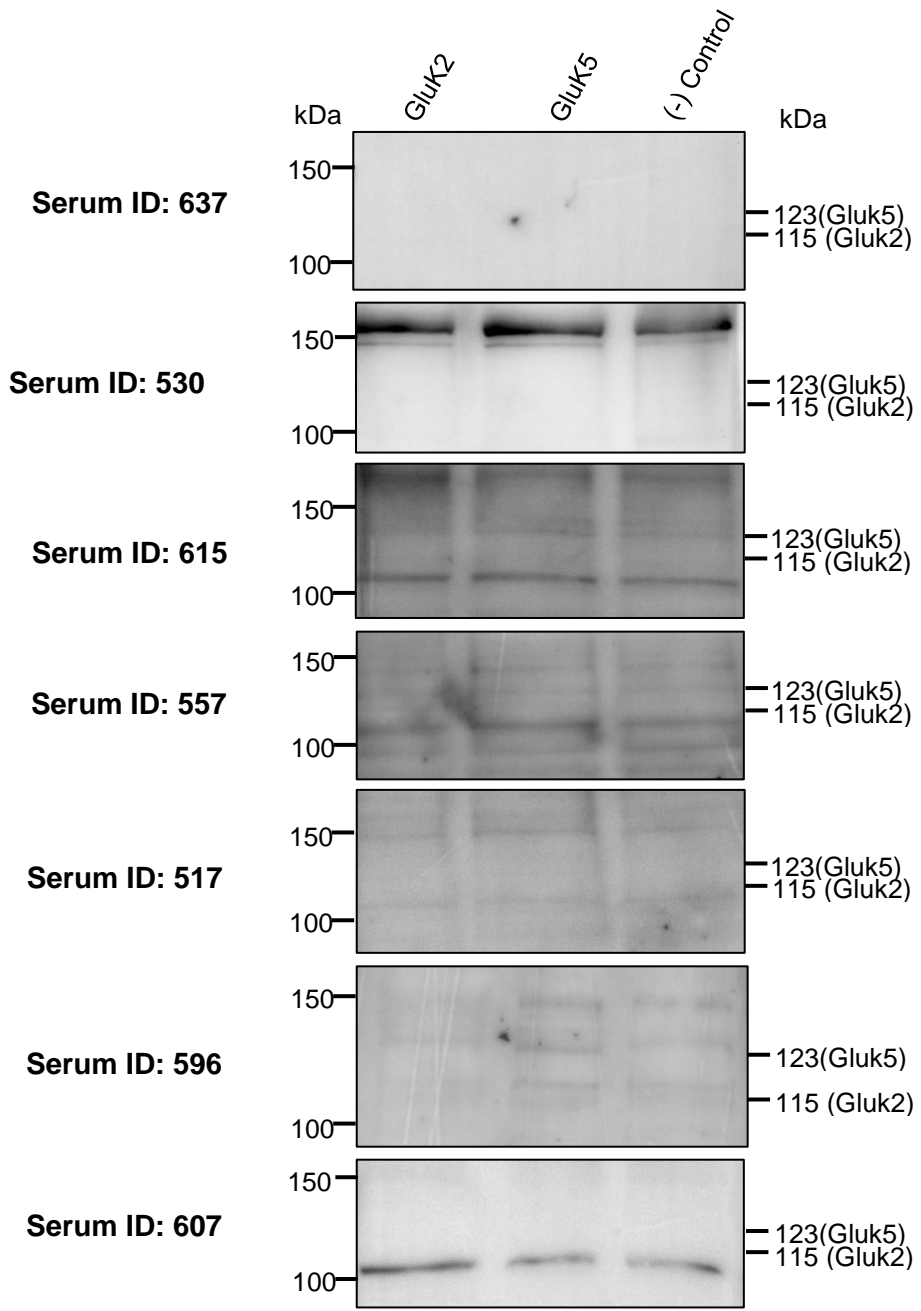
Figure 3.3. Detection of GluK2 and Gluk5 using T1D patient serum by immunoblots. Homogenates from HEK293T cells producing GluK2 or GluK5 proteins were prepared. Proteins (40 µg per lane) were separated by SDS-PAGE and transferred to immobilon membranes (Method section 3.2.2). Cell homogenates from untrasfected HEK293T cells were used as a negative control ((-) Control). Immunoblots were probed with T1D patient serum serum (1:200 dilution) overnight at 4°C. Immunoblots were then probed with a commercial secondary anti-human IgG antibody (0.55 µg/ml; Sigma-Aldrich®) for 1 hour. Immunoblots were imaged by the enhanced chemiluminescence detection system and Syngene gel imaging and analysis system (Syngene, Cambridge, UK). The serum sample ID is indicated on the let (Table 3.2 for sample details), along with the molecular weight markers (Bio-Rad®) in kilodaltons (kDa). The expected size of GluK2 and GluK5 is indicated on the right. Figure is representative of one independent experiment.

3.3.2 Glutamate receptor autoantibodies are not more frequently observed in T1D patient serum than in healthy controls

Cell-based assays have been shown to be an effective method to detect glutamate receptor autoantibodies from patient serum (van Coevorden-Hameete et al., 2016; Park et al., 2018). In addition, cell-based assays allow for screening of conformation-dependent antibodies and helps to prevent potential epitope sites from being altered or obscured by sample preparation (Gastaldi et al., 2017; Ricken et al., 2018). It was therefore decided to perform a cell-based assay to detect GluR autoantibodies.

To ensure that transfected HEK293T cells were over-expressing GluK2, GluK5, GluN1 or GluN1 and GluN2B (Methods section 3.2.2), cells were incubated with anti-GluK2 (Figure 3.4), anti-GluK5 (Figure 3.5), anti-GluN1 (Figure 3.6) or both anti-GluN1 and anti-GluN2B (Figure 3.5) commercial antibodies and probed with anti-rabbit IgG Alexa Flour 488 antibody (Sigma-Aldrich), as described in the Methods section 3.2.4. The transfection efficiency was then calculated from 4 randomly selected areas. GluK2, GluK5 and GluN1 transiently transfected cells had a transfection efficiency of 44% (±10.7% SD), 39% (±24.7% SD) and 36% (±14.4% SD), respectively. Finally, GluN1 and GluN2B co-transfected cells had a transfection efficiency of 31% (±9% SD) for GluN1 and 26% (±4.5% SD) for GluN2B (Figure 3.7).

To optimise the assay and evaluate the dilution of secondary antibody used, HEK293T were incubated with human serum (1:20 or 1:100 dilution) for 1 hour and probed with an anti-human IgG Alexa Flour 488 antibody in a range of dilutions (Sigma-Aldrich, Poole, UK; 2.67 – 0.04 µg/ml) (Methods section 3.2.3). There was minimal background fluorescence when 0.04 µg/ml secondary

antibody was used and still allowed visualisation of any serum autoantibody staining (Figure 3.8. and 3.9). All of the other dilutions produced very high background which would make it impossible to detect specific autoantibody staining. It was therefore decided to use 0.04 µg/ml of the secondary anti-human IgG Alex Flour 488 antibody (Sigma-Aldrich, Poole, UK). Previous studies have detected autoantibodies with patient sera diluted 1:100 (Irani et al., 2010; Vincent et al., 2018) and a further study recommended that 1:100 dilution of serum is the minimum dilution used for a similar cell-based assay (Chen and Chang, 2018) hence, this dilution was used for the current study.
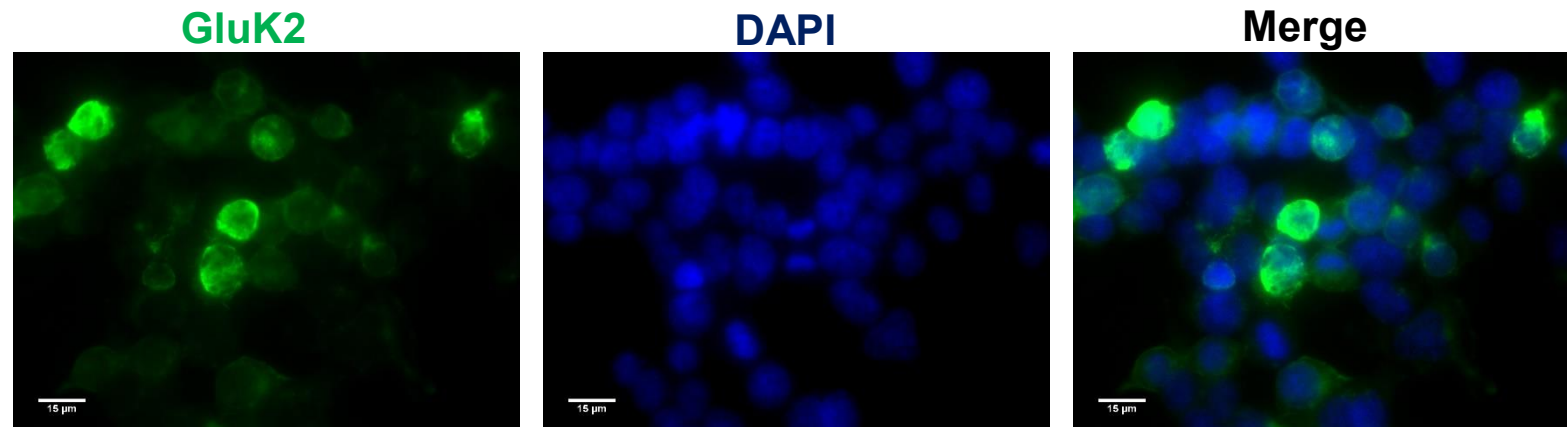
Figure 3.4. HEK293T cells over-express GluK2 protein when transiently transfected with GluK2 plasmid DNA. HEK293T cells were grown in 24 well plates on coverslips for 24 hours and then transfected with 500 ng GluK2 plasmids (Methods section 3.2.3) and incubated for a further 48 hours. Transfected HEK293T cells were then fixed with 100 % methanol and permeabilised with 0.2 % Triton X-100 in PBS. A rabbit polyclonal anti-GluK2/3 antibody (0.025 µg/ml; Millipore UK Limited) in 0.3 % BSA in PBS was incubated with the transfected HEK293T cells for 1 hour. After 1 hour the cells were washed with PBS and probed with Anti-Rabbit Alexa Flour 568 (0.4 µg/ml; Fisher Scientific, Loughborough, UK) 0.3 % BSA for 30 minutes. The slides were then mounted with DAKO fluorescence mounting medium (Agilent Technologies LDA, Stockport, UK) with 300 nM DAPI and visualised with Nikon Eclipse TE300 inverted microscope (magnification x 40) and scored (Methods section 3.2.6). GluK2 transfected HEK293T cells are shown in green and cell nucleus DAPI staining is shown in blue. Transfection efficiency was calculated from 4 randomly selected regions. Scale bar represents 15 µM.
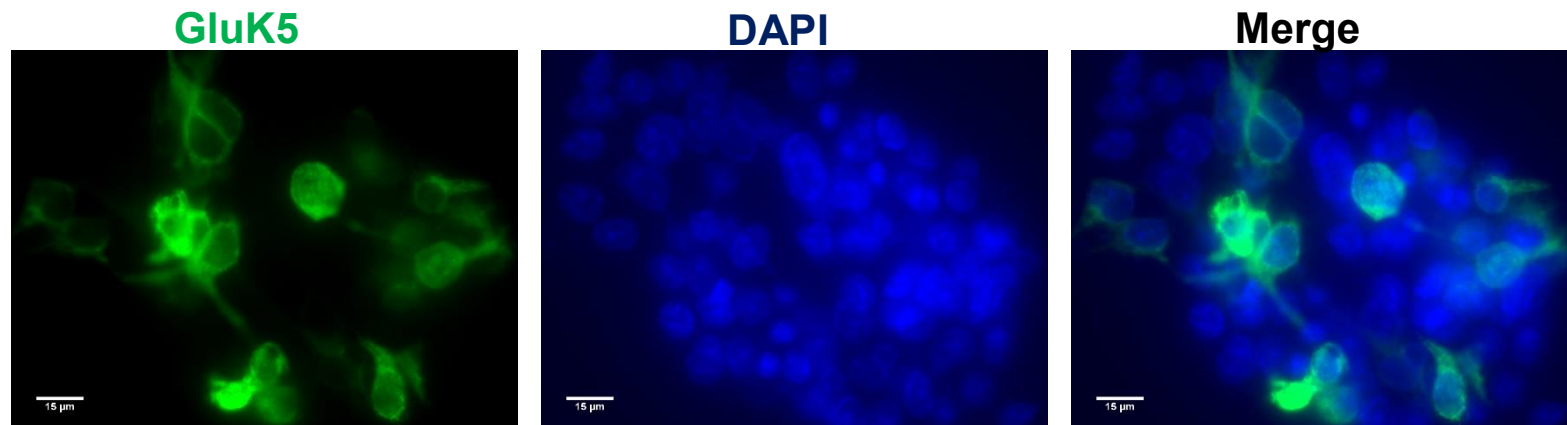
Figure 3.5. HEK293T cells over-express GluK5 protein when transiently transfected with GluK5 plasmid DNA. HEK293T cells

were grown in 24 well plates on coverslips for 24 hours and then transfected with 500 ng GluK5 plasmid (Methods section 3.2.3) and

incubated for a further 48 hours. Transfected HEK293T cells were then fixed with 100 % methanol and permeabilised with 0.2 % Triton

X-100 in PBS. A rabbit polyclonal anti-GRIK5 antibody (0.1 µg/ml; Millipore UK Limited) in 0.3 % BSA in PBS was incubated with the

transfected HEK293T cells for 1 hour. After 1 hour the cells were washed with PBS and probed with Anti-Rabbit Alexa Flour 568 (0.4

µg/ml; Fisher Scientific, Loughborough, UK) for 30 minutes. The slides were then mounted with DAKO fluorescence mounting medium

(Agilent Technologies LDA, Stockport, UK) with 300 nM DAPI and visualised with Nikon Eclipse TE300 inverted microscope

(magnification x 40) and scored (Methods section 3.2.6). GluK5 transfected HEK293T cells are shown in green and cell nucleus DAPI

staining is shown in blue. Transfection efficiency was calculated from 4 randomly selected regions. Scale bar represents 15 µM.
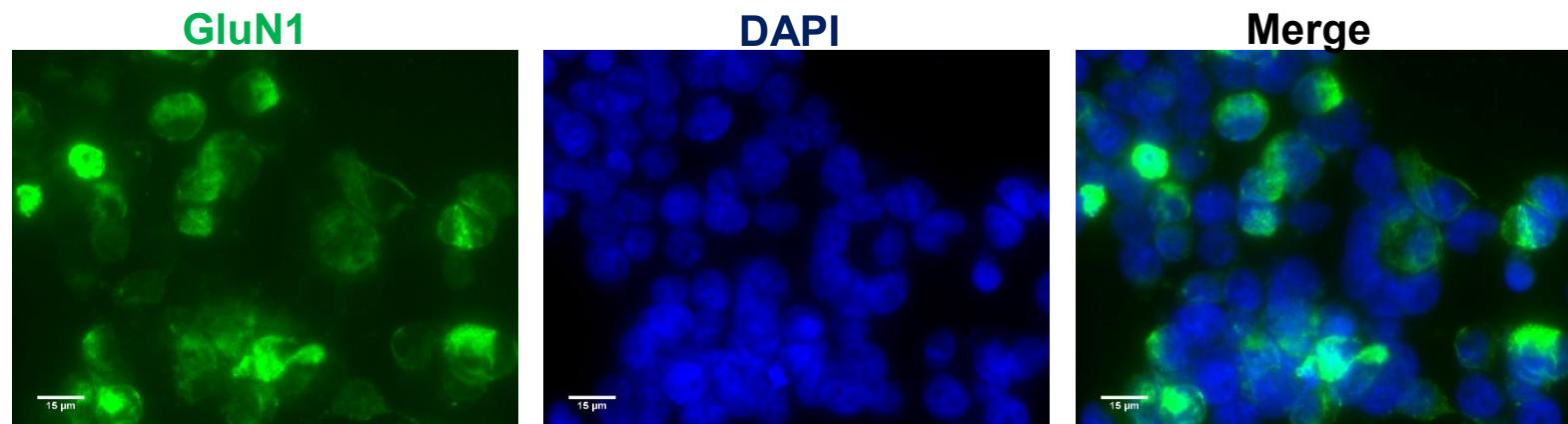
Figure 3.6. HEK293T cells over-express GluN1 protein when transiently transfected with GluN1 plasmid DNA. HEK293T cells were grown in 24 well plates on coverslips for 24 hours and then transfected with 500 ng GluN1 plasmid (Methods section 3.2.3) and incubated for a further 48 hours. Transfected HEK293T cells were then fixed with 100 % methanol and permeabilised with 0.2 % Triton X-100 in PBS. A rabbit polyclonal anti-NMDAR1 antibody (0.295µg/ml; Cell Signalling Technology®) in 0.3 % BSA in PBS was incubated with the transfected HEK293T cells for 1 hour. After 1 hour the cells were washed with PBS and probed with Anti-Rabbit Alexa Flour 568 (0.4 µg/ml; Fisher Scientific, Loughborough, UK) for 30 minutes. The slides were then mounted with DAKO fluorescence mounting medium (Agilent Technologies LDA, Stockport, UK) with 300 nM DAPI and visualised with Nikon Eclipse TE300 inverted microscope (magnification x 40) and scored (Method section 3.2.6). GluN1 transfected HEK293T cells are shown in green and cell nucleus DAPI staining is shown in blue. Transfection efficiency was calculated from 4 randomly selected regions. Scale bar represents 15 µM.
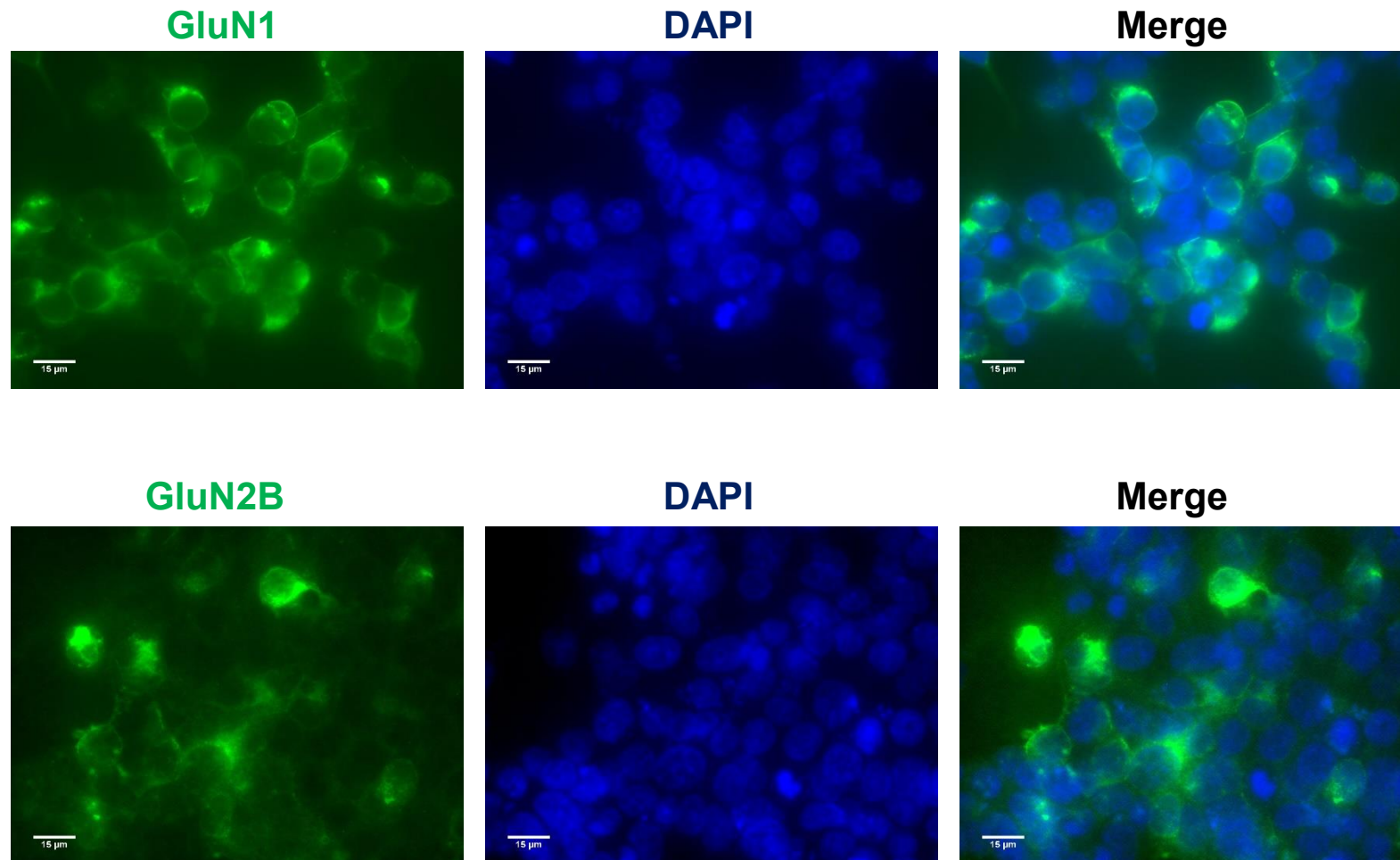
Figure 3.7. HEK293T cells over-express GluN1 and GluN2B protein when transiently transfected with GluN1 and GluN2B plasmid DNA. HEK293T cells were grown in 24 well plates on coverslips for 24 hours and then transfected with 100 ng GluN1 plasmid

and 400 ng GluN2B plasmid (Methods section 3.2.3) and incubated for a further 48 hours. Transfected HEK293T cells were then fixed with 100 % methanol and permeabilised with 0.2 % Triton X-100 in PBS. A) A rabbit polyclonal anti-NMDAR1 antibody (0.295µg/ml; Cell Signalling Technology®) or B) a rabbit polyclonal anti-NMDAR2B (0.2 µg/ml; Merck Millipore) in 0.3 % BSA in PBS was incubated with the transfected HEK293T cells for 1 hour. After 1 hour the cells were washed with PBS and probed with Anti-Rabbit Alexa Flour 488 (0.4 µg/ml; Fisher Scientific, Loughborough, UK) for 30 minutes. The slides were then mounted with DAKO fluorescence mounting medium (Agilent Technologies LDA, Stockport, UK) with 300 nM DAPI and visualised with Nikon Eclipse TE300 inverted microscope (magnification x 40) and scored (Method section 3.2.6). GluN1 or GluN2B transfected HEK293T cells are shown in green and cell nucleus DAPI staining is shown in blue. Transfection efficiency was calculated from 4 randomly selected regions. Scale bar represents 15 µM.

	Anti-Human IgG	DAPI	Merge
2.67 µg/ml			
0.4 µg/ml			
0.2 µg/ml			
0.04 µg/ml			
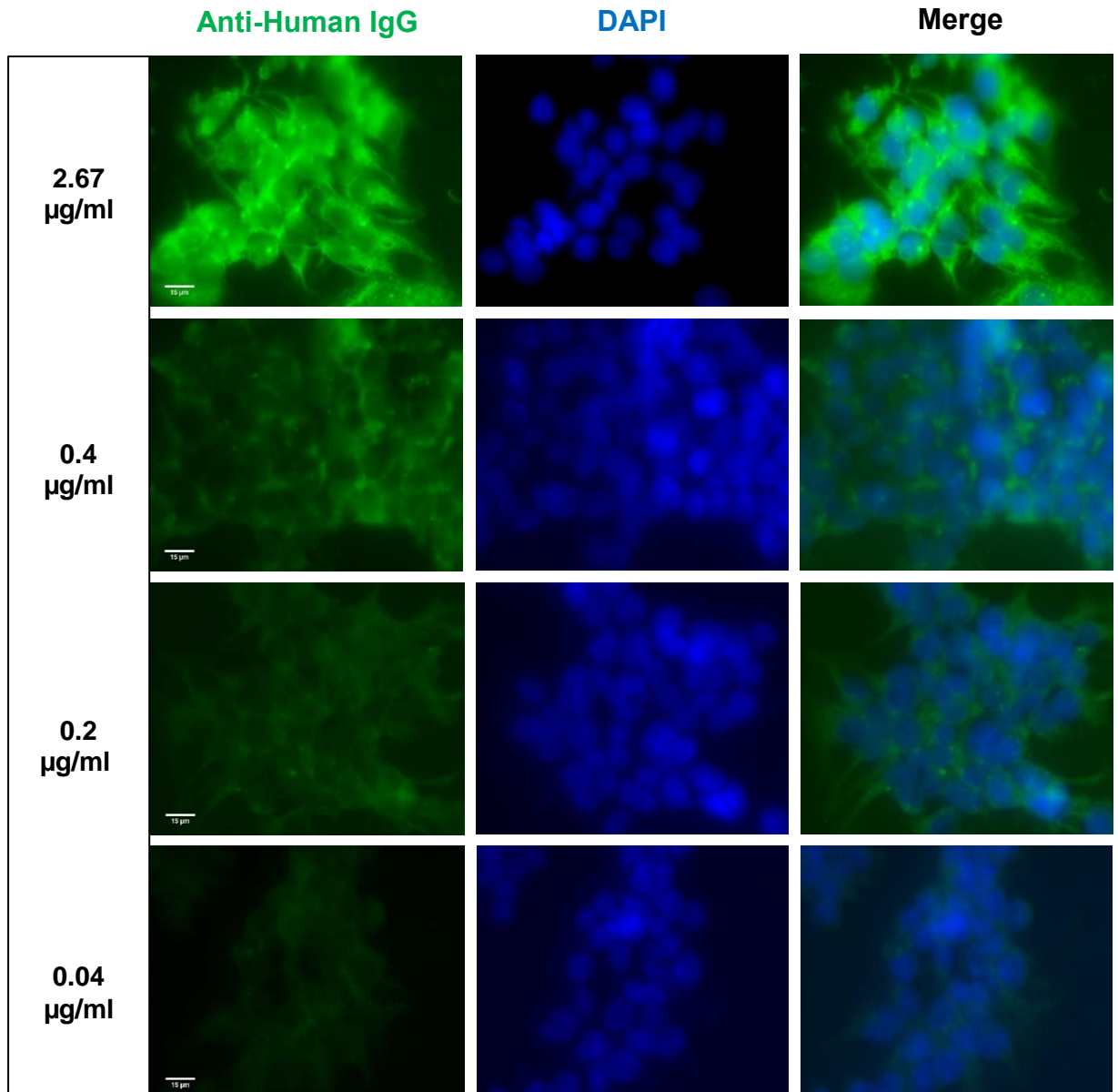
Figure 3.8. Optimisation of secondary anti-human IgG antibody used to detect positive staining from primary human serum antibodies (1:20 dilution). HEK293T cells were grown in 24 well plates on coverslips for 72 hours. Cells were then fixed with 100 % methanol and permeabilised with 0.2 % Triton X-100 in PBS. Human serum (1:20 dilution) in 0.3 % BSA in PBS was incubated with the cells for 1 hour. After 1 hour, cells were washed with PBS and probed with Anti-Human IgG Alexa Flour 488 (Fisher Scientific, Loughborough, UK) in PBS with 0.3 % BSA at varying dilutions (2.67 – 0.04 µg/ml) for 30 minutes. The

slides were then mounted with DAKO fluorescence mounting medium (Agilent Technologies LDA, Stockport, UK) containing 300 nM DAPI and visualised with Nikon Eclipse TE300 inverted microscope (magnification x 40). Human antibody binding is shown in green and cell nucleus DAPI staining is shown in blue. Anti-Human IgG antibody dilution used is indicated on the left. Scale bar represents 15 µM. Figure is representative of three separate images from one individual experiment.

Figure 3.9. Optimisation of secondary anti-human IgG antibody used to detect positive staining from primary human serum antibodies (1:100 dilution). HEK293T cells were grown in 24 well plates on coverslips for 72 hours. Cells were then fixed with 100 % methanol and permeabilised with 0.2 % Triton X-100 in PBS. Human serum (1:100 dilution) in 0.3 % BSA in PBS was incubated with the cells for 1 hour. After 1 hour, cells were washed with PBS and probed with Anti-Human IgG Alexa Flour 488 (Fisher Scientific, Loughborough, UK) in PBS with 0.3 % BSA at varying dilutions (2.67 – 0.04 µg/ml) for 30 minutes. The

slides were then mounted with DAKO fluorescence mounting medium (Agilent Technologies LDA, Stockport, UK) containing 300 nM DAPI and visualised with Nikon Eclipse TE300 inverted microscope (magnification x 40). Human antibody binding is shown in green and cell nucleus DAPI staining is shown in blue. Anti-Human IgG antibody dilution used is indicated on the left. Scale bar represents 15 µM. Figure is representative of three separate images from one individual experiment.

All serum samples were tested in duplicate with one slide probed simultaneously with a commercial GluK2, GluK5 or GluN1 antibody (Methods section Table 3.1). This allowed visualisation of GluR subunit over-expressing HEK293T cells and scoring for co-localisation of positive serum autoantibody staining to GluR subunits. The second slide was probed with serum only and acted as a control to ensure the commercial antibody binding to GluR subunits was not affecting serum sample autoantibody binding; thus, preventing visualisation of positive samples. Serum samples were only scored positively if autoantibody staining was seen on both slides. The scoring for the serum samples were carried out as described by Leite et al., 2008 (Methods section 3.2.6, Table 3.3). In the current study the highest score observed was 3 and any scores above 1 were considered positive.

Of the 40 T1D patient serum samples tested for GluK2 autoantibodies, 3 were positive (7.5%), which was not statistically significant compared to healthy control serum ($p = 0.337$), in which 2 samples were positive (5%). Representative examples of the serum samples are shown in Figure 3.10 and the scores are shown in Figure 3.11. Similarly, GluK5 autoantibodies were detected in 2 T1D patient samples (5%) and in 1 healthy control sample (3%) and no significant difference ($p = 0.704$) was found between groups (Figures 3.12 and 3.13). For both GluK2 and GluK5 the median score was 0.

T1D Samples tested for GluN1 autoantibodies revealed a higher number of positives compared to GluK2 and GluK5, however, this was also seen in the healthy control samples. From the T1D patient serum, 7 samples were found to be positive (18%), compared to 10 healthy control samples (28%), but there was no significant difference between groups ($p = 0.238$) (Figures 3.14 and 3.15).

Some studies have found that autoantibodies to NMDA receptors are only detectable when there is expression of functional heteromers and expression of single subunits alone did not allow autoantibody binding from serum samples (Dalmau et al., 2007). Previous studies have reported that co-transfection of GluN1 and GluN2B plasmid DNA at a 1:4 ratio, results in successful co-expression of GluN1 and GluN2B protein and formation of functional GluN1/GluN2B receptors (Domingues et al., 2006, 2007; Fan et al., 2009; Guo et al., 2017). Therefore, HEK293T cells in the current study were co-transfected with GluN1 and GluN2B plasmids at a 1:4 ratio, respectively. The current study has shown that HEK293T cells co-transfected with GluN1 and GluN2B plasmids over-express GluN1 or GluN2B subunit protein (Figure 3.7). The serum samples were then tested, as described in Methods section 3.2.4 with the co-transfected cells. From T1D serum there were 5 positive GluN1:GluN2B samples (13%), compared to 3 positive samples from healthy control serum (8%) (Figures 3.16 and 3.17). There was no significant difference between T1D serum and control serum ($p = 0.063$).

Overall, there was no significant difference observed between T1D and healthy control serum for any of the GluR subunits tested (Table 3.4, Figure 3.18).

Overview	GluK2	Serum + anti-human IgG	DAPI	Merge	Score
					3
					1
					0.5
					0
x 400	x 1000	x 1000	x 1000	x 1000	

157
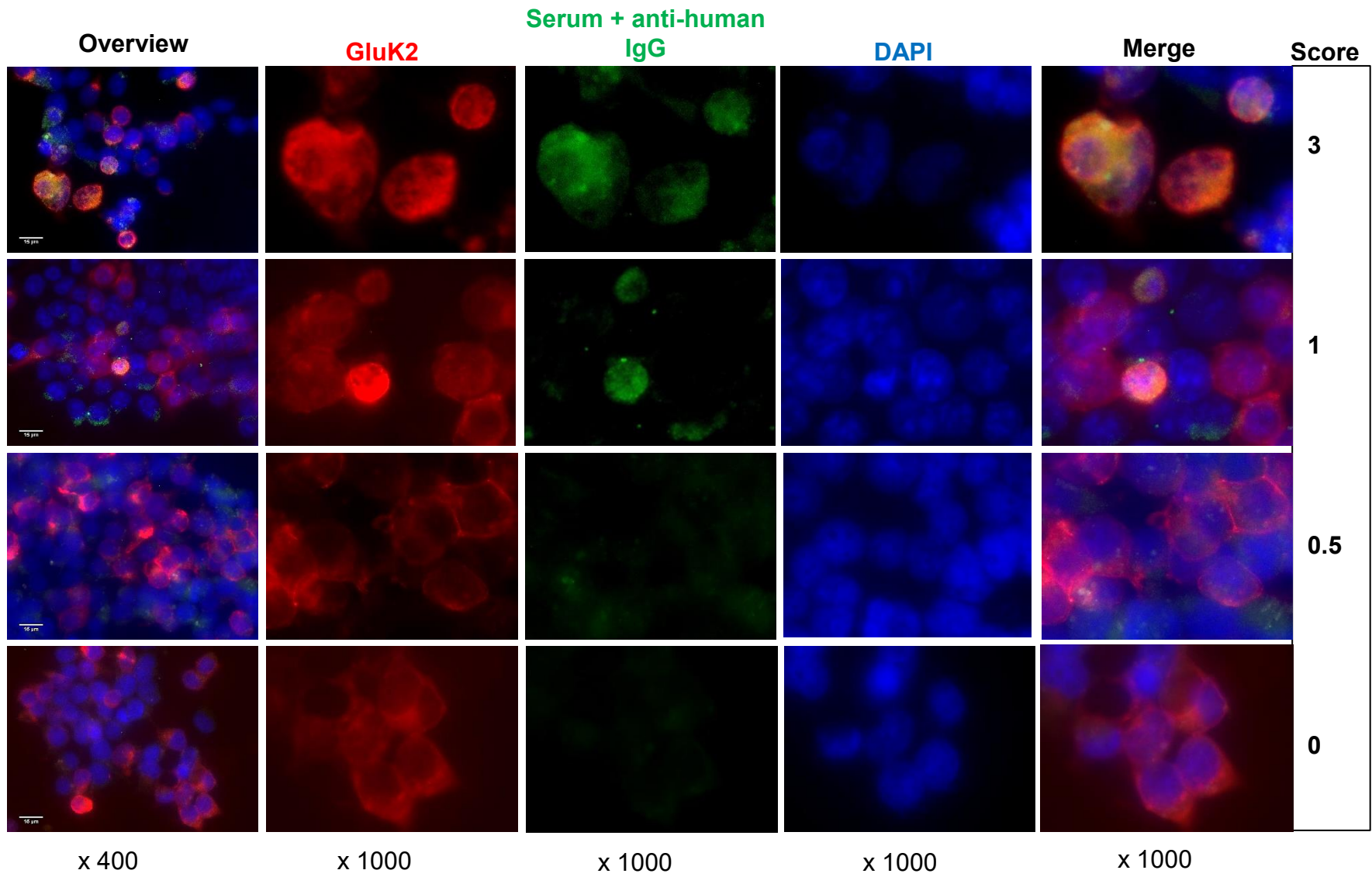
Figure 3.10. Detection of autoantibodies to GluK2 receptor subunit. HEK293T cells were grown in 24 well plates on coverslips for 24 hours and then transfected with 500 ng GluK2 plasmids (Methods section 3.2.3) and incubated for a further 48 hours. Transfected HEK293T cells were then fixed with 100 % methanol and permeabilised with 0.2 % Triton X-100 in PBS. A rabbit polyclonal anti-GluK2/3 antibody (0.025 µg/ml; Millipore UK Limited) and human serum (1:100 dilution) in 0.3 % BSA in PBS was incubated with the transfected HEK293T cells for 1 hour. After 1 hour the cells were washed with PBS and probed with Anti-Rabbit Alexa Flour 568 (0.4 µg/ml; Fisher Scientific, Loughborough, UK) and Anti-Human Alexa Flour 488 (0.04 µg/ml; Fisher Scientific, Loughborough, UK) in PBS and 0.3 % BSA for 30 minutes. The slides were then mounted with DAKO fluorescence mounting medium (Agilent Technologies LDA, Stockport, UK) with 300 nM DAPI and visualised with Nikon Eclipse TE300 inverted microscope (magnification x 40) and scored (Method section 3.2.4). Autoantibody binding of serum samples from T1D patient serum or control serum is shown in green, GluK2 transfected HEK293T cells are shown in red and cell nucleus DAPI staining is shown in blue. IgG binding score to GluK2 is indicated on the right. Scale bar represents 15 µM. Images are representative of the different scoring of autoantibody staining for GluK2 subunits from one independent experiment carried out in duplicate (one stained with human serum and anti-GluK2/3, the second with human serum only), in which 5 randomly selected regions were imaged and scored as outlined in Table 3.3.
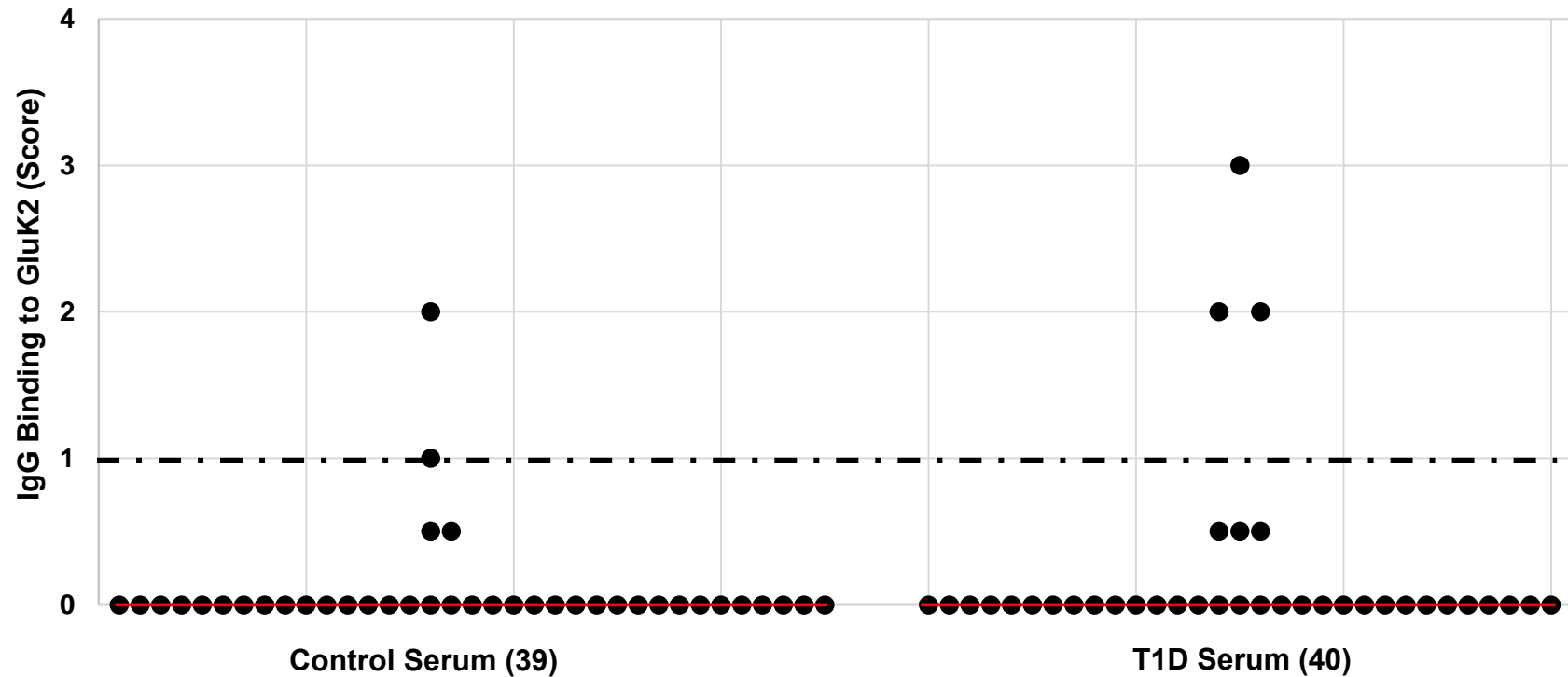
Figure 3.11. Autoantibody binding scores to GluK2. All serum samples were scored between 0 and 4 (as described in Methods section 3.2.4) from five separate images per serum sample tested in duplicate. The red line shown indicates the median values and the number of samples tested is in brackets. Serum samples were considered positive if they achieved a score of 1 or above, represented by the dotted line.
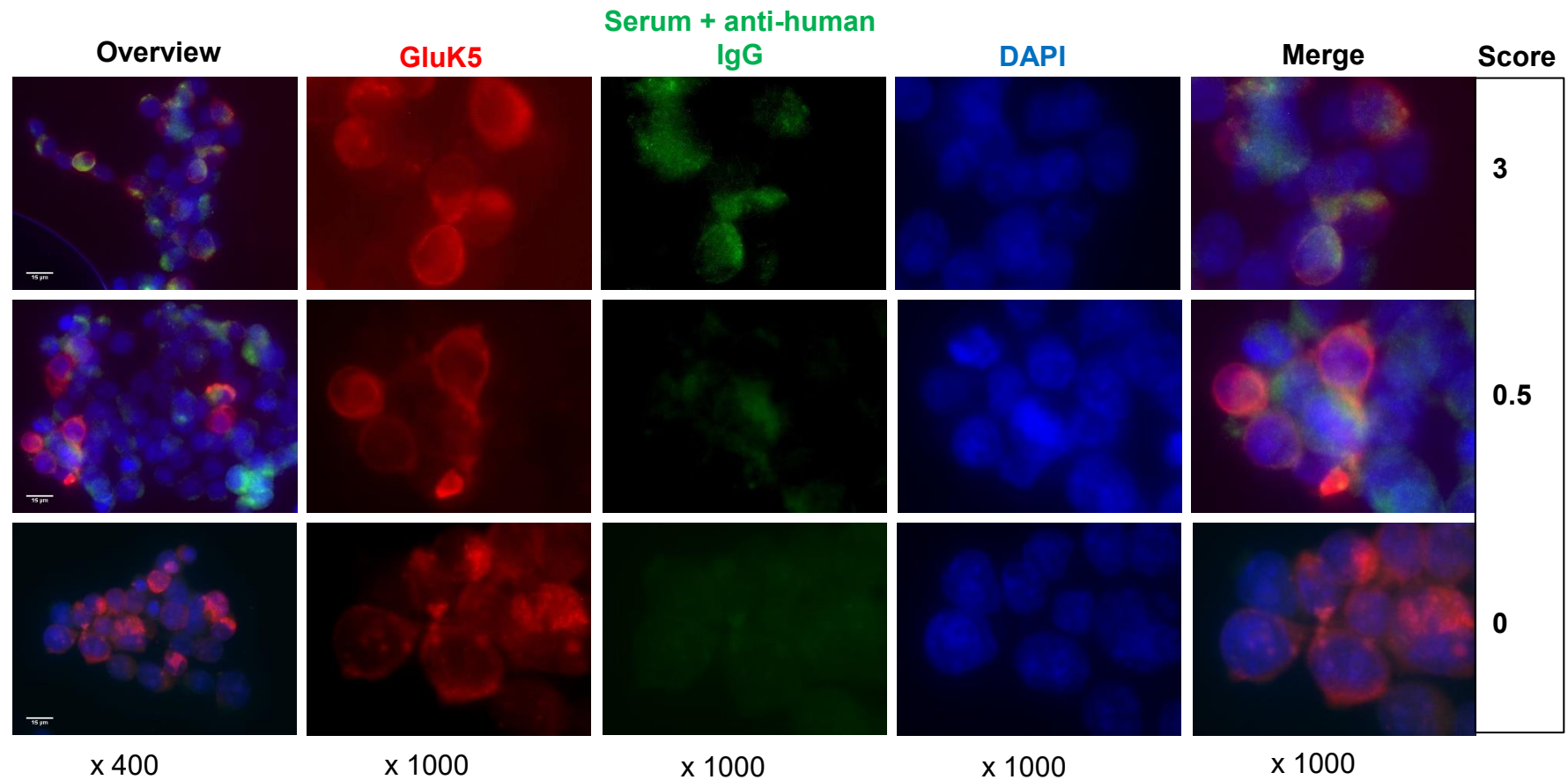
Figure 3.12. Detection of autoantibodies to GluK5 receptor subunits. HEK293T cells were grown in 24 well plates on coverslips for 24 hours and then transfected with 500 ng GluK5 plasmid (Methods section 3.2.3) and incubated for a further 48 hours. Transfected

HEK293T cells were then fixed with 100 % methanol and permeabolised with 0.2 % Triton X-100 in PBS. A rabbit polyclonal anti-GRIK5 antibody (0.1 µg/ml; Millipore UK Limited) and human serum (1:100 dilution) in 0.3 % BSA in PBS was incubated with the transfected HEK293T cells for 1 hour. After 1 hour the cells were washed with PBS and probed with Anti-Rabbit Alexa Flour 568 (0.4 µg/ml; Fisher Scientific, Loughborough, UK) and Anti-Human Alexa Flour 488 (0.04 µg/ml; Fisher Scientific, Loughborough, UK) for 30 minutes. The slides were then mounted with DAKO fluorescence mounting medium (Agilent Technologies LDA, Stockport, UK) with 300 nM DAPI and visualised with Nikon Eclipse TE300 inverted microscope (magnification x 40) and scored (Method section 3.2.4). Autoantibody binding of serum samples from T1D patient serum or control serum is shown in green, GluK5 transfected HEK293T cells are shown in red and cell nucleus DAPI staining is shown in blue. Scale bar represents 15 µM. Images are representative of the different scoring of autoantibody staining for GluK5 subunits from one independent experiment carried out in duplicate (one stained with human serum and anti-GluK5, the second with human serum only), in which 5 randomly selected regions were imaged and scored as outlined in Table 3.3.
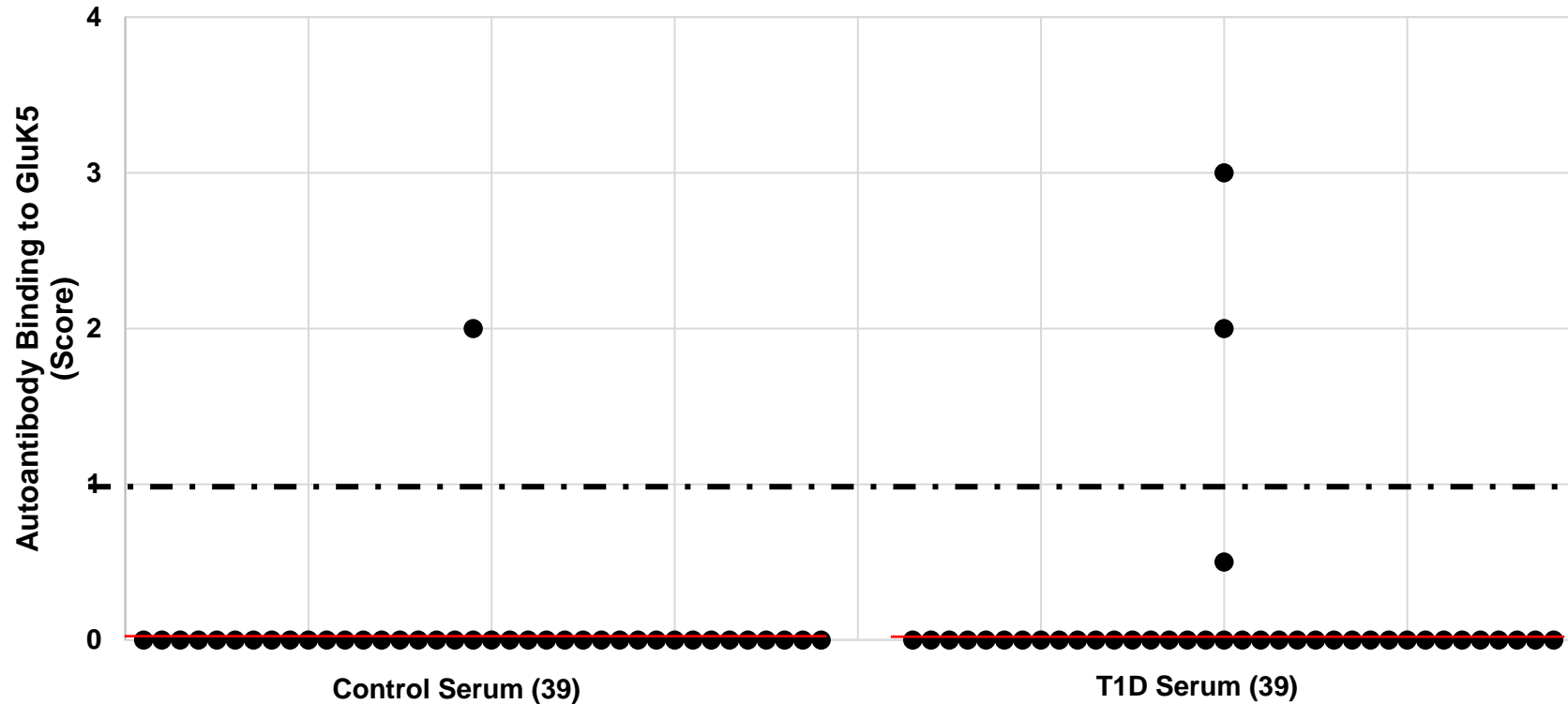
Figure 3.13. Autoantibody binding scores to GluK5. All serum samples were scored between 0 and 4 (as described in Methods section 3.2.4) from five separate images per serum sample tested in duplicate. The red line shown indicates the median values and the number of samples tested is in brackets. Serum samples were considered positive if they achieved a score of 1 or above, represented by the dotted line.

Overview	GluN1	Serum + anti-human IgG	DAPI	Merge	Score
x 400	x 1000	x 1000	x 1000	x 1000	

Score values (top to bottom): 2, 1, 0.5, 0

163
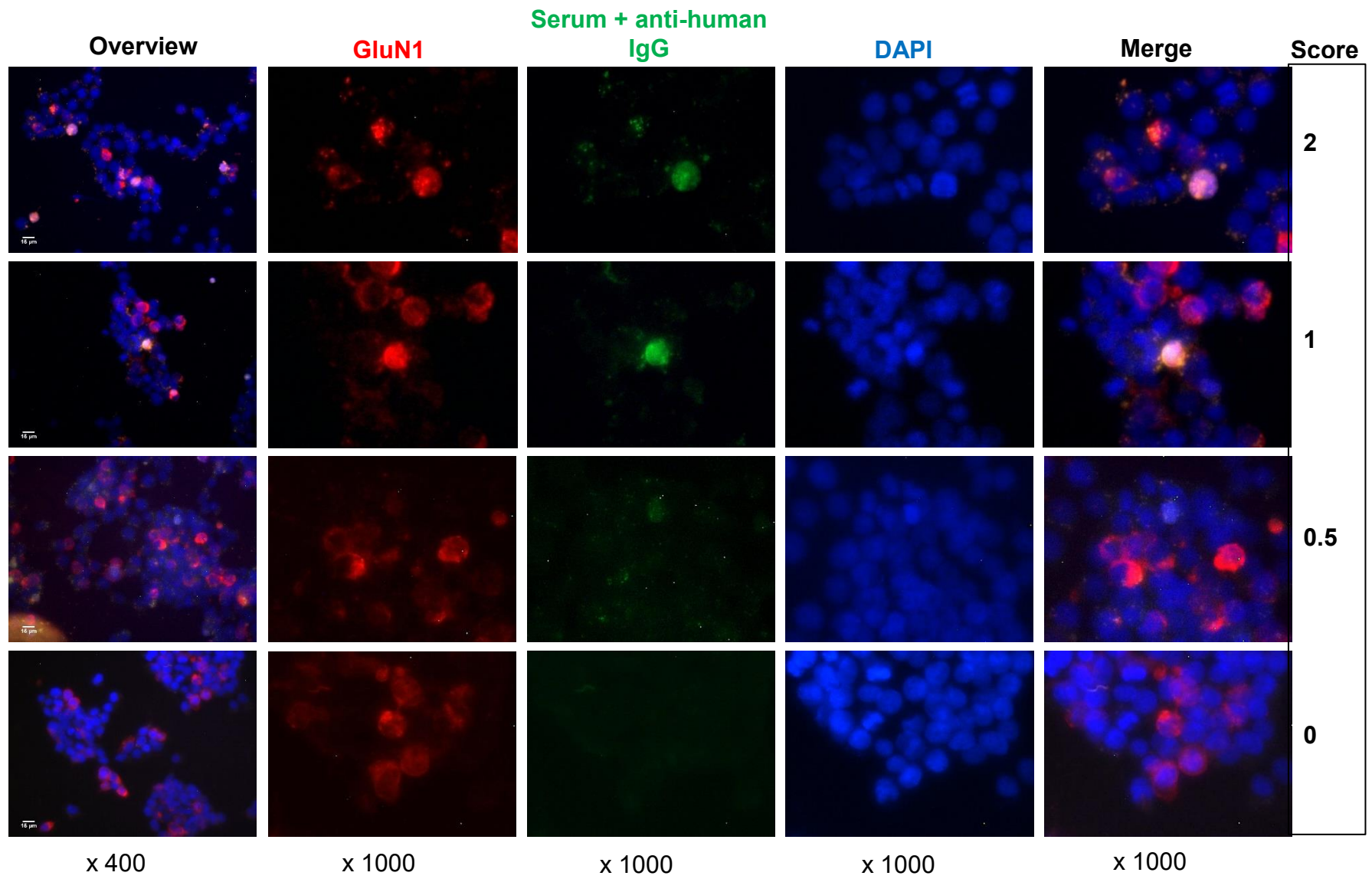
Figure 3.14. Detection of autoantibodies to GluN1 receptor subunit. HEK293T cells were grown in 24 well plates on coverslips for 24 hours and then transfected with 500 ng GluN1 plasmid (Methods section 3.2.3) and incubated for a further 48 hours. Transfected HEK293T cells were then fixed with 100 % methanol and permeabolised with 0.2 % Triton X-100 in PBS. A rabbit polyclonal anti-NMDAR1 antibody (0.295 µg/ml; Cell Signalling Technology®) and human serum (1:100 dilution) in 0.3 % BSA in PBS was incubated with the transfected HEK293T cells for 1 hour. After 1 hour the cells were washed with PBS and probed with Anti-Rabbit Alexa Flour 568 (0.4 µg/ml; Fisher Scientific, Loughborough, UK) and Anti-Human Alexa Flour 488 (0.04 µg/ml; Fisher Scientific, Loughborough, UK) for 30 minutes. The slides were then mounted with DAKO fluorescence mounting medium (Agilent Technologies LDA, Stockport, UK) with 300 nM DAPI and visualised with Nikon E80i Fluorescence Photomicroscope (magnification x 40) and scored (Methods section 3.2.6). Autoantibody binding of serum samples from T1D patient serum or control serum is shown in green, GluN1 transfected HEK293T cells are shown in red and cell nucleus DAPI staining is shown in blue. Scale bar represents 15 µM. Images are representative of the different scoring of autoantibody staining for GluN1 subunits from one independent experiment carried out in duplicate (one stained with human serum and anti-NMDAR1, the second with human serum only), in which 5 randomly selected regions were imaged and scored as outlined in Table 3.3.

Figure 3.15. Autoantibody binding scores to GluN1. All serum samples were scored between 0 and 4 (as described in Methods section 3.2.6) from five separate images per serum sample tested in duplicate. The red line shown indicates the median values and the number of samples tested is in brackets. Serum samples were considered positive if they achieved a score of 1 or above, represented by the dotted line.

	Overview	GluN1	Serum + anti-human IgG	DAPI	Merge	Score

x 400　　x 1000　　x 1000　　x 1000　　x 1000
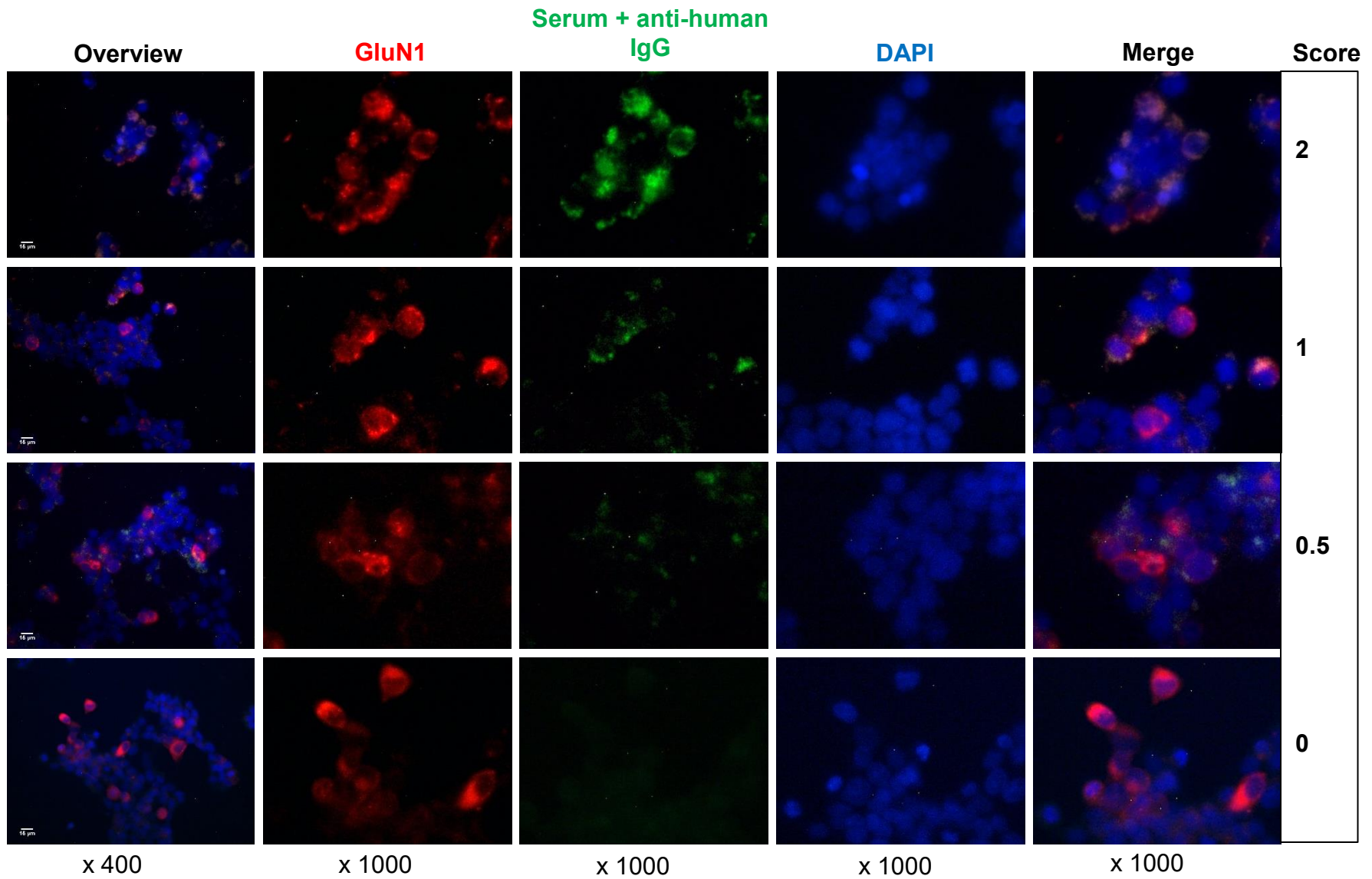
Figure 3.16. Detection of autoantibodies to GluN1 receptor subunit from HEK293T cells which have been co-transfected with GluN1 and GluN2B plasmids. HEK293T cells were grown in 24 well plates on coverslips for 24 hours and then transfected with 100 ng GluN1 plasmid and 400 ng GluN2B plasmid (Methods section 3.2.3) and incubated for a further 48 hours. Transfected HEK293T cells were then fixed with 100 % methanol and permeabolised with 0.2 % Triton X-100 in PBS. A rabbit polyclonal anti-NMDAR1 antibody (0.295 µg/ml; Cell Signalling Technology®) and human serum (1:100 dilution) in 0.3 % BSA in PBS was incubated with the transfected HEK293T cells for 1 hour. After 1 hour the cells were washed with PBS and probed with Anti-Rabbit Alexa Flour 568 (0.4 µg/ml; Fisher Scientific, Loughborough, UK) and Anti-Human Alexa Flour 488 (0.04 µg/ml; Fisher Scientific, Loughborough, UK) for 30 minutes. The slides were then mounted with DAKO fluorescence mounting medium (Agilent Technologies LDA, Stockport, UK) with 300 nM DAPI and visualised with Nikon E80i Fluorescence Photomicroscope (magnification x 40) and scored (Methods section 3.2.6). Autoantibody binding of serum samples from T1D patient serum or control serum is shown in green, GluN1 transfected HEK293T cells are shown in red and cell nucleus DAPI staining is shown in blue. Scale bar represents 15 µM. Images are representative of the different scoring of autoantibody staining for GluN1 subunits from one independent experiment carried out in duplicate (one stained with human serum and anti-NMDAR1, the second with human serum only), in which 5 randomly selected regions were imaged and scored as outlined in Table 3.3.

Figure 3.17. Autoantibody binding scores to GluN1 receptor subunit from HEK293T cells which have been co-transfected with GluN1 and GluN2B plasmids. All serum samples were scored between 0 and 4 (as described in Methods section 3.2.6) from five separate images per serum sample tested in duplicate. The red line shown indicates the median values and the number of samples tested is in brackets. Serum samples were considered positive if they achieved a score of 1 or above, represented by the dotted line.

Table 3.4. Results of GluR autoantibody detection from Type 1 Diabetic patient serum and healthy control serum. Results were compared by two-way Mann-Whitney U Test. NS = not significant.

	No. controls tested	% Control sera positives	No. T1D sera tested	% T1D sera positive	Statistical significance
GluN1	38	29%	39	18%	NS *(p = 0.0.238)*
GluN1:GluN2B	36	8%	39	13%	NS *(p = 0.063)*
GluK2	39	5%	40	8%	NS *(p = 0.337)*
GluK5	39	3%	39	5%	NS *(p = 0.704)*
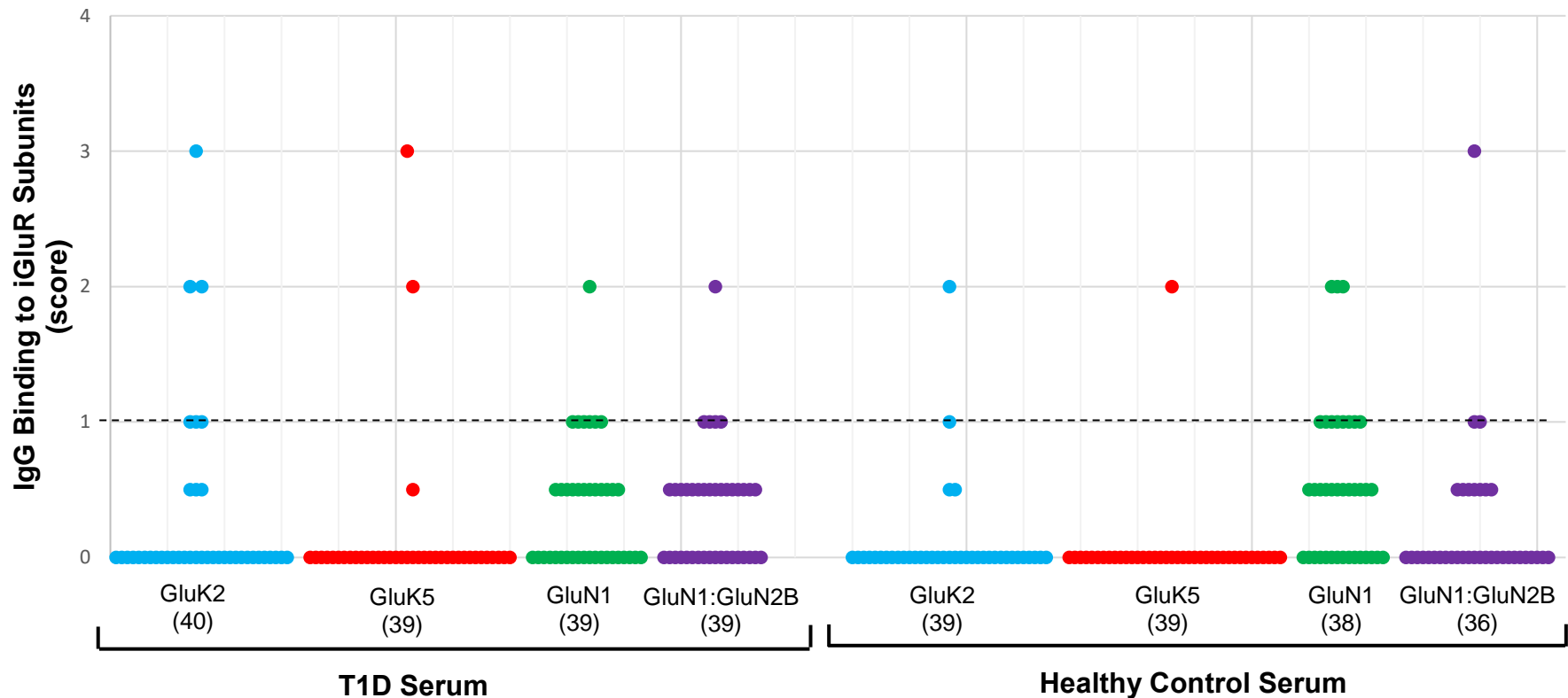
Figure 3.18. Autoantibody binding scores to GluR subunits. All serum samples were scored between 0 and 4 (as described in Methods section 3.2.6) from five separate images per serum sample tested in duplicate. The number of samples tested is in brackets and serum samples were considered positive if they achieved a score of 1 or above, represented by the dotted line.

3.4 Discussion

As previously discussed in section 1.4.4 several autoantibodies are already known to be associated with T1D and are successfully used as a predictor of disease (Jacobsen et al., 2018). Autoantibody testing has become an essential part in the diagnosis of T1D by health professionals, as well as being the corner stone of numerous studies investigating the prediction of T1D (Krischer et al., 2019; Uusitalo et al., 2018). Despite being an essential clinical tool, none of the currently known autoantibodies associated with T1D are thought to be the cause of disease and have so far not been able to aid in the prevention of T1D. It has been shown that some T1D sera which is immunoreactive to islet cells do not contain any of the currently known T1D associated autoantibodies (Wenzlau and Hutton, 2013). This, therefore, suggests that there are more autoantibodies associated with T1D yet to be discovered. Identifying the remaining autoantibody targets in T1D is essential as it will provide a fuller picture of the immune process in the disease and potentially identify the cause of the disease. Autoantibodies which target GluRs have already been shown to initiate disease within the CNS (Dalmau et al., 2017; Geis et al., 2019) and is discussed further in section 1.10. Numerous studies have also suggested indirect links with glutamate and GluRs and the pathogenesis of T1D as chronic exposure to glutamate resulted in cytotoxicity and β-cell death (Di Cairano et al., 2011; Boonnate et al., 2015; Oresic et al., 2008). Whilst a further study demonstrated that β-cell damage initiated by chronic glucose exposure was alleviated when *GluN1* was knocked out (Huang et al., 2017). It was therefore decided to investigate if autoantibodies which target GluRs were present in the serum of newly diagnosed T1D patients and confirm a direct link between GluRs and T1D.

3.4.1 <u>Immunoblotting is not an appropriate method for the detection of GluR autoantibodies from sera from T1D patients</u>

It has been shown that HEK293T transfection, followed by immunoblotting with patient serum can be an effective way to detect autoantibodies, as demonstrated by Dalmau et al., 2008 who used this method to identify anti-NMDAR autoantibodies in anti-NMDA-receptor encephalitis patient serum. Li et al., 2010 also used a similar method to characterise anti-pancreatic duodenal homeobox 1 autoantibodies in T1D patient serum. HEK293T cells over-expressed the GluR subunit proteins GluK2 and GluK5 following transfection with GluK2 or GluK5 plasmid DNA (Figure 3.1) and processed for immunoblotting. From the 27 serum samples tested no clear positives were found, due to non-specific bands in the GluK2/GluK5 lanes, as well as in the negative control. Previous studies have noted that use of immunoblotting to detect autoantibodies from sera can be difficult as there are often many non-specific bands on the blots, making the results hard to interpret (Banjara et al., 2017; Pumphrey et al., 2013; Vianello et al., 2005). This was also seen in the current study. To minimise non-specific bands, future studies could purify overexpressed GluR subunit proteins instead of using the whole protein homogenate so that the serum sample antibodies can only bind to GluR proteins and therefore increase the specificity of the assay (Gleichman et al., 2012). Detection of GluR autoantibodies by immunoblotting may not have been possible because the process of extracting GluK2/GluK5 protein lysate and its use in SDS-PAGE gels interferes with the proteins tertiary structure and therefore when the protein is used it is no longer in its native conformation. As a result of this, epitopes which are present in the native form may become hidden or destroyed during sample processing, thus preventing

autoantibody binding (Bass et al., 2017). This theory is supported by research, which has shown that GAD autoantibodies associated with T1D cannot be detected by immunoblotting due to changes in the GAD protein physiochemical structure caused by protein extraction for use with SDS-PAGE gels (Pihoker et al., 2005). It was therefore concluded that immunoblotting was not an appropriate method for the detection of GluR autoantibodies from patient serum and an alternative method needed to be used.

3.4.2 <u>Cell-based immunofluorescence assays can be used for the detection of GluR autoantibodies from patient serum</u>

To overcome some of the problems faced with using immunoblotting to detect autoantibodies a cell-based assay was decided to be used instead. Cell-based assays have been shown to be an effective method to detect glutamate receptor autoantibodies from patient serum (van Coevorden-Hameete et al., 2016; Park et al., 2018). Additionally, cell-based assays do not denature the proteins and helps to prevent potential epitope sites from being altered or obscured during sample preparation (Gastaldi et al., 2017; Ricken et al., 2018). Co-staining with a commercial GluR antibody enabled direct visualisation of HEK293T cells which were overexpressing GluR proteins and it could therefore be determined if autoantibody staining from patient serum was specifically targeting GluR overexpressing cells. This prevented reporting of false positives, a problem which is seen with this method of autoantibody assay if it is not known which specific cells are overexpressing the target protein (Gastaldi et al., 2017).

Human serum contains many naturally occurring antibodies which have the potential to react with proteins from the HEK293T cell line, resulting in non-specific primary antibody binding; an issue which has been observed in the

previous experiments using immunoblots (Figure 3.2 and 3.3.). Optimisation of the secondary antibody dilution was essential to try and reduce background fluorescence, whilst still allowing visualisation of positive primary GluR autoantibody staining. After optimisation a dilution of 1:100 for patient serum and 1:50,000 dilution for the secondary anti-human antibody was used.

3.4.3 No difference is observed in GluR autoantibody frequency in T1D patient serum compared to healthy age-matched controls

T1D patient serum and healthy age-matched controls were tested for the GluR subunits; GluK2, GluK5, GluN1 and GluN1 with GluN2B. We adopted the scoring for positive staining described by Leite et al., 2008 (Method section Table 3.3), which was also used in numerous other studies (Huda et al., 2017; Park et al., 2018; Tsonis et al., 2015). There was found to be no significant difference in samples positive for GluR autoantibodies between T1D patients and age-matched healthy controls (Figure 3.18). Our data indicates that autoantibodies to GluRs are not associated with T1D and there is no evidence that excitotoxicity driven by GluR autoantibodies causes β-cell loss in T1D for this group of patients.

The current study unexpectedly observed a large difference between the number of healthy control serum which contained autoantibodies to GluN1 and the number of healthy control serum which were positive for GluN1 autoantibodies when co-transfected with GluN2B. It was expected that the number of positive samples for both GluN1 and GluN1 co-transfected with GluN2B would be similar in the healthy control group, however, there was significantly more positives for GluN1 alone ($p = 0.01732$). Studies have demonstrated that binding of different GluN2 subunits to GluN1 results in different conformational changes to the receptor which can also lead to changes in receptor function and gating kinetics

(Hansen et al., 2018; Lind et al., 2017; Ryan et al., 2008). Therefore, the difference in number of positive samples may be because binding of GluN2B to GluN1 changes the structure of the receptor and as such may block autoantibody binding sites which are available when GluN1 is not bound to GluN2B and is instead bound to one of the other GluN2 (GluN2A, GluN2C or GluN2D) or GluN3 (GluN3A – B) subunits.

Intriguingly, research suggested that there are two endotypes for T1D which can be divided based on their insulitic profile (Arif et al., 2014; Endocrinology, 2019; Leete et al., 2016). The first subtype shows high infiltration of leukocytes, specifically CD20$^+$ cells, whilst the second subtype shows a low CD20$^+$ profile. The authors demonstrated that the two endotypes are split by age of onset, with CD20$^+$ high individuals being consistently diagnosed before the age of 7 years, whereas CD20$^+$ low individuals are diagnosed after the age of 13 years (Leete et al., 2016). Significantly, those diagnosed after 13 years of age retain 40 % of their insulin-containing islets, whereas those diagnosed under 7 do not retain these cells and their β-cell loss is more aggressive. The authors have suggested that the cause of T1D in the CD20$^+$ low individuals is more likely to be due to a functional deficit within the islets of Langerhans, rather than the result of total β-cell loss, as seen in the CD20$^+$ high endotype (Leete et al., 2016). It should therefore be noted that all serum samples used in this study were from newly diagnosed T1D patients over the age of 29 and may identify with the CD20$^+$ low endotype which is thought to result from islet dysfunction and later lead to autoimmunity and epitope spreading, rather than islet autoimmunity being the initiating cause of disease. The current study only used T1D patient samples which were positive for GAD autoantibodies and previous studies have identified

that GAD antibodies are more common in T1D patients diagnosed at a later age, compared to IAA and IA-2 antibodies which are more prevalent in those diagnosed young (Gillespie and Long, 2019; Tridgell et al., 2011) and are associated with faster disease progression (Gillespie and Long, 2019). This supports the conclusion that the current study has only tested one subset of T1D patients and future studies should aim to use samples from a wide range of ages and autoantibody profiles.

As discussed in section 1.5, researching causes of T1D is challenging as the clinical presentation of disease only occurs after the majority of β-cells have been destroyed (Figure 1.4, (Rojas et al., 2018)). As a result, by the point of diagnosis the immune system has already been activated and numerous changes in the immune response have occurred. Studies have identified that the autoantibody profile of an individual at the point of seroconversion and the point of diagnosis are often different and in some cases the initial autoantibody at seroconversion (IAA in the majority of T1D cases) had already disappeared by the time of diagnosis (Bauer et al., 2019; Ilonen et al., 2018). It is therefore possible that any currently unknown autoantibodies that might be the primary cause of T1D may have already also disappeared at the time of diagnosis and may be the reason for the lack of autoantibodies to GluR subunits in the current study. In conclusion, autoantibodies targeted towards GluRs are unlikely to be indicators of T1D, however, future work should aim to gather samples from patients of a more varied age-range.

As described in section 1.4.3 there are numerous models which have been suggested to lead to the development of T1D (Figure 1.7) and it may be that autoantibodies are not the initiating cause of T1D. For example, recent research

has suggested that viral infection is the initial cause of autoimmunity which leads to T1D (Hyöty et al., 2018; Principi et al., 2017). There are several viral mechanisms which are proposed to induce T1D. The first of which is viral molecular mimicking, where the virus contains structurally similar antigens to self-antigens which leads to confusion by the immune system and activation of T and B cells which target both virus and self-antigens, causing autoimmunity (Figure 3.19a). This is supported by research which has found that Coxsackievirus B's (CVB) P2-C protein sequence resembles human GAD (Kaufman et al., 1992). The second mechanism, termed the bystander effect, suggests that the proinflammatory and inflammatory mediators which are activated during viral infection cause islet cell damage and subsequent release of islet antigens from β-cells and increased autoantigen presentation by antigen presenting cells (APCs) (Figure 3.19b). A recent study investigating CVB induced T1D in NADPH oxidase-deficient Non-Obese Diabetic mice found they were protected from virus-induced autoimmune diabetes (Burg et al., 2018). Burg et al., 2018 proposed that this protection was due to impaired pro-inflammatory Toll-like receptor signalling in NADPH oxidase deficient NOD mice. Impaired Toll-like receptor signalling would prevent initiation of proinflammatory mediators, thus, stopping T1D progression via the bystander effect. Finally, as mentioned in section 1.4.4, and linked to the bystander effect, epitope spreading is thought to be linked with a persistent viral infection, triggering the release of more self-antigens as more tissue and cells become damaged which are then targeted by new autoreactive cells (Cornaby et al., 2015; Didona and Di Zenzo, 2018) (Figure 3.19c). This being said, there is a growing consensus that T1D is a heterogenous disorder with different subtypes which may have different causes from one individual to

another and present with the varying levels of β-cell loss and insulin production (Ahlqvist et al., 2018; Atkinson et al., 2015). As stated previously, it is therefore important that any future studies use a varied sample population of different age of onset, duration of disease and autoantibody profile in order to get a more indicative picture of the disease.
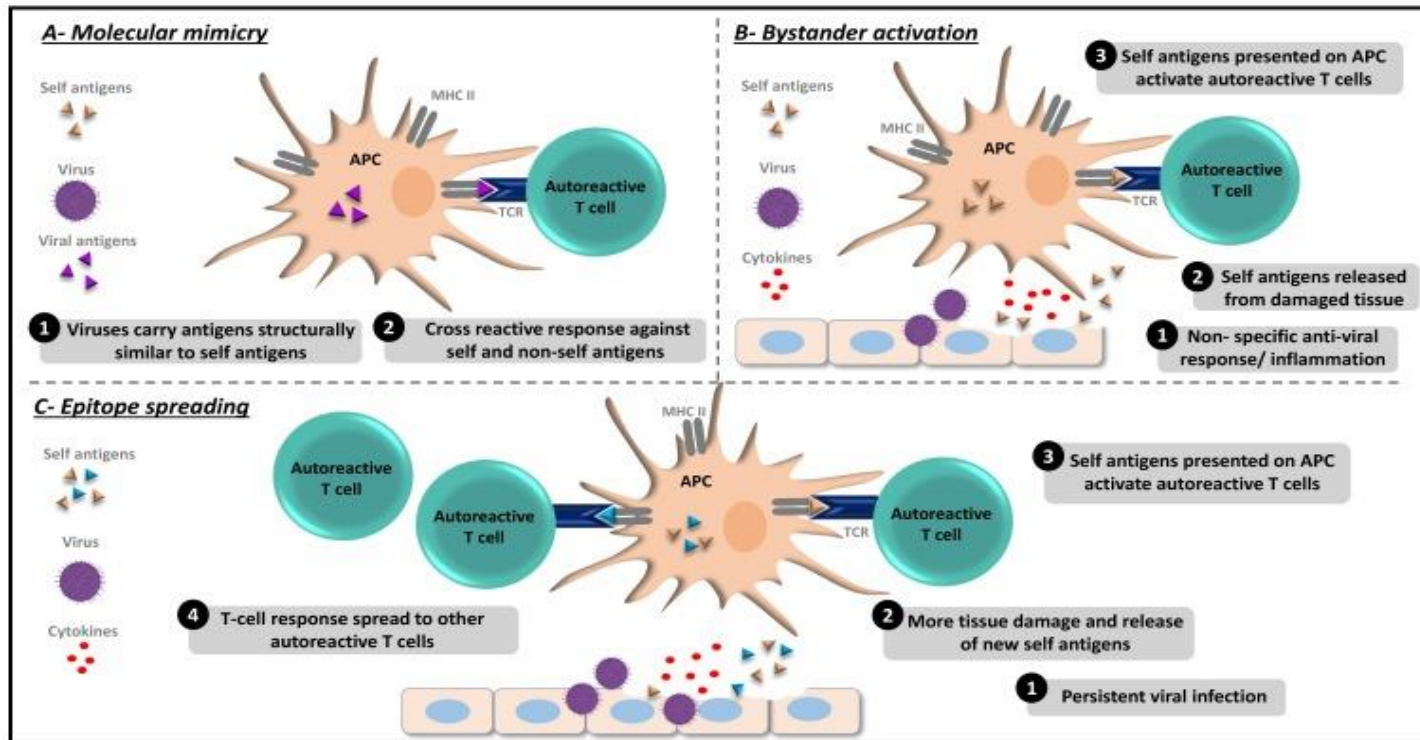
Figure 3.19. Mechanisms of virus induced T1D. A) Molecular mimicry; virus contains structurally similar antigens to self-antigens which leads to activation of T and B cells which target both virus and self-antigens. B) Bystander effect; proinflammatory and inflammatory mediators are activated during viral infection cause cell damage and subsequent release of islet antigens from β-cells and increased autoantigen presentation by antigen presenting cells (APCs). C) Epitope spreading; persistent viral infection triggers the release of more self-antigens as more tissue and cells become damaged which are then targeted by new autoreactive cells. Image taken from Smatti et al., 2019.

4. Conclusion and Future Work

4.1. Conclusion

The first aim of this study was to identify GluRs, specifically KAR subunits, expressed in the human β-cell line, EndoC-βH1. Experiments using RT-PCR identified the KAR subunits GluK2 and GluK5, as well as the auxiliary subunits Neto1 and Neto2 in EndoC-βH1 cells. In addition, the current study showed that GluK2 and GluN2B protein is produced by EndoC-βH1 cells. The expression of GluRs in pancreatic β-cells has produced varying results in the literature (Tables 1.1 – 1.3) due to the difficulty in firstly obtaining islets and then effectively sorting them into the different cell types of the islets of Langerhans. Until the development of the human β-cell line, EndoC-βH1, there was no pure β-cell line to conduct conclusive GluR expression experiments and therefore added to the variation of results seen in the literature as only murine cell lines were available (Tables 1.1 – 1.3). Specifically the presence of KARs in pancreatic β-cells has been identified by relatively few studies and with varying results (Benner et al., 2014; Bramswig et al., 2013; Cabrera et al., 2008; Dorrell et al., 2011; Eizirik et al., 2012; Huang et al., 2017; Inagaki et al., 1995; Kutlu et al., 2009; Nica et al., 2013). Only one study has identified GluK5 subunit protein (Molnár et al., 1995). The current study is therefore the first to identify GluK2 protein from human β-cells and provide evidence that human β-cells form functional KARs.

The second aim of the study was to elucidate what role KARs play in insulin secretion. GSIS experiments have shown that activation of KARs potentiates insulin secretion when in the presence of stimulatory glucose levels, but not at basal glucose concentrations. This study showed that GluK2 is translocated to

the surface when EndoC-βH1 cells are treated with stimulatory glucose concentrations, indicating that KARs trafficking is influenced by changes in glucose levels in pancreatic β-cells. This study has confirmed that KARs contribute in GSIS in β-cells. Overall, these findings demonstrate that GluRs play a role in hormone secretion in human β-cells and therefore mainting blood glucose levels in the body. GluRs could therefore provide valuable new insight into how β-cells respond to glucose and are a potential new target for drug development in controlling insulin levels in Diabetic patients, however, further research is still needed.

The final aim of the project was to identify if GluR subunits on the β-cell surface are targeted by the immune system in T1D. This is the first study which has aimed to identify a direct association between anti-GluR autoantibodies and T1D. The current study demonstrated that there was no significant difference seen between the number of T1D patient sera positive for GluR autoantibodies compared to healthy controls and it is therefore unlikely that GluRs are the primary autoantibody targets in newly diagnosed, adult T1D patients. However, the current study is limited in that it only used serum samples from an older age group and as discussed in section 3.4.3, research suggests that there are two T1D endotypes which are split by insulitic profile, with the first endotype presenting at a young age (before 7 years old) and the second occurring after 13 years old (Arif et al., 2014; Endocrinology, 2019; Leete et al., 2016). The current study only used patient samples of individuals over 13 years old and therefore only investigated GluRs in relation to one T1D endotype. Despite GluRs being unlikely to be associated with T1D, it was important to rule them out as potential targets by the immune system so that new cell-surface protein targets can now be investigated.

4.1.   Future Work

The current study has been able to begin to identify a role for GluRs in insulin secretion from human β-cells as it was able to identify GluR subunit proteins, as well as demonstrating that activation of KARs leads to increased GSIS. However, the current study has only just begun to understand GluRs in β-cells and what role they play in hormone secretion and glucose homeostasis. The current study was limited as it was unable to successfully produce a GluK2 knock-down EndoC-βH1 cell line and therefore relied on GluR agonists and antagonists to determine GluR function. It would be important for future studies to investigate the specific role of GluK2 in insulin secretion from pancreatic β-cells by creating a stable GluK2 knock-out EndoC-βH1 cell line. The current study found using lenti-viral knock-down unsuccessful in the EndoC-βH1 cell line, however, a recent study has identified that CRISPR-Cas9 is a more reliable and effective method for gene knock-down in this cell line (Grotz et al., 2020) and should be considered in future studies. This approach could also be used to investigated how Neto proteins influence GluK2 trafficking to the cell surface in β-cells, as within neuronal cells they are known to play a role in the function and trafficking of KARs (Evans et al., 2017, 2019) and it is yet to be confirmed if they have the same effect in β-cells. Knockdown of Neto proteins could help to identify if these proteins are involved in surface expression of KARs, as is seen in neuronal cells and therefore are also involved in insulin secretion.

Within the human body blood glucose levels can fluctuate from high to low over a range of concentrations, however, the current study only investigated the extremes of this range and only at two concentrations as a representation of stimulatory (20 mM) and non-stimulatory (0.5 mM) glucose. In order to elucidate

a fuller picture of GluRs within β-cells, it will also be useful to study their expression and effects over a range of glucose concentrations and time points to see if the effects of GluRs are directly correlated to glucose concentration. When β-cells are exposed to chronic glucose levels it results in cytotoxicity and cell damage (Huang et al., 2017, Cairano et al., 2011) and some research has suggested that NMDAR knock-down reduces β-cell death (Marquard et al., 2015). It would therefore be of interest to investigate the role of GluRs, specifically KARs, in β-cell damage when cells are exposed to chronic glucose levels and identify if KARs are able to provide protection from damage or if they are part of the cause.

The current study has also proposed a mechanism to demonstrate how KARs induce insulin secretion (Figure 2.24). However, future work is needed to identify the specific mechanism and signally pathway by which KARs interact to increase insulin secretion. Previous studies have demonstrated that kainate results in $[Ca^{2+}]_I$ in MIN6 cells (Gonoi et al., 1994; Inagaki et al., 1995), it would therefore be important to confirm that human EndoC-βH1 cells also increase $[Ca^{2+}]_I$ and that it is this influx of Ca^{2+} which potentiates insulin secretion. KARs are also able to induce metabotropic effects in neuronal cells (Falcón-Moya et al., 2018) and as described in section 2.4.6 it may be that interaction with the PKA signally pathway by KARs increases insulin secretion in β-cells. Identification of the specific signally pathways involved in KAR-induced insulin secretion could lead to new therapeutic targets which could be utilised to improve insulin secretion in diabetic patients.

The current study has been able to contribute new knowledge in the presence and role of GluRs on human β-cells. It has specifically identified GluR subunits

which are expressed by the human β-cell line EndoC-βH1 and has demonstrated that KARs are able to increase GSIS in β-cells. However, more work is needed to uncover how GluRs exert their effects on β-cells and if they can be utilised to protect β-cells from damage when under stress.

5. References

Ahlqvist, E., Storm, P., Käräjämäki, A., Martinell, M., Dorkhan, M., Carlsson, A., Vikman, P., Prasad, R.B., Aly, D.M., Almgren, P., et al. (2018). Novel subgroups of adult-onset diabetes and their association with outcomes: a data-driven cluster analysis of six variables. Lancet Diabetes Endocrinol. *6*, 361–369.

Aizawa, T., and Komatsu, M. (2005). Rab27a: a new face in β cell metabolism-secretion coupling. J. Clin. Invest. *115*, 227–230.

Akirav, E., Kushner, J.A., and Herold, K.C. (2008). β-Cell Mass and Type 1 Diabetes. Diabetes *57*, 2883–2888.

Alicic, R.Z., Rooney, M.T., and Tuttle, K.R. (2017). Diabetic Kidney Disease: Challenges, Progress, and Possibilities. Clin. J. Am. Soc. Nephrol. *12*, 2032–2045.

American Diabetes Association (2018). 2. Classification and Diagnosis of Diabetes: Standards of Medical Care in Diabetes-2018. Diabetes Care *41*, S13–S27.

Andersson, L.E., Valtat, B., Bagge, A., Sharoyko, V.V., Nicholls, D.G., Ravassard, P., Scharfmann, R., Spégel, P., and Mulder, H. (2015). Characterization of stimulus-secretion coupling in the human pancreatic EndoC-βH1 beta cell line. PloS One *10*, e0120879.

Andrade-Talavera, Y., Duque-Feria, P., Sihra, T.S., and Rodríguez-Moreno, A. (2013). Pre-synaptic kainate receptor-mediated facilitation of glutamate release involves PKA and Ca(2+) -calmodulin at thalamocortical synapses. J. Neurochem. *126*, 565–578.

Andreone, L., Gimeno, M.L., and Perone, M.J. (2018). Interactions Between the Neuroendocrine System and T Lymphocytes in Diabetes. Front. Endocrinol. *9*.

Antvorskov, J.C., Halldorsson, T.I., Josefsen, K., Svensson, J., Granström, C., Roep, B.O., Olesen, T.H., Hrolfsdottir, L., Buschard, K., and Olsen, S.F. (2018). Association between maternal gluten intake and type 1 diabetes in offspring: national prospective cohort study in Denmark. The BMJ *362*.

Arif, S., Leete, P., Nguyen, V., Marks, K., Nor, N.M., Estorninho, M., Kronenberg-Versteeg, D., Bingley, P.J., Todd, J.A., Guy, C., et al. (2014). Blood and Islet Phenotypes Indicate Immunological Heterogeneity in Type 1 Diabetes. Diabetes *63*, 3835–3845.

Arinuma, Y. (2018). Antibodies and the brain: anti-N-methyl-D-aspartate receptor antibody and the clinical effects in patients with systemic lupus erythematosus. Curr. Opin. Neurol. *31*, 294–299.

Arntfield, M.E., and van der Kooy, D. (2011). β-Cell evolution: How the pancreas borrowed from the brain: The shared toolbox of genes expressed by neural and

pancreatic endocrine cells may reflect their evolutionary relationship. BioEssays News Rev. Mol. Cell. Dev. Biol. *33*, 582–587.

Association, A.D. (2018). 2. Classification and Diagnosis of Diabetes: Standards of Medical Care in Diabetes—2018. Diabetes Care *41*, S13–S27.

Atkinson, M.A., Eisenbarth, G.S., and Michels, A.W. (2014). Type 1 diabetes. Lancet Lond. Engl. *383*, 69–82.

Atkinson, M.A., Herrath, M. von, Powers, A.C., and Clare-Salzler, M. (2015). Current Concepts on the Pathogenesis of Type 1 Diabetes—Considerations for Attempts to Prevent and Reverse the Disease. Diabetes Care *38*, 979–988.

Atouf, F., Czernichow, P., and Scharfmann, R. (1997). Expression of neuronal traits in pancreatic beta cells. Implication of neuron-restrictive silencing factor/repressor element silencing transcription factor, a neuron-restrictive silencer. J. Biol. Chem. *272*, 1929–1934.

Bader, E., Migliorini, A., Gegg, M., Moruzzi, N., Gerdes, J., Roscioni, S.S., Bakhti, M., Brandl, E., Irmler, M., Beckers, J., et al. (2016). Identification of proliferative and mature β-cells in the islets of Langerhans. Nature *535*, 430–434.

Balu, R., McCracken, L., Lancaster, E., Graus, F., Dalmau, J., and Titulaer, M.J. (2019). A score that predicts 1-year functional status in patients with anti-NMDA receptor encephalitis. Neurology *92*, e244–e252.

Banjara, M., Ghosh, C., Dadas, A., Mazzone, P., and Janigro, D. (2017). Detection of brain-directed autoantibodies in the serum of non-small cell lung cancer patients. PLOS ONE *12*, e0181409.

Barnes, M.R., and Gray, I.C. (2003). Bioinformatics for Geneticists (John Wiley & Sons).

Bass, J., Wilkinson, D., Rankin, D., Phillips, B., Szewczyk, N., Smith, K., and Atherton, P. (2017). An overview of technical considerations for Western blotting applications to physiological research. Scand. J. Med. Sci. Sports *27*, 4–25.

Bauer, W., Veijola, R., Lempainen, J., Kiviniemi, M., Härkönen, T., Toppari, J., Knip, M., Gyenesei, A., and Ilonen, J. (2019). Age at Seroconversion, HLA Genotype and Specificity of Autoantibodies in Progression of Islet Autoimmunity in Childhood. J. Clin. Endocrinol. Metab.

Bellamy, L., Casas, J.-P., Hingorani, A.D., and Williams, D. (2009). Type 2 diabetes mellitus after gestational diabetes: a systematic review and meta-analysis. Lancet Lond. Engl. *373*, 1773–1779.

Benner, C., van der Meulen, T., Cacéres, E., Tigyi, K., Donaldson, C.J., and Huising, M.O. (2014). The transcriptional landscape of mouse beta cells compared to human beta cells reveals notable species differences in long non-coding RNA and protein-coding gene expression. BMC Genomics *15*, 620.

Benussi, A., Alberici, A., Buratti, E., Ghidoni, R., Gardoni, F., Di Luca, M., Padovani, A., and Borroni, B. (2019). Toward a Glutamate Hypothesis of Frontotemporal Dementia. Front. Neurosci. *13*, 304.

Bernstein, J., Lee-Parritz, A., Quinn, E., Ameli, O., Craig, M., Heeren, T., Iverson, R., Jack, B., and McCloskey, L. (2019). After Gestational Diabetes: Impact of Pregnancy Interval on Recurrence and Type 2 Diabetes. BioResearch Open Access *8*, 59–64.

Bertrand, G., Gross, R., Puech, R., Loubatières-Mariani, M.M., and Bockaert, J. (1992). Evidence for a glutamate receptor of the AMPA subtype which mediates insulin release from rat perfused pancreas. Br. J. Pharmacol. *106*, 354–359.

Bingley, P.J., Christie, M.R., Bonifacio, E., Bonfanti, R., Shattock, M., Fonte, M.T., Bottazzo, G.F., and Gale, E.A. (1994). Combined analysis of autoantibodies improves prediction of IDDM in islet cell antibody-positive relatives. Diabetes *43*, 1304–1310.

Blakemore, L.J., Corthell, J.T., and Trombley, P.Q. (2018). Kainate Receptors Play a Role in Modulating Synaptic Transmission in the Olfactory Bulb. Neuroscience *391*, 25–49.

Bonifacio, E., Mathieu, C., Nepom, G.T., Ziegler, A.-G., Anhalt, H., Haller, M.J., Harrison, L.C., Hebrok, M., Kushner, J.A., Norris, J.M., et al. (2017). Rebranding asymptomatic type 1 diabetes: the case for autoimmune beta cell disorder as a pathological and diagnostic entity. Diabetologia *60*, 35–38.

Bonifacio, E., Beyerlein, A., Hippich, M., Winkler, C., Vehik, K., Weedon, M.N., Laimighofer, M., Hattersley, A.T., Krumsiek, J., Frohnert, B.I., et al. (2018). Genetic scores to stratify risk of developing multiple islet autoantibodies and type 1 diabetes: A prospective study in children. PLoS Med. *15*.

Bonner-Weir, S., Sullivan, B.A., and Weir, G.C. (2015). Human Islet Morphology Revisited. J. Histochem. Cytochem. *63*, 604–612.

Boonnate, P., Waraasawapati, S., Hipkaeo, W., Pethlert, S., Sharma, A., Selmi, C., Prasongwattana, V., and Cha'on, U. (2015). Monosodium Glutamate Dietary Consumption Decreases Pancreatic β-Cell Mass in Adult Wistar Rats. PloS One *10*, e0131595.

Borroni, B., Stanic, J., Verpelli, C., Mellone, M., Bonomi, E., Alberici, A., Bernasconi, P., Culotta, L., Zianni, E., Archetti, S., et al. (2017). Anti-AMPA GluA3 antibodies in Frontotemporal dementia: a new molecular target. Sci. Rep. *7*, 6723.

Bramswig, N.C., Everett, L.J., Schug, J., Dorrell, C., Liu, C., Luo, Y., Streeter, P.R., Naji, A., Grompe, M., and Kaestner, K.H. (2013). Epigenomic plasticity enables human pancreatic α to β cell reprogramming. J. Clin. Invest. *123*, 1275–1284.

Briant, L., Salehi, A., Vergari, E., Zhang, Q., and Rorsman, P. (2016). Glucagon secretion from pancreatic α-cells. Ups. J. Med. Sci. *121*, 113–119.

Brice, N.L., Varadi, A., Ashcroft, S.J.H., and Molnar, E. (2002). Metabotropic glutamate and GABA(B) receptors contribute to the modulation of glucose-stimulated insulin secretion in pancreatic beta cells. Diabetologia *45*, 242–252.

Brissova, M., Shostak, A., Fligner, C.L., Revetta, F.L., Washington, M.K., Powers, A.C., and Hull, R.L. (2015). Human Islets Have Fewer Blood Vessels than Mouse Islets and the Density of Islet Vascular Structures Is Increased in Type 2 Diabetes. J. Histochem. Cytochem. Off. J. Histochem. Soc. *63*, 637–645.

Burg, A.R., Das, S., Padgett, L.E., Koenig, Z.E., and Tse, H.M. (2018). Superoxide Production by NADPH Oxidase Intensifies Macrophage Anti-Viral Responses during Diabetogenic Coxsackievirus Infection. J. Immunol. Baltim. Md 1950 *200*, 61–70.

Cabrera, O., Berman, D.M., Kenyon, N.S., Ricordi, C., Berggren, P.-O., and Caicedo, A. (2006). The unique cytoarchitecture of human pancreatic islets has implications for islet cell function. Proc. Natl. Acad. Sci. U. S. A. *103*, 2334–2339.

Cabrera, O., Jacques-Silva, M.C., Speier, S., Yang, S.-N., Köhler, M., Fachado, A., Vieira, E., Zierath, J.R., Kibbey, R., Berman, D.M., et al. (2008). Glutamate is a positive autocrine signal for glucagon release. Cell Metab. *7*, 545–554.

Chen, C.-H., and Chang, Y.-S. (2018). A Simple Cell-based Immunofluorescence Assay to Detect Autoantibody Against the N-Methyl-D-Aspartate (NMDA) Receptor in Blood. J. Vis. Exp. JoVE.

Chia, J.S.J., McRae, J.L., Enjapoori, A.K., Lefèvre, C.M., Kukuljan, S., and Dwyer, K.M. (2018). Dietary Cows' Milk Protein A1 Beta-Casein Increases the Incidence of T1D in NOD Mice. Nutrients *10*.

Chiefari, E., Arcidiacono, B., Foti, D., and Brunetti, A. (2017). Gestational diabetes mellitus: an updated overview. J. Endocrinol. Invest. *40*, 899–909.

Chireh, B., Li, M., and D'Arcy, C. (2019). Diabetes increases the risk of depression: A systematic review, meta-analysis and estimates of population attributable fractions based on prospective studies. Prev. Med. Rep. *14*, 100822.

Cho, J.-H., Chen, L., Kim, M.-H., Chow, R.H., Hille, B., and Koh, D.-S. (2010). Characteristics and functions of {alpha}-amino-3-hydroxy-5-methyl-4-isoxazolepropionate receptors expressed in mouse pancreatic {alpha}-cells. Endocrinology *151*, 1541–1550.

van Coevorden-Hameete, M.H., Titulaer, M.J., Schreurs, M.W.J., de Graaff, E., Sillevis Smitt, P.A.E., and Hoogenraad, C.C. (2016). Detection and Characterization of Autoantibodies to Neuronal Cell-Surface Antigens in the Central Nervous System. Front. Mol. Neurosci. *9*.

Coppieters, K., and von Herrath, M. (2018). The Development of Immunotherapy Strategies for the Treatment of Type 1 Diabetes. Front. Med. *5*.

Cornaby, C., Gibbons, L., Mayhew, V., Sloan, C.S., Welling, A., and Poole, B.D. (2015). B cell epitope spreading: mechanisms and contribution to autoimmune diseases. Immunol. Lett. *163*, 56–68.

Da Silva Xavier, G. (2018). The Cells of the Islets of Langerhans. J. Clin. Med. *7*.

Dalmau, J., Tüzün, E., Wu, H., Masjuan, J., Rossi, J.E., Voloschin, A., Baehring, J.M., Shimazaki, H., Koide, R., King, D., et al. (2007). Paraneoplastic anti-N-methyl-D-aspartate receptor encephalitis associated with ovarian teratoma. Ann. Neurol. *61*, 25–36.

Dalmau, J., Gleichman, A.J., Hughes, E.G., Rossi, J.E., Peng, X., Lai, M., Dessain, S.K., Rosenfeld, M.R., Balice-Gordon, R., and Lynch, D.R. (2008). Anti-NMDA-receptor encephalitis: case series and analysis of the effects of antibodies. Lancet Neurol. *7*, 1091–1098.

Dalmau, J., Geis, C., and Graus, F. (2017). Autoantibodies to Synaptic Receptors and Neuronal Cell Surface Proteins in Autoimmune Diseases of the Central Nervous System. Physiol. Rev. *97*, 839–887.

Di Cairano, E.S., Davalli, A.M., Perego, L., Sala, S., Sacchi, V.F., La Rosa, S., Finzi, G., Placidi, C., Capella, C., Conti, P., et al. (2011). The glial glutamate transporter 1 (GLT1) is expressed by pancreatic beta-cells and prevents glutamate-induced beta-cell death. J. Biol. Chem. *286*, 14007–14018.

Didona, D., and Di Zenzo, G. (2018). Humoral Epitope Spreading in Autoimmune Bullous Diseases. Front. Immunol. *9*.

Diedisheim, M., Oshima, M., Albagli, O., Huldt, C.W., Ahlstedt, I., Clausen, M., Menon, S., Aivazidis, A., Andreasson, A.-C., Haynes, W.G., et al. (2018). Modeling human pancreatic beta cell dedifferentiation. Mol. Metab. *10*, 74–86.

Diez, J.A., Arrojo e Drigo, R., Zheng, X., Stelmashenko, O.V., Chua, M., Rodriguez-Diaz, R., Fukuda, M., Köhler, M., Leibiger, I., Tun, S.B.B., et al. (2017). Pancreatic Islet Blood Flow Dynamics in Primates. Cell Rep. *20*, 1490–1501.

Domingues, A., Oliveira, T.C., Laço, M.L.N., Macedo, T.R.A., Oliveira, C.R., and Rego, A.C. (2006). Expression of NR1/NR2B N-Methyl-d-Aspartate Receptors Enhances Heroin Toxicity in HEK293 Cells. Ann. N. Y. Acad. Sci. *1074*, 458–465.

Domingues, A., Almeida, S., da Cruz e Silva, E.F., Oliveira, C.R., and Rego, A.C. (2007). Toxicity of β-amyloid in HEK293 cells expressing NR1/NR2A or NR1/NR2B N-methyl-d-aspartate receptor subunits. Neurochem. Int. *50*, 872–880.

Dorrell, C., Abraham, S.L., Lanxon-Cookson, K.M., Canaday, P.S., Streeter, P.R., and Grompe, M. (2008). Isolation of major pancreatic cell types and long-term culture-initiating cells using novel human surface markers. Stem Cell Res. *1*, 183–194.

Dorrell, C., Schug, J., Lin, C.F., Canaday, P.S., Fox, A.J., Smirnova, O., Bonnah, R., Streeter, P.R., Stoeckert, C.J., Kaestner, K.H., et al. (2011). Transcriptomes of the major human pancreatic cell types. Diabetologia *54*, 2832–2844.

Dorrell, C., Schug, J., Canaday, P.S., Russ, H.A., Tarlow, B.D., Grompe, M.T., Horton, T., Hebrok, M., Streeter, P.R., Kaestner, K.H., et al. (2016). Human islets contain four distinct subtypes of β cells. Nat. Commun. *7*, 1–9.

Duarte, L.F., Farías, M.A., Álvarez, D.M., Bueno, S.M., Riedel, C.A., and González, P.A. (2019). Herpes Simplex Virus Type 1 Infection of the Central Nervous System: Insights Into Proposed Interrelationships With Neurodegenerative Disorders. Front. Cell. Neurosci. *13*, 46.

Eberhard, D. (2013). Neuron and beta-cell evolution: Learning about neurons is learning about beta-cells. BioEssays *35*, 584–584.

Eizirik, D.L., Sammeth, M., Bouckenooghe, T., Bottu, G., Sisino, G., Igoillo-Esteve, M., Ortis, F., Santin, I., Colli, M.L., Barthson, J., et al. (2012). The Human Pancreatic Islet Transcriptome: Expression of Candidate Genes for Type 1 Diabetes and the Impact of Pro-Inflammatory Cytokines. PLOS Genet *8*, e1002552.

Endocrinology, T.L.D.& (2019). Type 1 diabetes research: poised for progress. Lancet Diabetes Endocrinol. *7*, 1.

Evans, A.J., Gurung, S., Wilkinson, K.A., Stephens, D.J., and Henley, J.M. (2017). Assembly, Secretory Pathway Trafficking, and Surface Delivery of Kainate Receptors Is Regulated by Neuronal Activity. Cell Rep. *19*, 2613–2626.

Evans, A.J., Gurung, S., Henley, J.M., Nakamura, Y., and Wilkinson, K.A. (2019). Exciting Times: New Advances Towards Understanding the Regulation and Roles of Kainate Receptors. Neurochem. Res. *44*, 572–584.

Falcón-Moya, R., Losada-Ruiz, P., Sihra, T.S., and Rodríguez-Moreno, A. (2018). Cerebellar Kainate Receptor-Mediated Facilitation of Glutamate Release Requires Ca2+-Calmodulin and PKA. Front. Mol. Neurosci. *11*.

Falcón-Moya1, R., Sihra, T.S., and Rodríguez-Moreno, A. (2018). Kainate Receptors: Role in Epilepsy. Front. Mol. Neurosci. *11*.

Fan, J., Wu, X., Cao, Z., Chen, S., Owyang, C., and Li, Y. (2009). Up-regulation of anterior cingulate cortex NR2B receptors contributes to visceral pain responses in rats. Gastroenterology *136*, 1732-1740.e3.

Fang, Z., Yang, Y., Chen, X., Zhang, W., Xie, Y., Chen, Y., Liu, Z., and Yuan, W. (2017). Advances in Autoimmune Epilepsy Associated with Antibodies, Their Potential Pathogenic Molecular Mechanisms, and Current Recommended Immunotherapies. Front. Immunol. *8*, 395.

Fayfman, M., Pasquel, F.J., and Umpierrez, G.E. (2017). Management of Hyperglycemic Crises: Diabetic ketoacidosis and hyperglycemic hyperosmolar state. Med. Clin. North Am. *101*, 587–606.

Ferrara-Cook, C., Geyer, S.M., Evans-Molina, C., Libman, I.M., Becker, D.J., Gitelman, S.E., Redondo, M.J., and Type 1 Diabetes TrialNet Study Group (2020). Excess BMI Accelerates Islet Autoimmunity in Older Children and Adolescents. Diabetes Care.

Ferrari, S.L., Abrahamsen, B., Napoli, N., Akesson, K., Chandran, M., Eastell, R., El-Hajj Fuleihan, G., Josse, R., Kendler, D.L., Kraenzlin, M., et al. (2018). Diagnosis and management of bone fragility in diabetes: an emerging challenge. Osteoporos. Int. *29*, 2585–2596.

Ferreira, J.M., Burnett, A.L., and Rameau, G.A. (2011). Activity-Dependent Regulation of Surface Glucose Transporter-3. J. Neurosci. Off. J. Soc. Neurosci. *31*, 1991–1999.

Fièvre, S., Carta, M., Chamma, I., Labrousse, V., Thoumine, O., and Mulle, C. (2016). Molecular determinants for the strictly compartmentalized expression of kainate receptors in CA3 pyramidal cells. Nat. Commun. *7*, 12738.

Firdous, P., Nissar, K., Ali, S., Ganai, B.A., Shabir, U., Hassan, T., and Masoodi, S.R. (2018). Genetic Testing of Maturity-Onset Diabetes of the Young Current Status and Future Perspectives. Front. Endocrinol. *9*.

Fred, R.G., Kappe, C., Ameur, A., Cen, J., Bergsten, P., Ravassard, P., Scharfmann, R., and Welsh, N. (2015). Role of the AMP kinase in cytokine-induced human EndoC-βH1 cell death. Mol. Cell. Endocrinol. *414*, 53–63.

Frederiksen, B., Kroehl, M., Lamb, M.M., Seifert, J., Barriga, K., Eisenbarth, G.S., Rewers, M., and Norris, J.M. (2013). Infant Exposures and Development of Type 1 Diabetes Mellitus. JAMA Pediatr. *167*, 808–815.

Fukuyama, T., Takahashi, Y., Kubota, Y., Mogami, Y., Imai, K., Kondo, Y., Sakuma, H., Tominaga, K., Oguni, H., and Nishimura, S. (2015). Semi-quantitative analyses of antibodies to N-methyl-d-aspartate type glutamate receptor subunits (GluN2B & GluN1) in the clinical course of Rasmussen syndrome. Epilepsy Res. *113*, 34–43.

Gallyas, F., Ball, S.M., and Molnar, E. (2003). Assembly and cell surface expression of KA-2 subunit-containing kainate receptors. J. Neurochem. *86*, 1414–1427.

Garand, D., Mahadevan, V., and Woodin, M.A. (2019). Ionotropic and metabotropic kainate receptor signalling regulates Cl- homeostasis and GABAergic inhibition. J. Physiol. *597*, 1677–1690.

Gastaldi, M., Thouin, A., Franciotta, D., and Vincent, A. (2017). Pitfalls in the detection of N-methyl-d-aspartate-receptor (NMDA-R) antibodies. Clin. Biochem. *50*, 354–355.

Geis, C., Planagumà, J., Carreño, M., Graus, F., and Dalmau, J. (2019). Autoimmune seizures and epilepsy. J. Clin. Invest. *129*, 926–940.

Gillespie, K.M., and Long, A.E. (2019). What Have Slow Progressors Taught Us About T1D—Mind the Gap! Curr. Diab. Rep. *19*.

Giorgio, C., Incerti, M., Pala, D., Russo, S., Chiodelli, P., Rusnati, M., Cantoni, A.M., Di Lecce, R., Barocelli, E., Bertoni, S., et al. (2019). Inhibition of Eph/ephrin interaction with the small molecule UniPR500 improves glucose tolerance in healthy and insulin-resistant mice. Pharmacol. Res. *141*, 319–330.

Gleichman, A.J., Spruce, L.A., Dalmau, J., Seeholzer, S.H., and Lynch, D.R. (2012). Anti-NMDA receptor encephalitis antibody binding is dependent on amino acid identity of a small region within the GluN1 amino terminal domain. J. Neurosci. Off. J. Soc. Neurosci. *32*, 11082–11094.

Goldberg-Stern, H., Ganor, Y., Cohen, R., Pollak, L., Teichberg, V., and Levite, M. (2014). Glutamate receptor antibodies directed against AMPA receptors subunit 3 peptide B (GluR3B) associate with some cognitive/psychiatric/behavioral abnormalities in epilepsy patients. Psychoneuroendocrinology *40*, 221–231.

Gonoi, T., Mizuno, N., Inagaki, N., Kuromi, H., Seino, Y., Miyazaki, J., and Seino, S. (1994). Functional neuronal ionotropic glutamate receptors are expressed in the non-neuronal cell line MIN6. J. Biol. Chem. *269*, 16989–16992.

González-González, I.M., and Henley, J.M. (2013). Postsynaptic Kainate Receptor Recycling and Surface Expression Are Regulated by Metabotropic Autoreceptor Signalling. Traffic Cph. Den. *14*, 810–822.

Gorelick, J., Yarmolinsky, L., Budovsky, A., Khalfin, B., Klein, J.D., Pinchasov, Y., Bushuev, M.A., Rudchenko, T., and Ben-Shabat, S. (2017). The Impact of Diet Wheat Source on the Onset of Type 1 Diabetes Mellitus-Lessons Learned from the Non-Obese Diabetic (NOD) Mouse Model. Nutrients *9*.

Graham, F.L., Smiley, J., Russell, W.C., and Nairn, R. (1977). Characteristics of a Human Cell Line Transformed by DNA from Human Adenovirus Type 5. J. Gen. Virol. *36*, 59–72.

Granger, A.J., Gray, J.A., Lu, W., and Nicoll, R.A. (2011). Genetic analysis of neuronal ionotropic glutamate receptor subunits. J. Physiol. *589*, 4095–4101.

Green, A.D., Vasu, S., and Flatt, P.R. (2018). Cellular models for beta-cell function and diabetes gene therapy. Acta Physiol. Oxf. Engl. *222*.

Greger, I.H., Watson, J.F., and Cull-Candy, S.G. (2017). Structural and Functional Architecture of AMPA-Type Glutamate Receptors and Their Auxiliary Proteins. Neuron *94*, 713–730.

Gresa-Arribas, N., Titulaer, M.J., Torrents, A., Aguilar, E., McCracken, L., Leypoldt, F., Gleichman, A.J., Balice-Gordon, R., Rosenfeld, M.R., Lynch, D., et al. (2014). Antibody titres at diagnosis and during follow-up of anti-NMDA receptor encephalitis: a retrospective study. Lancet Neurol. *13*, 167–177.

Grotz, A.K., Abaitua, F., Navarro-Guerrero, E., Hastoy, B., Ebner, D., and Gloyn, A.L. (2020). A CRISPR/Cas9 genome editing pipeline in the EndoC-βH1 cell line to study genes implicated in beta cell function. Wellcome Open Res. *4*.

Guo, H., Camargo, L.M., Yeboah, F., Digan, M.E., Niu, H., Pan, Y., Reiling, S., Soler-Llavina, G., Weihofen, W.A., Wang, H.-R., et al. (2017). A NMDA-receptor calcium influx assay sensitive to stimulation by glutamate and glycine/D-serine. Sci. Rep. *7*, 1–13.

Gurgul-Convey, E., Mehmeti, I., Plötz, T., Jörns, A., and Lenzen, S. (2016). Sensitivity profile of the human EndoC-βH1 beta cell line to proinflammatory cytokines. Diabetologia.

Hadzic, M., Jack, A., and Wahle, P. (2017). Ionotropic glutamate receptors: Which ones, when, and where in the mammalian neocortex. J. Comp. Neurol. *525*, 976–1033.

Hansen, K.B., Yi, F., Perszyk, R.E., Furukawa, H., Wollmuth, L.P., Gibb, A.J., and Traynelis, S.F. (2018). Structure, function, and allosteric modulation of NMDA receptors. J. Gen. Physiol. *150*, 1081–1105.

Hart, N.J., and Powers, A.C. (2019). Use of human islets to understand islet biology and diabetes: progress, challenges and suggestions. Diabetologia *62*, 212–222.

Hastoy, B., Godazgar, M., Clark, A., Nylander, V., Spiliotis, I., van de Bunt, M., Chibalina, M.V., Barrett, A., Burrows, C., Tarasov, A.I., et al. (2018). Electrophysiological properties of human beta-cell lines EndoC-βH1 and -βH2 conform with human beta-cells. Sci. Rep. *8*, 16994.

Henderson, J.R., and Moss, M.C. (1985). A morphometric study of the endocrine and exocrine capillaries of the pancreas. Q. J. Exp. Physiol. Camb. Engl. *70*, 347–356.

Hernaus, D., and Amelsvoort, T. van (2018). Glutamate-dopamine matters in psychosis. Lancet Psychiatry *5*, 773–774.

Hex, N., Bartlett, C., Wright, D., Taylor, M., and Varley, D. (2012). Estimating the current and future costs of Type 1 and Type 2 diabetes in the UK, including direct health costs and indirect societal and productivity costs. Diabet. Med. J. Br. Diabet. Assoc. *29*, 855–862.

Hogan-Cann, A.D., and Anderson, C.M. (2016). Physiological Roles of Non-Neuronal NMDA Receptors. Trends Pharmacol. Sci.

Hong, S.W., Jiang, Y., Kim, S., Li, C.J., and Lee, D. (2014). Target Gene Abundance Contributes to the Efficiency of siRNA-Mediated Gene Silencing. Nucleic Acid Ther. *24*, 192–198.

Huang, Q., Merriman, C., Zhang, H., and Fu, D. (2017a). Coupling of Insulin Secretion and Display of a Granule-resident Zinc Transporter ZnT8 on the Surface of Pancreatic Beta Cells. J. Biol. Chem. *292*, 4034–4043.

Huang, X.-T., Li, C., Peng, X.-P., Guo, J., Yue, S.-J., Liu, W., Zhao, F.-Y., Han, J.-Z., Huang, Y.-H., Yang-Li, Y.-L., et al. (2017b). An excessive increase in glutamate contributes to glucose-toxicity in β-cells via activation of pancreatic NMDA receptors in rodent diabetes. Sci. Rep. *7*.

Huda, S., Waters, P., Woodhall, M., Leite, M.I., Jacobson, L., De Rosa, A., Maestri, M., Ricciardi, R., Heckmann, J.M., Maniaol, A., et al. (2017). IgG-specific cell-based assay detects potentially pathogenic MuSK-Abs in seronegative MG. Neurol. Neuroimmunol. Neuroinflammation *4*.

Hyöty, H., Leon, F., and Knip, M. (2018). Developing a vaccine for type 1 diabetes by targeting coxsackievirus B. Expert Rev. Vaccines *17*, 1071–1083.

Iacobucci, G.J., and Popescu, G.K. (2018). Kinetic models for activation and modulation of NMDA receptor subtypes. Curr. Opin. Physiol. *2*, 114–122.

Ilonen, J., Lempainen, J., Hammais, A., Laine, A.-P., Härkönen, T., Toppari, J., Veijola, R., Knip, M., and Finnish Pediatric Diabetes Register (2018). Primary islet autoantibody at initial seroconversion and autoantibodies at diagnosis of type 1 diabetes as markers of disease heterogeneity. Pediatr. Diabetes *19*, 284–292.

Inagaki, N., Kuromi, H., Gonoi, T., Okamoto, Y., Ishida, H., Seino, Y., Kaneko, T., Iwanaga, T., and Seino, S. (1995). Expression and role of ionotropic glutamate receptors in pancreatic islet cells. FASEB J. Off. Publ. Fed. Am. Soc. Exp. Biol. *9*, 686–691.

Insel, R.A., Dunne, J.L., Atkinson, M.A., Chiang, J.L., Dabelea, D., Gottlieb, P.A., Greenbaum, C.J., Herold, K.C., Krischer, J.P., Lernmark, Å., et al. (2015). Staging presymptomatic type 1 diabetes: a scientific statement of JDRF, the Endocrine Society, and the American Diabetes Association. Diabetes Care *38*, 1964–1974.

Irani, S.R., Alexander, S., Waters, P., Kleopa, K.A., Pettingill, P., Zuliani, L., Peles, E., Buckley, C., Lang, B., and Vincent, A. (2010). Antibodies to Kv1 potassium channel-complex proteins leucine-rich, glioma inactivated 1 protein and contactin-associated protein-2 in limbic encephalitis, Morvan's syndrome and acquired neuromyotonia. Brain J. Neurol. *133*, 2734–2748.

Jack, A., Hamad, M.I.K., Gonda, S., Gralla, S., Pahl, S., Hollmann, M., and Wahle, P. (2018). Development of Cortical Pyramidal Cell and Interneuronal Dendrites: a Role for Kainate Receptor Subunits and NETO1. Mol. Neurobiol.

Jacobsen, L.M., Haller, M.J., and Schatz, D.A. (2018). Understanding Pre-Type 1 Diabetes: The Key to Prevention. Front. Endocrinol. *9*.

Jahan, M., Johnström, P., Selvaraju, R.K., Svedberg, M., Winzell, M.S., Bernström, J., Kingston, L., Schou, M., Jia, Z., Skrtic, S., et al. (2018). The development of a GPR44 targeting radioligand [11C]AZ12204657 for in vivo assessment of beta cell mass. EJNMMI Res. *8*.

Jansson, L., Barbu, A., Bodin, B., Drott, C.J., Espes, D., Gao, X., Grapensparr, L., Källskog, Ö., Lau, J., Liljebäck, H., et al. (2016). Pancreatic islet blood flow and its measurement. Ups. J. Med. Sci. *121*, 81–95.

Jayanarayanan, S., Anju, T.R., Smijin, S., and Paulose, C.S. (2015). Vitamin D3 supplementation increases insulin level by regulating altered IP3 and AMPA receptor expression in the pancreatic islets of streptozotocin-induced diabetic rat. J. Nutr. Biochem. *26*, 1041–1049.

Juan-Mateu, J., Rech, T.H., Villate, O., Lizarraga-Mollinedo, E., Wendt, A., Turatsinze, J.-V., Brondani, L.A., Nardelli, T.R., Nogueira, T.C., Esguerra, J.L.S., et al. (2017). Neuron-enriched RNA-binding Proteins Regulate Pancreatic Beta Cell Function and Survival. J. Biol. Chem. *292*, 3466–3480.

Kamalova, A., and Nakagawa, T. (2020). AMPA receptor structure and auxiliary subunits. J. Physiol.

Kapadia, M., Bijelić, D., Zhao, H., Ma, D., Stojanovich, L., Milošević, M., Andjus, P., and Šakić, B. (2017). Effects of sustained i.c.v. infusion of lupus CSF and autoantibodies on behavioral phenotype and neuronal calcium signaling. Acta Neuropathol. Commun. *5*, 70.

Kaufman, D.L., Erlander, M.G., Clare-Salzler, M., Atkinson, M.A., Maclaren, N.K., and Tobin, A.J. (1992). Autoimmunity to two forms of glutamate decarboxylase in insulin-dependent diabetes mellitus. J. Clin. Invest. *89*, 283–292.

Kilinc, D. (2018). The Emerging Role of Mechanics in Synapse Formation and Plasticity. Front. Cell. Neurosci. *12*.

Köhler, M., Daré, E., Ali, M.Y., Rajasekaran, S.S., Moede, T., Leibiger, B., Leibiger, I.B., Tibell, A., Juntti-Berggren, L., and Berggren, P.-O. (2012). One-step purification of functional human and rat pancreatic alpha cells. Integr. Biol. Quant. Biosci. Nano Macro *4*, 209–219.

Köhr, G., Eckardt, S., Lüddens, H., Monyer, H., and Seeburg, P.H. (1994). NMDA receptor channels: subunit-specific potentiation by reducing agents. Neuron *12*, 1031–1040.

Komatsu, M., Sato, Y., Yamada, S., Yamauchi, K., Hashizume, K., and Aizawa, T. (2002). Triggering of Insulin Release by a Combination of cAMP Signal and Nutrients. Diabetes *51*, S29–S32.

Korol, S.V., Jin, Z., Jin, Y., Bhandage, A.K., Tengholm, A., Gandasi, N.R., Barg, S., Espes, D., Carlsson, P.-O., Laver, D., et al. (2018). Functional Characterization of Native, High-Affinity GABAA Receptors in Human Pancreatic β Cells. EBioMedicine *30*, 273–282.

Kracht, M.J.L., de Koning, E.J.P., Hoeben, R.C., Roep, B.O., and Zaldumbide, A. (2018). Bioluminescent reporter assay for monitoring ER stress in human beta cells. Sci. Rep. *8*.

Krischer, J.P., Liu, X., Vehik, K., Akolkar, B., Hagopian, W.A., Rewers, M.J., She, J.-X., Toppari, J., Ziegler, A.-G., Lernmark, Å., et al. (2019). Predicting Islet Cell Autoimmunity and Type 1 Diabetes: An 8-Year TEDDY Study Progress Report. Diabetes Care *42*, 1051–1060.

Krizhanovskii, C., Kristinsson, H., Elksnis, A., Wang, X., Gavali, H., Bergsten, P., Scharfmann, R., and Welsh, N. (2017). EndoC-βH1 cells display increased sensitivity to sodium palmitate when cultured in DMEM/F12 medium. Islets *9*, e1296995.

Kuljanin, M., Elgamal, R.M., Bell, G.I., Xenocostas, A., Lajoie, G.A., and Hess, D.A. (2019). Human Multipotent Stromal Cell Secreted Effectors Accelerate Islet Regeneration. Stem Cells Dayt. Ohio *37*, 516–528.

Kutlu, B., Burdick, D., Baxter, D., Rasschaert, J., Flamez, D., Eizirik, D.L., Welsh, N., Goodman, N., and Hood, L. (2009). Detailed transcriptome atlas of the pancreatic beta cell. BMC Med. Genomics *2*, 3.

Ladépêche, L., Planagumà, J., Thakur, S., Suárez, I., Hara, M., Borbely, J.S., Sandoval, A., Laparra-Cuervo, L., Dalmau, J., and Lakadamyali, M. (2018). NMDA Receptor Autoantibodies in Autoimmune Encephalitis Cause a Subunit-Specific Nanoscale Redistribution of NMDA Receptors. Cell Rep. *23*, 3759–3768.

Lai, M., Hughes, E.G., Peng, X., Zhou, L., Gleichman, A.J., Shu, H., Matà, S., Kremens, D., Vitaliani, R., Geschwind, M.D., et al. (2009). AMPA receptor antibodies in limbic encephalitis alter synaptic receptor location. Ann. Neurol. *65*, 424–434.

Laimighofer, M., Lickert, R., Fuerst, R., Theis, F.J., Winkler, C., Bonifacio, E., Ziegler, A.-G., and Krumsiek, J. (2019). Common patterns of gene regulation associated with Cesarean section and the development of islet autoimmunity – indications of immune cell activation. Sci. Rep. *9*.

Lambeth, L.S., Van Hateren, N.J., Wilson, S.A., and Nair, V. (2010). A direct comparison of strategies for combinatorial RNA interference. BMC Mol. Biol. *11*, 77.

Lampasona, V., Pittman, D.L., Williams, A.J., Achenbach, P., Schlosser, M., Akolkar, B., and Winter, W.E. (2019). Islet Autoantibody Standardization Program 2018 Workshop: Interlaboratory Comparison of Glutamic Acid Decarboxylase Autoantibody Assay Performance. Clin. Chem.

Lawlor, N., Márquez, E.J., Orchard, P., Narisu, N., Shamim, M.S., Thibodeau, A., Varshney, A., Kursawe, R., Erdos, M.R., Kanke, M., et al. (2019). Multiomic Profiling Identifies cis-Regulatory Networks Underlying Human Pancreatic β Cell Identity and Function. Cell Rep. *26*, 788-801.e6.

Lee, C.J., Labrakakis, C., Joseph, D.J., and MacDermott, A.B. (2004). Functional similarities and differences of AMPA and kainate receptors expressed by cultured rat sensory neurons. Neuroscience *129*, 35–48.

Lee, Y.-B., Han, K., Kim, B., Jin, S.-M., Lee, S.-E., Jun, J.E., Ahn, J., Kim, G., and Kim, J.H. (2019). High Proportion of Adult Cases and Prevalence of Metabolic Syndrome in Type 1 Diabetes Mellitus Population in Korea: A Nationwide Study. Diabetes Metab. J. *43*, 76–89.

Leete, P., Willcox, A., Krogvold, L., Dahl-Jørgensen, K., Foulis, A.K., Richardson, S.J., and Morgan, N.G. (2016). Differential Insulitic Profiles Determine the Extent of β-Cell Destruction and the Age at Onset of Type 1 Diabetes. Diabetes *65*, 1362–1369.

Leite, M.I., Jacob, S., Viegas, S., Cossins, J., Clover, L., Morgan, B.P., Beeson, D., Willcox, N., and Vincent, A. (2008). IgG1 antibodies to acetylcholine receptors in "seronegative" myasthenia gravis. Brain J. Neurol. *131*, 1940–1952.

Lemelman, M.B., Letourneau, L., and Greeley, S.A.W. (2018). Neonatal Diabetes Mellitus: An Update on Diagnosis and Management. Clin. Perinatol. *45*, 41–59.

Levite, M. (2014). Glutamate receptor antibodies in neurological diseases: anti-AMPA-GluR3 antibodies, anti-NMDA-NR1 antibodies, anti-NMDA-NR2A/B antibodies, anti-mGluR1 antibodies or anti-mGluR5 antibodies are present in subpopulations of patients with either: epilepsy, encephalitis, cerebellar ataxia, systemic lupus erythematosus (SLE) and neuropsychiatric SLE, Sjogren's syndrome, schizophrenia, mania or stroke. These autoimmune anti-glutamate receptor antibodies can bind neurons in few brain regions, activate glutamate receptors, decrease glutamate receptor's expression, impair glutamate-induced signaling and function, activate blood brain barrier endothelial cells, kill neurons, damage the brain, induce behavioral/psychiatric/cognitive abnormalities and ataxia in animal models, and can be removed or silenced in some patients by immunotherapy. J. Neural Transm. Vienna Austria 1996 *121*, 1029–1075.

Li, S.-W., Koya, V., Li, Y., Donelan, W., Lin, P., Reeves, W.H., and Yang, L.-J. (2010). Pancreatic duodenal homeobox 1 protein is a novel beta-cell-specific autoantigen for type I diabetes. Lab. Investig. J. Tech. Methods Pathol. *90*, 31–39.

Lind, G.E., Mou, T.-C., Tamborini, L., Pomper, M.G., Micheli, C.D., Conti, P., Pinto, A., and Hansen, K.B. (2017). Structural basis of subunit selectivity for competitive NMDA receptor antagonists with preference for GluN2A over GluN2B subunits. Proc. Natl. Acad. Sci. *114*, E6942–E6951.

Longo, P.A., Kavran, J.M., Kim, M.-S., and Leahy, D.J. (2013). Transient Mammalian Cell Transfection with Polyethylenimine (PEI). Methods Enzymol. *529*, 227–240.

Lund-Blix, N.A., Dydensborg Sander, S., Størdal, K., Nybo Andersen, A.-M., Rønningen, K.S., Joner, G., Skrivarhaug, T., Njølstad, P.R., Husby, S., and Stene, L.C. (2017). Infant Feeding and Risk of Type 1 Diabetes in Two Large Scandinavian Birth Cohorts. Diabetes Care *40*, 920–927.

Ma, C., Wang, C., Zhang, Q., and Lian, Y. (2019). Emerging role of prodromal headache in patients with anti-N-methyl-D-aspartate receptor encephalitis. J. Pain Res. *12*, 519–526.

Magi, S., Piccirillo, S., and Amoroso, S. (2019). The dual face of glutamate: from a neurotoxin to a potential survival factor-metabolic implications in health and disease. Cell. Mol. Life Sci. CMLS *76*, 1473–1488.

Magne, F., Puchi Silva, A., Carvajal, B., and Gotteland, M. (2017). The Elevated Rate of Cesarean Section and Its Contribution to Non-Communicable Chronic Diseases in Latin America: The Growing Involvement of the Microbiota. Front. Pediatr. *5*.

Mahan, V.L. (2019). Neurointegrity and europhysiology: astrocyte, glutamate, and carbon monoxide interactions. Med. Gas Res. *9*, 24–45.

Mahdipour, E., Salmasi, Z., and Sabeti, N. (2019). Potential of stem cell-derived exosomes to regenerate β islets through Pdx-1 dependent mechanism in a rat model of type 1 diabetes. J. Cell. Physiol.

Manto, M., Dalmau, J., Didelot, A., Rogemond, V., and Honnorat, J. (2010). In vivo effects of antibodies from patients with anti-NMDA receptor encephalitis: further evidence of synaptic glutamatergic dysfunction. Orphanet J. Rare Dis. *5*, 31.

Marquard, J., Otter, S., Welters, A., Stirban, A., Fischer, A., Eglinger, J., Herebian, D., Kletke, O., Klemen, M.S., Stožer, A., et al. (2015). Characterization of pancreatic NMDA receptors as possible drug targets for diabetes treatment. Nat. Med. *21*, 363–372.

Marshall, J.J., Xu, J., and Contractor, A. (2018). Kainate Receptors Inhibit Glutamate Release Via Mobilization of Endocannabinoids in Striatal Direct Pathway Spiny Projection Neurons. J. Neurosci. *38*, 3901–3910.

Martin, S., and Henley, J.M. (2004). Activity-dependent endocytic sorting of kainate receptors to recycling or degradation pathways. EMBO J. *23*, 4749–4759.

Mayer, M.L. (2017). The Challenge of Interpreting Glutamate-Receptor Ion-Channel Structures. Biophys. J. *113*, 2143–2151.

McLaughlin, K.A., Richardson, C.C., Williams, S., Bonifacio, E., Morgan, D., Feltbower, R.G., Powell, M., Rees Smith, B., Furmaniak, J., and Christie, M.R. (2015). Relationships between major epitopes of the IA-2 autoantigen in Type 1 diabetes: Implications for determinant spreading. Clin. Immunol. Orlando Fla *160*, 226–236.

Migues, P.V., Liu, L., Archbold, G.E.B., Einarsson, E.Ö., Wong, J., Bonasia, K., Ko, S.H., Wang, Y.T., and Hardt, O. (2016). Blocking Synaptic Removal of GluA2-Containing AMPA Receptors Prevents the Natural Forgetting of Long-Term Memories. J. Neurosci. Off. J. Soc. Neurosci. *36*, 3481–3494.

Molnár, E., Váradi, A., McIlhinney, R.A., and Ashcroft, S.J. (1995). Identification of functional ionotropic glutamate receptor proteins in pancreatic beta-cells and in islets of Langerhans. FEBS Lett. *371*, 253–257.

Moore, C.B., Guthrie, E.H., Huang, M.T.-H., and Taxman, D.J. (2010). Short Hairpin RNA (shRNA): Design, Delivery, and Assessment of Gene Knockdown. Methods Mol. Biol. Clifton NJ *629*, 141–158.

Mørkholt, A.S., Kastaniegaard, K., Trabjerg, M.S., Gopalasingam, G., Niganze, W., Larsen, A., Stensballe, A., Nielsen, S., and Nieland, J.D. (2018). Identification of brain antigens recognized by autoantibodies in experimental autoimmune encephalomyelitis-induced animals treated with etomoxir or interferon-β. Sci. Rep. *8*, 1–11.

Nakayama, M., Simmons, K.M., and Michels, A.W. (2015). Molecular Interactions Governing Autoantigen Presentation in Type 1 Diabetes. Curr. Diab. Rep. *15*, 113.

Ndiaye, F.K., Ortalli, A., Canouil, M., Huyvaert, M., Salazar-Cardozo, C., Lecoeur, C., Verbanck, M., Pawlowski, V., Boutry, R., Durand, E., et al. (2017). Expression and functional assessment of candidate type 2 diabetes susceptibility genes identify four new genes contributing to human insulin secretion. Mol. Metab. *6*, 459–470.

Negrete-Díaz, J.V., Sihra, T.S., Flores, G., and Rodríguez-Moreno, A. (2018). Non-canonical Mechanisms of Presynaptic Kainate Receptors Controlling Glutamate Release. Front. Mol. Neurosci. *11*.

Nica, A.C., Ongen, H., Irminger, J.-C., Bosco, D., Berney, T., Antonarakis, S.E., Halban, P.A., and Dermitzakis, E.T. (2013). Cell-type, allelic, and genetic signatures in the human pancreatic beta cell transcriptome. Genome Res. *23*, 1554–1562.

Nirmalan, N., and Nirmalan, M. (2017). Hormonal control of metabolism: regulation of plasma glucose. Anaesth. Intensive Care Med. *18*, 502–507.

O'Donovan, S.M., Sullivan, C.R., and McCullumsmith, R.E. (2017). The role of glutamate transporters in the pathophysiology of neuropsychiatric disorders. NPJ Schizophr. *3*.

Oleson, B.J., McGraw, J.A., Broniowska, K.A., Annamalai, M., Chen, J., Bushkofsky, J.R., Davis, D.B., Corbett, J.A., and Mathews, C.E. (2015). Distinct differences in the responses of the human pancreatic β-cell line EndoC-βH1 and human islets to proinflammatory cytokines. Am. J. Physiol. - Regul. Integr. Comp. Physiol. *309*, R525–R534.

Opendak, M., Zanca, R.M., Anane, E., Serrano, P.A., and Sullivan, R.M. (2018). Developmental transitions in amygdala PKC isoforms and AMPA receptor expression associated with threat memory in infant rats. Sci. Rep. *8*, 14679.

Orav, E., Dowavic, I., Huupponen, J., Taira, T., and Lauri, S.E. (2019). NETO1 Regulates Postsynaptic Kainate Receptors in CA3 Interneurons During Circuit Maturation. Mol. Neurobiol.

Oresic, M., Simell, S., Sysi-Aho, M., Näntö-Salonen, K., Seppänen-Laakso, T., Parikka, V., Katajamaa, M., Hekkala, A., Mattila, I., Keskinen, P., et al. (2008). Dysregulation of lipid and amino acid metabolism precedes islet autoimmunity in children who later progress to type 1 diabetes. J. Exp. Med. *205*, 2975–2984.

Otter, S., and Lammert, E. (2016). Exciting Times for Pancreatic Islets: Glutamate Signaling in Endocrine Cells. Trends Endocrinol. Metab. TEM *27*, 177–188.

Palacios-Filardo, J., Aller, M.I., and Lerma, J. (2016). Synaptic Targeting of Kainate Receptors. Cereb. Cortex *26*, 1464–1472.

Park, K.H., Waters, P., Woodhall, M., Lang, B., Smith, T., Sung, J.-J., Kim, K.-K., Lim, Y.-M., Kim, J.-E., Kim, B.-J., et al. (2018). Myasthenia gravis seronegative for acetylcholine receptor antibodies in South Korea: Autoantibody profiles and clinical features. PLoS ONE *13*.

Parsons, W.J., Ramkumar, V., and Stiles, G.L. (1988). Isobutylmethylxanthine stimulates adenylate cyclase by blocking the inhibitory regulatory protein, Gi. Mol. Pharmacol. *34*, 37–41.

Patterson, C.C., Harjutsalo, V., Rosenbauer, J., Neu, A., Cinek, O., Skrivarhaug, T., Rami-Merhar, B., Soltesz, G., Svensson, J., Parslow, R.C., et al. (2019). Trends and cyclical variation in the incidence of childhood type 1 diabetes in 26 European centres in the 25 year period 1989–2013: a multicentre prospective registration study. Diabetologia *62*, 408–417.

Patterson, S., Irwin, N., Guo-Parke, H., Moffett, R.C., Scullion, S.M., Flatt, P.R., and McClenaghan, N.H. (2016). Evaluation of the role of N-methyl-D-aspartate (NMDA) receptors in insulin secreting beta-cells. Eur. J. Pharmacol. *771*, 107–113.

Paul, D.S., Teschendorff, A.E., Dang, M.A.N., Lowe, R., Hawa, M.I., Ecker, S., Beyan, H., Cunningham, S., Fouts, A.R., Ramelius, A., et al. (2016). Increased DNA methylation variability in type 1 diabetes across three immune effector cell types. Nat. Commun. *7*.

Pawaskar, M., Iglay, K., Witt, E.A., Engel, S.S., and Rajpathak, S. (2018). Impact of the severity of hypoglycemia on health - Related quality of life, productivity, resource use, and costs among US patients with type 2 diabetes. J. Diabetes Complications *32*, 451–457.

Pechnick, R.N., and Poland, R.E. (2004). Comparison of the effects of dextromethorphan, dextrorphan, and levorphanol on the hypothalamo-pituitary-adrenal axis. J. Pharmacol. Exp. Ther. *309*, 515–522.

Pedersen, M.G., Tagliavini, A., and Henquin, J.-C. (2019). Calcium signaling and secretory granule pool dynamics underlie biphasic insulin secretion and its

amplification by glucose: experiments and modeling. Am. J. Physiol. Endocrinol. Metab. *316*, E475–E486.

Peng, X., Hughes, E.G., Moscato, E.H., Parsons, T.D., Dalmau, J., and Balice-Gordon, R.J. (2015). Cellular plasticity induced by anti-α-amino-3-hydroxy-5-methyl-4-isoxazolepropionic acid (AMPA) receptor encephalitis antibodies. Ann. Neurol. *77*, 381–398.

Perillo, M., Paganos, P., Mattiello, T., Cocurullo, M., Oliveri, P., and Arnone, M.I. (2018). New Neuronal Subtypes With a "Pre-Pancreatic" Signature in the Sea Urchin Stongylocentrotus purpuratus. Front. Endocrinol. *9*, 650.

Peters, L.L., Thornton, C., de Jonge, A., Khashan, A., Tracy, M., Downe, S., Feijen-de Jong, E.I., and Dahlen, H.G. (2018). The effect of medical and operative birth interventions on child health outcomes in the first 28 days and up to 5 years of age: A linked data population-based cohort study. Birth Berkeley Calif *45*, 347–357.

Petrovic, M.M., Viana da Silva, S., Clement, J.P., Vyklicky, L., Mulle, C., González-González, I.M., and Henley, J.M. (2017). Metabotropic action of postsynaptic kainate receptors triggers hippocampal long-term potentiation. Nat. Neurosci. *20*, 529–539.

Pfeifer, C.R., Shomorony, A., Aronova, M.A., Zhang, G., Cai, T., Xu, H., Notkins, A.L., and Leapman, R.D. (2015). Quantitative analysis of mouse pancreatic islet architecture by serial block-face SEM. J. Struct. Biol. *189*, 44–52.

Pickard, L., Noël, J., Henley, J.M., Collingridge, G.L., and Molnar, E. (2000). Developmental changes in synaptic AMPA and NMDA receptor distribution and AMPA receptor subunit composition in living hippocampal neurons. J. Neurosci. Off. J. Soc. Neurosci. *20*, 7922–7931.

Pihoker, C., Gilliam, L.K., Hampe, C.S., and Lernmark, A. (2005). Autoantibodies in diabetes. Diabetes *54 Suppl 2*, S52-61.

Pociot, F. (2017). Type 1 diabetes genome-wide association studies: not to be lost in translation. Clin. Transl. Immunol. *6*, e162.

Prasad, R.B., and Groop, L. (2016). Single-Cell Sequencing of Human Pancreatic Islets—New Kids on the Block. Cell Metab. *24*, 523–524.

Principi, N., Berioli, M.G., Bianchini, S., and Esposito, S. (2017). Type 1 diabetes and viral infections: What is the relationship? J. Clin. Virol. Off. Publ. Pan Am. Soc. Clin. Virol. *96*, 26–31.

Pumphrey, S.A., Pizzirani, S., Pirie, C.G., Anwer, M.S., and Logvinenko, T. (2013). Western blot patterns of serum autoantibodies against optic nerve antigens in dogs with goniodysgenesis-related glaucoma. Am. J. Vet. Res. *74*, 621–628.

Raghavan, S., Vassy, J.L., Ho, Y., Song, R.J., Gagnon, D.R., Cho, K., Wilson, P.W.F., and Phillips, L.S. (2019). Diabetes Mellitus–Related All-Cause and

Cardiovascular Mortality in a National Cohort of Adults. J. Am. Heart Assoc. Cardiovasc. Cerebrovasc. Dis. *8*.

Rath, A., Glibowicka, M., Nadeau, V.G., Chen, G., and Deber, C.M. (2009). Detergent binding explains anomalous SDS-PAGE migration of membrane proteins. Proc. Natl. Acad. Sci. *106*, 1760–1765.

Ravassard, P., Hazhouz, Y., Pechberty, S., Bricout-Neveu, E., Armanet, M., Czernichow, P., and Scharfmann, R. (2011). A genetically engineered human pancreatic β cell line exhibiting glucose-inducible insulin secretion. J. Clin. Invest. *121*, 3589–3597.

Regnell, S.E., and Lernmark, Å. (2017). Early prediction of autoimmune (type 1) diabetes. Diabetologia *60*, 1370–1381.

Reiner, A., and Levitz, J. (2018). Glutamatergic Signaling in the Central Nervous System: Ionotropic and Metabotropic Receptors in Concert. Neuron *98*, 1080–1098.

Rewers, M., and Ludvigsson, J. (2016). Environmental risk factors for type 1 diabetes. Lancet Lond. Engl. *387*, 2340–2348.

Ribeiro, F.M., Vieira, L.B., Pires, R.G.W., Olmo, R.P., and Ferguson, S.S.G. (2017). Metabotropic glutamate receptors and neurodegenerative diseases. Pharmacol. Res. *115*, 179–191.

Richter, E.A., and Hargreaves, M. (2013). Exercise, GLUT4, and skeletal muscle glucose uptake. Physiol. Rev. *93*, 993–1017.

Ricken, G., Schwaiger, C., De Simoni, D., Pichler, V., Lang, J., Glatter, S., Macher, S., Rommer, P.S., Scholze, P., Kubista, H., et al. (2018). Detection Methods for Autoantibodies in Suspected Autoimmune Encephalitis. Front. Neurol. *9*.

Röder, P.V., Wu, B., Liu, Y., and Han, W. (2016). Pancreatic regulation of glucose homeostasis. Exp. Mol. Med. *48*, e219.

Rodnoi, P., Rajkumar, M., Moin, A.S.M., Georgia, S.K., Butler, A.E., and Dhawan, S. (2017). Neuropeptide Y expression marks partially differentiated β cells in mice and humans. JCI Insight *2*.

Rodriguez-Diaz, R., Abdulreda, M.H., Formoso, A.L., Gans, I., Ricordi, C., Berggren, P.-O., and Caicedo, A. (2011). Innervation patterns of autonomic axons in the human endocrine pancreas. Cell Metab. *14*, 45–54.

Rogers, M.A.M., Kim, C., Banerjee, T., and Lee, J.M. (2017). Fluctuations in the incidence of type 1 diabetes in the United States from 2001 to 2015: a longitudinal study. BMC Med. *15*.

Rojas, J., Bermudez, V., Palmar, J., Martínez, M.S., Olivar, L.C., Nava, M., Tomey, D., Rojas, M., Salazar, J., Garicano, C., et al. (2018). Pancreatic Beta

Cell Death: Novel Potential Mechanisms in Diabetes Therapy. J. Diabetes Res. *2018*.

Rorsman, P., and Ashcroft, F.M. (2018). Pancreatic β-Cell Electrical Activity and Insulin Secretion: Of Mice and Men. Physiol. Rev. *98*, 117–214.

Rorsman, P., and Braun, M. (2013). Regulation of insulin secretion in human pancreatic islets. Annu. Rev. Physiol. *75*, 155–179.

Roshanravan, H., Kim, E.Y., and Dryer, S.E. (2016). NMDA Receptors as Potential Therapeutic Targets in Diabetic Nephropathy: Increased Renal NMDA Receptor Subunit Expression in Akita Mice and Reduced Nephropathy Following Sustained Treatment With Memantine or MK-801. Diabetes *65*, 3139–3150.

Ryan, T.J., Emes, R.D., Grant, S.G., and Komiyama, N.H. (2008). Evolution of NMDA receptor cytoplasmic interaction domains: implications for organisation of synaptic signalling complexes. BMC Neurosci. *9*, 6.

Rzeski, W., Turski, L., and Ikonomidou, C. (2001). Glutamate antagonists limit tumor growth. Proc. Natl. Acad. Sci. *98*, 6372–6377.

Saab, A.S., Tzvetavona, I.D., Trevisiol, A., Baltan, S., Dibaj, P., Kusch, K., Möbius, W., Goetze, B., Jahn, H.M., Huang, W., et al. (2016). Oligodendroglial NMDA Receptors Regulate Glucose Import and Axonal Energy Metabolism. Neuron *91*, 119–132.

Saberzadeh-Ardestani, B., Karamzadeh, R., Basiri, M., Hajizadeh-Saffar, E., Farhadi, A., Shapiro, A.M.J., Tahamtani, Y., and Baharvand, H. (2018). Type 1 Diabetes Mellitus: Cellular and Molecular Pathophysiology at A Glance. Cell J. Yakhteh *20*, 294–301.

Sakamoto, S., Putalun, W., Vimolmangkang, S., Phoolcharoen, W., Shoyama, Y., Tanaka, H., and Morimoto, S. (2018). Enzyme-linked immunosorbent assay for the quantitative/qualitative analysis of plant secondary metabolites. J. Nat. Med. *72*, 32–42.

Santiago, A.R., Gaspar, J.M., Baptista, F.I., Cristóvão, A.J., Santos, P.F., Kamphuis, W., and Ambrósio, A.F. (2009). Diabetes changes the levels of ionotropic glutamate receptors in the rat retina. Mol. Vis. *15*, 1620–1630.

Schmitz, D., Mellor, J., Breustedt, J., and Nicoll, R.A. (2003). Presynaptic kainate receptors impart an associative property to hippocampal mossy fiber long-term potentiation. Nat. Neurosci. *6*, 1058–1063.

Selvaraj, K., Gowthamarajan, K., Karri, V.V.S.R., Barauah, U.K., Ravisankar, V., and Jojo, G.M. (2017). Current treatment strategies and nanocarrier based approaches for the treatment and management of diabetic retinopathy. J. Drug Target. *25*, 386–405.

Sheng, N., Shi, Y.S., and Nicoll, R.A. (2017). Amino-terminal domains of kainate receptors determine the differential dependence on Neto auxiliary subunits for trafficking. Proc. Natl. Acad. Sci. U. S. A. *114*, 1159–1164.

Shi, X., Huang, G., Wang, Y., Liu, Z., Deng, C., Li, X., Zheng, P., and Zhou, Z. (2019). Tetraspanin 7 autoantibodies predict progressive decline of beta cell function in individuals with LADA. Diabetologia 62, 399–407.

Siller, A.F., Lugar, H., Rutlin, J., Koller, J.M., Semenkovich, K., White, N.H., Arbelaez, A.M., Shimony, J., and Hershey, T. (2016). Severity of clinical presentation in youth with type 1 diabetes is associated with differences in brain structure. Pediatr. Diabetes n/a-n/a.

Sillevis Smitt, P., Kinoshita, A., De Leeuw, B., Moll, W., Coesmans, M., Jaarsma, D., Henzen-Logmans, S., Vecht, C., De Zeeuw, C., Sekiyama, N., et al. (2000). Paraneoplastic cerebellar ataxia due to autoantibodies against a glutamate receptor. N. Engl. J. Med. 342, 21–27.

Smart, T.G., and Paoletti, P. (2012). Synaptic neurotransmitter-gated receptors. Cold Spring Harb. Perspect. Biol. 4.

Smatti, M.K., Cyprian, F.S., Nasrallah, G.K., Al Thani, A.A., Almishal, R.O., and Yassine, H.M. (2019). Viruses and Autoimmunity: A Review on the Potential Interaction and Molecular Mechanisms. Viruses 11.

So, M., Elso, C.M., Tresoldi, E., Pakusch, M., Pathiraja, V., Wentworth, J.M., Harrison, L.C., Krishnamurthy, B., Thomas, H.E., Rodda, C., et al. (2018). Proinsulin C-peptide is an autoantigen in people with type 1 diabetes. Proc. Natl. Acad. Sci. U. S. A. 115, 10732–10737.

Spitzer, S., Volbracht, K., Lundgaard, I., and Káradóttir, R.T. (2016). Glutamate signalling: A multifaceted modulator of oligodendrocyte lineage cells in health and disease. Neuropharmacology.

Steiner, D.J., Kim, A., Miller, K., and Hara, M. (2010). Pancreatic islet plasticity: Interspecies comparison of islet architecture and composition. Islets 2, 135–145.

Sun, H., Lu, L., Zuo, Y., Wang, Y., Jiao, Y., Zeng, W.-Z., Huang, C., Zhu, M.X., Zamponi, G.W., Zhou, T., et al. (2014). Kainate receptor activation induces glycine receptor endocytosis through PKC deSUMOylation. Nat. Commun. 5.

Suzuki, E., and Kamiya, H. (2016). PSD-95 regulates synaptic kainate receptors at mouse hippocampal mossy fiber-CA3 synapses. Neurosci. Res. 107, 14–19.

Teraoku, H., and Lenzen, S. (2017). Dynamics of Insulin Secretion from EndoC-βH1 β-Cell Pseudoislets in Response to Glucose and Other Nutrient and Nonnutrient Secretagogues. J. Diabetes Res. 2017.

Thomas, N.J., Jones, S.E., Weedon, M.N., Shields, B.M., Oram, R.A., and Hattersley, A.T. (2018). Frequency and phenotype of type 1 diabetes in the first six decades of life: a cross-sectional, genetically stratified survival analysis from UK Biobank. Lancet Diabetes Endocrinol. 6, 122–129.

Tizaoui, K., Kim, S.H., Jeong, G.H., Kronbichler, A., Lee, K.S., Lee, K.H., and Shin, J.I. (2019). Association of PTPN22 1858C/T Polymorphism with

Autoimmune Diseases: A Systematic Review and Bayesian Approach. J. Clin. Med. *8*.

Tomas, A., Jones, B., and Leech, C. (2019). New Insights into Beta-Cell GLP-1 Receptor and cAMP Signaling. J. Mol. Biol.

Toniolo, A., Cassani, G., Puggioni, A., Rossi, A., Colombo, A., Onodera, T., and Ferrannini, E. (2019). The diabetes pandemic and associated infections: suggestions for clinical microbiology. Rev. Med. Microbiol. *30*, 1–17.

Tönnes, J., Stierli, B., Cerletti, C., Behrmann, J.T., Molnár, E., and Streit, P. (1999). Regional distribution and developmental changes of GluR1-flop protein revealed by monoclonal antibody in rat brain. J. Neurochem. *73*, 2195–2205.

Tridgell, D.M., Spiekerman, C., Wang, R.S., and Greenbaum, C.J. (2011). Interaction of Onset and Duration of Diabetes on the Percent of GAD and IA-2 Antibody–Positive Subjects in the Type 1 Diabetes Genetics Consortium Database. Diabetes Care *34*, 988–993.

Tsonis, A.I., Zisimopoulou, P., Lazaridis, K., Tzartos, J., Matsigkou, E., Zouvelou, V., Mantegazza, R., Antozzi, C., Andreetta, F., Evoli, A., et al. (2015). MuSK autoantibodies in myasthenia gravis detected by cell based assay — A multinational study. J. Neuroimmunol. *284*, 10–17.

Tsonkova, V.G., Sand, F.W., Wolf, X.A., Grunnet, L.G., Kirstine Ringgaard, A., Ingvorsen, C., Winkel, L., Kalisz, M., Dalgaard, K., Bruun, C., et al. (2018). The EndoC-βH1 cell line is a valid model of human beta cells and applicable for screenings to identify novel drug target candidates. Mol. Metab. *8*, 144–157.

Tuomilehto, J. (2013). The Emerging Global Epidemic of Type 1 Diabetes. Curr. Diab. Rep. *13*, 795–804.

Twomey, E.C., and Sobolevsky, A.I. (2018). Structural Mechanisms of Gating in Ionotropic Glutamate Receptors. Biochemistry *57*, 267–276.

Tyka, K., Jörns, A., Turatsinze, J.-V., Eizirik, D.L., Lenzen, S., and Gurgul-Convey, E. (2019). MCPIP1 regulates the sensitivity of pancreatic beta-cells to cytokine toxicity. Cell Death Dis. *10*.

Uusitalo, U., Lee, H.-S., Andrén Aronsson, C., Vehik, K., Yang, J., Hummel, S., Silvis, K., Lernmark, Å., Rewers, M., Hagopian, W., et al. (2018). Early Infant Diet and Islet Autoimmunity in the TEDDY Study. Diabetes Care *41*, 522–530.

Vianello, M., Keir, G., Giometto, B., Betterle, C., Tavolato, B., and Thompson, E.J. (2005). Antigenic differences between neurological and diabetic patients with anti-glutamic acid decarboxylase antibodies. Eur. J. Neurol. *12*, 294–299.

Vincent, A., Pettingill, P., Pettingill, R., Lang, B., Birch, R., Waters, P., Irani, S.R., Buckley, C., Watanabe, O., Arimura, K., et al. (2018). Association of Leucine-Rich Glioma Inactivated Protein 1, Contactin-Associated Protein 2, and Contactin 2 Antibodies With Clinical Features and Patient-Reported Pain in Acquired Neuromyotonia. JAMA Neurol. *75*, 1519–1527.

Vishnoi, S., Raisuddin, S., and Parvez, S. (2016). Glutamate Excitotoxicity and Oxidative Stress in Epilepsy: Modulatory Role of Melatonin. J. Environ. Pathol. Toxicol. Oncol. Off. Organ Int. Soc. Environ. Toxicol. Cancer *35*, 365–374.

Wallis, J.L., Irvine, M.W., Jane, D.E., Lodge, D., Collingridge, G.L., and Bortolotto, Z.A. (2015). An interchangeable role for kainate and metabotropic glutamate receptors in the induction of rat hippocampal mossy fiber long-term potentiation in vivo. Hippocampus *25*, 1407–1417.

Watanabe-Iida, I., Konno, K., Akashi, K., Abe, M., Natsume, R., Watanabe, M., and Sakimura, K. (2016). Determination of kainate receptor subunit ratios in mouse brain using novel chimeric protein standards. J. Neurochem. *136*, 295–305.

Weaver, C.D., Yao, T.L., Powers, A.C., and Verdoorn, T.A. (1996). Differential expression of glutamate receptor subtypes in rat pancreatic islets. J. Biol. Chem. *271*, 12977–12984.

Wendt, A., and Eliasson, L. (2020). Pancreatic α-cells - The unsung heroes in islet function. Semin. Cell Dev. Biol.

Weng, J., Zhou, Z., Guo, L., Zhu, D., Ji, L., Luo, X., Mu, Y., and Jia, W. (2018). Incidence of type 1 diabetes in China, 2010-13: population based study. The BMJ *360*.

Wenzlau, J.M., and Hutton, J.C. (2013). Novel diabetes autoantibodies and prediction of type 1 diabetes. Curr. Diab. Rep. *13*, 608–615.

Wiśniewski, K., and Car, H. (2002). (S)-3,5-DHPG: a review. CNS Drug Rev. *8*, 101–116.

Wu, W., Hodges, E., Redelius, J., and Höög, C. (2004). A novel approach for evaluating the efficiency of siRNAs on protein levels in cultured cells. Nucleic Acids Res. *32*, e17.

Wu, Y., Fortin, D.A., Cochrane, V.A., Chen, P.-C., and Shyng, S.-L. (2017). NMDA receptors mediate leptin signaling and regulate potassium channel trafficking in pancreatic β-cells. J. Biol. Chem. *292*, 15512–15524.

Wu, Z.-Y., Zhu, L.-J., Zou, N., Bombek, L.K., Shao, C.-Y., Wang, N., Wang, X.-X., Liang, L., Xia, J., Rupnik, M., et al. (2012). AMPA receptors regulate exocytosis and insulin release in pancreatic β cells. Traffic Cph. Den. *13*, 1124–1139.

Yi, Z., Waseem Ghani, M., Ghani, H., Jiang, W., Waseem Birmani, M., Ye, L., Bin, L., Cun, L.G., Lilong, A., and Mei, X. (2020). Gimmicks of gamma-aminobutyric acid (GABA) in pancreatic β-cell regeneration through transdifferentiation of pancreatic α- to β-cells. Cell Biol. Int.

You, W.-P., and Henneberg, M. (2016). Type 1 diabetes prevalence increasing globally and regionally: the role of natural selection and life expectancy at birth. BMJ Open Diabetes Res. Care *4*, e000161.

Yu, W., and Miller, R.F. (1995). NBQX, an improved non-NMDA antagonist studied in retinal ganglion cells. Brain Res. *692*, 190–194.

Zampieri, S., Ghirardello, A., Doria, A., Tonello, M., Bendo, R., Rossini, K., and Gambari, P.F. (2000). The use of Tween 20 in immunoblotting assays for the detection of autoantibodies in connective tissue diseases. J. Immunol. Methods *239*, 1–11.

Zeng, H., Shen, E.H., Hohmann, J.G., Oh, W.S., Bernard, A., Royall, J.J., Glattfelder, K.J., Sunkin, S.M., Morris, J.A., Guillozet-Bongaarts, A.L., et al. (2012). Large-scale cellular-resolution gene profiling in human neocortex reveals species-specific molecular signatures. Cell *149*, 483–496.

Zhang, H., Liu, R., Deng, T., Wang, X., Lang, H., Qu, Y., Duan, J., Huang, D., Ying, G., and Ba, Y. (2016). The microRNA-124-iGluR2/3 pathway regulates glucagon release from alpha cells. Oncotarget *7*, 24734–24743.

Zhao, H., Lomash, S., Chittori, S., Glasser, C., Mayer, M.L., and Schuck, P. (2017). Preferential assembly of heteromeric kainate and AMPA receptor amino terminal domains. ELife *6*.

Zhong, F., and Jiang, Y. (2019). Endogenous Pancreatic β Cell Regeneration: A Potential Strategy for the Recovery of β Cell Deficiency in Diabetes. Front. Endocrinol. *10*.

Zhou, Y., and Danbolt, N.C. (2014). Glutamate as a neurotransmitter in the healthy brain. J. Neural Transm. Vienna Austria 1996 *121*, 799–817.

Zhu, S., and Gouaux, E. (2017). Structure and symmetry inform gating principles of ionotropic glutamate receptors. Neuropharmacology *112*, 11–15.

Zhu, Y., and Zhang, C. (2016). Prevalence of Gestational Diabetes and Risk of Progression to Type 2 Diabetes: a Global Perspective. Curr. Diab. Rep. *16*, 7.

Ziegler, A.G., Rewers, M., Simell, O., Simell, T., Lempainen, J., Steck, A., Winkler, C., Ilonen, J., Veijola, R., Knip, M., et al. (2013). Seroconversion to multiple islet autoantibodies and risk of progression to diabetes in children. JAMA *309*, 2473–2479.

IDF diabetes atlas - 2017 Atlas.

6. Appendix

6.1.   Appendix I

shRNA sequencing results from Source Biosciences.

shRNA_integrated_into_pSUPER-neo-GFP; Primer_30nt_M13R (provided by Source Biosciences)

```
NNNNNNNNNNNNNCCTCACTAAAGGGACNAAAGCTGGTACCGGGCCCCCCCTCGAGAAAAACCT
CTGATTATGCTTTCCTAATCTCTTGAATTAGGAAAGCATAATCAGAGGGGGGATCTGTGGTCTC
ATACAGAACTTATAAGATTCCCAAATCCAAAGACATTTCACGTTTATGGTGATTTCCCAGAACA
CATAGCGACATGCAAATATTGCAGGGCGCCACTCCCCTGTCCCTCACAGCCATCTTCCTGCCAG
GGCGCACGCGCGCTGGGTGTTCCCGCCTAGTGACACTGGGCCCGCGATTCCTTGGAGCGGGTTG
ATGACGTCAGCGTTCGAATTCTACCGGGTAGGGGAGGCGCTTTTCCCAAGGCAGTCTGGAGCAT
GCGCTTTAGCAGCCCCGCTGGGCACTTGGCGCTACACAAGTGGCCTCTGGCCTCGCACACATTC
CACATCCACCGGCCGGTAGGCGCCAACCGGCTCCGTTCTTTGGTGGCCCCTTCGCGCCACCTTC
TACTCCTCCCCTAGTCAGGAAGTTCCCCCCCGCCCCGCAGCTCGCGTCGTGCAGGACGTGACAA
ATGGAAGTAGCACGTCTCACTAGTCTCGTGCAGATGGACAGCACCGCTGAGCAATGGAAGCGGG
TAGGCCTTTGGGGCAGCGGCCAATAGCAGCTTTGCTCCTTCGCTTTCTGGGCTCANANGCTGGG
AANGGGTGGGTCCGGGGGCGGGCTCANGGGCGGGCTCNNGGGCGGGGCGGGCGCCCGAAAGTCC
TCCGGANGNCCGGCATTCTGCACGCTTCAAAAGCGCACGTCTGCCGCGCTGTTCTCCTCTTCCT
CATCTCCGGGNCTTTTNNACCTGCAGCCCAAGCTAGCTTACNNGTCGCCACCNTGGTGAGCAAG
GGCGANGANCTGTTCACCGGGGTGGTGNCCATCCTGGTCGAGCTGNACGGCGACGTAAACNGCC
ACANNTTCAGCGTGTCCNGCGAGGGCGNNGGNNGATGCCACCTANNNNAGCTGANCCNGANGNT
TNATCTGCNCNNCNGNAGCTGCCCGNGCCCTGGGCCACCCNCGTGACNNCCTGACTANNGCGNG
CNNNGNGTNNNNNNGCTACNCCNACCNCCNTGNANCAGCNNGANTNCNTNNANNTCNGNCNNNC
NCNNANGNNNANGTNCANNNNNNNNNNNNNNTTNTTNANGNACNANGNNANNTNNNNNNNNNNCN
ANGNNNANNNNNANGNNNNNCCNNNNNANCNCNNNNNNNNNNAANNNNNNNNNNNNNNNNGANNN
NNNCNNGNNNANNNGNNNNNNNNNNNNNNNNNTNNNNNNNNNCNNNANNNNNN
```

shRNA integrated into pXLG3-PX-GFP-IRES-WPRE

```
NNNNNNANNCGCGGGCCNGTGTCNCTAGGCGGGANNACCCAGCGCGCGTGCGCCCTGGCAGGAA
GATGGCTGTGAGGGACAGGGGAGTGGCGCCCTGCAATATTTGCATGTCGCTATGTGTTCTGGGA
AATCACCATAAACGTGAAATGTCTTTGGATTTGGGAATCTTATAAGTTCTGTATGAGACCACAG
ATCCCCCCTCTGATTATGCTTTCCTAATTCAAGAGATTAGGAAAGCATAATCAGAGGTTTTTCT
CGAGGGGGGGCCCGGTACCAGCTTTTGTTCCCTTTAGTGAGGGTTAATTTCGAGCTTGGCGTAA
TCATGGTCATAGCTGTTTCCTGTGTGAAATTGTTATCCGCTCACAATTCCACACAACATACGAG
CCGGAAGCATAAAGTGTAAAGCCTGGGGTGCCTAATGAGTGAGCTAACTCACATTAATTGCGTT
GCGCTCACTGCCCGCTTTCCAGTCGGGAAACCTGTCGTGCCAGCTGCATTAATGAATCGGCCAA
CGCGCGGGGAGAGGCGGTTTGCGTATTGGGCGCTCTTCCGCTTCCTCGCTCACTGACTCGCTGC
GCTCGGTCGTTCGGCTGCGGCGAGCGGTATCAGCTCACTCAAAGGCGGTAATACGGTTATCCAC
AGAATCAGGGGATAACGCAGGAAAGAACATGTGAGCAAAAGGCCAGCAAAAGGCCAGGAACCGT
AAAAAGGCCGCGTTGCTGGCGTTTTTCCATAGGCTCCGCCCCCCTGACGAGCATCACAAAAATC
GACGCTCAAGTCAGAGGTGGCGAAACCCGACAGGACTATAAAGATACCAGGCGTTTCCCCCTGG
AAGCTCCCTCGTGCGCTCTCCTGTTCCGACCCTGCCGCTTACCGGATACCTGTCCGCCTTTCTC
CCTTCGGGAAGCGTGGCGCTTTCTCATAGCTCACGCTGTAGGTATCTCAGTTCGGTGTAGGTCG
TTCGCTCCAAGCTGGGCTGTGTGCACGAACCCCCCGTTCAGCCCGACCGCTGCGCCTTATCCGG
TAACTATCGTCTTGAGTCCAACCCGGTAAGACACGACTTATCGCCACTGGCAGCAGCCACTGGT
AACAGGATTAGCAGAGCGAGGTATGTAGGCGGTGCTACAGAGTTCTTGAAGTGGTGGCCTAACT
ACGGCTACACTAAANNAACAGTATTTGGTATCTGCGCTCTGCTGAANCCAGTTACCTTCGGAAA
AANNAGTTGGTAGCTCTTGATCCGGCAANCAANCCACCGCNGGNNAGCGGTGGNTTTTTTTTGT
TTGCAANCNNCCAANTTACCCNNCNNAAAAAAANGGATCTNNNGAANNNTCCTTTNGATCTTTT
NCTACGGGGNNCNGANNNNNNNAATGGAANCGAAANNTNCCNGTTTAAGGNATTTTNGGNCNNTG
AAANTTNTCCAAAAAGGNNNNNCCCCNNNAANNNCCNTTNAAANTTNAAAANGGNANNTTTNAA
ANCCNNNNNNAANNNNNNNNNNNNNNNNAANCTTTGGNNCNNNNNNNNTTCNNNNNGNNTNNNNNN
CCNNNNNNAGNCNTNNNNNNNNNNNCCGAANNNGGCNNNNATCNNANNNNNNNNNNNTATNNNNNN
NNNNNTCNNNNNNNGGNNNTNNNNNNNNNNNANNNNNNGGNNNNNNNNNNNNNNNCNNNNGNNNNCC
NNANGNNNNNNNNNNNNAANCCCNNNGNANNCCCNACNNNNNNCCNNGNNNNCCNNNTNTTTTN
CNNNNNNNNNANGNCCNNNCCNNNNCNNNNNNNGNNNNNNNAANNNNNANNNNNNNNNGNNNNN
NNNNNNNTNNNATNNCCNCCNNNNANCNANNNNANNNNNANNNNNNGTNNTNNNNNANGNNNNNN
NNNNNNANNNNNGNNNNNNNCNNNTTCANANNNNNNTNNNNNNNNNTNATTTTNNTNNNNNNNTN
NNGNNNANAANNNNNNNNTNAATNNC
```

6.2. Appendix II

Protein FASTA sequences taken from UniProt

https://www.uniprot.org/uniprot/Q63273

Anti-GRIK5 Antibody (Millipore UK Limited) protein target sequence highlighted in yellow. Differences between the human and rat sequence are highlighted in red.

Human GRIK5 Protein Sequence

```
MPAELLLLLIVAFASPSCQVLSSLRMAAILDDQTVCGRGERLALALAREQINGIIEVPAK
ARVEVDIFELQRDSQYETTDTMCQILPKGVVSVLGPSSSPASASTVSHICGEKEIPHIKV
GPEETPRLQYLRFASVSLYPSNEDVSLAVSRILKSFNYPSASLICAKAECLLRLEELVRG
FLISKETLSVRMLDDSRDPTPLLKEIRDDKVSTIIIDANASISHLILRKASELGMTSAFY
KYILTTMDFPILHLDGIVEDSSNILGFSMFNTSHPFYPEFVRSLNMSWRENCEASTYLGP
ALSAALMFDAVHVVSAVRELNRSQEIGVKPLACTSANIWPHGTSLMNYLRMVEYDGLTG
RVEFNSKGQRTNYTLRILEKSRQGHREIGVWYSNRTLAMNATTLDINLSQTLANKTLVVT
TILENPYVMRRPNFQALSGNERFEGFCVDMLRELAELLRFYRLRLVEDGLYGAPEPNGS
WTGMVGELINRKADLAVAAFTITAEREKVIDFSKPFMTLGISILYRVHMGRKPGYFSFLD
PFSPAVWLFMLLAYLAVSCVLFLAARLSPYEWYNPHPCLRARPHILENQYTLGNSLWFPV
GGFMQQGSEIMPRALSTRCVSGVWWAFTLIIISSYTANLAAFLTVQRMEVPVESADDLAD
QTNIEYGTIHAGSTMTFFQNSRYQTYQRMWNYMQSKQPSVFVKSTEEGIARVLNSRYAFL
LESTMNEYHRRLNCNLTQIGGLLDTKGYGIGMPLGSPFRDEITLAILQLQENNRLEILKR
KWWEGGRCPKEEDHRAKGLGMENIGGIFIVLICGLIIAVFVAVMEFIWSTRRSAESEEVS
VCQEMLQELRHAVSCRKTSRSRRRRPGGPSRALLSLRAVREMRLSNGKLYSAGAGGDAG
SAHGGPQRLLDDPGPPSGARPAAPTPCTHVRVCQECRRIQALRASGAGAPPRGLGVPAEA
```
==TSPPRPRPGP====AGPRELA====EHE==

Rat GRIK5 Protein Sequence

```
MPAELLLLLIVAFANPSCQVLSSLRMAAILDDQTVCGRGERLALALAREQINGIIEVPAK
ARVEVDIFELQRDSQYETTDTMCQILPKGVVSVLGPSSSPASASTVSHICGEKEIPHIKV
GPEETPRLQYLRFASVSLYPSNEDVSLAVSRILKSFNYPSASLICAKAECLLRLEELVRG
FLISKETLSVRMLDDSRDPTPLLKEIRDDKVSTIIIDANASISHLVLRKASELGMTSAFY
KYILTTMDFPILHLDGIVEDSSNILGFSMFNTSHPFYPEFVRSLNMSWRENCEASTYPGP
ALSAALMFDAVHVVSAVRELNRSQEIGVKPLACTSANIWPHGTSLMNYLRMVEYDGLTG
RVEFNSKGQRTNYTLRILEKSRQGHREIGVWYSNRTLAMNATTLDINLSQTLANKTLVVT
TILENPYVMRRPNFQALSGNERFEGFCVDMLRELAELLRFYRLRLVEDGLYGAPEPNGS
WTGMVGELINRKADLAVAAFTITAEREKVIDFSKPFMTLGISILYRVHMGRKPGYFSFLD
PFSPAVWLFMLLAYLAVSCVLFLAARLSPYEWYNPHPCLRARPHILENQYTLGNSLWFPV
GGFMQQGSEIMPRALSTRCVSGVWWAFTLIIISSYTANLAAFLTVQRMEVPVESADDLAD
QTNIEYGTIHAGSTMTFFQNSRYQTYQRMWNYMQSKQPSVFVKSTEEGIARVLNSRYAFL
LESTMNEYHRRLNCNLTQIGGLLDTKGYGIGMPLGSPFRDEITLAILQLQENNRLEILKR
KWWEGGRCPKEEDHRAKGLGMENIGGIFVVLICGLIIAVFVAVMEFIWSTRRSAESEEVS
VCQEMLQELRHAVSCRKTSRSRRRRPGGPSRALLSLRAVREMRLSNGKLYSAGAGGDAG
AHGGPQRLLDDPGPPGGPRPQAPTPCTHVRVCQECRRIQALRASGAGAPPRGLGTPAEA
```
==T====SPPRPRPGPTGPRELTEHE==

6.3.   Appendix III

Lentivus knock-down of GluK2 in neuronal cells from University of Bristol

Figure 3-13: Loss of total and surface GluK2 does not alter the total or surface levels of GluK5. Surface biotinylation was performed on DIV 15 hippocampal neurones post 5 days GluK2 KD to isolate surface proteins and determine surface and total GluK2 and GluK5 levels by western blotting.

A. Representative western blot images of surface and total levels of GluK2 and GluK5 post 5 days GluK2 KD. GAPDH was used as an internal control to determine no internal proteins were biotinylated.

B-E. Quantification of separate surface and total protein levels of GluK2 total (B), GluK2 surface (C), GluK5 total (D) and GluK5 surface (E) shown in A. The total levels of proteins were normalised to respective GAPDH levels. Surface/Total ratio was determined to obtain surface reads. N=7 independent dissections, ns $p>0.05$, ****$p<0.0001$; Unpaired t-test; error bars=S.D.

6.4. Appendix IIII

PCR sequencing results from Source Biosciences.

GluK2 Forward Primer: CATGCAGCAAGGTTCTGAGC

Sequence Amplified:

```
CATTTCTTCGTATACTGCTAACTTAGCCGCCTTTCTGACAGTGGAACGCATGGAATCCCCTATT
GACTCTGCTGATGATTTAGCTAAACAAACCAAGATAGAATATGGAGCAGTAGAGGATGGTGCAA
CCATGACTTTTTTCAAGAAATCAAAAATCTCCACGTATGACAAAATGTGGGCCTTTATGAGTAG
CAGAAGGCAGTCAGTGCTGGTCAAAAGTAATGAAGAAGGAATCCAGCGAGTCCTCACCTCTGAT
TATGCTTTCCTAATGGAGTCAACAACCATCGAGTTTGTTACCCAGCGGAACTGTAACCTGACAC
AGATTGGCGGCCTTATAGACTCTAAAGGTTATGGCGTTGGCACTCCCATGGGTTCTCCATATCG
AGACAAAATTACCATAGCAATTCTTCAGCTGCAAGAGGAAGGCAAACAA
```

GluK5 Forward Primer: AGAACCAACTACACCCTGCG

Sequence Amplified:

```
GAGANTGGGGTGTGGTNCTCTANNNGCACCNTGGNCATGAATGCCTCCACCCTGGACNTCAACC
TGTCTCAAACACTGGCCAGCAAGACCCTGGTGGTCACAACCATCCTGGAGAACCCATACGTCAT
GCGCCGGCCCAACTTCCAGGCCCTGTCGGGGAACGAACGCTTCGAGGGCTTCTGCGTGGACATG
CTGCGGGAGCTGGCCGAGCTGCTGCGCTTCCGCTACCGCCTGCGGTTGGTGGAGGATGGGCTGT
ACGGGGCGCCCGAGCCCAACGGCTCCTGGACGGGCATGGTTGGCGAGCTCATCAACCGGAAGGC
AGAC
```

Neto1 Forward Primer: CACCAGTGGGACTGTCATTG

Sequence Amplified:

```
TTATCNTCTCTGTCATCGTACAGATCAAACAGCCTCGTAAAAAGTATGTCCAAAGGAAATCAGA
CTTTGACCAGACAGTTTTCCAGGAGGTATTTGAACCTCCTCATTATGAGTTATGCACTCTCAGA
GGGACAGGAGCTACAGCTGACTTTGCAGATGTGGCAGAA
```

Neto2 Forward Primer: TTTGCTTCGCCAAATTATCC

Sequence Amplified:

GNATCTACATTTTGGANCTNGCTNNNNNGTNNNNNNNNNAGAGCTNTNGNACCNTTTGATGAAC
ATTNTTATATAGAACCATCATTTGAGTGTCGGTTTGATCACTTGGAAGTTCGAGATGGGCCATT
TGGTTTCTCTCCTCTTATAGATCGTTACTGTGGCGTGAAAAGCCCTCCATTAAA